# Antimicrobial Metallohelices: Discovery and Mechanistic Investigation

**by**

**Daniel H Simpson**

A thesis submitted in partial fulfilment of the requirements of the degree of Doctor of Philosophy in Mathematical Biology and Biophysical Chemistry

Department of Chemistry and MOAC Doctoral Training Centre,

University of Warwick

June 2017

# Table of Contents

# List of Figures

# List of Schemes

# List of Tables

# Frequently Used Abbreviations

| | |
|---|---|
| AMR | Antimicrobial Resistance |
| ASR | Acid Stress Response |
| CAMHB | Cation-Adjusted Müller-Hinton Broth |
| CAMP | Cationic Antimicrobial Peptide |
| DNA | Deoxyribonucleic Acid |
| EHEC/UPEC | Enterohaemorrhagic/Uropathogenic *Escherichia coli* |
| ESKAPE | *Enterococcus faecium*, *Staphylococcus aureus*, *Klebsiella pneumoniae*, *Acinetobacter baumannii*, *Pseudomonas aeruginosa* and *Enterobacter* spp. |
| $IC_{50}$ | Half-maximal inhibitory concentration |
| LPS | Lipopolysaccharide |
| MBC | Minimum Bactericidal Concentration |
| MIC | Minimum Inhibitory Concentration |
| MOA | Mode of Action |
| MRSA | Methicillin-resistant *Staphylococcus aureus* |
| NMR | Nuclear Magnetic Resonance |
| $OD_{600}$ | Optical Density at wavelength 600 nm |
| PBS | Phosphate-Buffered Saline |
| RM | Resistant Mutant |
| RNA | Ribonucleic Acid |
| SAR | Structure-Activity Relationship |
| SNP | Single Nucleotide Polymorphism |
| WGS | Whole Genome Sequencing |
| WT | Wild Type (*n.*) or Wild-Type (*adj.*) |
| XRD | X-Ray Diffraction |

# Acknowledgements

First and foremost I would like to offer my utmost thanks and appreciation to my principal supervisor, Prof. Peter Scott, for the opportunity to work on this project, as well as all the guidance, support and knowledge over the last four years (golf and cycling notwithstanding). Many thanks too to all members of the Scott group of the last four years for keeping the laboratory running smoothly, and making it a far more bearable workplace. My thanks to: Connah, Paul, Hualong, Shaun, Tom, and more MChems than I can possibly remember, although special mention does go to Pratik, Andy and Kate whose projects were important influences on my own. I would also like to extend my gratitude to the now graduated members who taught me the basics: Drs Suzanne Howson, Nikola Chmel, Chris Kay, Alan Faulkner, and Becky Kaner.

For their immense support and assistance on the biological aspects of this project, I must offer my sincere thanks to my supervisor in Life Sciences, Prof. David Roper, and primary collaborator, Dr Nicholas Waterfield. Both, along with their groups, were not only critical in providing much needed expertise and resources, but were extremely welcoming and patient towards this chemist trying very hard to become an accomplished microbiologist.

I would like to thank all those at Warwick who assisted with specific aspects of my project. In acquiring funding for my work *via* the EPSRC and encouraging my personal development, I would like to thank the MOAC doctoral training centre, especially the academic/administrative staff, and fellow members of the 2012 cohort. For their advice and guidance, I am grateful to my advisory panel: Drs Christophe Corre, David Fox, and Nikola Chmel. Within the Department of Chemistry I would like to thank: Dr Guy Clarkson for gleefully handling the crystallography (in spite of

many dubious ‘crystals’); Ivan Prokes and Rob Perry (NMR); Lijiang Song and Phil Aston (Mass spec.); Prof. Alison Rodger for use of her group’s spectroscopic equipment; Science City for use of TGA equipment and the necessary training. At the School of Life Sciences I am grateful to Daniel McFeely for teaching me the basics of microbiology and screening, the Dowson and Roper groups for the provision of strains and equipment, and the media prep staff for the probable gallons of media they were willing to prepare at short notice - Cerith Harries in particular for also helping me practice my Welsh.

Additionally my sincere thanks to the Microbiology and Infection Division, namely members of lab M116 for briefly accepting me as one of their own, and Drs Gemma Kay and Alexia Hapeshi in particular for being excellent collaborators and advisors. Thanks also to Dr Chrystala Constantinidou for providing pathogenic *E. coli* strains, Pavelas Sazinas and Emily Stokes for their support with RNA-seq, and both the bioinformatics team and the Waterfield group for working through the *omics* analyses.

Finally, I have to personally thank those close to me. I would never have got this far in life without the steadfast support of my family, particularly my parents: Mark and Tina, to whom I am extremely grateful. I would also like to thank my old teachers, Dafydd Jenkins and Jonathan Thomas, for encouraging my early interest in mathematics and science. Above all I must thank Lucy, who has helped me through the highs and lows of the last few years; I hope she understands how grateful I am. I am also indebted to her family for their tremendous support.

# Declaration

This thesis is submitted to the University of Warwick in support of an application for the degree of Doctor of Philosophy. The work performed in this thesis was carried out in the Department of Chemistry, School of Life Sciences, and Medical School of the University of Warwick between October 2013 and June 2017. Unless stated otherwise, it is the work of the author and has not been submitted in whole or in part for any previous degree at this or any other university.

# Publications Arising From This Work

## Chapter 1

D. H. Simpson & P. Scott, Chapter 7: *Antimicrobial Metallodrugs*, in: *Inorganic and Organometallic Transition Metal Complexes with Biological Molecules and Living Cells*, ed. K. K. W. Lo, Elsevier Academic Press Inc., 2017.

# Summary

**Chapter 1** outlines the potential of coordination and organometallic complexes in antimicrobial chemotherapy. Various historical examples are reviewed and their advantages and disadvantages discussed. Recent developments are then described, which have allowed the design of complexes with well-defined 3-dimensional structures, but in which the metal acts as a structural template rather than a reaction centre. Finally, consideration is given to the prospects for such compounds making a substantial contribution to the currently rather uncertain future of antimicrobial chemotherapy.

**Chapter 2** describes the discovery, synthesis and characterisation of new Class Ia (*exo*-pyridine) flexicates with varying ligand functionality, as well as some of the underlying challenges. The helicating effect of the linker connecting these bimetallic structures is subsequently explored, by investigating their structure, physical properties and aqueous stability.

**Chapter 3** focuses on the screening of water-soluble Class Ia flexicates for antimicrobial activity against various bacteria, allowing the establishment of lead compounds against Gram-negative bacteria. Various assays are then used in order to make further preclinical evaluations of the lead compounds and/or better understand the nature of the observed antimicrobial activity. For example, eukaryote toxicity and effect upon membrane integrity are assessed.

**Chapter 4** explores the use of tandem *omics* techniques (genomics, transcriptomics and proteomics) as means to develop credible hypotheses regarding the mechanism behind the potent activity of the lead compound against a pathogenic *E. coli* strain. The initial study describes the selection and characterisation of *E. coli* mutants

tolerant the lead compound. Responses of the cell at the RNA and protein level respectively are then measured in response to the addition of the lead compound, at a sub-lethal dose.

**Chapter 5** Infers general conclusions from across this thesis and conveys suggestions for future work that may further expand this field.

**Chapter 6** details the experimental procedures used to carry out the work in this thesis.

**Appendix** contains tables of crystallographic data

# Ligands Used in this Thesis

$L^a$

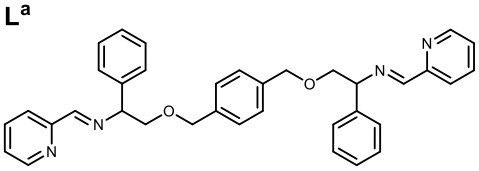

$L^b$

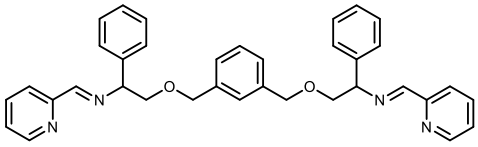

$L^c$

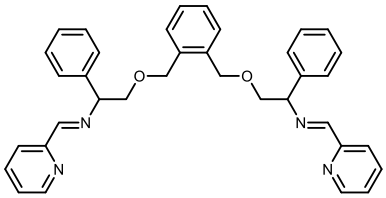

$L^d$

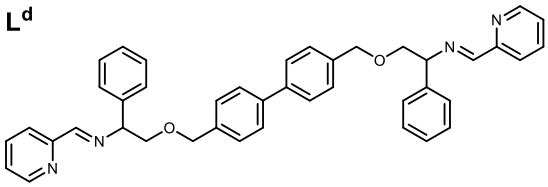

$L^e$

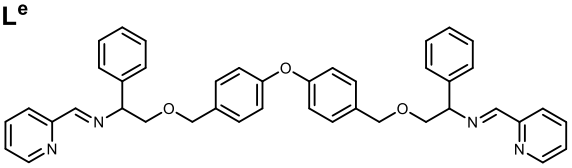

$L^f$

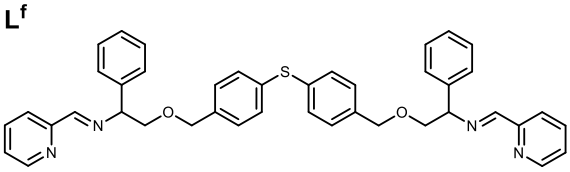

$L^g$

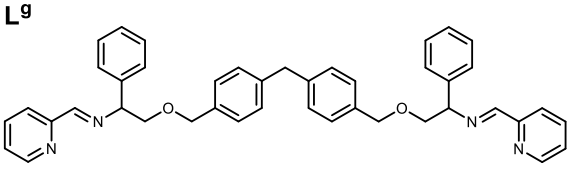

**L$^{h}$**

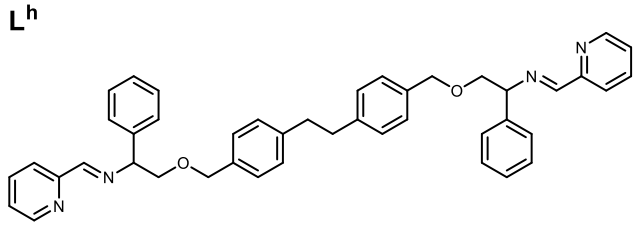

**L$^{i}$**

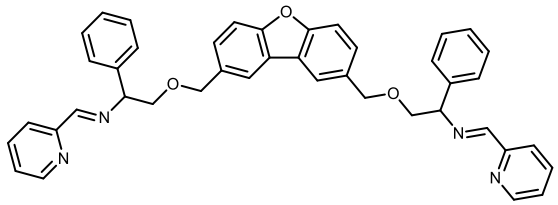

# Chapter 1

# Antimicrobial Metallodrugs

## 1.1 Introduction

The development of antibiotics in the early 20th century revolutionised the field of medicine, preventing countless deaths from diseases caused by microbial pathogens. In the early 21st century, issues such as immunodeficiency – increasingly common in the age of HIV/AIDS and for patients undergoing cancer chemotherapy – have boosted the demand for agents to combat opportunistic infections.[1, 2] Our ability to respond to such challenges is however threatened by the rise of antimicrobial resistance (AMR), creating an extensive problem for the medical establishment,[3-7] with infection by drug-resistant pathogens now a prominent and growing cause of global mortality.[8]

### 1.1.1 Antimicrobial resistance and the case for metallo-antimicrobials

Whilst the genetic changes required for bacterial resistance are substantial, rapid cell division at human body temperature (~20 min for *Escherichia coli*) and the vast number of bacteria involved in infections means that these changes occur often. DNA replication produces on average 1 error in every $10^7$ bases[9, 10] and in a typical bacterial genome of ~$3 \times 10^6$ base pairs , this is equivalent to approximately 0.3 errors per generation.[10] Although only a few resistant mutations are produced, those mutants survive and flourish where other drug-susceptible bacteria die. This rapid adaptation ensures that antibiotic-resistant strains often appear soon after clinical use of a drug,[10-12] Methicillin-resistant *Staphylococcus aureus* (MRSA), multidrug-

resistant *Mycobacterium tuberculosis* (MDR-TB) and fluoroquinolone-resistant *Pseudomonas aeruginosa* (FQRPA) are much-publicised examples.[8, 13, 14]

While some of the mechanisms by which microbes resist drug action are more generalised, many depend on specific molecular recognition of the active antimicrobial[15-19] (Figure 1.1). For example, drug-deactivating enzymes produced by microbes (*e.g.* β-lactamases) commonly provide resistance to natural product or closely related, 'semi-synthetic' agents which contain structures and chemical motifs familiar to biology.[20] In contrast, such enzymes are not evolved and have not been found for 'purely synthetic' antimicrobials, leading to the argument that the ideal compound might be produced by rational design rather than by the modification of a natural product[21, 22] or indeed by exploratory phenotypic screening (*vide infra*).

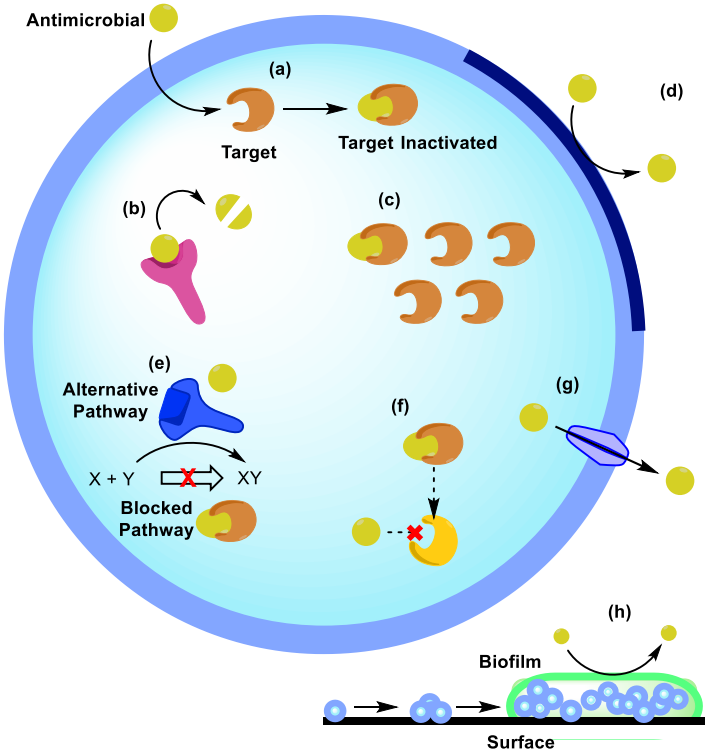


**Figure 1.1: Routes of antimicrobial resistance [AMR]:** (a) demonstrates a simple antimicrobial mode of action; (b) enzymatic inactivation of the antimicrobial; (c) target overproduction; (d) changes to cellular permeability; (e) a pathway blocked by the drug is circumvented by the creation or use of an alternative pathway; (f) target modification/mutation; (g) efflux pumping; (h) a surface-bound bacterium forms an impermeable biofilm.

Transition metal complexes, representing in many cases completely anthropogenic chemistry, thus emerge as an alternative source of chemotherapeutic antimicrobial agents.[23, 24] They offer structural diversity not available to organic chemistry alone, alongside a range of ligand exchange kinetics, redox activities, and tunable electrostatic topologies.[25] However, synthetic transitional metal complexes, *e.g.* simple *tris*-chelate complexes used by Dwyer (*vide infra*), have traditionally offered these features at the cost of a lack of functional complexity in comparison to biomolecules and synthetic organic compounds. Also, while the unique properties of metal complexes create new opportunities for interactions with biological machinery, possibly leading to new modes-of-action, they also present new questions in respect of biological compatibility and transport. Such considerations will be crucial design of synthetic metallodrugs, and are briefly addressed here.

### 1.1.2. Metallodrugs and the bacterial cell envelope

Before a complex may access an endocellular target it is required to somehow cross the bacterial cell envelope, which provides defense against chemical and physical stresses from the environment. This barrier may prove to be a considerable challenge to synthetic chemotherapeutics.[26] This brief account of the issues facing metallodrugs in respect of cellular entry follows the prevailing assumption that passive diffusion is the principal route of ingress, although there is a highly credible argument for a carrier-mediated view of drug uptake *i.e.* that drugs predominantly enter cells *via* promiscuous proteinaceous carriers.[27-29]

Pathogenic bacteria are commonly classified as Gram-positive or -negative according to the response of the outer surface of the cell to the Gram test, developed

in 1884.[30] Gram-positive bacteria such as *Staphylococcus*, *Streptococcus* and *Bacillus* stain purple on exposure to crystal violet (hexamethyl pararosaniline chloride).[31] They have a substantial layer of peptidoglycan (murein); a 3D lattice structure formed from a sugar polymer, crosslinked *via* oligopeptide side-chains (Figure 1.2). The exterior is decorated with teichoic acids – polymers of *e.g.* glycerol phosphate and carbohydrates – whose function is to bind metal cations, providing rigidity. Biosynthesis of peptidoglycan is unique to bacteria, and this process is thus an important antibacterial target (*e.g.* by the β-lactams).[32] Gram-negative bacteria such as *Escherichia*, *Yersinia* and *Pseudomonas* are enveloped by both inner and outer membranes separated by a periplasm containing relatively little peptidoglycan;[31] they stain pink with the application of Gram staining assays. The outer membrane consists of phospholipids and lipopolysaccharides (LPSs), which are found on the cell surface, directed outward. LPSs are a unique feature to these bacteria, their amphiphillic, negatively charged nature allows them to confer a negatively charged layer to the outer cell membrane,[33] which is stabilised using divalent cations. The double plasma membrane studded with LPSs in Gram-negative species makes them a problematic target for many drug molecules. Before a complex may access an endocellular target it is required to somehow cross the bacterial cell envelope, which provides defense against chemical and physical stresses from the environment. This barrier may prove to be a considerable challenge to synthetic chemotherapeutics.[26]

The lipophilicity of a complex is taken as a good measure of its ability to pass into the cell by diffusion, and in some cases increased lipophilicity correlates with antimicrobial potency (*vide infra*). The standard method of evaluating the lipophilicity of a molecule is by measuring the partition between octanol and water

*i.e.* log(P), for example by using the "shake-flask" method.[34] This criterion is part of "*Lipinski's rule of five*" (see below). Ideal lipophilicity for antimicrobial activity lies within a target, organism-dependent range, high enough to be able to cross the cell membrane, but low enough to be sufficiently soluble in an aqueous medium (*i.e.* amphiphilic).[35] Advantageously for coordination complexes, the combination of metals centres that are usually charged (hydrophilic) and lipophilic organic ligands may give rise to systems of amphipathic topography. This would imply their hydrophobicity could be optimised in this respect. Relating changes in structure, geometry and physical properties of a complex to their influence upon biological activity may lead to the development of structure-activity relationships or quantitative structure-activity relationships (SARs/QSARs); a common exercise in drug design and development.[36]

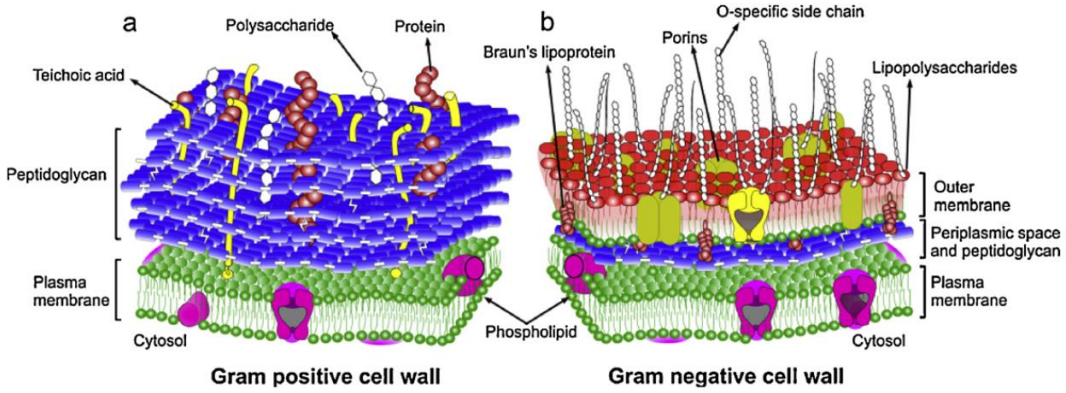


**Figure 1.2: The bacterial cell wall:** (a) The Gram-positive envelope. (b) The Gram-negative envelope. In Gram-positive bacteria, the lipidic plasma membrane with embedded proteins is covered by a multilayered peptidoglycan shell decorated with polysaccharides, teichoic acids and proteins. In Gram-negative bacteria, a thin peptidoglycan layer surrounds the plasma membrane and is covered by an asymmetrical outer membrane containing lipopolysaccharides, which lies on the peptidoglycan layer. Reprinted from *Micron*, Vol 48 (12), Tripathi P., Beaussart A., Andre G., Rolain T., Lebeer S., Vanderleyden J., Hols P., and Dufrêne Y. F., Towards a nanoscale view of lactic acid bacteria, p. 1323–1330, Copyright 2012, with permission from Elsevier.[37]

In more extreme instances of amphiphilicity, metal complexes may, like detergents, be able to destroy the integrity of the lipid bilayer of the cell wall and thus

compromise the bacterium.[38] This is not thought of as a viable antibacterial route however, as any untargeted mechanism generally compromising the cell wall is likely to also severely damage eukaryotic cell membranes, leading to low selectivity and unacceptable toxicity towards humans. The high positive charge on some metal complexes may naturally lead to surfactancy in this context, and this mechanism needs to be excluded *via* standard tests such as red blood cell lysis assays.[39]

### 1.1.3 Lipinski's rule of five and other criteria

It is common practice to assess the orally active "drug-likeness" of a molecule according to *Lipinski's rule of five*: this places a limit on the acceptable number of hydrogen bond donors and acceptors (5 and 10 respectively), a molecular weight <500 Daltons and a log(P) value (water-octanol partition coefficient) no greater than 5, with others later refining this to a -0.4 to +5.6 range from observations using large drug databases.[40] Suitable candidates will break at most one criterion.

These guidelines were developed from observation of the properties of successful drug molecules of the time, and so are naturally biased towards small compounds of natural or synthetic-organic origin. While these particular guidelines may therefore not be appropriate for application to metal complex design, the underlying physico-chemical issues remain. It thus makes sense for metallo-organic chemists to consider overarching criteria for properties of their chosen region of chemical space at the start of discovery programs. It is quite a challenge for example to synthesise complexes that combine water solubility and stability, stereochemical purity and ready availability. Without these properties however the molecule is most unlikely to progress out of the chemistry lab and into the clinic, regardless of *in vitro* activity.

### 1.1.4 Molecular targets in the cell

Coordination and organometallic chemistry are not yet *generally* equipped to address specific biomolecular targets *i.e.* to make a compound for a specific receptor as in the target-oriented approach to drug discovery, although elegant approaches are emerging.[41, 42] There are nevertheless great opportunities to take part in the resurgence of phenotypic drug discovery.[43-45] where the biological targets of a drug (see examples below) are established after the observation of the useful biological effect. Indeed, it has been asserted that this approach has led to a disproportionately high number of first-in-class drugs with novel mechanisms of action (1999-2008).[46, 47]

DNA is fundamentally important to the machinery governing cells and their proliferation. It is involved directly or indirectly in all cellular functions, through the coding of proteins *via* genes, making DNA a key antimicrobial target, particular for reactive-at-metal metallodrugs.[48] The major 'canonical' form observed biologically, B-DNA has a wide, shallow major groove and a relatively deep and narrow minor groove. This anionic structure lends itself to various interactions with coordination complexes,[49, 50] *e.g.* by dative or covalent bonds, shape selectivity or *via* the stacked bases[51] (shown in Figure 1.3). Such binding or reactions may alter its shape, reactivity, chemistry, and ultimately the function of DNA.

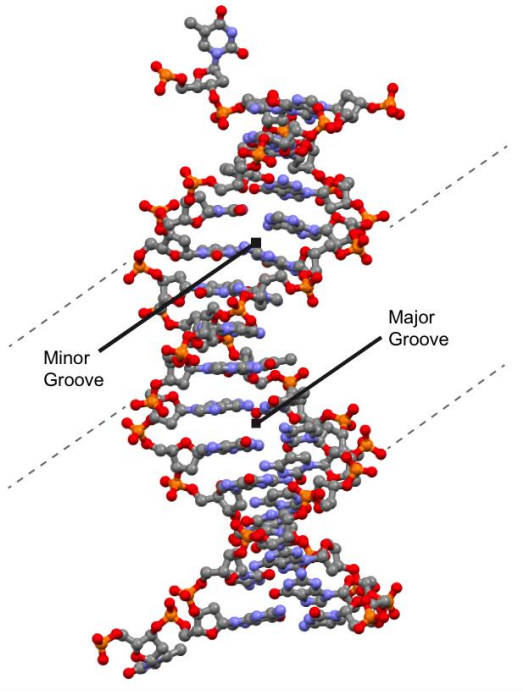


**Figure 1.3: A short B-DNA sequence.** Based on coordinates obtained from the Nucleic Acid Database project (NDB), based at Rutgers University (NDB ID: NA2970 PDB ID: 4Q10).[52]

Within the bacterium, the chromosomal DNA exists as a supercoiled; non-organelle bound structure: the nucleoid. Maintenance of the topological integrity of this chromosomal DNA is enacted by two enzymes classes; topoisomerases and DNA gyrases, both of which control the extent of the supercoiling,[53] making these enzymes useful antimicrobial targets in their own right.

Composed almost entirely of RNA, the complex machinery of the bacterial ribosome tackles the task of translating the encoded information of DNA into proteins that catalyse the cellular processes of the cell.[54] This important function makes RNA a potential target, in particular the ribosome complex. RNA rarely takes the B-form observed in DNA[55] (Figure 1.3), though it may be considered chemically similar and can produce analogous structures at a local level. In rapidly growing bacterial cells, most of the ribosomes appear in the aggregated form of polysomes, where several

ribosomes carry out translation on a single RNA transcript (messenger RNA) of a particular gene.[56]

The demand for structural and chemical diversity required for the biocatalysis supporting life falls overwhelmingly to the polypeptides. Protein complexity is built in at the primary structural level from the large pool of chemically diverse common amino acids monomers available (>20), increased through the secondary structures available (α-helices, β-sheets), and increased again at the tertiary and quaternary structure levels (macrostructure, co-factor inclusion).[57] Targeting these diverse species poses quite a challenge to drug designers, and no antimicrobial metallodrugs have been developed to our knowledge with this specific purpose, although protein inhibiting metallodrugs have been developed as anticancer agents;[25] notably Meggers and co-workers' staurosporine-mimetic, Ru(II) protein kinase inhibitors.[58]

### 1.1.5 Preliminary screening for antimicrobial activity

Most of the studies reported in this chapter include some kind of antimicrobial screening as part of the early discovery process. The essentials are summarised here, with an excellent summary of more detailed advice available.[39]

The measurement of the ability of a candidate to inhibit the growth of a bacterium – the minimum inhibitory concentration (MIC) usually reported in μg/ml – may be carried out using standardised protocols.[59] This allows rapid comparability to existing antimicrobials. MIC values may also be contrasted with the toxicity of a compound to eukaryote as a rough measure of its selectivity (for prokaryotes), using another rapid *in vitro* method to measure half-maximal inhibitory concentration ($IC_{50}$

usually in μM or nM) against eukaryote cells. Further, the minimum bactericidal concentration (MBC in μg/ml) – the lowest concentration of an antibacterial agent required to kill rather than merely inhibit growth of a particular bacterium – can be determined readily.[59] A wide range of other studies are available, and these are mentioned in the relevant section below.

Against the background outlined at the start of this section of the need for drugs that may suffer less from the acquisition of resistance, and of considering the practical barriers which must be overcome, we explore here the recruitment of transition metal coordination chemistry for the development of new classes of antimicrobial chemotherapeutics. Alongside naturally occurring metallodrugs, increasingly sophisticated antimicrobial complexes are now being developed and tested. These metallodrugs broadly fall into two categories: (i) those using a labile or reactive metal centre as an implicit part of their mode-of-action - particularly those natural products that are 'activated' by metal coordination, and; (ii) those using metal ions as a template. The latter area is of increasing interest as we gain better control over complex stoichiometry and stereochemistry.[25]

## 1.2 Redox-active Metal Complexes

The intrinsic antimicrobial (antibacterial) activity of certain group 11 metal ions or solubilised atoms is well known.[60] Copper and, particularly, silver vessels would be used by early civilizations to store water because of an understanding that this would help disinfect it.[61] Since then Cu, Ag and other transition metal ions have been shown in water to be bactericidal, primarily *via* in-cell redox activity (notably cycles

of Fenton/Haber-Wiess reactions[60]) and/or sporadic interference with native metal cofactors as per the Irving-Williams series[62] even at low concentration.[63, 64] However, aqua or other simple complexes would not be suitable for use in antimicrobial chemotherapy because of their generally low solubility in water, poor stability and resultant potential for toxicity in humans.[65]

In this context we note that some complexes that are unsuitable as drugs find commercial use as topical antimicrobial agents. The antifungal/antibacterial zinc pyrithione[66] (pyrithione = *N*-hydroxypyridine-2-thione) present in many shampoos is used to treat forms of dermatitis and dandruff. While Zn(II) is not a redox active metal, it was determined that the complex acts by increasing cellular *copper* levels, leading to loss of activity of iron-sulfur cluster-containing proteins. It is this proposed that pyrithione acts as a copper ionophore, enabling copper to enter cells and distribute across intracellular membranes.[67] The topical antibacterial natural product bacitracin – a cyclic peptide – is active as a complex of a range of divalent metal ions[68] and is used in *e.g.* Zn and Ag preparations.

Research on complexes which are designed to release antimicrobial metals into solution by triggers such as local redox activity has appeared. Screening of copper complexes by Wolschendorf and co-workers led to the discovery of antibacterial complexes that are implied to release copper ions.[69, 70] Fromm and co-workers developed silver coordination species, some of which comprise polynuclear frameworks, with antimicrobial properties.[71] Useful approaches for work in this area would be to promote selective ingress into prokaryote cells or to create systems for organism-specific release. Such hypothetical ‘stealth’ complexes could be similar in

nature to complexes where the metal centre acts as a structural template *e.g.* helicates or siderephore complexes and their analogues (*vide infra*).

### 1.2.1 Bleomycin

Bleomycin (Figure 1.4), also known as blenoxane and occasionally abbreviated BLM, was discovered in 1966 as a Cu(II)-chelating antibiotic derived from a culture of the strain *Streptomyces verticullus*,[72] although the complexes Fe and Co are the most studied.[73-75] Although bleomycin and its derivatives are noted anti-cancer and antiviral agents,[76, 77] they have also shown promising prokaryote (*Bacillus subtilis*) toxicity.[78] The iron complex is considered to be the *in vivo* active species due to the relative abundance of iron in living organisms relative to other transition metals. In the Fe(II)-chelate form and in the presence of dioxygen ($O_2$) and a reducing agent, bleomycin actively cleaves DNA in a directed manner.[75] It is a key example of a compound where the organic component provides an element of targeting but the principal payload is the metal ion.

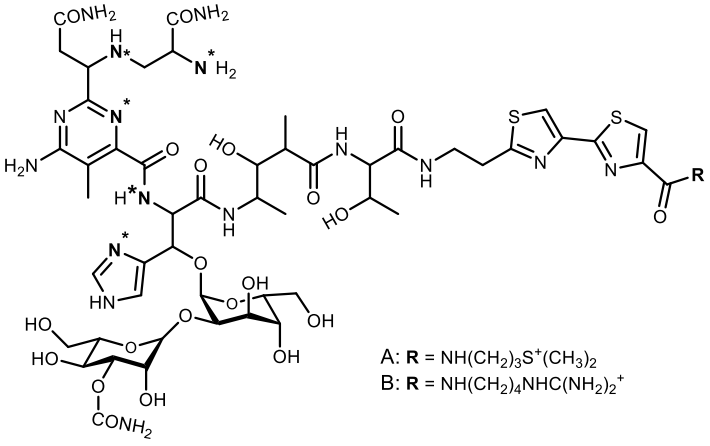


**Figure 1.4: Structure of 'free' bleomycin (A and B variants).** The metal binding sites, proposed through spectroscopic studies, are marked *.[79]

The nature of the coordination geometry of the complex formed by chelation of a metal ion by bleomycin has been thoroughly studied. Electron spin-echo envelope spectroscopy of complexes allowed, through detection of hyperfine splitting of $^{14}N$, identification of the heteroatoms involved in binding[79] as well as the presence of a distorted five or six coordinate coordination sphere (the sixth being a possible site for a monodentate ligand). Determination of the structure of a Cu(II) complex of a bleomycin intermediate, lacking the sugar and peptidyl bithiazole moieties, but inclusive of all metal binding sites has appeared.[80] Nuclear magnetic resonance (NMR) studies, using diamagnetic Zn(II) species on bleomycin itself as well as the structurally similar tallysomycin as chelators has been used to probe the coordination of bleomycin.[81, 82]

The proposed antimicrobial mechanism of action involves the formation of an 'active form' where the BLM-Fe(II) reacts (most likely *via* a superoxide intermediate) to form a peroxy species BLM-Fe(III)-OOH with the peroxy species occupying the sixth coordination site of the distorted octahedron, as observed by Raman spectroscopy.[83] O-O bond cleavage results in the generation of O=Fe(IV)-BLM or O=Fe(V)-BLM which oxides ribose moieties in DNA, in regions immediately preceding a 5'-GC-3' or 5'-GT-3' sequence, causing the ribose moiety and thus the DNA structure to break down.[75, 84, 85]

Despite the good early candidacy of such bleomycin complexes, they have largely been ruled out as a prospect for a clinical antimicrobial role. Issues include the lack of specificity for prokaryote DNA, the severity/irreversibility of DNA double strand scission, and evidence for human toxicity (causing lung fibrosis).[86]

### 1.2.2 Streptonigrin and the anthracyclines

Streptonigrin (SN) is a quinone-based antibiotic,[87] which as a whole undergoes a dramatic structural change upon metal binding [(Figure 1.5(a)], towards an active form.[88] The anthracyclines (ACs - notably daunomycin and adriamycin) are constructed of four fused rings linked to a pyran derivative [Figure 1.5(b)], which may be a pyranose sugar, or group of sugars, in more complex examples.[89] Although their core structures vary, these compounds share notable key features; (i) both were originally isolated from the *Streptomyces* genus (although synthetic derivatives are known);[90-92] (ii) they contain moieties that allow specific binding/intercalation of DNA (their primary target, although ACs may also bind DNA topoisomerase enzymes);[93, 94] and (iii) whilst both are quinone-based antibiotics in their own right (as unbound species), they require binding of a redox-active metal in order to be fully active. For the latter, evidence suggests that the increase in activity is caused by improving DNA binding by modification of geometry and electrostatic topography, and the availability of localised catalysis of radical species formation.[95, 96] It is suggested that anthracyclines may be bound to one, or two metal ions simultaneously, using their opposing β-ketophenolate moieties.[97]

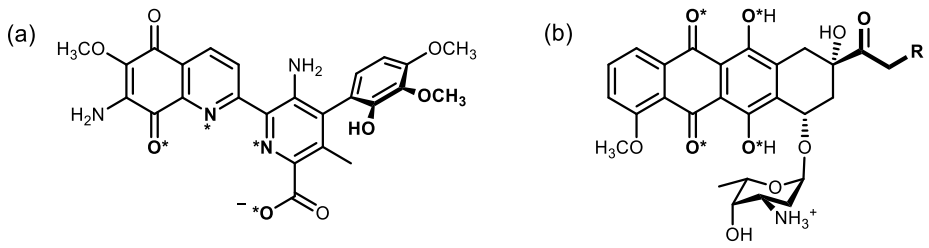


**Figure 1.5: Structures of quinone-based antibiotics:** (a) streptonigin and (b) the simple anthracyclines daunomycin (R = H) and adriamycin (R = OH). Proposed metal binding sites are marked *.

The antimicrobial effects of SN towards *E. coli* and *B. subtilis*, were described in the 1960-70s.[98, 99] The mechanism has been linked to its generation of $O_2^-$ and/or peroxides, a feature closely associated with the presence of iron and copper, leading

to the inhibition of DNA synthesis.[100] Similarly, metal-AC complexes [notably 1:1 complexes with Fe(III)] are implicated in the induction of DNA cleavage *via* increased generation of radicals,[101, 102] especially in the presence of reducing agents such as NADH. Reportedly this activity occurs through (metal-assisted) reduction to semiquinone forms, as with other quinone-based drugs;[103] a process found to be inhibited by the enzymes catalase[104] and superoxide dismutase[105] as would be expected for a mechanism dependent upon reactive superoxides and peroxides. Intercalation of the free anthracycline in DNA, combined with limited redox activity of the organic nucleus, accounts for the mild antibacterial effect of metal-free species, particularly against *B. subtilis* strains lacking DNA-repair mechanisms.[106]

Some antifungal activity (daunomycin) has also been noted.[107]

## 1.3 Complexes with Reactive Metal Centres

Numerous attempts have been made to screen reactive-at-metal species for antimicrobial activity, with varying results. Prominent historic examples have been reviewed in detail, notably by Ming.[108]

Although cisplatin [*cis*-diamminedichloridoplatinum(II)] is renowned for its anticancer activity, and been thoroughly reviewed accordingly alongside other platinum compounds,[109-111] it was discovered serendipitously as a drug candidate by Barnett Rosenberg in the 1960s *via* its ability to inhibit cell division in *E. coli*.[112] Other than its completely synthetic origin, it is differentiated from the earlier antimicrobial species discussed in this section in that the metal does not contribute to

the mechanism of action *via* redox activity, but as a reaction centre in the formation of strong crosslinking bonds with the target biomolecule DNA *in vivo*.[50]

Focus for synthetic reactive-at-metal antimicrobials has been with the aim of controlling and modulating reactivity in order to reduce the side effects seen in chemotherapeutic use. Attempts have subsequently been made to 'tame' cisplatin-like heavy transition metal complexes using strongly bound *N*-heterocyclic carbene (NHC) ancillary ligands.[113] While *bis* complexes such as that of Figure 1.6(a) have modest activity,[114] Panda, Ghosh and co-workers[115] reported a slightly more potent complex of gold chloride [Figure 1.6(b)] in Gram-positive *B. subtilis*, although this and similar examples tested were inactive against Gram-negative *E. coli*. Gurovic, Silbestri and co-workers[116] synthesised much more soluble gold and silver complexes *e.g.* Figure 1.6(c), but the MIC values reported were extremely high. In contrast, bimetallic compounds *e.g.* Figure 1.6(d) were screened by Mandal and co-workers for their antimicrobial activities against multiple keratitis-associated human eye pathogens, revealing some impressive MIC figures and the ability to eradicate biofilm on contact lenses.[117] An alternative strategy for controlled reactivity is the use of metal centres with 'intermediate' reactivity, for example Co(III) complexes with non-innocent (redox) ligands.[118]

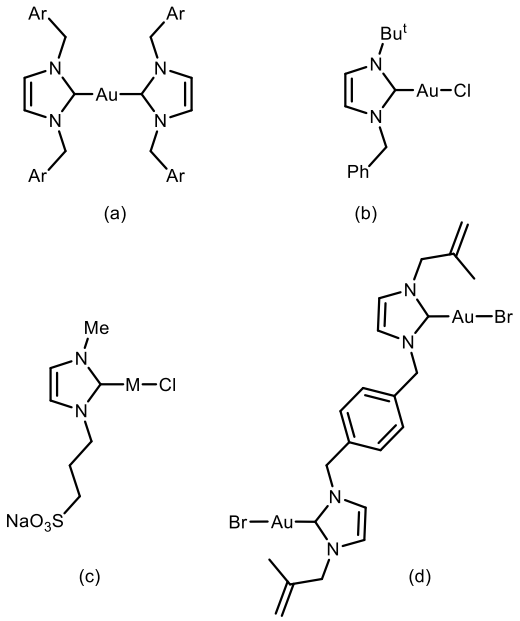


**Figure 1.6: *N*-heterocyclic carbene complexes used in antimicrobial screening.**

## 1.4 Complexes Which Release Carbon Monoxide

The ability of coordination complexes to act as small molecule carriers, particularly CO-releasing molecules (CORMs), has been explored as a source of chemotherapeutic agents - including antimicrobials.[119]

The efforts initially of Saraiva[120] and later Poole in particular[121] have driven the antimicrobial research of CORMs, and in spite of the analytical challenge involved demonstrating CO release under biological conditions.[122] Modest antimicrobial effects of prototypic examples have been described[120] which were markedly improved in comparison with the use of carbon monoxide alone. This perhaps suggests selective release, or a synergistic effect of the remaining complex.[121] Interestingly, these complexes would appear to affect 'non-traditional' targets (*e.g.* cellular respiration).[123] Figure 1.7 shows two notable CORMs; Ru(II)-based

'CORM-3', noted for its water solubility owing to the use of glycinate and chloride ligands, and a Mn(I)-based 'photoCORM', capable of releasing CO upon irradiation with near-ultraviolet light, with an initially uncoordinated pyridyl group capping the now free octahedral site.[121]

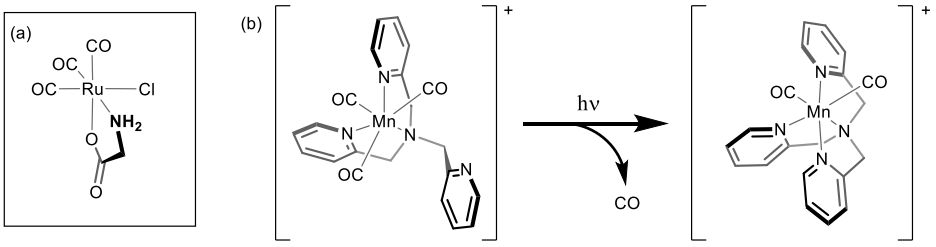


**Figure 1.7: Notable CORM-type complexes studied as potential antimicrobial *metallodrugs*:** (a) CORM-3 [tricarbonylchloro(glycinato)ruthenium(II)] and (b) the '*photoCORM*' $[Mn(CO)_3(tpa\text{-}\kappa^3N)]^+$,[124] showing the action of CO release with UV-irradiation.

The use of electromagnetic radiation to photoactivate an inert metallodrug precursor at the site of infection, has garnered some interest.[125, 126] However, the poor penetrability of shorter-wavelength light into the body[127] and the often-widespread nature of infection needs to be considered.

## 1.5 Metal Centres as Structural Templates

Rather than using metal centred redox activity or substitution chemistry to permanently damage DNA or other biomolecular target(s), more subtle inhibitory mechanisms are being addressed with complexes where the metal is intended to be purely structure-forming. Indeed, depending on the nature of the ligands, the control of stereochemistry becomes important, and this is an area where much development is needed.[25] Nevertheless, systems with promising antimicrobial activity along with supporting studies towards an understanding of underlying mechanism(s) have been reported.

### 1.5.1 Early advances: simple *tris*-complexes

A very early body of work, which nevertheless continues to inspire new research, was described by Dwyer and co-workers in the 1950-60s.[128, 129] These researchers tested simple complexes of transition metals with small, symmetric bidentate ligands, such as the examples shown in Figure 1.8. These complexes were found to have variable activity against strains of *Escherichia, Staphylococcus* and *Salmonella* respectively, with the placement of exosteric groups (*e.g.* methyl groups) proving an important influence on antibacterial activity observed.

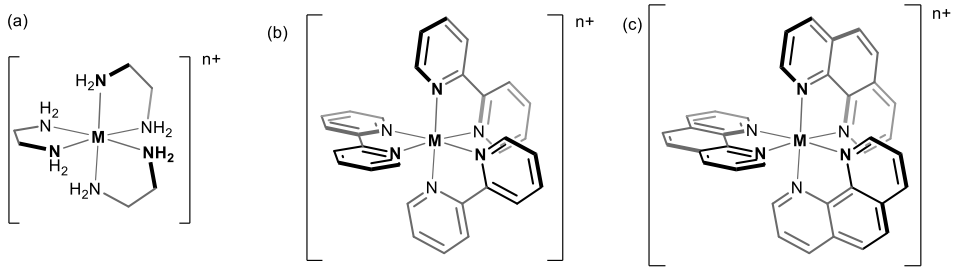


**Figure 1.8: Simple *tris*-chelate metal complexes** using: bidentate N-donor ligands (a) ethylenediamine, (b) 2,2′-bipyridine and (c) 1,10-phenanthroline. Complexes are shown as Δ-isomers although the study used both Δ and Λ enantiomers separately, or racemic mixtures. M = Co, Ru, Ni, Fe, Os. [128, 129]

### 1.5.2 DNA-intercalating ruthenium complexes

Many tris(bipyridine) and related complexes of Ru(II) are known – these are very inert and not expected to mediate any sort of metal-centred activity. Their ability to intercalate DNA is however well studied[49, 50] using *e.g.* NMR, linear dichroism (LD) and circular dichroism (CD).[130, 131] The complex Δ-$[Ru(bpy)_2(dppz)]^{2+}$ for example co-crystalises with B-DNA containing a base-pair mismatch as shown in Figure 1.9.[132]

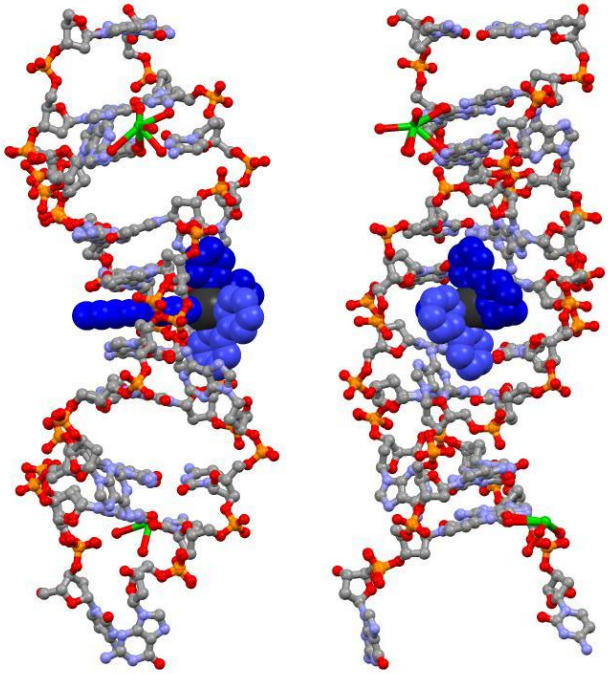

**Figure 1.9: B-DNA complex of Δ-[Ru(bby)$_2$(dppz)]$^{2+}$.** The complex is shown as a spacefill model in blue/grey. One dppz ligand intercalates two B-DNA base pairs. Structure is shown from two perspectives (90° rotation about the vertical axis). Only the double helix and a single complex are shown for clarity. Created from RCSB Protein Data Bank structure (PDB ID: 4E1U).[132]

While much of the motivation for use of these complexes is in the arena of cancer,[133-138] Aldrich-Wright and co-workers published in 2010 an account of the antimicrobial potential of three Ru(II)-based DNA intercalators (Figure 1.10).[139] Using standardised screening techniques[59] MICs were determined against four Gram-positive bacterial strains [*B. subtilis* 168, Methicillin-sensitive *S. aureus* (MSSA) 160 and MRSA strains 41 & 252]. The results appeared to follow earlier reported trends in ability to intercalate DNA; [Ru(phen)$_2$(dpq)]$^{2+}$ showed little or no potency, [Ru(bpy)$_2$(dpqC)]$^{2+}$ showed middling activity (MIC: 16-64 μg/ml) and [Ru(2,9-Me$_2$phen)$_2$(dppz)]$^{2+}$ displayed the highest potency with MICs ranging from 8 μg/ml for MSSA160 to a remarkable 2 μg/ml for MRSA252. MBCs (minimum bacteriocidal concentration) of two to four times the corresponding MICs support a bacteriocidal rather than an inhibitory (bacteriostatic) mode of action. In contrast, no

activity was found against Gram-negative *E. coli*, perhaps because of the low permeability of the cell envelope.

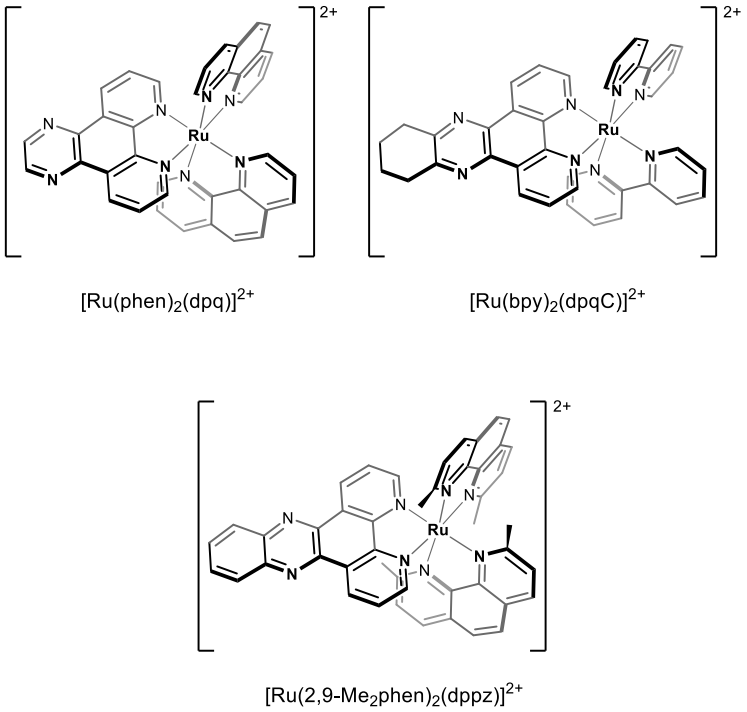


**Figure 1.10: DNA-intercalating complexes studied by Aldrich-Wright and co-workers:** dpq = dipyrido[3,2-d:2',3'-f]-quinoxaline), dpqC = dipyrido[3,2-a:2',3'-c]-(6,7,8,9-tetrahydro)-phenazine), dppz = dipyrido[3,2-a:2',3'-c]-phenazine. Complexes shown as Δ isomers.

In further work, a time-kill assay using $[Ru(2,9\text{-}Me_2phen)_2(dppz)]^{2+}$ was carried out. This established the rate with which live bacteria are killed *via* measurement of the population growth/decline from a set initial population. In the presence of 1 μg/ml (0.5 of the MIC) or less, MRSA252 continued to increase in population. At 8 μg/ml (the MBC) and 32 μg/ml population showed a sharp decline, suggesting a relatively rapid mode of action. Further, the nematode worm *Caenorhabditis elegans* (*C. elegans*), a multicellular eukaryote and noted infection model[140, 141], was infected by MRSA252, then subjected to various concentrations of $[Ru(2,9\text{-}Me_2phen)_2(dppz)]^{2+}$ *i.e.* an infection/recovery experiment. Over several days, the number of surviving worms was monitored (Figure 1.11). It was observed that a relatively low concentration of $[Ru(2,9\text{-}Me_2phen)_2(dppz)]^{2+}$ (1 μg/ml) showed little improvement

over the control, where all worms died by day six in both cases, though with a slightly slower rate with complex present. Concentrations of 8 and 32 μg/ml showed marked improvement over the control with ~80% nematode survival at day six.

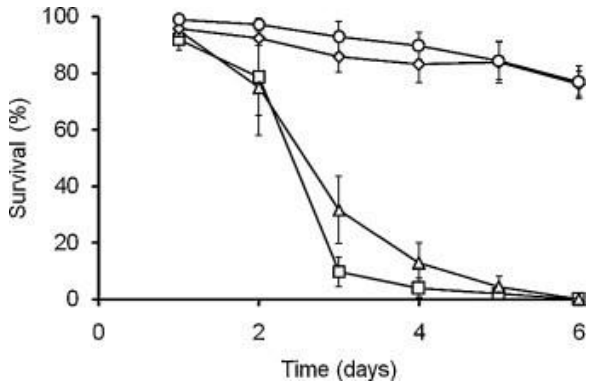


**Figure 1.11: Survival of age-synchronised *C. elegans* in the presence of $[Ru(Me_2phen)_2dppz]^{2+}$:** after an initial 1 h incubation with *S. aureus* MRSA252 the number of living worms was scored daily. Circles, 32 μg/ml; diamonds, 8 μg/ml; triangles, 1 μg/ml; squares, no compound added (control). Reprinted from the European Journal of Pharmaceutical Sciences, Vol 42 (4), Bolhuis A., Hand L., Marshall J. E., Richards A. D., Rodger A. and Aldrich-Wright J., *Antimicrobial activity of ruthenium-based intercalators*, p. 313–317, Copyright 2011, with permission from Elsevier.[139]

Overall these experiments create one of the more advanced cases for potential use of inert metal complexes as antimicrobials; relatively low MIC, a rapid mode of action relative to infection spread, direct evidence for recovery from otherwise fatal infection in a higher eukaryote, and a credible mechanistic hypothesis. Significant questions remain however, such as selectivity of the compounds here or in higher organisms, and the issue of enantiomeric separation.[131, 142-147]

### 1.5.3 Oligonuclear ruthenium complexes

O'Reilly *et al.* found that "dimers" of $[Ru(phen)_2(Me_2bpy)]^{2+}$ units linked *via* an alkyl chains (Figure 1.12, n = 5, 7, 10) are excellent and robust DNA-groove binders, and more efficient than the mononuclear analogues. The binding strength was found to increase with the linker chain length as this allows it to 'follow' the helical DNA

structure.[148-150] Aldrich-Wright and co-workers also demonstrated enhanced binding, compared with its mononuclear analogue, of a dinuclear Ru(II) complex incorporating a 2-mercaptoethyl ether linker.[151] Similarly, Lincoln and Thomas demonstrated extremely high binding affinity of Ru(II) dinuclear complexes at DNA sites.[152-155] Keene and Collins have presented an extensive body of work in this area, including discovery of antimicrobials and study of mechanism(s) of action.[156]

The $[(Ru(phen)_2)_2(\mu\text{-}bb_n)]^{4+}$ (abbreviated to $Rubb_n$) systems in separated stereoisomeric forms (Δ,Δ or Λ,Λ, excluding the *meso* isomer)[157] were studied alongside various controls.[158] $Rubb_{12\text{-}16}$ complexes were found to be active against a range of pathogenic bacteria, particularly Gram-positive *S. aureus*, both methicillin-susceptible (ATCC 25923) and 'clinical wild type' MRSA (MICs of 1-2 μg/ml). Activities against Gram-negative *E. coli* ATCC 25922 (2-4 μg/ml) and ATCC 27853 *P. aeruginosa* ATCC 27853 (8-16 μg/ml) were more modest but nevertheless promising. Against all Gram-negative and Gram-positive organisms tested, the Δ,Δ-isomers were found to be marginally the more active. Interestingly, relatively short (n = 2, 5), and heteroatom-linked dinuclear complexes were shown to have little or no activity.

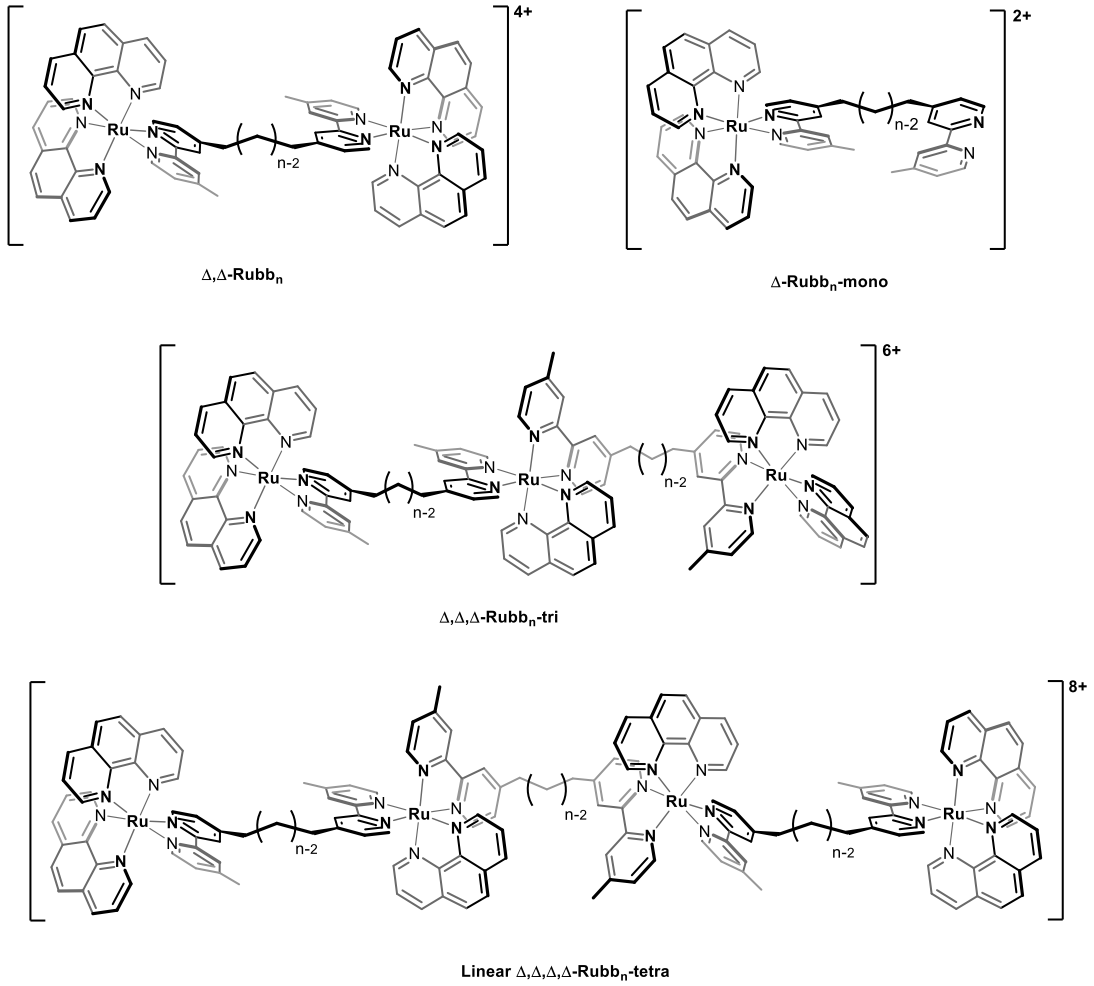


**Figure 1.12: Oligonuclear ruthenium complexes used by Collins, Keene *et al.*:** Rubb$_n$, Rubb$_n$-mono [Rubb$_n$ lacking a second Ru$^{II}$(phen)$_2$ centre], trinuclear and linear tetranuclear analogues. All metal centres shown in the Δ configuration, and where applicable with methylene bridges anchored *trans* across Ru(II) centres.

Selectivity for the 'lead' Δ,Δ-Rubb$_{12\text{-}16}$ complexes was assessed subsequently. Human red blood cell lysis (indicating membrane disruption) and toxicity to THP-1 (monocytic leukemia) cells increased with chain length, but the most promising candidate tested (ΔΔ-Rubb$_{12}$) gave $HC_{50}$ and $IC_{50}$ values respectively over 100-fold higher than the *S. aureus* MIC.[158] Later screening by the same team showed a lower toxicity to hamster kidney (BHK), human embryonic kidney (HEK-293) and human liver carcinoma (HEP-G2) cell lines.[159]

Microbial cellular uptake for this class of compound was measured for these complexes *via* their inherent fluorescence.[160] Uptake fell with lower linker chain

length *n* reflecting the trend in log *P* values[158] $Rubb_{16}$ > $Rubb_{12}$ > $Rubb_{7}$ suggesting that the higher hydrophobicity is beneficial, although it is difficult to deconvolute other effects of the longer chain such as increased mechanical flexibility. At the same time, monometallic species $Rubb_n$-mono which contain a pendant ligand (n = 7, 12) and $[Ru(Me_4phen)_3]^{2+}$ did not follow the same trend, even though $[Ru(Me_4phen)_3]^{2+}$, a compound remarkably similar to those used in the early work of Dwyer,[128, 129] was shown here to be a potent antimicrobial (MIC range: 0.5 μg/ml vs. *S aureus* to 32 μg/ml vs. *P. aeruginosa*). This may well indicate that the mechanisms of cellular uptake and/or antimicrobial action of $Rubb_n$ systems are different from mononuclear Ru(II) systems.

Uptake into Gram-negative bacteria was significantly less than for Gram-positives for $Rubb_n$ systems, and shown in all cases to occur in an energy-independent manner (passive diffusion) as, for example, dead or ATP-inhibited cells would still accumulate the complexes.[160, 161] Further, the dinuclear complexes significantly depolarise and permeablise the cell membrane of *S. aureus*,[161] although it is worth noting that this occurred at concentrations double the corresponding MICs.[158]

Cellular localization of $Rubb_n$ in *E. coli* MG1665 was studied using wide-field fluorescence microscopy (Figure 1.13).[159] $Rubb_{16}$, the most hydrophobic $Rubb_n$ complex reported, was found to concentrate in the vicinity of RNA (polysomes) *in vivo*, despite the significant membrane activity reported previously.[161] In the context of the pedigree described above of $Rubb_n$ systems as DNA-groove binders, an RNA/polysome-targeting mechanism is feasible, which could halt translation of RNA to proteins, thereby preventing protein synthesis. A preference for the RNA-

rich nucleolus over chromosomal DNA for all linear $Rubb_{12}$ systems in eukaryotic cell lines was observed *via* co-localization studies using confocal microscopy.[162]

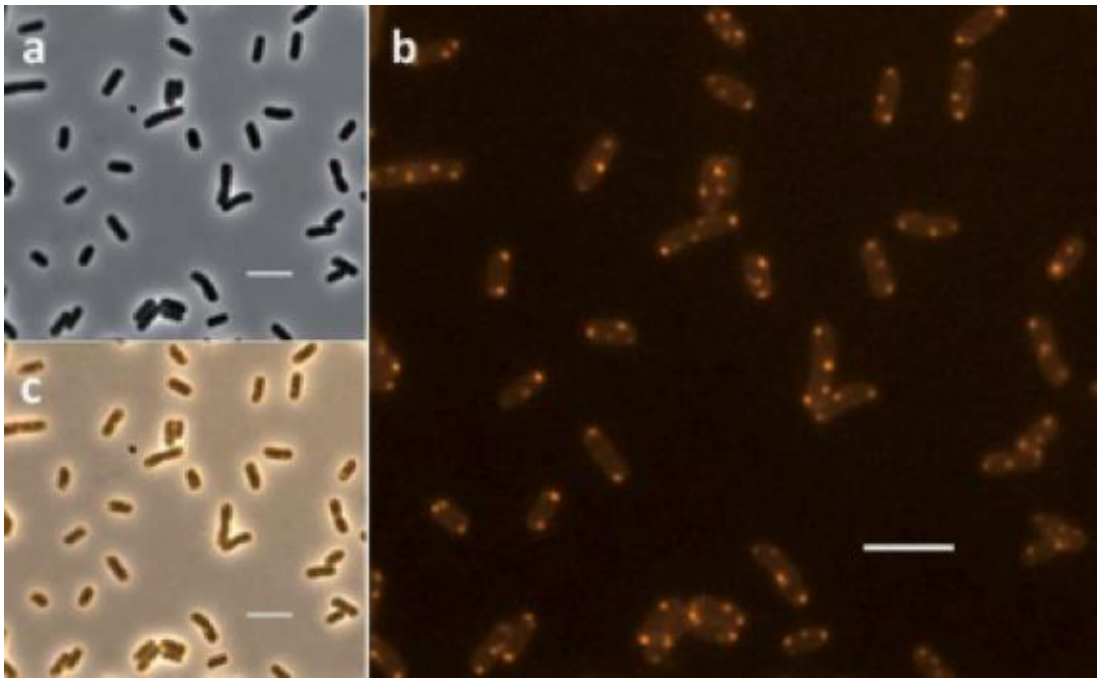


**Figure 1.13: $Rubb_{16}$ localisation in E. coli MG1665 cells at the MIC of 4 mg/ml.** Fluorescence microscopy images show: (a) phase-contrast: (b) $Rubb_{16}$ phosphorescence; and (c) merged. Scale bar = 5 μm. This image and others from the same work illustrate the concentration of $Rubb_{16}$ at the RNA-based polysomes.[159] - Published by The Royal Society of Chemistry.

The concepts above were extended through the study of oligonuclear $Rubb_n$ complexes (Figure 1.12) built through modular syntheses.[163] The application of similar methodology to earlier work[158] showed that these complexes have strong antimicrobial activity; several MICs against *S. aureus* were below 1 μM, with low MICs against Gram-negatives *E. coli* (1-6 μM) and to a lesser extent, *P. aeruginosa* (9-50 μM). Linear species with chain lengths n = 12, 16, were found to be more active, and in particular the linear tetranuclear complexes were more active than the branched species. This is consistent with the hypothetical target as RNA with the compounds acting as polynucleotide groove binders.[159] Furthermore while the trinuclear species were found to be the most lipophilic (log *P*) and showed relatively high uptake, they were not as active as their linear-tetranuclear counterparts. Unlike

their dinuclear counterparts, cellular uptake of Rubb$_n$-tri and linear Rubb$_n$-tetra (Figure 1.12) in the Gram-negative species was greater than or equal to that observed in the Gram-positives, and yet the MICs for Gram-positive species were significantly lower. This may suggest in this instance that the resistance of Gram-negative species to these compounds is not the result of the protective membrane but because intracellular processes are for some reason less susceptible.[160, 161]

### 1.5.4 Siderophore analogues

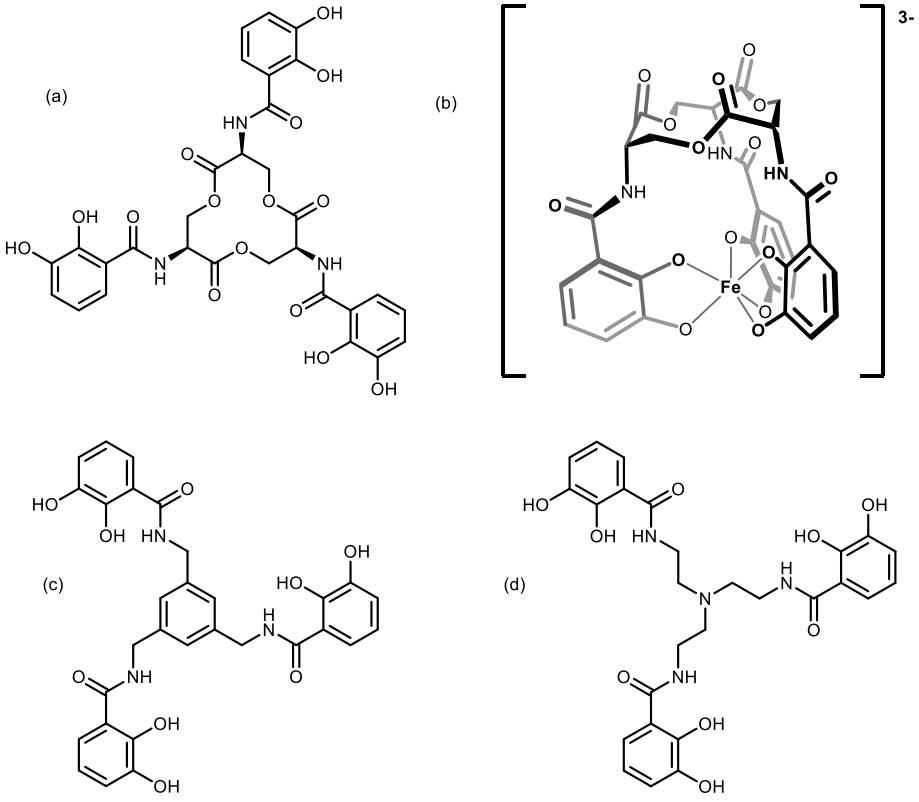


**Figure 1.14: Siderophore and analogue chemistry of Raymond *et al.*** (a) the catechol ligand enterobactin (ent) from *E. coli*; (b) structure of [Fe$^{III}$(ent)]$^{3-}$ based on a crystallographic study of [V(ent)$_3$]$^{2-}$; (c) 1,3,5-*tris*[(2,3-dihyroxybenzoyl)aminomethyl]benzene (MECAM); (d) 1,3,5-N,N',N'' -*tris*(2,3-dihydroxybenzoylamide)tri(aminoethyl)amine (TRENCAM).

Siderophores are molecules produced by bacteria in order to sequester iron[164] in competition with strategies evolved in the host organism such as nutritional immunity.[165, 166] Enterobactin [Figure 1.14(a)][167, 168] is the strongest Fe(III)-binding

siderophore known, ($K$ = $10^{52}$ $M^{-1}$).[169] The chiral backbone, biosynthesised from a tri-lactone of the amino acid L-serine, preorganises for Δ configuration at the metal;[170] the structure of Figure 1.14(b) is based on the analogue Δ-$[V(ent)]^{2-}$, reported by Karpishin & Raymond.[171]

Raymond and co-workers conducted a detailed study of the uptake of siderophore complexes in *E. coli*, underpinning our understanding of bacterial uptake of ferric iron. Of particular interest to this chapter was the ability of a Rh(III) complex $[Rh(MECAM)]^{3-}$ [ligand shown in Figure 1.14(c)] to inhibit bacterial uptake of the $[Fe(ent)]^{3-}$ complex[167] nominally *via* the *E. coli* FepA receptor protein; a critical pathway for essential iron uptake in *E. coli*.[172, 173] $[Fe(TRENCAM)]^{3-}$ [174] [ligand shown in Figure 1.14(d)] and in particular $[Fe(MECAM)]^{3-}$ were later found to be taken up by the iron-starved Gram-negative, enterobactin-dependent species, *Bordetella bronchiseptica* using the same BfeA outer membrane receptor as enterobactin.[175] Other $[Fe(ent)]^{3-}$ mimics have shown similar uptake in *Salmonella typhimurium* through enterobactin receptors; IroN and FepA.[176] Work on the TRENCAM ligand and its complexes has led to an intriguing set of supramolecular structures, which are bicapped, rather than monocapped; two TREN [*tris*(2-aminoethyl)amine] moieties link the three catechol bidentate units to two axial tertiary amine 'hubs' at either pole of the complex.[177]

Through this work we can see that a siderophore analogue might be used to block the uptake of iron or to ferry more toxic ions into the prokaryote cell in 'Trojan horse' strategy.

### 1.5.5 Metallohelices

Myriad coordination architectures formed through the application of ligands designed to span multiple metal centres have been reported, including helicates,[178-181] knots,[182] grids,[183, 184] catenanes,[185] rotaxanes,[186] boxes[187] and cages[188] amongst others.[189] Rather few of these have been shown to have any kind of potential use as drug molecules, probably because of the difficulty in making water-compatible compounds in significant quantities. This practical barrier arises because inert metal ions such as Ru(II), which are expected to give water-stable compounds, give mixtures of kinetic products on reaction with polydentate ligands, leading to low yields. On the other hand, the cleaner thermodynamic products produced by relatively labile metals are almost invariably subject to hydrolysis in water or biological media.

Lehn's prototypical helicate chemistry[181] (Figure 1.15) has nevertheless inspired a number of workers to explore the idea that such compounds might provide entry to a new area of biomimetic chemical space unavailable to organic chemistry.[190, 191]

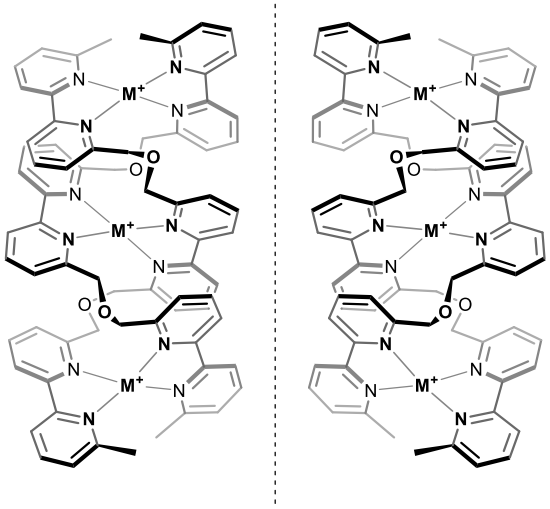

**Figure 1.15: Lehn's prototypic helicate structure:** showing the two optical isomers (M = Cu or Ag).[181, 192]

In 1997, Hannon and co-workers reported a synthesis of a helicate structure $[Fe_2L^H_3]^{4+}$ from simple starting materials;[193] an aromatic diamine, 2-picolinaldehyde, and an Fe(II) source that provides the anchoring octahedral metal centres (Figure 1.16). The rigid ligand system mechanically couples the helical coordination environments, requiring them to adopt the same stereochemistry (Δ,Δ, or Λ,Λ). The ensuing triple-helix structure has a well-defined pitch. The reported syntheses of this compound involve the use of weakly-coordinating anions ($PF_6^-$) for ease of isolation, followed by exchange with chloride to provide water solubility.

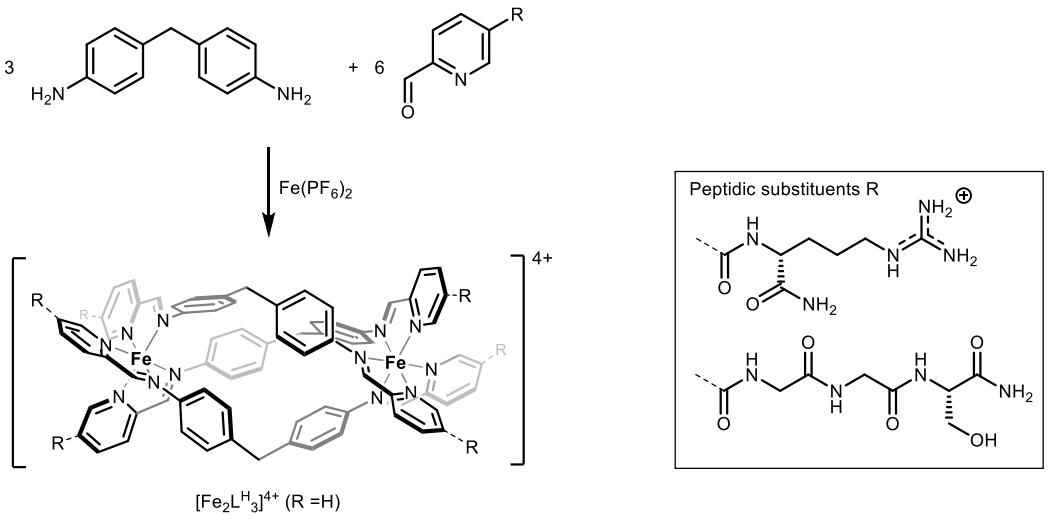


**Figure 1.16: Hannon's Fe(II) helicate, shown as the Λ,Λ isomer.**

Related examples include the results of simple modifications to the original Fe(II) helicate: replacing the bridging methylene with O; several peripheral modifications;[194] Ru(II) analogue(s).[195, 196] The latter, along with the original bis-Fe(II) helicate, is reported to be resolvable into enantiomers using a brine elution on a cellulose column or even paper,[194, 197] as supported by circular dichroism, although without quantification of the optical purity (*e.g.* through the use of an NMR shift reagent such as TRISPHAT).[198] Helicates with arginine[199] and a short peptide fragments[200] (Figure 1.16) were subsequently reported *via* multi-step route. Helicity

was seen to be controlled to within the limit of signal:noise for the NMR spectra observed.[199] Great attention has been given to the ability of these helicates to bind DNA motifs *in vitro*, especially the B-DNA major groove[196, 201, 202] and three-way junctions (3WJ)[199, 203-205] inducing conformational changes.[196]

The helicate $[Fe_2L^H_3]^{4+}$ of Figure 1.16 as the chloride salt was subject to *in vivo* screening as an antimicrobial agent.[206] MICs of 32 μg/ml against Gram-positive *B. subtilis* strain 168, and 64 μg/ml against Gram-negative *E. coli* strain GM2163, respectively. Both MBCs were less than four times the MIC, and although the potencies are rather low this was taken as confirming a bacteriocidal mode of action.[39] Unfortunately the compound was found to be incompatible with standard broth[59] so a special in-house medium was devised. This makes comparison with other compounds difficult. Spectroscopic analysis of the DNA extracted from *B. subtilis* after exposure to the helicate at 100 μM indicated a ~3.7-fold rise in the absorbance at 575 nm compared to that of a control sample, which presumably had a very low absorbance in this region. Further work is needed to establish a link between the ability of this helicate to bind DNA and the antimicrobial or other activity. A time-kill assay supports a rapid cell death for *B. subtilis* and SDS-PAGE (protein electrophoresis) assays suggest a loss in overall protein production and an upregulation of stress proteins in that bacterium, although this may be due to membrane damage.

The low stability of $[Fe_2L^H_3]^{4+}$ to hydrolysis in water has been noted.[42] As mentioned above such matters must always be a consideration for labile metal assemblies and we recommend that simple kinetic stability studies are performed. If the helicate architecture is merely a vehicle for delivery of organic components, then in the case

of $[Fe_2L^H_3]^{4+}$ that is a mixture of a relatively benign aldehyde and a carcinogenic and toxic[207, 208] diamine component. Despite these limitations, this work is tantalizing and has inspired others to consider how safer, more tractable and more drug-like metallohelices can be synthesised. In progressing this work, a number of criteria need to be considered if any helicate or related compound can ever find its way to the clinic. Specifically the complexes need to be readily available on a reasonable scale in optically pure form, have good solubility and high stability in water, and be capable of derivatization so that structures can be optimised. While these criteria are challenging, and made more so by the need, as alluded to above, to use inherently labile metals, we are unlikely to see practical progress if we do not address them.[191]

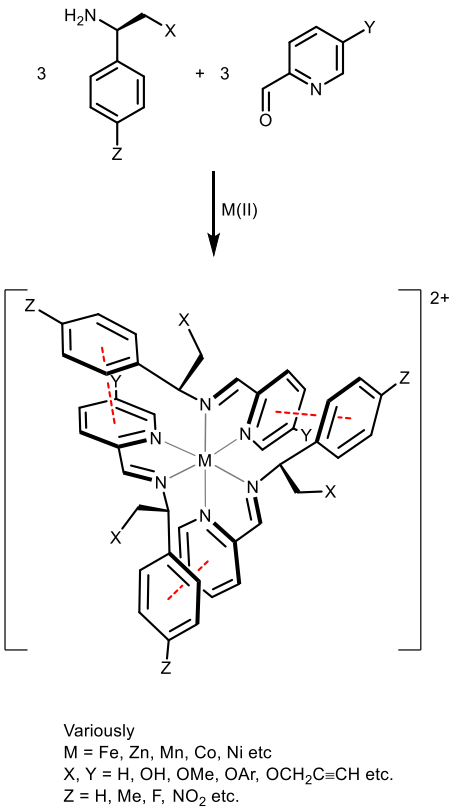


**Figure 1.17: Highly diastereoselective self-assembly of M(II) complexes:** α-phenyliminopyridine ligands from optically pure amines and pyridine-2-aldehydes engage in synergistic π-stacking arrangements as part of the mechanism of stereoselection.[209-211]

Scott and co-workers' approach to this problem was to avoid reliance on the helicate paradigm of mechanical coupling for stereochemical control at the metal, and instead

to develop a diastereoselective synthesis of monometallic complexes which might be used to form the end units of a helicate-like structure. Following the development of several prototype ligand designs for this purpose[212-215] a very simple but highly effective synthesis of highly stereochemically pure complexes of various first row transition metal was developed (Figure 1.17).[209-211] For diamagnetic Fe(II) the selectivity for a single *fac* diastereoisomer (~200:1) is delivered in this α-phenyliminopyridine system by a combination of optimal stereodirecting steric effects and a series of hydrophobic arene π-interactions. The latter also provides the complexes with remarkable stability to hydrolysis (*vide infra*).

The next step of linking two such monometallic units together proceeded smoothly, and the subsequent so-called flexicates[216] were comprised of two diastereomerically pure tris(chelate)Fe(II) units linked at either side by relatively flexible chains. Two structural classes are readily available: a diamine linker leading to *exo*-pyridine (alternatively class Ia), and a dialdehyde leading to *exo*-imine (alternatively class Ib) architectures (Figure 1.18).

MICs were determined in standard media against MRSA strain 252 and *E. coli* strain MC4100.[216] It was found that the more flexible architectures of the *exo*-imine *flexicates* (Figure 1.18) showed little or no antibiotic activity. In stark contrast, the more rigid system of the *exo*-pyridine class of flexicate had much higher antimicrobial activity with MICs of 8 μg/ml against Gram-positive MRSA for both isomers and MICs of 8 and 4 μg/ml for Δ and Λ isomers respectively against Gram-negative *E. coli.* Similar MICs were observed in pathogenic *MRSA* USA300, and *E. coli* TOP10.[42] MBCs in these organisms of *ca* 2 × MIC suggest a bacteriocidal mode

of action. Promisingly, the same flexicates were found to have low toxicity ($LC_{50}$ of 400-500 μg/ml) towards the nematode *C. elegans*.[216]

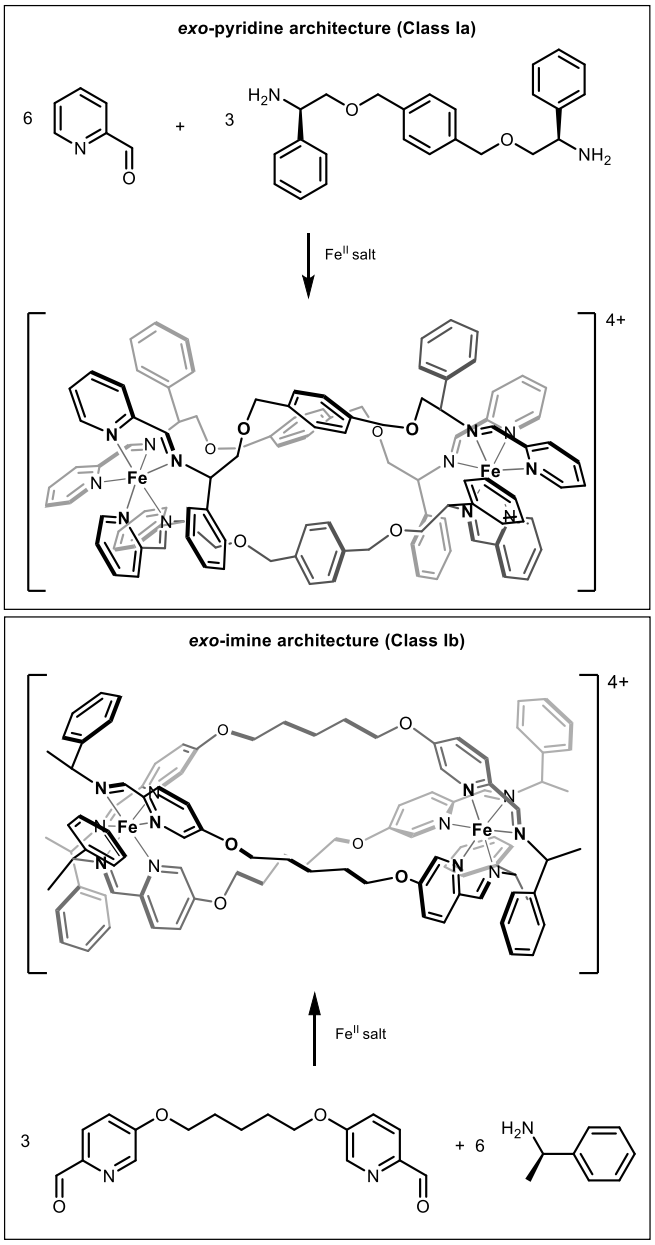


**Figure 1.18: Subcomponent self-assemblies of two flexicate architectures.**[216]

As with the Hannon helicate, there is evidence for binding to DNA architectures in some of these compounds. Binding affinities were generally stronger for Λ complexes and markedly stronger for the more rigid, antimicrobial *exo*-imine architectures (Figure 1.18), and evidence was presented from LD spectra for binding into the major groove.[216] A more detailed analysis of the biophysical interactions

with different DNA motifs was presented.[217] Atomic force microscopy (AFM) revealed that the enantiomers caused supercoiling of ctDNA, and DNase I footprinting supported B-DNA major groove binding for this complex as well as suggesting a sequence selectivity for 5'-CACATA and 5'-CACTAT sequences. The interaction of this flexicate with DNA motifs that are potential chemotherapeutic targets was demonstrated: four-way (Holliday) junctions (4WJ) – implemented in homologous genetic recombination,[218] 3WJs (both T-shaped and Y-shaped variations) and double stranded DNA (dsDNA) with bulges of different sizes. In contrast, in all such studies the exo-imine architecture gave essentially no DNA binding.[217]

At this stage while the correlation between the DNA interactions seen *in vitro* and the antibiotic activity may be coincidental, it is noteworthy that a wide selection of further *exo*-imine flexicates[219] with little or no binding affinity for cell-free DNA were also inactive as antimicrobials. At the same time observations of low toxicity to the amoeba, *Acanthamoeba polyphaga* and an apparent probiotic effect in the moth larvae, *Manduca sexta*, in which the systemic distribution of the complex was observed, are highly encouraging.

Inspired by the structures of small antimicrobial peptides such as human cathelicidin LL-37,[220, 221] Scott used a new set of supramolecular design principles to develop a synthesis of a range of functionalised, optically pure amphipathic metallohelices.[42] These highly water-stable "triplex" metallohelices (Figure 1.19) are comprised of three directional strands arranged head-to-tail, leading, *via* the helix fold, to structures with a polar functionalised face opposite a hydrophobic ridge. Perhaps surprisingly, given their high toxicity to cancer cell lines, antimicrobial activity for at

least the parent complexes against *MRSA* and *E. coli* was negligible (MICs all >128 μg/ml).

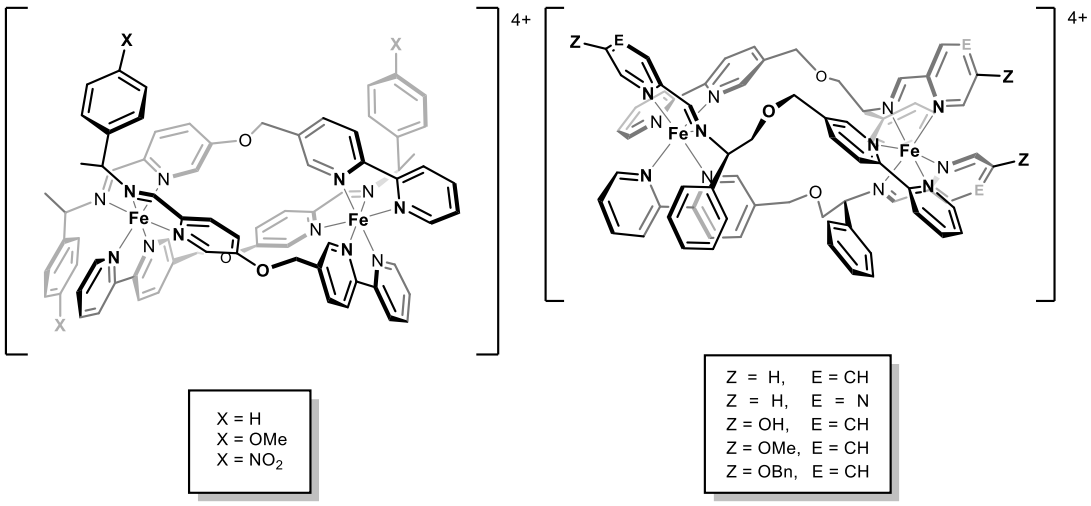


**Figure 1.19: Cationic units of optically pure *triplex metallohelices*** [42]

Crowley and co-workers reported a simple synthesis of a dinuclear Ru(II) triple helicates using a Huisgen alkyne-azide cycloaddition ('click') reaction to furnish a pyridine-triazole bidentate unit at either end of a symmetric AB-BA ligand.[222] Here also, negligible antimicrobial activity was observed (MICs >256 μg/ml) for this, or indeed the Hannon helicate which was used as a control.

## 1.6 Outlook

Antimicrobial transition metal complexes that rely on metal-centred redox or reactivity, generally cause lesions to a DNA target by producing highly reactive species such as peroxides in the vicinity, or by forming new covalent bonds (cross-linking). Despite the use in many cases of ligands designed to confer selectivity of the metallo-antimicrobial towards DNA, these drugs are likely to be promiscuous as

a natural consequence of overt reactivity at the metal centre. Poor selectivity towards the microbial target and depletion by unspecific binding are inevitable.[223] Many reactive-at-metal metallodrugs have thus found greater clinical acceptance as anticancer agents, or as topical treatments of infection. Overall however the feasibility of use of new systems such as NHC complexes of gold and silver in antimicrobial treatments must be low given the affinity of these ions to ubiquitous thiol groups *in vivo*.[116]

More promising reactive-at-metal antimicrobials display improved activity by making use of the way coordination chemistry may be used to define the geometry of their complexes, allowing engineered targeting of the endocellular target; there may be potential for development towards the targeted delivery of reactive metal species, using complexes engineered to carefully contain reactivity until required; a 'Trojan horse' strategy.[224]

Since the late 1980s major developments in supramolecular-coordination chemistry have allowed the design of myriad transition metal complexes with well-defined geometries with no overtly reactive metal centre. These architectures have been discussed for some time as useful in the design of synthetic antimicrobials as they could be engineered to have a geometry ideal for inhibiting a particular cellular process, whilst simultaneously evading the resistance mechanisms suffered by natural products, as their chemistry is unfamiliar to nature. Despite this attention, it is only since the mid-1990s that such complexes have been reported with appropriate properties to be used in medicinal research, and since 2010 that substantial works on screening for antimicrobial potential and mechanisms of action have appeared.

The most promising examples thus far of antimicrobial complexes of this type have been the ruthenium-based, intercalators of Aldrich-Wright, the oligonuclear ruthenium systems of Collins and Keene, and dinuclear iron metallohelix systems. As with reactive-at-metal complexes, much attention has been given to their interaction with DNA *in vitro*.[50, 225] Little attention has been given this far to interactions with other prokaryote cellular structures such as membrane chemistry or the possibility of protein-protein interactions (PPIs). The latter are crucial to the vast majority of cellular processes as well as offering high specificity. Meggers and co-workers[58] show there is a precedent for targeting PPIs with coordination complexes through precise architectural design. In this context, self-assembling bimetallic helicate-based systems show great promise because of their structural similarity to α-helices, but control over surface topology, so readily provided in nature, is in its infancy.[42]

If inert template complexes are versatile enough to be tailored to provide potent and selective antibiotic agents, then it is argued that their synthetic design ought to be driven by a better and fuller understanding of their molecular interactions within (and at the surface of) the prokaryote pathogen, *i.e.* understanding by what mechanism(s) it has any antibacterial effect. Advances in high-throughput assays in molecular biology and computation methods, for example, are making such awareness ever easier to achieve. As well as a scarcity of mechanistic understanding, it is also noted that to date the few inert template coordination complexes that have been reported to have biological activity have only been tested against a few genera (*Bacillus*, *Staphyloccocus*, *Escherichia*), and the selectivity for prokaryotes over eukaryotes *in vivo* has rarely been studied.

The demonstrated usefulness of CORM-type complexes as CO release vectors adds another potential weapon in the fight against microbial infection, and the idea of small molecule releasing complexes may well be expanded towards other useful small molecules than may benefit from targeted delivery (nitrous oxide, hydrogen sulfide, *etc.*).

There is a growing interest in the field towards synergistic combinations of drugs; hitting different prokaryote biomolecular targets in complimentary fashion, hopefully reducing resistance and toxic side effects, and allowing the 'repurposing' of existing chemic space.[226-229] This has not been widely studied for coordination complexes, the report of Wolschendorf and co-workers of copper ion releasing complexes acting synergistically with disulfiram, being an exception.[70] Some of the potential of coordination complexes may be realised here as they may act on pathways (protein synthesis, DNA replication, iron intake, *etc.*) that could sensitise the pathogen to traditional chemotherapeutics.

The chemistry necessary to develop the well-defined structures with tailored properties is rapidly advancing. It is proposed that in order to effectively guide this research to reach its full potential in antimicrobial chemotherapy, we must employ a rigorous approach to fully understanding the potency, selectivity, cell wall activity and mechanisms of action of each complex type, using a wide range of organisms. We need to conduct this interdisciplinary work with a view to advancing towards *in vivo* trials. Realistically, in order to make such an investment, coordination and organometallic chemists should be asking themselves hard questions about their chosen system. Can it ever be produced and used as a drug in humans? What are the barriers to acceptance by regulators and industry? Given the increasingly strict

limitations on heavy metal impurities in drugs[230] the deliberate use of such metals outside existing cancer treatments is perhaps unlikely. In the fight against antimicrobial resistance there is nevertheless a need to explore chemical space outside that of natural antibiotics, and so long as we address practical criteria of safety and utility, the unique structures of metallo-organic chemistry provide a very promising avenue.

# 1.7 References for Chapter 1


1. J. T. Brooks, J. E. Kaplan, K. K. Holmes, C. Benson, A. Pau and H. Masur, *Clin. Infect. Dis.*, 2009, **48**, 609-611.

2. A. G. Freifeld, E. J. Bow, K. A. Sepkowitz, M. J. Boeckh, J. I. Ito, C. A. Mullen, Raad, II, K. V. Rolston, J. A. H. Young and J. R. Wingard, *Clin. Infect. Dis.*, 2011, **52**, E56-E93.

3. R. Gaynes, *Infect. Dis. Clin. North Am.*, 1997, **11**, 757-&.

4. R. Gaynes and D. Monnet, in *Antibiotic Resistance: Origins, Evolution, Selection and Spread*, Wiley, London, 1997, pp. 47-56.

5. S. L. Knobler, S. M. Lemon, M. Najafi and T. Burroughs, *WHO Global Strategy for Containment of Antimicrobial Resistance: Executive Summary*, National Academies Press (US), Washington DC, 2003.

6. M. A. Fischbach and C. T. Walsh, *Science*, 2009, **325**, 1089-1093.

7. D. M. Livermore, *Int. J. Antimicrob. Agents*, 2012, **39**, 283-294.

8. H. W. Boucher, G. H. Talbot, J. S. Bradley, J. E. Edwards, D. Gilbert, L. B. Rice, M. Scheld, B. Spellberg and J. Bartlett, *Clin. Infect. Dis.*, 2009, **48**, 1-12.

9. J. Cairns, J. Overbaugh and S. Miller, *Nature*, 1988, **335**, 142-145.

10. C. Walsh, *Antibiotics: Actions, Origins, Resistance*, ASM Press, Washington, DC, 2003.

11. S. R. Palumbi, *Science*, 2001, **293**, 1786-1790.

12. G. G. Perron, A. E. G. Lee, Y. Wang, W. E. Huang and T. G. Barraclough, *Proc. R. Soc. Lond., Ser. B: Biol. Sci.*, 2012, **279**, 1477-1484.

13. S. R. Gill, D. E. Fouts, G. L. Archer, E. F. Mongodin, R. T. DeBoy, J. Ravel, I. T. Paulsen, J. F. Kolonay, L. Brinkac, M. Beanan, R. J. Dodson, S. C. Daugherty, R. Madupu, S. V. Angiuoli, A. S. Durkin, D. H. Haft, J. Vamathevan, H. Khouri, T. Utterback, C. Lee, G. Dimitrov, L. X. Jiang, H. Y. Qin, J. Weidman, K. Tran, K. Kang, I. R. Hance, K. E. Nelson and C. M. Fraser, *J. Bacteriol.*, 2005, **187**, 2426-2438.

14. M. Zignol, M. S. Hosseini, A. Wright, C. Lambregts-van Weezenbeek, P. Nunn, C. J. Watt, B. G. Williams and C. Dye, *J. Infect. Dis.*, 2006, **194**, 479-485.

15. R. M. Donlan and J. W. Costerton, *Clin. Microbiol. Rev.*, 2002, **15**, 167-193.

16. H. Nikaido, *Science*, 1994, **264**, 382-388.

17. P. F. McDermott, R. D. Walker and D. G. White, *Int. J. Toxicol.*, 2003, **22**, 135-143.

18. K. Poole, *J. Antimicrob. Chemother.*, 2005, **56**, 20-51.

19. J. H. Jorgensen, M. A. Pfaller, K. C. Carroll, G. Funke, M. L. Landry, S. S. Richter and D. W. Warnock, *Manual of Clinical Microbiology, 11th Edition*, American Society of Microbiology, 2015.

20. G. D. Wright, *Adv. Drug Del. Rev.*, 2005, **57**, 1451-1470.

21. B. G. Spratt, *Science*, 1994, **264**, 388-393.

22. I. Chopra, *J. Antimicrob. Chemother.*, 2013, **68**, 496-505.

23. S. M. Mandal, A. Roy, A. K. Ghosh, T. K. Hazra, A. Basak and O. L. Franco, *Front. Pharmacol.*, 2014, **5**, 12.

24. J. L. Hobman and L. C. Crossman, *J. Med. Microbiol.*, 2015, **64**, 471-497.

25. E. Meggers, *Chem. Commun.*, 2009, 1001-1010.

26. R. E. W. Hancock, *Trends Microbiol.*, 1997, **5**, 37-42.

27. P. D. Dobson and D. B. Kell, *Nat. Rev. Drug Discov.*, 2008, **7**, 205-220.

28. D. B. Kell and S. G. Oliver, *Front. Pharmacol.*, 2014, **5**.

29. D. B. Kell, *Nat. Rev. Drug Discov.*, 2016, **15**, 143-143.

30. J. Mann and M. J. C. Crabbe, *Bacteria and Antibacterial Agents*, Spektrum University Science Books, Oxford, 1996.

31. G. M. de Tejada, S. Sanchez-Gomez, I. Razquin-Olazaran, I. Kowalski, Y. Kaconis, L. Heinbockel, J. Andra, T. Schurholz, M. Hornef, A. Dupont, P. Garidel, K. Lohner, T. Gutsmann, S. A. David and K. Brandenburg, *Curr. Drug Targets*, 2012, **13**, 1121-1130.

32. A. Teo and D. Roper, *Antibiotics*, 2015, **4**, 495.

33. C. Erridge, E. Bennett-Guerrero and I. R. Poxton, *Microb. Infect.*, 2002, **4**, 837-851.

34. A. Paschke, P. L. Neitzel, W. Walther and G. Schuurmann, *J. Chem. Eng. Data*, 2004, **49**, 1639-1642.

35. V. Pliska, B. Testa, H. Waterbeemd, R. Mannhold, H. Kubinyi and H. Timmerman, *Lipophilicity in Drug Action and Toxicology*, Wiley, Published Online, 2008.

36. J. A. Arnott and S. L. Planey, *Expert Opin. Drug Discov.*, 2012, **7**, 863-875.

37. P. Tripathi, A. Beaussart, G. Andre, T. Rolain, S. Lebeer, J. Vanderleyden, P. Hols and Y. F. Dufrêne, *Micron*, 2012, **43**, 1323-1330.

38. S. Schuck, M. Honsho, K. Ekroos, A. Shevchenko and K. Simons, *Proc. Natl. Acad. Sci. USA*, 2003, **100**, 5795-5800.

39. A. J. O'Neill and I. Chopra, *Expert Opin. Investig. Drugs*, 2004, **13**, 1045-1063.

40. A. K. Ghose, V. N. Viswanadhan and J. J. Wendoloski, *J. Comb. Chem.*, 1999, **1**, 55-68.

41. S. Blanck, J. Maksimoska, J. Baumeister, K. Harms, R. Marmorstein and E. Meggers, *Angew. Chem. Int. Ed.*, 2012, **51**, 5244-5246.

42. A. D. Faulkner, R. A. Kaner, Q. M. A. Abdallah, G. Clarkson, D. J. Fox, P. Gurnani, S. E. Howson, R. M. Phillips, D. I. Roper, D. H. Simpson and P. Scott, *Nat. Chem.*, 2014, **6**, 797-803.

43. J. A. Lee, M. T. Uhlik, C. M. Moxham, D. Tomandl and D. J. Sall, *J. Med. Chem.*, 2012, **55**, 4527-4538.

44. U. S. Eggert, *Nat. Chem. Biol.*, 2013, **9**, 206-209.

45. F. Sams-Dodd, *Drug Discov. Today*, 2013, **18**, 211-217.

46. D. C. Swinney and J. Anthony, *Nat. Rev. Drug Discov.*, 2011, **10**, 507-519.

47. J. G. Moffat, J. Rudolph and D. Bailey, *Nat. Rev. Drug Discov.*, 2014, **13**, 588-602.

48. A. Bolhuis and J. R. Aldrich-Wright, *Bioorg. Chem.*, 2014, **55**, 51-59.

49. B. M. Zeglis, V. C. Pierre and J. K. Barton, *Chem. Commun.*, 2007, 4565-4579.

50. B. J. Pages, D. L. Ang, E. P. Wright and J. R. Aldrich-Wright, *Dalton Trans.*, 2015, **44**, 3505-3526.

51. C. Oguey, N. Foloppe and B. Hartmann, *PLOS ONE*, 2010, **5**.

52. B. C. Narayanan, J. Westbrook, S. Ghosh, A. I. Petrov, B. Sweeney, C. L. Zirbel, N. B. Leontis and H. M. Berman, *Nucleic Acids Res.*, 2014, **42**, D114-D122.

53. J. C. Wang, *Annu. Rev. Biochem.*, 1996, **65**, 635-692.

54. P. Nissen, J. Hansen, N. Ban, P. B. Moore and T. A. Steitz, *Science*, 2000, **289**, 920-930.

55. J. R. Arias-Gonzalez, *Integr. Biol.*, 2014, **6**, 904-925.

56. J. R. Warner, P. M. Knopf and A. Rich, *Proc. Natl. Acad. Sci. USA*, 1963, **49**, 122-129.

57. B. Alberts, A. Johnson, J. Lewis, M. Raff, K. Roberts and P. Walter, *Molecular Biology of the Cell*, Garland, Oxford, 2002.

58. L. Feng, Y. Geisselbrecht, S. Blanck, A. Wilbuer, G. E. Atilla-Gokcumen, P. Filippakopoulos, K. Kraling, M. A. Celik, K. Harms, J. Maksimoska, R. Marmorstein, G. Frenking, S. Knapp, L. O. Essen and E. Meggers, *J. Am. Chem. Soc.*, 2011, **133**, 5976-5986.

59. BSAC, *J. Antimicrob. Chemother.*, 1991, **27 Suppl D**, 1-50.

60. J. A. Lemire, J. J. Harrison and R. J. Turner, *Nature Rev. Microbiol.*, 2013, **11**, 371-384.

61. J. W. Alexander, *Surg. Infect. (Larchmt.)*, 2009, **10**, 289-292.

62. H. Irving and R. J. P. Williams, *J. Chem. Soc.*, 1953, 3192-3210.

63. L. Macomber and J. A. Imlay, *Proc. Natl. Acad. Sci. USA*, 2009, **106**, 8344-8349.

64. J. J. Harrison, H. Ceri, C. A. Stremick and R. J. Turner, *Environ. Microbiol.*, 2004, **6**, 1220-1227.

65. L. M. Gaetke and C. K. Chow, *Toxicology*, 2003, **189**, 147-163.

66. D. Wisher, *J. Med. Libr. Assoc.*, 2012, **100**, 75-76.

67. N. L. Reeder, J. Kaplan, J. Xu, R. S. Youngquist, J. Wallace, P. Hu, K. D. Juhlin, J. R. Schwartz, R. A. Grant, A. Fieno, S. Nemeth, T. Reichling, J. P. Tiesman, T. Mills, M. Steinke, S. L. Wang and C. W. Saunders, *Antimicrob. Agents Chemother.*, 2011, **55**, 5753-5760.

68. K. J. Stone and Stroming.Jl, *Proc. Natl. Acad. Sci. USA*, 1971, **68**, 3223-&.

69. M. Haeili, C. Moore, C. J. C. Davis, J. B. Cochran, S. Shah, T. B. Shrestha, Y. Zhang, S. H. Bossmann, W. H. Benjamin, O. Kutsch and F. Wolschendorf, *Antimicrob. Agents Chemother.*, 2014, **58**, 3727-3736.

70. A. G. Dalecki, M. Haeili, S. Shah, A. Speer, M. Niederweis, O. Kutsch and F. Wolschendorf, *Antimicrob. Agents Chemother.*, 2015, **59**, 4835-4844.

71. I. Chevrier, J. L. Sague, P. S. Brunetto, N. Khanna, Z. Rajacic and K. M. Fromm, *Dalton Trans.*, 2013, **42**, 217-231.

72. H. Umezawa, K. Maeda, T. Takeuchi and Y. Okami, *J. Antibiot.*, 1966, **19**, 200-209.

73. D. H. Petering, R. W. Byrnes and W. E. Antholine, *Chem. Biol. Interact.*, 1990, **73**, 133-182.

74. R. X. Xu, D. Nettesheim, J. D. Otvos and D. H. Petering, *Biochemistry*, 1994, **33**, 907-916.

75. R. M. Burger, *Chem. Rev.*, 1998, **98**, 1153-1169.

76. Takeshit.M, S. B. Horwitz and A. P. Grollman, *Virology*, 1974, **60**, 455-465.

77. A. Gothelf, L. M. Mir and J. Gehl, *Cancer Treat. Rev.*, 2003, **29**, 371-387.

78. B. I. Sikic, M. Rozencweig and S. K. Carter, *Bleomycin Chemotherapy*, Elsevier Science, 2013.

79. R. M. Burger, A. D. Adler, S. B. Horwitz, W. B. Mims and J. Peisach, *Biochemistry*, 1981, **20**, 1701-1704.

80. Y. Itaka, H. Nakamura, T. Nakatani, Y. Muraoka, A. Fujii, T. Takita and H. Umezawa, *J. Antibiot. (Tokyo)*, 1978, **31**, 1070-1072.

81. D. Williamson, I. J. McLennan, A. Bax, M. P. Gamcsik and J. D. Glickson, *J. Biomol. Struct. Dyn.*, 1990, **8**, 375-398.

82. A. M. Calafat, H. Won and L. G. Marzilli, *J. Am. Chem. Soc.*, 1997, **119**, 3656-3664.

83. C. Rajani, J. R. Kincaid and D. H. Petering, *J. Am. Chem. Soc.*, 2004, **126**, 3829-3836.

84. S. A. Kane and S. M. Hecht, *Prog. Nucleic Acid Res. Mol. Biol.*, 1994, **49**, 313-352.

85. S. M. Hecht, *Acc. Chem. Res.*, 1986, **19**, 383-391.

86. E. Azambuja, J. F. Fleck, R. G. Batista and S. S. M. Barreto, *Pulm. Pharmacol. Ther.*, 2005, **18**, 363-366.

87. T. J. Donohoe, C. R. Jones, A. F. Kornahrens, L. C. A. Barbosa, L. J. Walport, M. R. Tatton, M. O'Hagan, A. H. Rathi and D. B. Baker, *J. Org. Chem.*, 2013, **78**, 12338-12350.

88. M. M. Harding and G. V. Long, *Curr. Med. Chem.*, 1997, **4**, 405-420.

89. R. B. Weiss, G. Sarosy, K. Clagettcarr, M. Russo and B. Leylandjones, *Cancer Chemother. Pharmacol.*, 1986, **18**, 185-197.

90. W. S. Marsh, A. L. Garretson and E. M. Wesel, *Antibiot. Chemother.*, 1961, **11**, 151-157.

91. J. Niemi, M. Metsa-Ketela, G. Schneider and P. Mantsala, in *Anthracycline Chemistry and Biology I: Biological Occurence and Biosynthesis, Synthesis and Chemistry: Biological Occurence and Biosynthesis, Synthesis and Chemistry*, ed. K. Krohn, Springer-Verlag Berlin, Berlin, 2008, vol. 282, pp. 75-99.

92. A. Fujiwara and T. Hoshino, *CRC Crit. Rev. Biotechnol.*, 1986, **3**, 133-157.

93. L. Lothstein, M. Israel and T. W. Sweatman, *Drug Resist. Updat.*, 2001, **4**, 169-177.

94. P. B. Jensen, B. S. Sorensen, M. Sehested, E. J. F. Demant, E. Kjeldsen, E. Friche and H. H. Hansen, *Biochem. Pharmacol.*, 1993, **45**, 2025-2035.

95. J. R. White, *Biochem. Biophys. Res. Commun.*, 1977, **77**, 387-391.

96. A. Eizaguirre, M. Yanez and L. A. Eriksson, *Phys. Chem. Chem. Phys.*, 2012, **14**, 12505-12514.

97. M. M. L. Fiallo, H. Drechsel, A. Garnier-Suillerot, B. F. Matzanke and H. Kozlowski, *J. Med. Chem.*, 1999, **42**, 2844-2851.

98. E. M. Gregory and Fridovic.I, *J. Bacteriol.*, 1973, **114**, 1193-1197.

99. H. L. White and J. R. White, *Mol. Pharmacol.*, 1968, **4**, 549-565.

100. A. D. Bolzan and M. S. Bianchi, *Mutat. Res. - Rev. Mut. Res.*, 2001, **488**, 25-37.

101. M. Sterba, O. Popelova, A. Vavrova, E. Jirkovsky, P. Kovarikova, V. Gersl and T. Simunek, *Antioxid. Redox Signal.*, 2013, **18**, 899-929.

102. J. R. F. Muindi, B. K. Sinha, L. Gianni and C. E. Myers, *FEBS Lett.*, 1984, **172**, 226-230.

103. C. Asche, *Mini-Rev. Med. Chem.*, 2005, **5**, 449-467.

104. R. Cone, S. K. Hasan, J. W. Lown and A. R. Morgan, *Can. J. Biochem.*, 1976, **54**, 219-223.

105. J. M. C. Gutteridge, *Biochem. Pharmacol.*, 1984, **33**, 3059-3062.

106. A. Yoshimoto, T. Oki and T. Inui, *J. Antibiot.*, 1978, **31**, 92-94.

107. B. S. Kim, S. S. Moon and B. K. Hwang, *J. Agric. Food. Chem.*, 2000, **48**, 1875-1881.

108. L. J. Ming, *Med. Res. Rev.*, 2003, **23**, 697-762.

109. L. Kelland, *Nat. Rev. Cancer*, 2007, **7**, 573-584.

110. P. C. A. Bruijnincx and P. J. Sadler, in *Advances in Inorganic Chemistry, Vol 61: Metal Ion Controlled Reactivity*, eds. R. VanEldik and C. D. Hubbard, Elsevier Academic Press Inc, San Diego, 2009, vol. 61, pp. 1-62.

111. S. Dasari and P. B. Tchounwou, *Eur. J. Pharmacol.*, 2014, **740**, 364-378.

112. B. Rosenberg, L. Vancamp and T. Krigas, *Nature*, 1965, **205**, 698-699.

113. S. Budagumpi and S. Endud, *Organometallics*, 2013, **32**, 1537-1562.

114. İ. Özdemir, A. Denizci, H. T. Öztürk and B. Çetinkaya, *Appl. Organomet. Chem.*, 2004, **18**, 318-322.

115. S. Ray, R. Mohan, J. K. Singh, M. K. Samantaray, M. M. Shaikh, D. Panda and P. Ghosh, *J. Am. Chem. Soc.*, 2007, **129**, 15042-15053.

116. G. A. Fernández, M. S. Vela Gurovic, N. L. Olivera, A. B. Chopa and G. F. Silbestri, *J. Inorg. Biochem.*, 2014, **135**, 54-57.

117. T. Samanta, G. Roymahapatra, W. F. Porto, S. Seth, S. Ghorai, S. Saha, J. Sengupta, O. L. Franco, J. Dinda and S. M. Mandal, *PLoS ONE*, 2013, **8**, e58346.

118. E. L. Chang, C. Simmers and D. A. Knight, *Pharmaceuticals*, 2010, **3**, 1711.

119. B. E. Mann, in *Medicinal Organometallic Chemistry*, eds. G. Jaouen and N. MetzlerNolte, Springer-Verlag Berlin, Berlin, 2010, vol. 32, pp. 247-285.

120. L. S. Nobre, J. D. Seixas, C. C. Romao and L. M. Saraiva, *Antimicrob. Agents Chemother.*, 2007, **51**, 4303-4307.

121. L. K. Wareham, R. K. Poole and M. Tinajero-Trejo, *J. Biol. Chem.*, 2015, **290**, 18999-19007.

122. S. McLean, B. E. Mann and R. K. Poole, *Anal. Biochem.*, 2012, **427**, 36-40.

123. K. S. Davidge, G. Sanguinetti, C. H. Yee, A. G. Cox, C. W. McLeod, C. E. Monk, B. E. Mann, R. Motterlini and R. K. Poole, *J. Biol. Chem.*, 2009, **284**, 4516-4524.

124. C. Nagel, S. McLean, R. K. Poole, H. Braunschweig, T. Kramer and U. Schatzschneider, *Dalton Trans.*, 2014, **43**, 9986-9997.

125. N. A. Smith and P. J. Sadler, *Philos. Transact. A Math. Phys. Eng. Sci.*, 2013, **371**, 13.

126. R. F. Donnelly, N. C. Fletcher, P. J. McCague, J. Donnelly, P. A. McCarron and M. M. Tunney, *Lett. Drug Des. Discov.*, 2007, **4**, 175-179.

127. J. P. Celli, B. Q. Spring, I. Rizvi, C. L. Evans, K. S. Samkoe, S. Verma, B. W. Pogue and T. Hasan, *Chem. Rev.*, 2010, **110**, 2795-2838.

128. F. P. Dwyer, E. C. Gyarfas, W. P. Rogers and J. H. Koch, *Nature*, 1952, **170**, 190-191.

129. F. P. Dwyer, I. K. Reid, A. Shulman, G. M. Laycock and S. Dixson, *Aust. J. Exp. Biol. Med. Sci.*, 1969, **47**, 203-218.

130. M. Eriksson, M. Leijon, C. Hiort, B. Norden and A. Graslund, *Biochemistry*, 1994, **33**, 5031-5040.

131. C. Hiort, P. Lincoln and B. Norden, *J. Am. Chem. Soc.*, 1993, **115**, 3448-3454.

132. H. Song, J. T. Kaiser and J. K. Barton, *Nat. Chem.*, 2012, **4**, 615-620.

133. H. M. Chen, J. A. Parkinson, S. Parsons, R. A. Coxall, R. O. Gould and P. J. Sadler, *J. Am. Chem. Soc.*, 2002, **124**, 3064-3082.

134. A. M. Krause-Heuer, R. Grunert, S. Kuhne, M. Buczkowska, N. J. Wheate, D. D. Le Pevelen, L. R. Boag, D. M. Fisher, J. Kasparkova, J. Malina, P. J. Bednarski, V. Brabec and J. R. Aldrich-Wright, *J. Med. Chem.*, 2009, **52**, 5474-5484.

135. H. K. Liu and P. J. Sadler, *Acc. Chem. Res.*, 2011, **44**, 349-359.

136. T. Nhukeaw, P. Temboot, K. Hansongnern and A. Ratanaphan, *BMC Cancer*, 2014, **14**, 19.

137. J. G. Collins, A. D. Sleeman, J. R. Aldrich-Wright, I. Greguric and T. W. Hambley, *Inorg. Chem.*, 1998, **37**, 3133-3141.

138. I. Greguric, J. R. Aldrich-Wright and J. G. Collins, *J. Am. Chem. Soc.*, 1997, **119**, 3621-3622.

139. A. Bolhuis, L. Hand, J. E. Marshall, A. D. Richards, A. Rodger and J. Aldrich-Wright, *Eur. J. Pharm. Sci.*, 2011, **42**, 313-317.

140. D. O'Callaghan and A. Vergunst, *Curr. Opin. Microbiol.*, 2010, **13**, 79-85.

141. M. Artal-Sanz, L. de Jong and N. Tavernarakis, *Biotechnol. J.*, 2006, **1**, 1405-1418.

142. C. Hiort, B. Norden and A. Rodger, *J. Am. Chem. Soc.*, 1990, **112**, 1971-1982.

143. R. T. Watson, J. L. Jackson, J. D. Harper, K. A. KaneMaguire, L. A. P. KaneMaguire and N. A. P. KaneMaguire, *Inorg. Chim. Acta*, 1996, **249**, 5-7.

144. K. Kano and H. Hasegawa, *Chem. Lett.*, 2000, 698-699.

145. C. X. Jiang, M. Y. Tong, D. W. Armstrong, S. Perera, Y. Bao and F. M. MacDonnell, *Chirality*, 2009, **21**, 208-217.

146. N. C. Fletcher, R. T. Brown and A. P. Doherty, *Inorg. Chem.*, 2006, **45**, 6132-6134.

147. J. Lacour, S. Torche-Haldimann, J. J. Jodry, C. Ginglinger and F. Favarger, *Chem. Commun.*, 1998, 1733-1734.

148. F. M. O'Reilly and J. M. Kelly, *J. Phys. Chem. B*, 2000, **104**, 7206-7213.

149. F. M. O'Reilly and J. M. Kelly, *New J. Chem.*, 1998, **22**, 215-217.

150. F. O'Reilly, J. Kelly and A. Kirsch-De Mesmaeker, *Chem. Commun.*, 1996, 1013-1014.

151. J. Aldrich-Wright, C. Brodie, E. C. Glazer, N. W. Luedtke, L. Elson-Schwab and Y. Tor, *Chem. Commun.*, 2004, 1018-1019.

152. B. Onfelt, L. Gostring, P. Lincoln, B. Norden and A. Onfelt, *Mutagenesis*, 2002, **17**, 317-320.

153. P. Nordell and P. Lincoln, *J. Am. Chem. Soc.*, 2005, **127**, 9670-9671.

154. C. Rajput, R. Rutkaite, L. Swanson, I. Haq and J. A. Thomas, *Chem. Eur. J.*, 2006, **12**, 4611-4619.

155. P. Lincoln and B. Norden, *Chem. Commun.*, 1996, 2145-2146.

156. F. F. Li, J. G. Collins and F. R. Keene, *Chem. Soc. Rev.*, 2015, **44**, 2529-2542.

157. J. L. Morgan, C. B. Spillane, J. A. Smith, D. P. Buck, J. G. Collins and R. Keene, *Dalton Trans.*, 2007, 4333-4342.

158. F. F. Li, Y. Mulyana, M. Feterl, J. M. Warner, J. G. Collins and F. R. Keene, *Dalton Trans.*, 2011, **40**, 5032-5038.

159. F. F. Li, E. J. Harry, A. L. Bottomley, M. D. Edstein, G. W. Birrell, C. E. Woodward, F. R. Keene and J. G. Collins, *Chem. Sci.*, 2014, **5**, 685-693.

160. F. F. Li, M. Feterl, Y. Mulyana, J. M. Warner, J. G. Collins and F. R. Keene, *J. Antimicrob. Chemother.*, 2012, **67**, 2686-2695.

161. F. F. Li, M. Feterl, J. M. Warner, F. R. Keene and J. G. Collins, *J. Antimicrob. Chemother.*, 2013, **68**, 2825-2833.

162. X. Li, A. K. Gorle, T. D. Ainsworth, K. Heimann, C. E. Woodward, J. Grant Collins and F. Richard Keene, *Dalton Trans.*, 2015, **44**, 3594-3603.

163. A. K. Gorle, M. Feterl, J. M. Warner, L. Wallace, F. R. Keene and J. G. Collins, *Dalton Trans.*, 2014, **43**, 16713-16725.

164. S. C. Andrews, A. K. Robinson and F. Rodriguez-Quinones, *FEMS Microbiol. Rev.*, 2003, **27**, 215-237.

165. James E. Cassat and Eric P. Skaar, *Cell Host & Microbe*, **13**, 509-519.

166. M. I. Hood and E. P. Skaar, *Nat. Rev. Microbiol.*, 2012, **10**, 525-537.

167. D. J. Ecker, L. D. Loomis, M. E. Cass and K. N. Raymond, *J. Am. Chem. Soc.*, 1988, **110**, 2457-2464.

168. I. G. Obrien, G. B. Cox and F. Gibson, *Biochim. Biophys. Acta*, 1970, **201**, 453-&.

169. C. J. Carrano and K. N. Raymond, *J. Am. Chem. Soc.*, 1979, **101**, 5401-5404.

170. T. D. P. Stack, T. B. Karpishin and K. N. Raymond, *J. Am. Chem. Soc.*, 1992, **114**, 1512-1514.

171. T. B. Karpishin and K. N. Raymond, *Angew. Chem. Int. Ed.*, 1992, **31**, 466-468.

172. S. K. Buchanan, B. S. Smith, L. Venkatramani, D. Xia, L. Esser, M. Palnitkar, R. Chakraborty, D. van der Helm and J. Deisenhofer, *Nat. Struct. Biol.*, 1999, **6**, 56-63.

173. K. N. Raymond, E. A. Dertz and S. S. Kim, *Proc. Natl. Acad. Sci. USA*, 2003, **100**, 3584-3588.

174. S. J. Rodgers, C. W. Lee, C. Y. Ng and K. N. Raymond, *Inorg. Chem.*, 1987, **26**, 1622-1625.

175. M. T. Anderson and S. K. Armstrong, *J. Bacteriol.*, 2006, **188**, 5731-5740.

176. W. Rabsch, W. Voigt, R. Reissbrodt, R. M. Tsolis and A. J. Baumler, *J. Bacteriol.*, 1999, **181**, 3610-3612.

177. M. Albrecht, S. J. Franklin and K. N. Raymond, *Inorg. Chem.*, 1994, **33**, 5785-5793.

178. M. Scherer, D. L. Caulder, D. W. Johnson and K. N. Raymond, *Angew. Chem. Int. Ed.*, 1999, **38**, 1588-1592.

179. M. Albrecht, *Chem. Eur. J.*, 2000, **6**, 3485-3489.

180. M. Albrecht, E. Isaak, M. Baumert, V. Gossen, G. Raabe and R. Frohlich, *Angew. Chem. Int. Ed.*, 2011, **50**, 2850-2853.

181. J. M. Lehn, A. Rigault, J. Siegel, J. Harrowfield, B. Chevrier and D. Moras, *Proc. Natl. Acad. Sci. USA*, 1987, **84**, 2565-2569.

182. R. S. Forgan, J. P. Sauvage and J. F. Stoddart, *Chem. Rev.*, 2011, **111**, 5434-5464.

183. M. Ruben, J. Rojo, F. J. Romero-Salguero, L. H. Uppadine and J. M. Lehn, *Angew. Chem. Int. Ed.*, 2004, **43**, 3644-3662.

184. P. N. W. Baxter, J. M. Lehn, J. Fischer and M. T. Youinou, *Angew. Chem. Int. Ed.*, 1994, **33**, 2284-2287.

185. J. F. Ayme, J. Lux, J. P. Sauvage and A. Sour, *Chem. Eur. J.*, 2012, **18**, 5565-5573.

186. J. C. Chambron, V. Heitz and J. P. Sauvage, *J. Am. Chem. Soc.*, 1993, **115**, 12378-12384.

187. P. J. Stang and D. H. Cao, *J. Am. Chem. Soc.*, 1994, **116**, 4981-4982.

188. N. Ousaka, S. Grunder, A. M. Castilla, A. C. Whalley, J. F. Stoddart and J. R. Nitschke, *J. Am. Chem. Soc.*, 2012, **134**, 15528-15537.

189. F. R. Keene, *Dalton Trans.*, 2011, **40**, 2405-2418.

190. G. Maayan and M. Albrecht, *Metallofoldamers: Supramolecular Architectures from Helicates to Biomimetics*, Wiley, 2013.

191. R. A. Kaner and P. Scott, *Future Med. Chem.*, 2015, **7**, 1-4.

192. T. M. Garrett, U. Koert, J. M. Lehn, A. Rigault, D. Meyer and J. Fischer, *J. Chem. Soc., Chem. Commun.*, 1990, 557-558.

193. M. J. Hannon, C. L. Painting, A. Jackson, J. Hamblin and W. Errington, *Chem. Commun.*, 1997, 1807-1808.

194. J. Kerckhoffs, J. C. Peberdy, I. Meistermann, L. J. Childs, C. J. Isaac, C. R. Pearmund, V. Reudegger, S. Khalid, N. W. Alcock, M. J. Hannon and A. Rodger, *Dalton Trans.*, 2007, 734-742.

195. J. C. Peberdy, J. Malina, S. Khalid, M. J. Hannon and A. Rodger, *J. Inorg. Biochem.*, 2007, **101**, 1937-1945.

196. M. J. Hannon, V. Moreno, M. J. Prieto, E. Moldrheim, E. Sletten, I. Meistermann, C. J. Isaac, K. J. Sanders and A. Rodger, *Angew. Chem. Int. Ed.*, 2001, **40**, 880-884.

197. M. J. Hannon, I. Meistermann, C. J. Isaac, C. Blomme, J. R. Aldrich-Wright and A. Rodger, *Chem. Commun.*, 2001, 1078-1079.

198. J. Lacour, C. Ginglinger, F. Favarger and S. TorcheHaldimann, *Chem. Commun.*, 1997, 2285-2286.

199. L. Cardo, V. Sadovnikova, S. Phongtongpasuk, N. J. Hodges and M. J. Hannon, *Chem. Commun.*, 2011, **47**, 6575-6577.

200. L. Cardo and M. J. Hannon, *Inorg. Chim. Acta*, 2009, **362**, 784-792.

201. I. Meistermann, V. Moreno, M. J. Prieto, E. Moldrheim, E. Sletten, S. Khalid, P. M. Rodger, J. C. Peberdy, C. J. Isaac, A. Rodger and M. J. Hannon, *Proc. Natl. Acad. Sci. USA*, 2002, **99**, 5069-5074.

202. C. Uerpmann, J. Malina, M. Pascu, G. J. Clarkson, V. Moreno, A. Rodger, A. Grandas and M. J. Hannon, *Chem. Eur. J.*, 2005, **11**, 1750-1756.

203. A. Oleksi, A. G. Blanco, R. Boer, I. Uson, J. Aymami, A. Rodger, M. J. Hannon and M. Coll, *Angew. Chem. Int. Ed.*, 2006, **45**, 1227-1231.

204. J. Malina, M. J. Hannon and V. Brabec, *Chem. Eur. J.*, 2007, **13**, 3871-3877.

205. L. Cerasino, M. J. Hannon and E. Sletten, *Inorg. Chem.*, 2007, **46**, 6245-6251.

206. A. D. Richards, A. Rodger, M. J. Hannon and A. Bolhuis, *Int. J. Antimicrob. Agents*, 2009, **33**, 469-472.

207. S. H. Kenyon, J. Bhattacharyya, C. J. Benson and P. L. Carmichael, *Toxicology*, 2004, **196**, 65-75.

208. T. Wellner, L. Lueersen, K. H. Schaller, J. Angerer, H. Drexler and G. Korinth, *Food Chem. Toxicol.*, 2008, **46**, 1960-1968.

209. S. E. Howson, L. E. N. Allan, N. P. Chmel, G. J. Clarkson, R. J. Deeth, A. D. Faulkner, D. H. Simpson and P. Scott, *Dalton Trans.*, 2011, **40**, 10416-10433.

210. C. P. Sebli, S. E. Howson, G. J. Clarkson and P. Scott, *Dalton Trans.*, 2010, **39**, 4447-4454.

211. S. E. Howson, L. E. N. Allan, N. P. Chmel, G. J. Clarkson, R. van Gorkum and P. Scott, *Chem. Commun.*, 2009, 1727-1729.

212. I. J. Munslow, A. J. Clarke, R. J. Deeth, I. Westmoreland and P. Scott, *Chem. Commun.*, 2002, 1868-1869.

213. I. J. Munslow, A. R. Wade, R. J. Deeth and P. Scott, *Chem. Commun.*, 2004, 2596-2597.

214. E. J. Crust, A. J. Clarke, R. J. Deeth, C. Morton and P. Scott, *Dalton Trans.*, 2004, 4050-4058.

215. I. Westmoreland, I. J. Munslow, A. J. Clarke, G. Clarkson, R. J. Deeth and P. Scott, *J. Organomet. Chem.*, 2006, **691**, 2228-2236.

216. S. E. Howson, A. Bolhuis, V. Brabec, G. J. Clarkson, J. Malina, A. Rodger and P. Scott, *Nat. Chem.*, 2012, **4**, 31-36.

217. V. Brabec, S. E. Howson, R. A. Kaner, R. M. Lord, J. Malina, R. M. Phillips, Q. M. A. Abdallah, P. C. McGowan, A. Rodger and P. Scott, *Chem. Sci.*, 2013, **4**, 4407-4416.

218. F. W. Stahl, *Genetics*, 1994, **138**, 241-246.

219. R. A. Kaner, S. J. Allison, A. D. Faulkner, R. M. Phillips, D. I. Roper, S. L. Shepherd, D. H. Simpson, N. R. Waterfield and P. Scott, *Chem. Sci.*, 2016.

220. M. Zanetti, R. Gennaro and D. Romeo, *FEBS Lett.*, 1995, **374**, 1-5.

221. U. H. N. Durr, U. S. Sudheendra and A. Ramamoorthy, *Biochim. Biophys. Acta*, 2006, **1758**, 1408-1425.

222. S. V. Kumar, W. K. C. Lo, H. J. L. Brooks and J. D. Crowley, *Inorg. Chim. Acta*, 2015, **425**, 1-6.

223. A. I. Ivanov, J. Christodoulou, J. A. Parkinson, K. J. Barnham, A. Tucker, J. Woodrow and P. J. Sadler, *J. Biol. Chem.*, 1998, **273**, 14721-14730.

224. U. Mollmann, L. Heinisch, A. Bauernfeind, T. Kohler and D. Ankel-Fuchs, *BioMetals*, 2009, **22**, 615-624.

225. M. J. Hannon, *Chem. Soc. Rev.*, 2007, **36**, 280-295.

226. S. K. Kasiakou, A. Michalopoulos, E. S. Soteriades, G. Samonis, G. J. Sermaides and M. E. Falagas, *Antimicrob. Agents Chemother.*, 2005, **49**, 3136-3146.

227. T. P. T. Cushnie and A. J. Lamb, *Int. J. Antimicrob. Agents*, 2011, **38**, 99-107.

228. L. Ejim, M. A. Farha, S. B. Falconer, J. Wildenhain, B. K. Coombes, M. Tyers, E. D. Brown and G. D. Wright, *Nat. Chem. Biol.*, 2011, **7**, 348-350.

229. T. Roemer and C. Boone, *Nat. Chem. Biol.*, 2013, **9**, 222-231.

230. D. R. Abernethy, A. J. DeStefano, T. L. Cecil, K. Zaidi and R. L. Williams, *Pharm. Res.*, 2010, **27**, 750-755.

# Chapter 2

## **New Class Ia Flexicates** From a Range of Optically Pure Diamines

### 2.1 Introduction

In Chapter 1, the potential of metallohelices as antimicrobial metallodrugs was discussed. The prototype class Ia (*exo*-pyridine) flexicate, $[Fe_2\mathbf{L}^{\mathbf{a}}{}_3]Cl_4$, showed promise in this field, having potent antimicrobial activity and remarkably high aqueous stability.[1] However, for reasons described later, no other flexicates of this class had been synthesised, and remarkably the analogous compounds of class Ib (*exo*-imine) and the related triplex metallohelices showed essentially no antimicrobial activity.[2, 3] It was thus a high priority to investigate the synthesis of new class Ia metallohelices for testing as antimicrobials.

This chapter will focus on the development of class Ia flexicates from diamine bridging units of varying sizes and architectures, in order to investigate the effect upon the assembly and structure of the system.

### 2.2 Synthesis of Optically Pure Diamine Bridges

A range of diamines derived from symmetric benzylic dihalides were targeted so as to provide a range of structural diversity (Scheme 2.1), such as: (i) the *meta*- and *ortho*-analogues of our previously reported[1] *para*-xylenyl system **3a**, *i.e.* **3b** and **3c**, are designed to investigate the effect of increasing fold angle; (ii) the 4,4'-biphenyl **3d** is

an elongated analogue of **3a**; (iii) the Ar-E-Ar systems **3e-h** incorporate potentially helicating 'hinges' and positions for secondary interactions; (iv) the more rigid dibenzofuran **3i**. These diamines were later incorporated into class Ia flexicates as described below (Scheme 2.4).

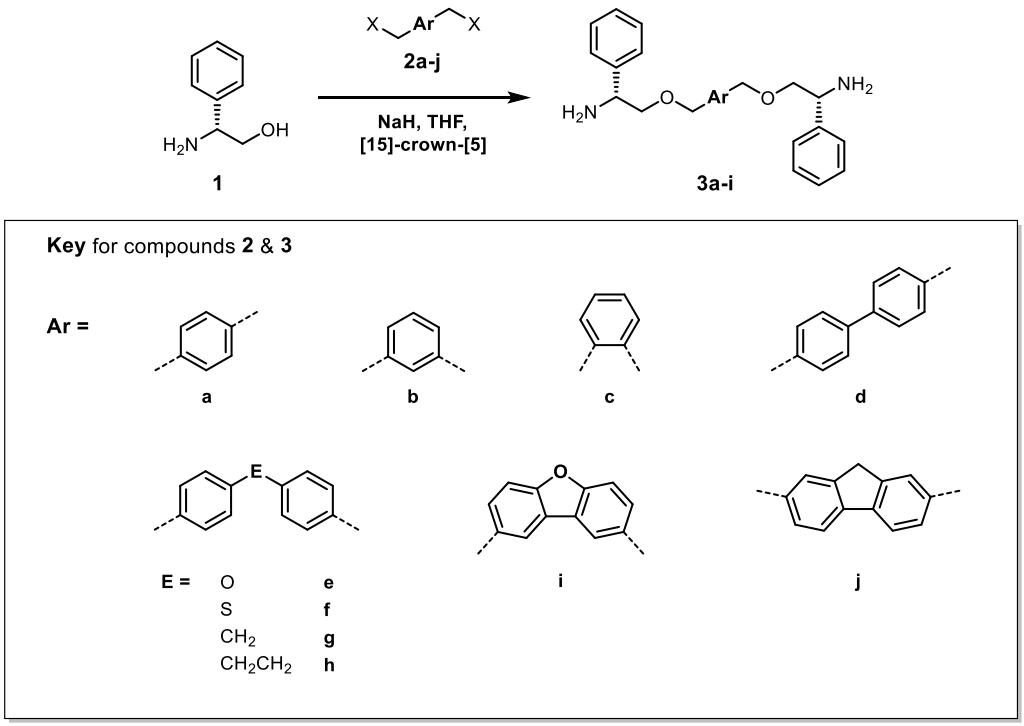


**Scheme 2.1: Synthetic routes to (*R*,*R*)-diamines (3a-i) from (*R*)-1 [(*R*)-2-phenylglycinol]**, through etherification of the corresponding benzylic dihalide (**2a-i**), mediated by sodium hydride and [15]-crown-[5] in THF. Corresponding (*S*,*S*)-diamines were similarly synthesised from (*S*)-**1**. The fluorene-bridged diamine **3j** could not be isolated for reasons discussed below.

### 2.2.1 Xylenyl & biphenyl linkers (3a-d)

Attempts to reproduce the synthesis of the previously reported[1] diamine enantiomers **3a** (Scheme 2.1) were unsuccessful. In these experiments, the reaction mixture was observed to be heterogeneous, containing a large quantity of solid material, and separation of the products was not achieved. Since the mass spectrum of the product material was essentially the same as that of the pure diamine it is proposed that samples contained some products of *N*-alkylation. NMR spectra were consistent with this

hypothesis. Further, attempts to apply the same conditions to the synthesis of *meta*-substituted enantiomers **3b** from **2b** (α,α'-dibromo-*m*-xylene) gave a similar result. It was suspected that this apparently capricious behaviour was a result of changes in the condition of starting materials and solvents *etc.*, but extensive studies showed no improvement, and new conditions were thus investigated. The use of an *N*-protection strategy was not attempted since this had been studied and abandoned by earlier group members. After a large number of experiments using various solvents and other conditions we turned to the work of Aspinall, Greeves *et al.*[4] who showed that the addition of [15]-crown-[5] improved the rate of *O*-alkylation in similar etherification reactions mediated by sodium hydride. Treatment of *p*-, *m*- and *o*- *bis*-bromomethylxylenes (**2a-c**) with 2.1 equivalents of 2-phenylglycinol (**1**) in the presence of NaH and 1-2 equivalents of [15]-crown-[5] (Scheme 2.1) led to homogeneous reaction mixtures in THF. After Kugelrohr distillation of the product to remove crown ether and excess aminoalcohol, the aminoethers **3a**, **3b** and **3c** were readily isolated, with negligible impurities present. NMR spectra of **3b** are shown in Figure 2.1.

Using the same modified etherification, commercially-available 4,4'-*bis*(chloromethyl)-1,1'-biphenyl (**2d**) was converted to **3d** as shown in Scheme 2.1.

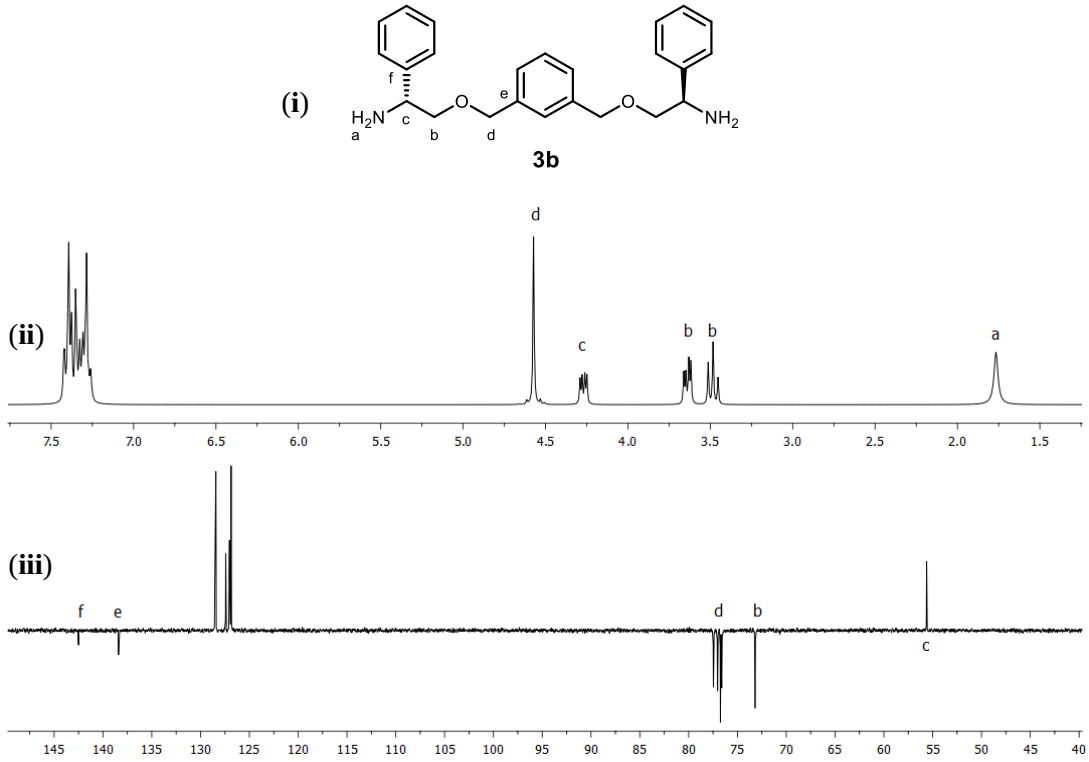


**Figure 2.1: NMR spectra of 3b**: (i) Structure of (*R,R*)-**3b;** (ii) 300 MHz $^{1}$H-NMR spectrum; (iii) 75 MHz $^{13}$C{$^{1}$H}-NMR spectrum. Spectra recorded in $CDCl_3$ ($\delta_H$ 7.26, $\delta_C$ 77) at 298 K.

## 2.2.2 Ar-E-Ar linkers (3e-h)

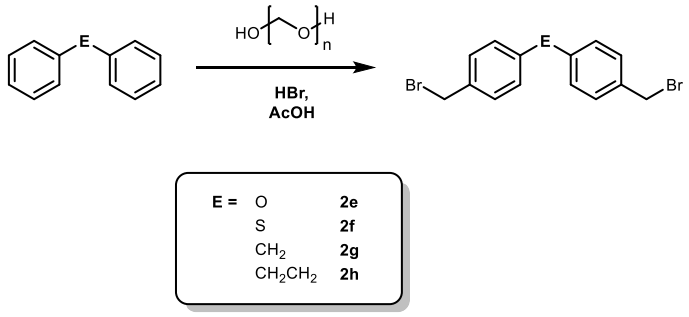


**Scheme 2.2: Synthetic routes to Ar-E-Ar dibromide intermediates 2e-h**, later incorporated into diamines **3e-h**.

The diamines of Scheme 2.1 containing an Ar-E-Ar linkage (**3e-h**) were furnished from the commercially-available compounds Ph-E-Ph (E = O, S, $CH_2$, $CH_2CH_2$) *via* a halomethylation method similar to that described by Belfield and co-workers[5, 6] *i.e.* using excess acidified formaldehyde/hydrobromic acid, to give dibromides **2e-h** (Scheme 2.2). Various reaction conditions were attempted, and suitable parameters

determined *via* $^{1}$H-NMR study of crude products. It was found that optimal reaction conditions correlated with the π-electron donating ability of the central atom E, *e.g.* optimal temperature increased as E varied: *alkyl* > S > O. Washing with water followed by recrystallisation from toluene/*n*-hexane or toluene/DCM gave the desired product in 40-60 % yield. This method gave excellent regioselectivity, as illustrated by the $^{1}$H-NMR spectrum (Figure 2.2) of **2e** [*bis*-4-(bromomethyl)phenyl ether].

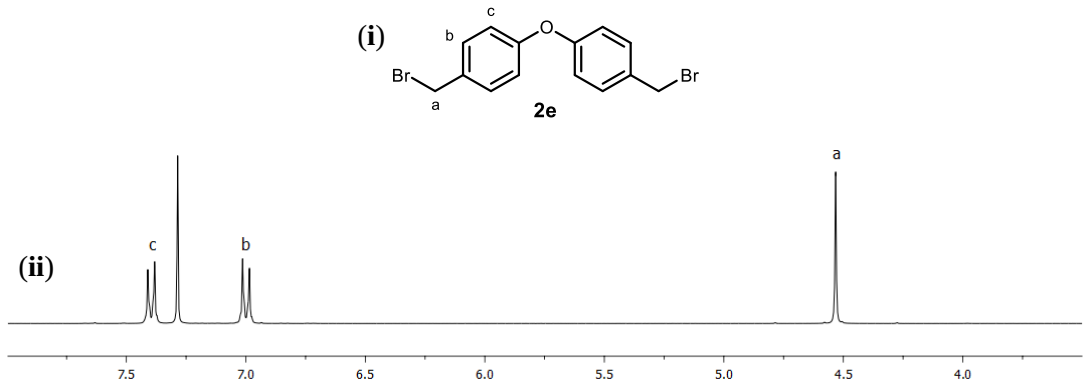


**Figure 2.2: $^{1}$H-NMR spectrum of 2e**: (i) Structure of **2e** [*bis*-4-(bromomethyl)phenyl ether]; (ii) 300 MHz $^{1}$H-NMR spectrum of this product recorded in $CDCl_3$ ($\delta_H$ 7.26) at 298 K.

### 2.2.3 Dibenzofuran linker (3i) and fluorene analogue

In order to develop rigid analogues of the Ar-E-Ar linkers, we considered the use of dibenzofuran, dibenzothiofuran, *N*-protected carbazole and fluorene systems. Attempts were made to extend the bromomethylation reaction described in the previous section. Of these, the dibenzofuran and fluorene systems were successful in giving single, suitable products with 2,8- and 2,7-substitution respectively (Scheme 2.3). In the remaining systems, a mixture of products was observed by NMR spectroscopy, presumably because each aromatic ring has two competing *para*-directing substituents. The dibenzofuran dibromide system **2i** was smoothly converted to **3i** (Scheme 2.1), but the fluorene derivative **2j** gave an inseparable mixture of

products, perhaps due to the relatively low p$K_a$ of the protons of the central methylene group (22.6 in DMSO).[7]

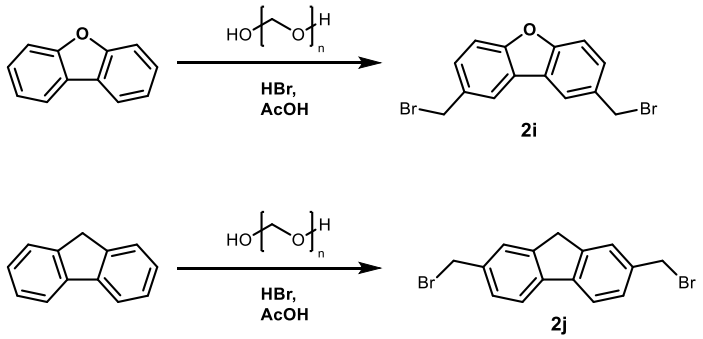


**Scheme 2.3: *bis*-Bromomethylation of dibenzofuran and 9H-fluorene** to give single products; 2,8-*bis*(bromomethyl)dibenzofuran (**2i**) and 2,7-*bis*(bromomethyl)-9H-fluorene (**2j**).

### 2.2.4 Determining the optical purity of diamine systems 3a-b

The α-iminophenyl unit present in flexicate systems leads to very high levels of diastereoselection in those self-assembled products, as determined by NMR spectroscopy.[8, 9] For the example of the *S*,*S* diamine, the presence of a small amount of the *meso* (*R*,*S*) compound might in principle lead to the formation of mesocate[10] *i.e.* Δ,Λ–$[M_2(R,S\text{-}L)_3]^{2+}$ (L = ditopic helicand). However, this would require a high level of *meso*-ligand self-selection; this is unlikely given that helication effects would lead to such a structure being very high energy. Hence this impurity is more likely to lead to the formation of other types of misassembled complex such as coordination polymers which would be detected by NMR spectroscopy. Further, at high levels of optical purity of *S*,*S* diamine, the presence of *R*,*R* compound is statistically unlikely. Nevertheless, and although we start with optically pure aminoalcohol, we do rely on the optical purity of the diamine in asserting the optical purity of the complex. Investigations of chiral HPLC analysis of these products, including a collaboration with a commercial analytical laboratory, had in the past proved fruitless, so we set out to determine optical purity by other means.

The diamines (*R*/*S*)-**3a** and (*R*/*S*)-**3b** were synthesised using racemic phenylglycinol. These mixtures could not be distinguished from the nominally optically pure products *e.g.* (*R*,*R*)-**3a**, by NMR spectroscopy. Therefore a chiral derivatisation method was employed,[11] whereby samples of nominally *S*,*S*-, *R*,*R*- and racemic (*i.e. S*,*S*/*R*,*R*/*S*,*R*) diamine were converted to the corresponding diamides using (*R*)-(+)-Mosher's acid (α-methoxy-α-trifluoromethyl-phenylacetic acid) and the products analysed by $^{1}$H-NMR spectroscopy. The spectra for **3b** isomers are shown in Figure 2.3. The diamide derivative of the racemic diamine gave two resonances in the ratio 1:1 (green line) indicating again that the stereogenic centres are isolated as far as can be determined by $^{1}$H-NMR spectroscopy at 400 MHz, but also that local diastereomeric units containing *S*- and *R*-amines could be distinguished *via* the $^{1}$H chemical shift of the methoxy group in (*R*)-(+)-Mosher's acid. The diastereomeric diamides of (*R*,*R*)-**3b** (blue line) and (*S*,*S*)-**3b** (red line) gave essentially a single resonance for the OMe unit. Thus, the total enantiomeric excess of all amine-derived chiral centres could be measured for a given sample (found to be >98 % e.e.). These results suggest that the etherification and purification methods described in section 2.2.1 led to the production of optically pure diamine bridges without significant racemisation.

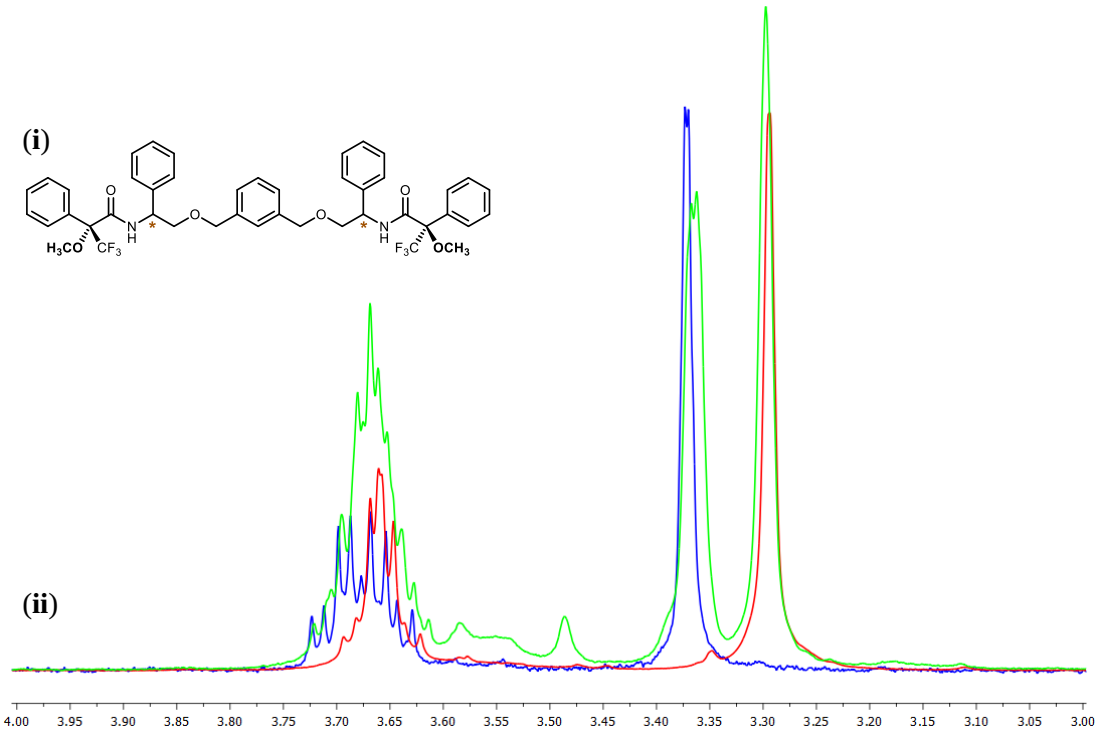


**Figure 2.3: Determination of the optical purity of 3b systems** through the synthesis of (*R*)-(+)-Mosher's acid derivatives (i) - the structure of which is shown here with bridge-derived chiral centres highlighted *. Overlaid 400 MHz $^1$H-NMR spectra in $CDCl_3$ are shown for three samples (ii); nominal (*R,R*)-**3b** derivative in blue, nominal (*S,S*)-**3b** derivative in red, and the derivative(s) of an **3b** isomeric mixture in green. Only the 3-4 ppm region containing the δ = 3.25-3.40 shift corresponding to -$OCH_3$ protons is shown. Spectra were recorded at 298 K.

# 2.3 New Zn(II) Flexicates

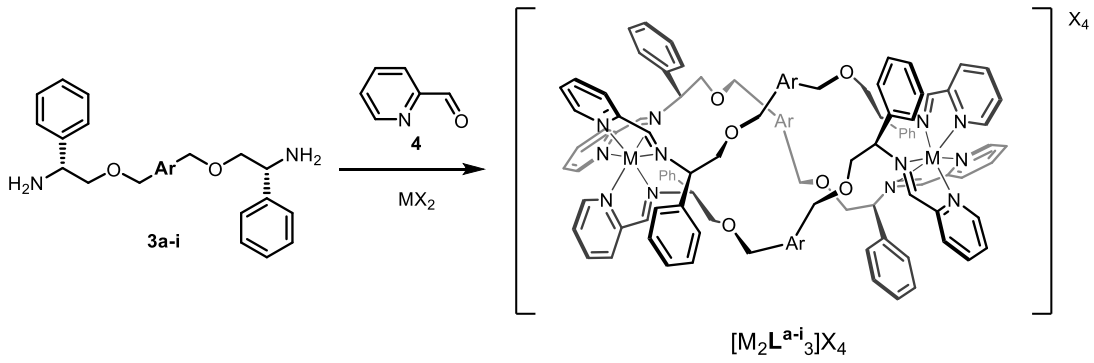


**Scheme 2.4: Synthetic routes to class Ia flexicates $\Delta_M$-$[M_2L^{a\text{-}i}{}_3]X_4$ from (*R,R*)-diamines, 3a-i**. Complexes synthesised from two metal sources are discussed in this chapter: zinc(II) perchlorate, and iron(II) chloride. Corresponding $\Lambda_M$ flexicates were similarly synthesised from diamines (*S,S*)-**3a-i**.

The synthesis of all class Ia flexicates of the type $[Zn_2\mathbf{L}_3][ClO_4]_4$ followed the same method as previously reported for $\Delta_{Zn}$-$[Zn_2\mathbf{L}^{\mathbf{a}}_3][ClO_4]_4$, *via* (*R*,*R*)-**3a** (Scheme 2.4);[1] allowing the components 2-pyridinecarboxaldehyde [**4**] (6 eq.), the appropriate diamine bridge [**3**] (3 eq.), and zinc(II) perchlorate hexahydrate (2 eq.) to self-assemble in acetonitrile at ambient temperature. Precipitation by addition of excess ethyl acetate and drying *in vacuo* gave the desired bimetallic species, with unoptimised yields of 50-80 %. These complexes were characterised by multinuclear NMR, mass spectroscopy, and microanalysis. Typical features of interest are discussed herein, with particular interest paid to those complexes where a single crystal suitable for XRD could be grown. It is worth noting that perchlorate salts pose an explosion risk, particularly when heated, and should therefore only used on a small scale and never exposed to excess heat.

### 2.3.1 Xylenyl & biphenyl linkers: $[Zn_2L^{a\text{-}d}_3][ClO_4]_4$

Before introducing new class Ia flexicates, it is useful to review the prototype assembly, $[Zn_2\mathbf{L}^{\mathbf{a}}_3][ClO_4]_4$ in the context of this chapter, as new structural comparisons can now be drawn.

The cationic unit of the complex comprises two octahedral metal centres of similar configuration to our earlier monometallic self-assembling systems,[8, 9] spanned by three *p*-xylenyl units. The crystal structure reported by Howson *et al.* (Figure 2.4) is intriguing for two main reasons (discussed below).

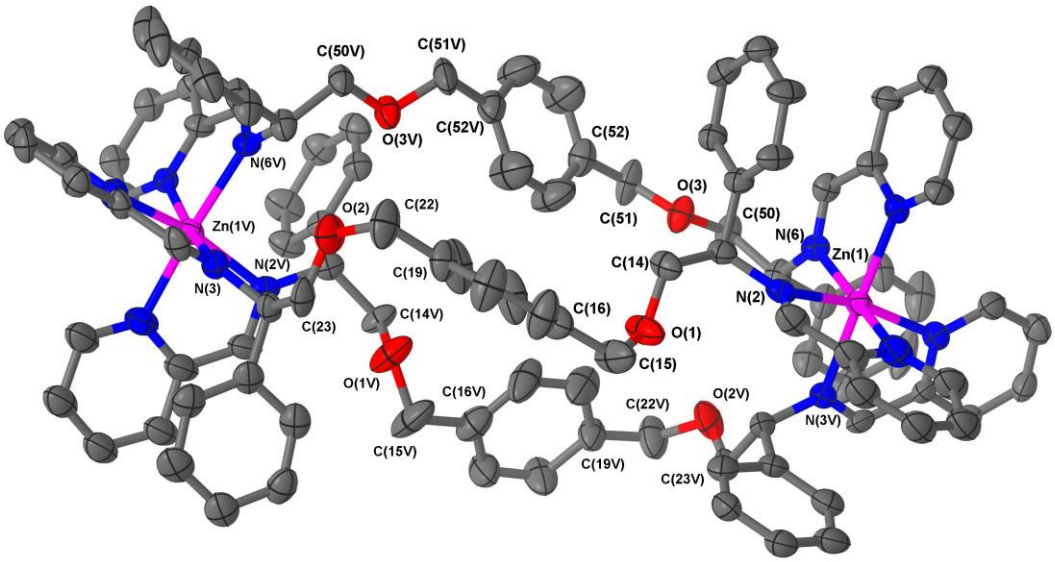


**Figure 2.4: Structure of the cationic unit in $\Delta_{Zn}$-$[Zn_2L^a_3][ClO_4]_4 \cdot 2CH_3CN \cdot 3H_2O \cdot ½CH_3OH$**, reproduced from the work of Howson *et al.*[1] Ellipsoids modelled at 50% probability. Hydrogen atoms, solvent molecules and counterions removed for clarity. Zn(II) ions are shown in pink, nitrogen atoms in blue, oxygen atoms in red, and carbon atoms in dark grey.

Firstly, the bridging groups are seen to deviate considerably from threefold symmetry. Two distinct orientations are observed; (i) bridges containing O(1) and O(2) are more folded, with acute torsion angles (<70°) at C(19)-C(22)-O(2)-C(23) and C(16)-C(15)-O(1)-C(14); (ii) the bridge containing O(3) in contrast traces effectively a linear transit between the Zn centres with a torsion angle at C(52)-C(51)-O(3)-C(50) of 173.9°. Nonetheless, the $[Zn_2\mathbf{L}^a_3]^{4+}$ complex is only slightly bent along the nominal $C_3$ axis, with the angle between the two imine N atom [N(2)-N(3)-N(6)] planes being 8.2°.

Secondly, although the complex displays overall axial chirality, the helicity of the bridging *p*-xylenyl groups opposes that of the metal coordination environments, giving a heterohelical structure. The pitch or 'twist' of the bridges along the nominal $C_3$ axis may be measured by taking the torsion angles between two Zn-N(imine) bonds of the same ligand, along the Zn-Zn axis [*e.g.* N(6V)-Zn(1V)-Zn(1)-N(6)]. It was found that for the two folded bridges, this angle was 20.3°, whereas the more linear bridge was rotated by 63.3°. These angles characterise this metallohelix as being not particularly

twisted at all. By comparison, the poly-bipyridine ligands of Lehn's archetypal Cu(I) helicate make ~180° rotation about the molecule's long axis, per additional metal unit.[12]

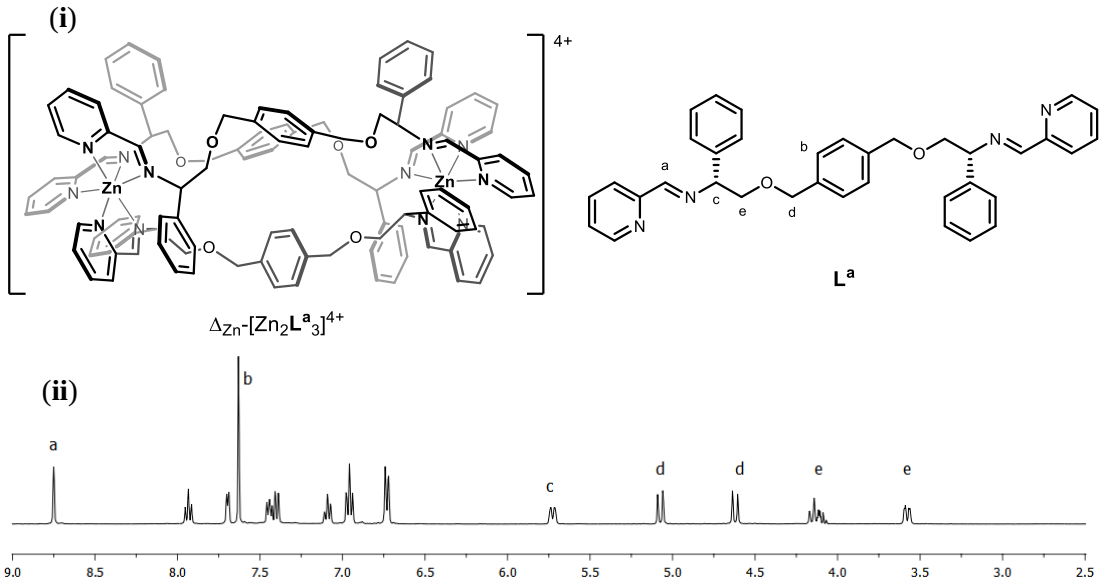


**Figure 2.5: $^1$H-NMR spectrum of $[Zn_2L^a_3][ClO_4]_4$:** (i) Structure of the assembled $\Delta_{Zn}$ flexicate (cationic unit) and its ligand, (*R,R*)-$\mathbf{L^a}$. (ii) The 400 MHz $^1$H-NMR spectrum of this flexicate, reproduced from the work of Howson *et al.* (recorded at 298 K in $d^3$-acetonitrile).

In contrast with the low symmetry structure of $[Zn_2\mathbf{L^a}_3]^{4+}$ observed in the solid state, the solution NMR spectra of $[Zn_2\mathbf{L^a}_3][ClO_4]_4$ (Figure 2.5) and the analogue $[Fe_2\mathbf{L^a}_3]Cl_4$ (Figure 2.15, *vide infra*) at room temperature indicate that the three ligands/bridges are equivalent on this timescale, suggesting either that the system is $D_3$ symmetric or, perhaps more likely, that a dynamic structure exists in solution. Overall, it is clear that the *p*-xylenyl bridge provided by $\mathbf{L^a}$ does not induce optimal topography in the bimetallic, *i.e.* this is not an ideal helicands for the class Ia flexicate system. Indeed, it was recognised in the first publication of this type of molecule that helication was not a requirement here for diastereomerically pure self-assembly – hence the name "flexicate" was coined for this type of metallohelical structure.

The *m*-xylenyl linkage of **3b** gave the new flexicate, $[Zn_2\mathbf{L^b}_3][ClO_4]_4$. As for $[Zn_2\mathbf{L^a}_3][ClO_4]_4$,[1] the $^1$H-NMR spectrum (Figure 2.6) of this complex is consistent with a threefold symmetric complex; only a single set of ligand peaks are present. A striking feature of the $^1$H-NMR spectrum of this complex is the strongly downfield-shifted singlet for the three isolated *m*-xylenyl protons which results from their orientation towards a deshielding environment at the centre of the complex (*vide infra*). This contrasts with the observations for a related *m*-xylenyl linked class Ib Zn(II) flexicate by Kaner *et al.*,[2] which gave a number of conformers associated with orientations of the bridging units.

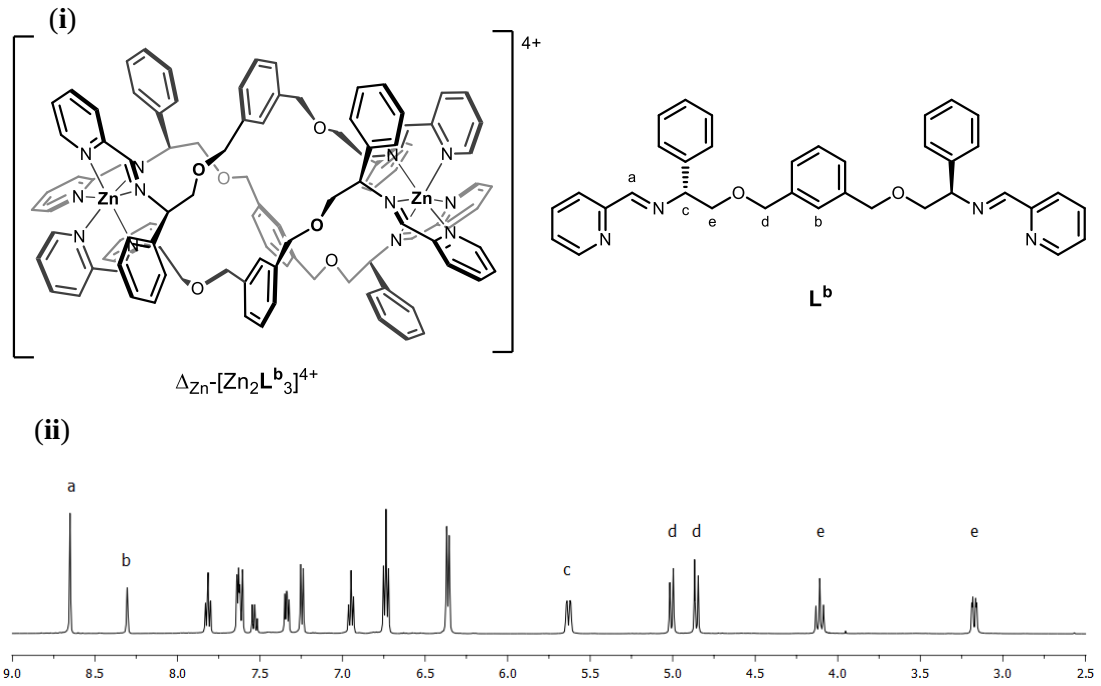


**Figure 2.6: $^1$H-NMR spectrum of $[Zn_2\mathbf{L^b}_3][ClO_4]_4$**: (i) Structure of the assembled $\Delta_{Zn}$ flexicate (cationic unit) and its ligand, (*R*,*R*)-**L$^b$;** (ii) 500 MHz $^1$H-NMR spectrum recorded in $d^3$-acetonitrile at 298 K.

Slow vapour diffusion of ethyl acetate into a concentrated acetonitrile solution of $\Delta_{Zn}$-$[Zn_2\mathbf{L^b}_3][ClO_4]_4$ afforded single crystals suitable for XRD.† The cationic unit of the

† Crystallographic data for this and other compounds discussed in this chapter were obtained and solved by Dr Guy Clarkson (University of Warwick). Tabulated crystallographic data for these complexes are included in the appendix.

compound, shown in Figure 2.7, crystallised in space group $P2_1$ along with four perchlorate counterions and two acetonitrile molecules. The octahedral Zn coordination environments of this structure are similar to those for $[Zn_2\mathbf{L}^{\mathbf{a}}{}_3][ClO_4]_4$ (*vide supra*) and all previous related structures, featuring the familiar inter-ligand $\pi$-$\pi$ stacking interactions.

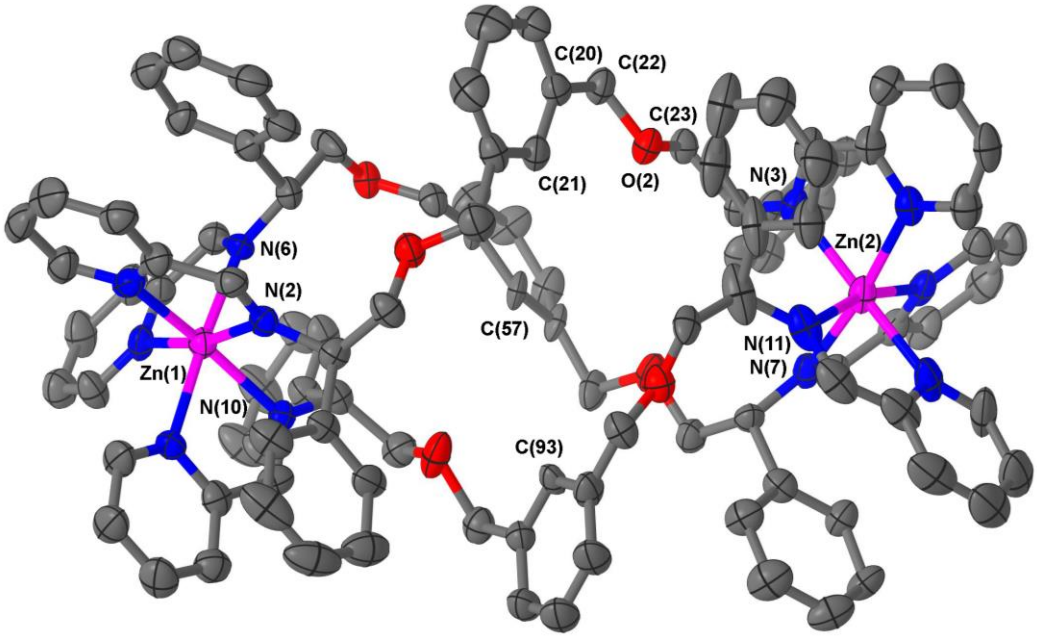


**Figure 2.7: Structure of the cation unit of $\Delta_{Zn}$-$[Zn_2L^b{}_3][ClO_4]_4\cdot 2CH_3CN$.** Ellipsoids modelled at 50% probability. Hydrogen atoms, solvent molecules and counterions removed for clarity. Zn(II) ions are shown in pink, nitrogen atoms in blue, oxygen atoms in red, and carbon atoms in dark grey.

The overall size and shape of $[Zn_2\mathbf{L}^{\mathbf{b}}{}_3]^{4+}$ is more markedly folded or "concertinaed" than $[Zn_2\mathbf{L}^{\mathbf{a}}{}_3]^{4+}$; the inter-metallic distance is substantially shortened (12.4 Å *vs.* 14.0 Å) while the circumference of the molecule is increased, as evidenced by the average distance between the centroids of each xylenyl aromatic ring: 7.6 Å, *vs.* 6.3 Å for $[Zn_2\mathbf{L}^{\mathbf{a}}{}_3]^{4+}$. Correspondingly the *m*-xylenyl bridge also folds with a more pronounced helical turn along the metal-metal axis: torsion angles between Zn-N(imine) bonds from the same ligand, along the Zn-Zn axis [*e.g.* N(6)-Zn(1)-Zn(2)-N(7)] range from 100.9° to 101.0°. It should be noted however that as with $[Zn_2\mathbf{L}^{\mathbf{a}}{}_3]^{4+}$ the *P*-helicity

generated by each $\Lambda_{Zn}$ centre is inverted at the *C*-stereogenic centre such that the bridge units fold with *M* helicity. Hence, the structure is homochiral, but not homohelical.[13]

The distortions from threefold symmetry observed in $[Zn_2\mathbf{L^a}_3]^{4+}$ are not so apparent in $[Zn_2\mathbf{L^b}_3]^{4+}$ and the conformations assumed by each $\mathbf{L^b}$ ligand are rather similar. For example all $C^{Ph}$-$CH_2$-O-$CH_2$ torsion angles [*e.g.* C(20)-C(22)-O(2)-C(23)], fall within the range 170-180°. The structure shows very slight bending along the nominal $C_3$ axis, with an angle between imine N atom planes [N(2)-N(6)-N(10) and N(3)-N(7)-N(11)] of 9.4°, comparable to $[Zn_2\mathbf{L^a}_3]^{4+}$.

The crystal structure of $[Zn_2\mathbf{L^b}_3][ClO_4]_4$ shows that all the *m*-xylenyl groups are oriented such that the C-H groups at C(21), C(57), and C(93) point towards the centre of the complex, in contrast to a structure detected in a related class Ib complex.[2] Since the plane of each xylenyl group intersects this cavity, the centre of the complex is expected to be a rather deshielding environment as a result of the coinciding ring currents. This explains the unusually downfield-shifted $^1$H-NMR signals for these H nuclei as shown in Figure 2.6.

In contrast to the above, the *o*-xylenyl system **3c** formed a mixture of products on treatment with aldehyde and zinc perchlorate (see Figure 2.8). Evidently while the ligand $\mathbf{L^c}$ is formed, it is not suitably configured to form a bimetallic complex.

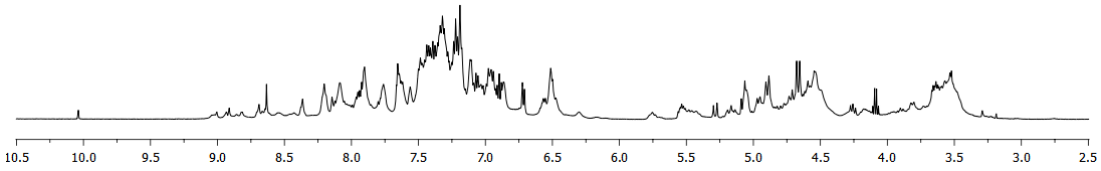


**Figure 2.8: $^1$H-NMR spectrum of the attempted synthesis of $[Zn_2L^c{}_3][ClO_4]_4$** recorded at 298 K in *d*$^3$-acetonitrile, using a 500 MHz spectrometer.

The biphenyl-linked diamine, **3d**, gave the flexicate $[Zn_2\mathbf{L}^{\mathbf{d}}{}_3][ClO_4]_4$. The $^1$H-NMR of this species shown in Figure 2.9 is consistent with the presence of a single, threefold symmetric complex.

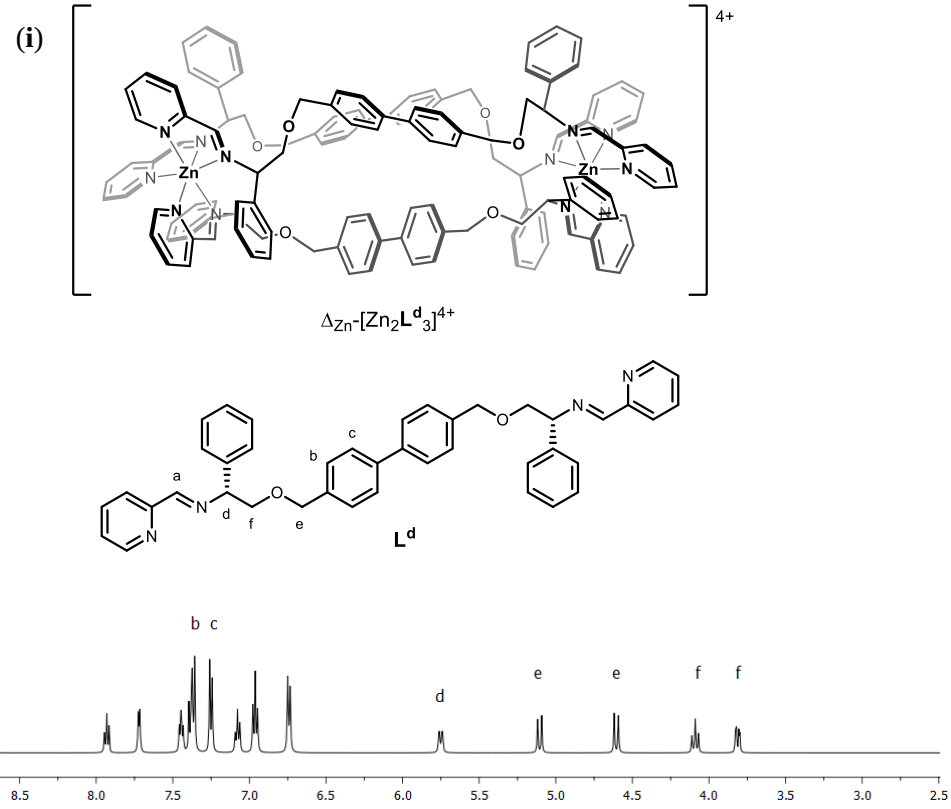


**Figure 2.9: $^1$H-NMR spectrum of $[Zn_2L^d{}_3][ClO_4]_4$**: (i) Structure of the assembled $\Delta_{Zn}$ flexicate (cationic unit) and its ligand, (*R*,*R*)-$\mathbf{L}^{\mathbf{d}}$**;** (ii) 500 MHz $^1$H-NMR spectrum recorded in *d*$^3$-acetonitrile at 298 K.

As may be expected given the structural similarity between 4,4'-substituted biphenyl and *p*-xylenyl linkers, the $^1$H-NMR spectrum of $[Zn_2\mathbf{L}^{\mathbf{d}}{}_3][ClO_4]_4$ bears a closer resemblance to the $^1$H-NMR spectrum of $[Zn_2\mathbf{L}^{\mathbf{a}}{}_3][ClO_4]_4$ (Figure 2.5) than of $[Zn_2\mathbf{L}^{\mathbf{b}}{}_3][ClO_4]_4$. The biphenyl protons can be discerned in that spectrum, as a pair of mutually coupled doublets.

### 2.3.2 Ar-E-Ar linkers: $[Zn_2L^{e\text{-}h}{}_3][ClO_4]_4$

Syntheses of Zn(II) flexicates $[Zn_2\mathbf{L}^{\mathbf{e\text{-}h}}{}_3][ClO_4]_4$ from diamine bridges **3e-h** were attempted. The $^1$H-NMR spectra of the resulting species are shown in Figure 2.10. The spectra of ether-linked $[Zn_2\mathbf{L}^{\mathbf{e}}{}_3][ClO_4]_4$, thioether-linked $[Zn_2\mathbf{L}^{\mathbf{f}}{}_3][ClO_4]_4$, and methylene-linked $[Zn_2\mathbf{L}^{\mathbf{g}}{}_3][ClO_4]_4$ indicate the presence of effectively a single conformer in each case. However, the spectrum of ethylene-linked $[Zn_2\mathbf{L}^{\mathbf{h}}{}_3][ClO_4]_4$ is marked out by the presence of numerous minor peaks alongside a series of major peaks corresponding to the target threefold symmetric flexicate.

The effect of temperature upon the mixture present in $[Zn_2\mathbf{L}^{\mathbf{h}}{}_3][ClO_4]_4$ was investigated through the use of variable temperature $^1$H-NMR studies. Spectra obtained in the temperature range 253 to 333 K (-20 to 60 °C), are shown in Figure 2.11. At 253 K one major species with signals corresponding to the target threefold symmetric flexicate is apparent. Notably, the imine region shows three small peaks in the approximate ratio 1:1:1 (as indicated in Figure 2.11), which could indicate the presence of a minor species with three inequivalent sets of imine units.

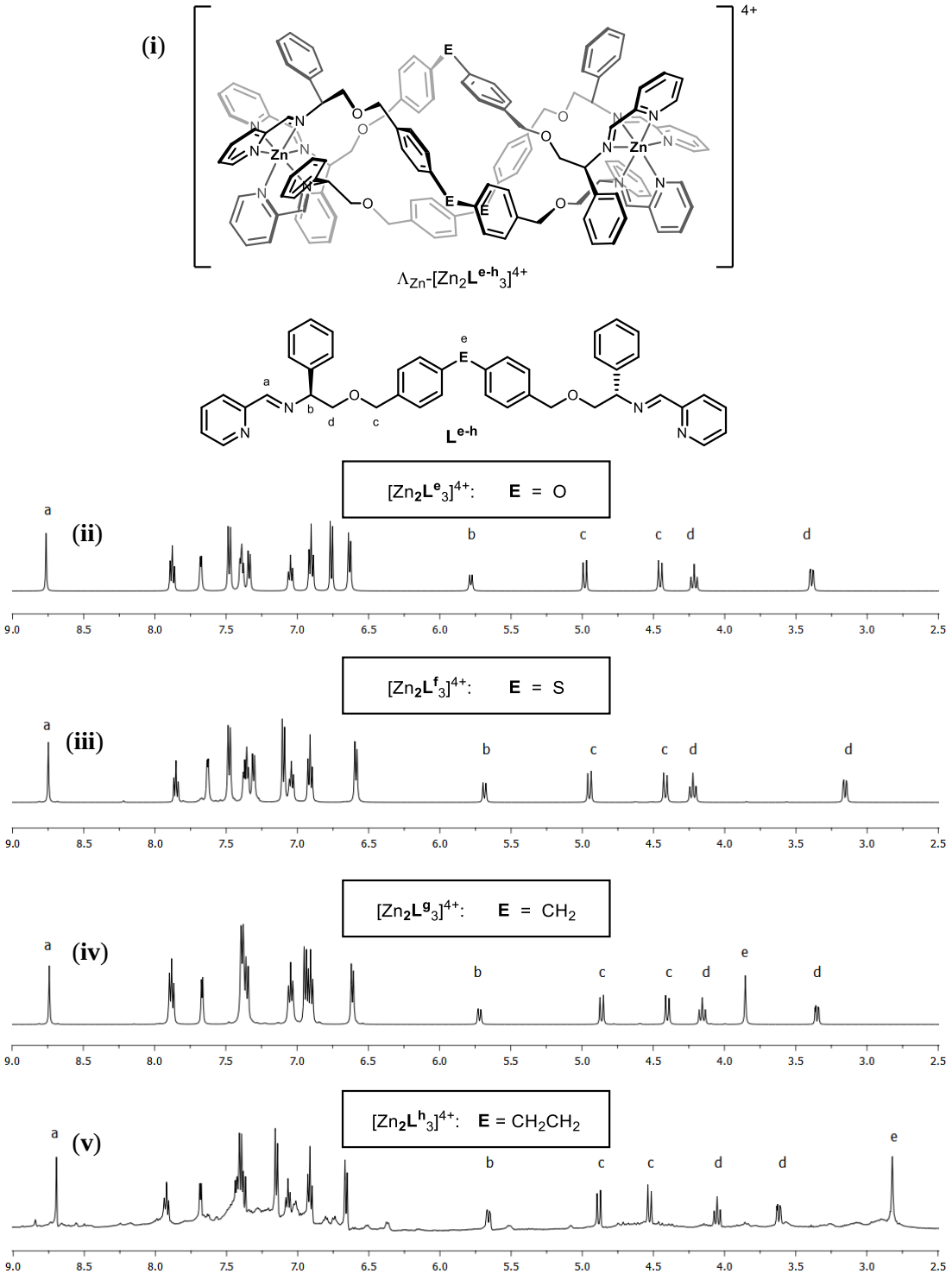


**Figure 2.10: $^1$H-NMR spectra of $[Zn_2L^{e\text{-}h}{}_3][ClO_4]_4$:** (i) Generic structure ($\Lambda_{Zn}$ cationic unit) for these assembled flexicates and the generic structure [(*S*,*S*) isomer] of their ligands [$\mathbf{L^{e\text{-}h}}$]; $^1$H-NMR spectra of (ii) $[Zn_2\mathbf{L^e}_3][ClO_4]_4$; (iii) $[Zn_2\mathbf{L^f}_3][ClO_4]_4$; (iv) $[Zn_2\mathbf{L^g}_3][ClO_4]_4$; (v) nominally $[Zn_2\mathbf{L^h}_3][ClO_4]_4$. Spectra recorded in *d*$^3$-acetonitrile at 298 K, using a 500 MHz spectrometer.

Other less well resolved minor peaks are also present. With increasing temperature these peaks broaden and increase in intensity relative to the imine peak for the major product, and by 333 K the lower symmetry compound is probably the most abundant.

There is also a pronounced broadening of peaks attributed to the higher symmetry species. These observations indicate that the two species are in equilibrium and that the rate of exchange increases with temperature, although even at 333 K, the rate is relatively slow on the NMR chemical shift timescale. It is worth noting that we cannot exclude the presence of species containing tetrahedral Zn(II) centres, since these would also be diamagnetic, although we have never observed such compounds previously in studies of this ligand type.

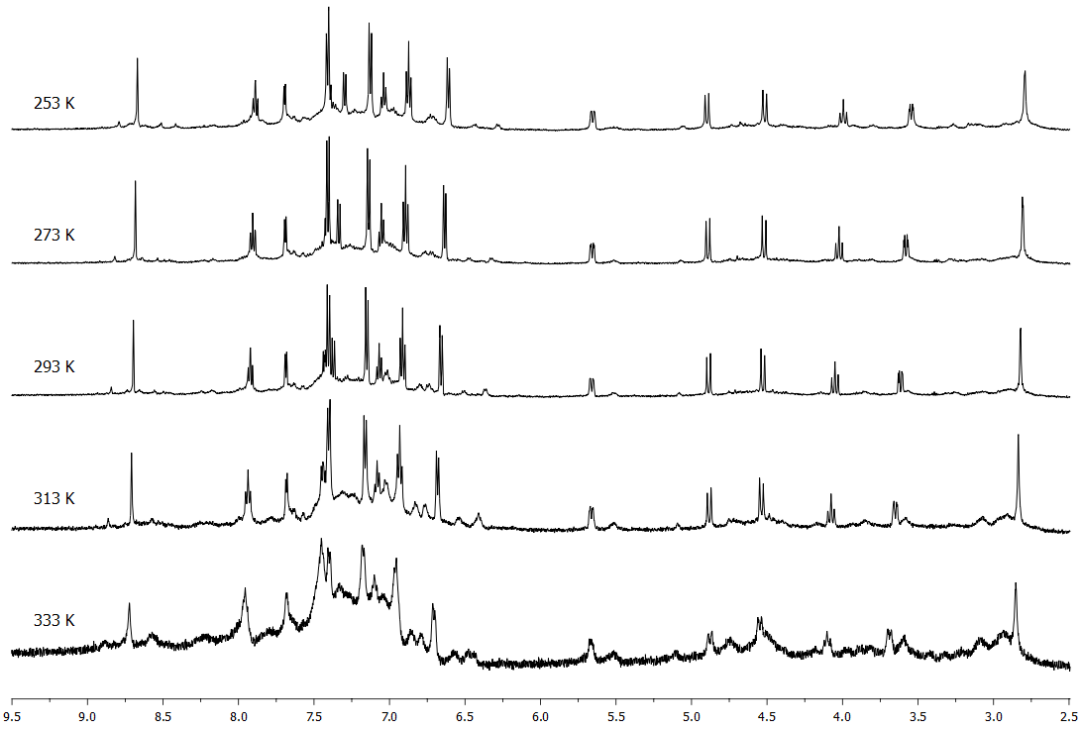


**Figure 2.11: Variable temperature $^1$H-NMR spectra of $[Zn_2L^h_3][ClO_4]_4$** in $d^3$-acetonitrile. Spectra recorded at 20 K increments from 253 K (-20 °C) to 333 K (60 °C), using a 500 MHz spectrometer.

Slow diffusion of ethyl acetate into a concentrated acetonitrile solution of thioether-linked $[Zn_2\mathbf{L}^f_3][ClO_4]_4$, prepared by mixing samples of the two antipodes, afforded single crystals suitable for XRD. A structure belonging to the space group C2/*c* was obtained, with a unit cell containing four $\Lambda_{Zn,}$ and four $\Delta_{Zn}$ $[Zn_2\mathbf{L}^f_3]^{4+}$ complexes, along with four counterions, five water molecules, and six acetonitrile molecules per complex. The $\Lambda_{Zn}$ cationic unit observed in this structure, is shown in Figure 2.12.

Naturally, the longer bridge of $[Zn_2\mathbf{L}^{f}_3]^{4+}$ results in a longer complex than those xylenyl-linked examples discussed previously, with an inter-metal distance of 17.4 Å. Interestingly, the 'hinge' created by the sulfur atoms appears to aid the folding process by allowing the bridge to arch outwards, with the two flanking *p*-tolyl units able to orient separately, and furthermore allowing the bridge a remarkable twist along the metal-metal axis: torsion angles between Zn-N(imine) bonds from the same ligand range 167.3° to 179.1°. As a consequence of this arching of the bridge the sulfur atoms protrude from the helix and the system appears to have a larger circumference than earlier examples (S-S distances range 8.0 Å to 9.2 Å). The moderate variation in S-S distances of $[Zn_2\mathbf{L}^{f}_3]^{4+}$ are consistent with a slightly anisotropic structure, perhaps due in part to the bulkiness of the sulfur atoms, which could make a more symmetric arrangement sterically challenging.

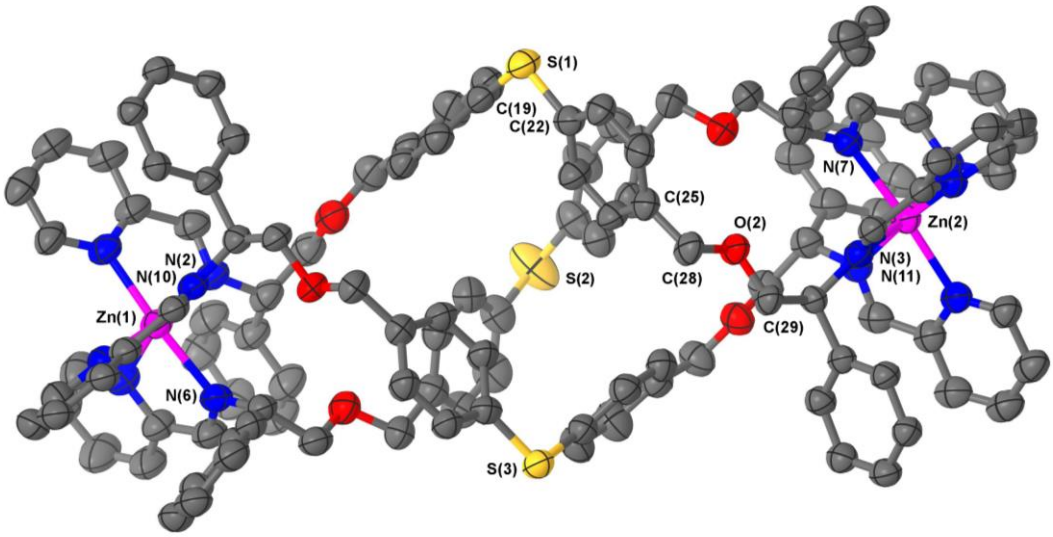


**Figure 2.12: Structure of the $\Lambda_{Zn}$ cation unit of $[Zn_2L^{f}_3][ClO_4]_4\cdot 6CH_3CN\cdot 5H_2O$.** Ellipsoids modelled at 50% probability. Hydrogen atoms, solvent molecules and counterions removed for clarity. Zn(II) ions are shown in pink, nitrogen atoms in blue, oxygen atoms in red, sulfur atoms in yellow, and carbon atoms in dark grey.

The structure does not appear to be distorted significantly from threefold symmetry; the C-S-C bond angles [*e.g.* C(19)-S(1)-C(22)] fall within a narrow range (103-104°), virtually identical to that measured for diphenyl sulphide.[14] The $C^{Ph}$-$CH_2$-O-$CH_2$

torsion angles [*e.g.* C(25)-C(28)-O(2)-C(29)] range from 162° to 171°; slightly lower than the essentially antiperiplanar arrangement in *meta*-bridged $[Zn_2\mathbf{L}^{\mathbf{b}}{}_3]^{4+}$ and within a smaller range than observed in the distorted structure, $[Zn_2\mathbf{L}^{\mathbf{a}}{}_3]^{4+}$. An angle between imine *N*-atom planes [N(2)-N(6)-N(10) and N(3)-N(7)-N(11)] of 9.9° (comparable to $[Zn_2\mathbf{L}^{\mathbf{a\text{-}b}}{}_3]^{4+}$ structures) is also supportive there being little torsional strain in this complex.

### 2.3.3 Dibenzofuran linker: $[Zn_2L^{i}{}_3][ClO_4]_4$

The (2,8-substituted) dibenzofuran linkage incorporated *via* **3i** gave flexicate $[Zn_2\mathbf{L}^{\mathbf{i}}{}_3][ClO_4]_4$, the $^1$H-NMR spectrum of which is shown in Figure 2.13.

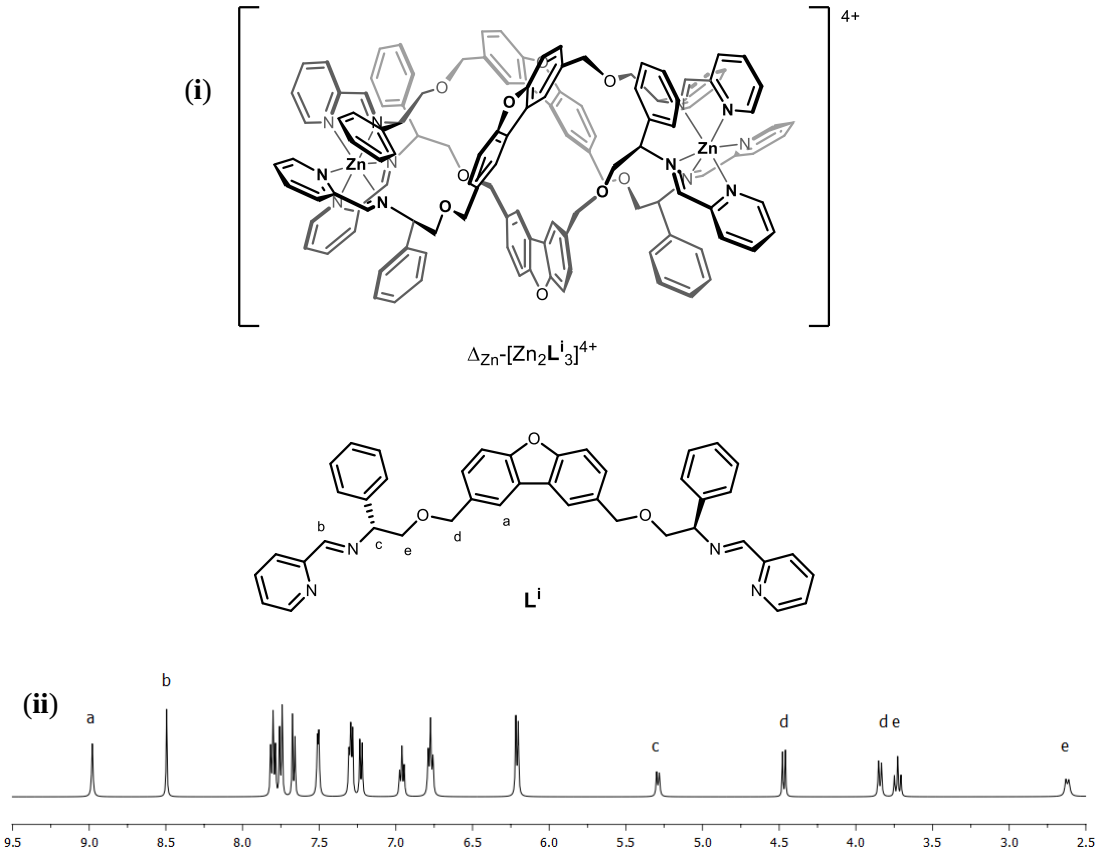


**Figure 2.13: $^1$H-NMR spectrum of $[Zn_2L^{i}{}_3][ClO_4]_4$**: (i) Structure of the assembled $\Delta_{Zn}$ flexicate (cationic unit) and its ligand, (*R*,*R*)-$\mathbf{L}^{\mathbf{i}}$; (ii) 500 MHz $^1$H-NMR spectrum recorded in $d^3$-acetonitrile at 298 K.

In the $^{1}$H-NMR spectrum of $[Zn_2\mathbf{L}^{\mathbf{i}}{}_3][ClO_4]_4$, resonance for the dibenzofuran 1- and 9-H atoms **a** (Figure 2.13) appears at 9.0 ppm *c.f.* 7.8 ppm in the amine **3i** (recorded in $CDCl_3$). This large downfield shift arises, as in $[Zn_2\mathbf{L}^{\mathbf{b}}{}_3][ClO_4]_4$ above, because these groups are directed toward the centre of the assembly. An additional similarity to the spectrum of $[Zn_2\mathbf{L}^{\mathbf{b}}{}_3][ClO_4]_4$ is that large chemical shift differences were observed within each pair of diastereotopic methylene protons **d** and **e**.

Slow diffusion of ethyl acetate into a concentrated acetonitrile solution of racemic $[Zn_2\mathbf{L}^{\mathbf{i}}{}_3][ClO_4]_4$, prepared by mixing samples of the two antipodes, afforded single crystals suitable for XRD. The compound crystallised in the space group P-1 and the unit cell contains two $\Lambda_{Zn,}$ and two $\Delta_{Zn}$ $[Zn_2\mathbf{L}^{\mathbf{i}}{}_3]^{4+}$ complexes, counterions, four acetonitrile and six water molecules. The $\Delta_{Zn}$ cationic unit is shown in Figure 2.14.

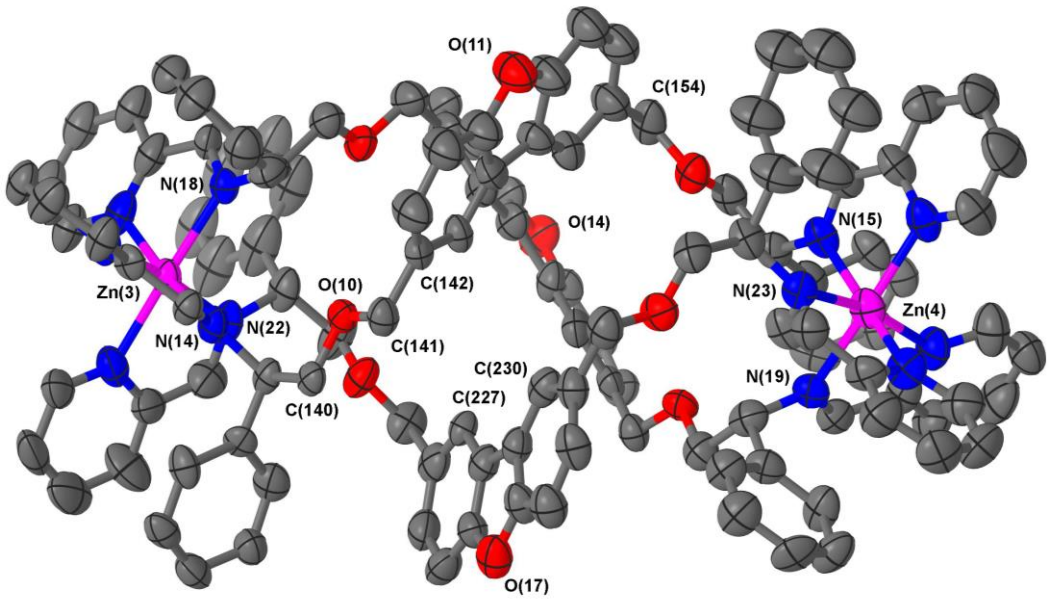


**Figure 2.14: Structure of the $\Delta_{Zn}$ cation unit of $[Zn_2L^{i}{}_3][ClO_4]_4{\cdot}CH_3CN{\cdot}1.5H_2O$.** Ellipsoids modelled at 50% probability. Hydrogen atoms, solvent molecules and counterions removed for clarity. Zn(II) ions are shown in pink, nitrogen atoms in blue, oxygen atoms in red, and carbon atoms in dark grey.

The intermetallic distance in $[Zn_2\mathbf{L}^{\mathbf{i}}{}_3]^{4+}$ of 14.4 Å is rather smaller than that observed in the related structure $[Zn_2\mathbf{L}^{\mathbf{f}}{}_3]^{4+}$ (17.4 Å), corresponding to a more compact concertina fold. Correspondingly the circumference is slightly larger, with distances

between 'apex' O atoms [O(11), O(14) and O(17)] falling into a narrow range (9.9-10.1 Å). These three atoms form an approximate equilateral triangle, indicating high symmetry of the system. There is also a lack of distortion arising from ring strain: each $C^{Ph}$-$CH_2$-O-$CH_2$ torsion angle [*e.g.* C(142)-C(141)-O(10)-C(140)] falls into the range 173-180° (effectively antiperiplanar). As alluded to above, one consequence of this efficient helication is that the CH groups at C(227) and C(230) are directed inwards leading to a strong downfield shift in the $^1$H-NMR spectrum. In addition, the angle between imine N atom planes [N(2)-N(6)-N(10) and N(3)-N(7)-N(11)] is exceptionally shallow at 3.3°. Torsion angles between Zn-N(imine) bonds from the same ligand, along the Zn-Zn axis range 159.8° to 162.5°, greater than $[Zn_2\mathbf{L}^{\mathbf{b}}{}_3]^{4+}$ and less than $[Zn_2\mathbf{L}^{\mathbf{f}}{}_3]^{4+}$, however this in line with $[Zn_2\mathbf{L}^{\mathbf{i}}{}_3]^{4+}$ having the intermediate inter-metal distance of the three.

## 2.4 New Water-Soluble Fe(II) Flexicates

Water compatible systems suitable for antimicrobial screening were prepared by self-assembly using adaptations of the method previously reported (Scheme 2.4).[1] In all cases, enantiomers $[Fe_2\mathbf{L}_3]Cl_4$ were synthesised by heating 2-pyridinecarboxaldehyde [**4**] (6 eq.) and the appropriate diamine bridge [**3**] (3 eq.) with anhydrous iron(II) chloride (2 eq.) under reflux in methanol. Upon removal of volatiles under reduced pressure, the desired bimetallic product was obtained in high yield. The NMR spectra of $[Fe_2\mathbf{L}^{\mathbf{a}}{}_3]Cl_4{\cdot}6H_2O$[1] obtained in this way are shown in Figure 2.15.

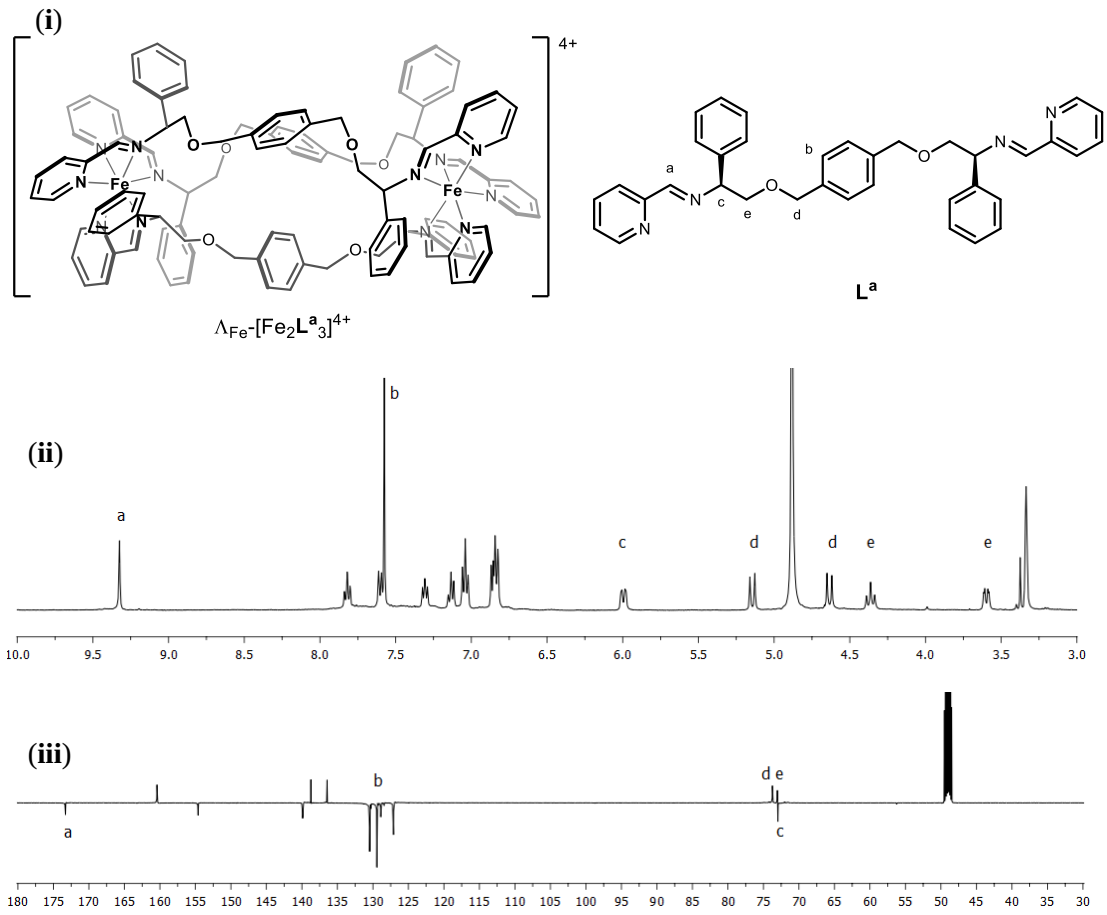


**Figure 2.15: NMR spectra of $[Fe_2L^a_3]Cl_4 \cdot 6H_2O$:** (i) Structure of the assembled $\Lambda_{Fe}$ flexicate (cationic unit) and its ligand, (*S*,*S*)-$\mathbf{L}^a$; (ii) 400 MHz $^1$H-NMR spectrum, showing the presence of water at 4.87 ppm; (iii) 100 MHz $^{13}C\{^1H\}$-NMR spectrum. Spectra recorded in *d*$^4$-methanol ($\delta_H$ 3.31, $\delta_C$ 49) at 298 K.

New $[Fe_2\mathbf{L}_3]Cl_4$ complexes were characterised *via* multinuclear NMR techniques, mass spectrometry, circular dichroism (CD) spectroscopy, microanalysis, thermo-gravimetric analysis (TGA), IR and UV-visible spectroscopies. In addition, experiments were conducted to assess the suitability of these complexes as antimicrobial candidates, *e.g.* aqueous stability studies. Key observations, typical of this class, are included in this chapter. Full characterisation data sets are included in Chapter 6.

### 2.4.1 Structure

$^{1}$H and $^{13}$C NMR spectra of $[Fe_2\mathbf{L}_3]Cl_4$ species were similar to their $[Zn_2\mathbf{L}_3][ClO_4]_4$ counterparts, suggesting strong structural similarity. Typically, $^{1}$H-NMR spectra were slightly broader and contain a large peak at 4.87 ppm due to the presence of water of crystallisation. The NMR spectra of $[Fe_2\mathbf{L}^{\mathbf{b}}_3]Cl_4$ are shown in Figure 2.16.

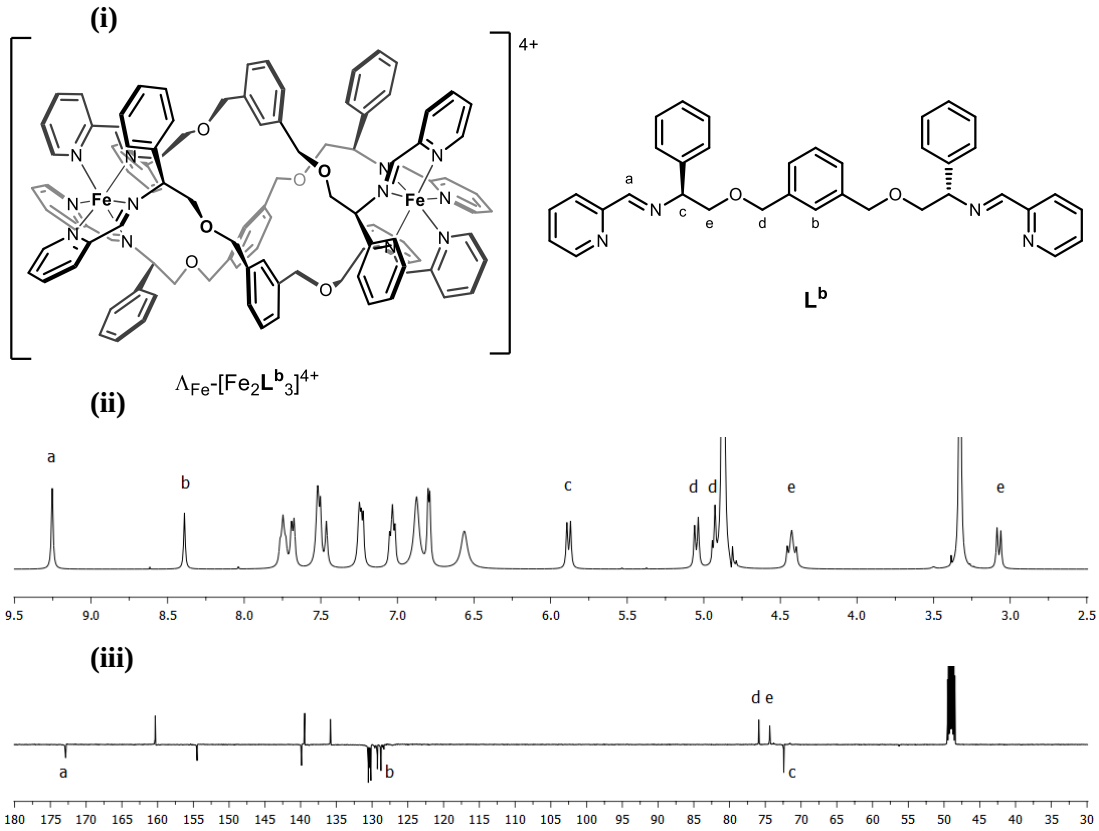


**Figure 2.16: NMR spectra of $[Fe_2\mathbf{L}^{\mathbf{b}}_3]Cl_4\cdot 6.5H_2O$:** (i) Structure of the assembled $\Lambda_{Fe}$ flexicate (cationic unit) and its ligand, (*S*,*S*)-$\mathbf{L}^{\mathbf{b}}$; (ii) 400 MHz $^{1}$H-NMR spectrum, showing the presence of water at 4.87 ppm; (iii) 100 MHz $^{13}$C{$^{1}$H}-NMR spectrum. Spectra recorded in *d*$^{4}$-methanol ($\delta_H$ 3.31, $\delta_C$ 49) at 298 K.

As for $[Zn_2\mathbf{L}^{\mathbf{c}}_3][ClO_4]_4$, the *o*-xylenyl bridged complex, $[Fe_2\mathbf{L}^{\mathbf{c}}_3]Cl_4$, could not be isolated.

Whilst NMR spectra of $[Fe_2\mathbf{L}^{\mathbf{h}}_3]Cl_4$ did not appear to be as complicated as its Zn(II) analogue, the $^{1}$H-NMR spectrum of this species was significantly broader than other compounds described in this section, although all peaks were in the usual ppm range

and few impurities were detected (Figure 2.17). The $^{13}$C-NMR spectrum was assigned readily.

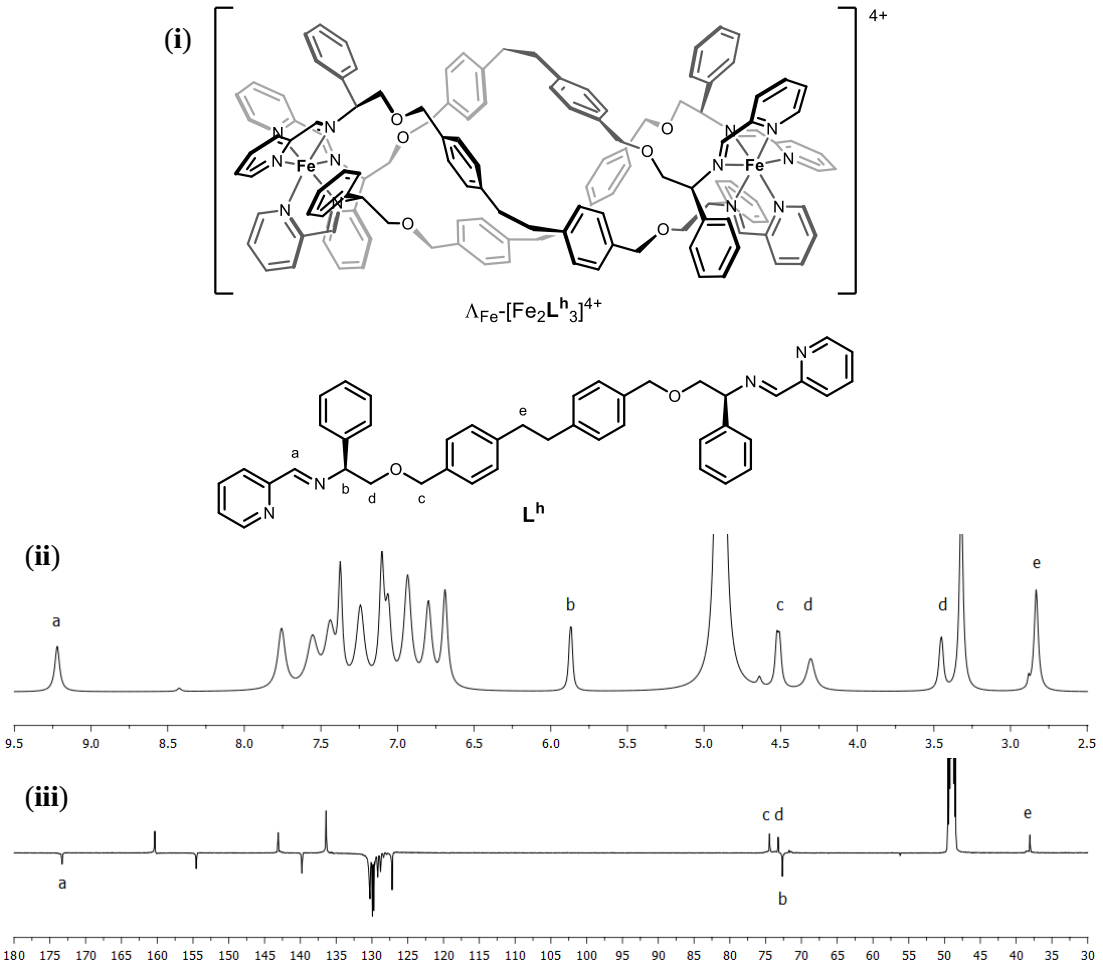


**Figure 2.17: NMR spectra of [Fe$_2$L$^h_3$]Cl$_4$·11.5H$_2$O:** (i) Structure of the assembled $\Lambda_{Fe}$ flexicate (cationic unit) and its ligand, (*S*,*S*)-**L$^h$**; (ii) 400 MHz $^1$H-NMR spectrum, showing the presence of water at 4.87 ppm; (iii) 100 MHz $^{13}$C{$^1$H}-NMR spectrum. Spectra recorded in *d*$^4$-methanol ($\delta_H$ 3.31, $\delta_C$ 49) at 298 K.

With the exception of [Fe$_2$**L**$^c_3$]Cl$_4$, each [Fe$_2$**L**$_3$]Cl$_4$ Ia flexicate gave excellent electrospray-ionisation mass spectrometry (ESI-MS) data, whereby the [Fe$_2$**L**$_3$]$^{4+}$ complex could easily be discriminated. This is in contrast to the [Zn$_2$**L**$_3$]$^{4+}$ counterparts, where the tetracation was typically not observed by the same method. For example, $\Lambda_{Fe}$-[Fe$_2$**L**$^h_3$]Cl$_4$ gave a strong peak of m/z 521.9, corresponding to the molecular ion. High resolution ESI-MS analysis of this complex shown in Figure 2.18 revealed that the isotopic peaks contributing to this signal are separated by ~0.25 mass

units, confirming a tetracationic charge and thus the dinuclear structure, as opposed to *e.g.* 8+ charged tetrahedral assemblies.[15, 16]

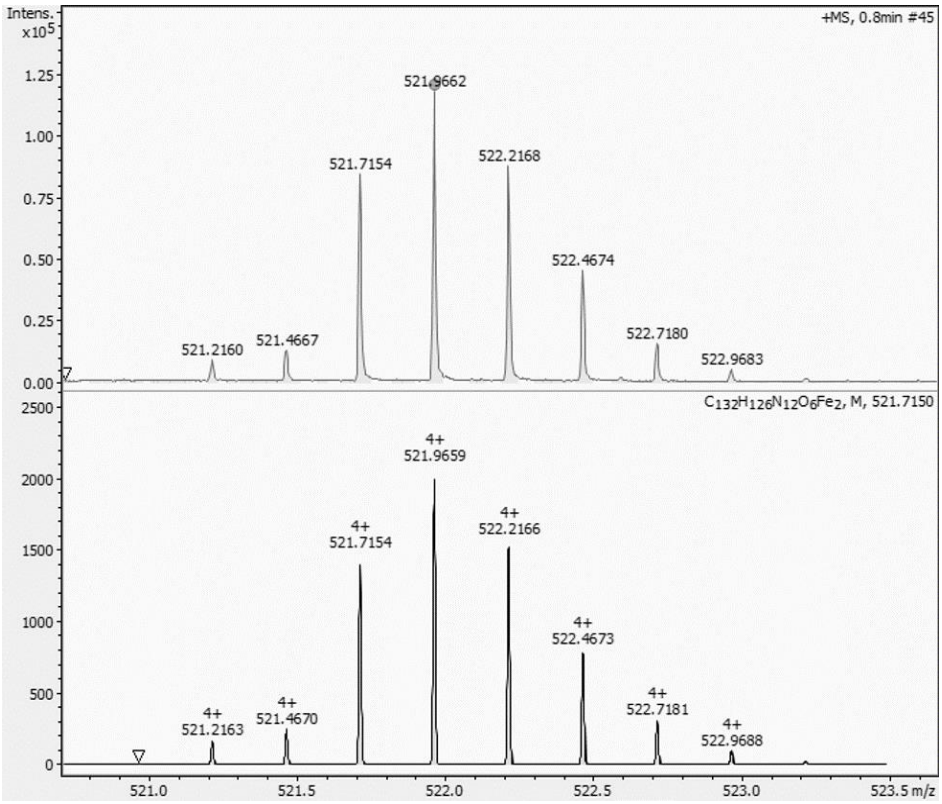


**Figure 2.18: High-resolution ESI mass spectrum of $\Lambda_{Fe}$-$[Fe_2L^h_3]Cl_4$** (top) focusing on the peak corresponding to the $[Fe_2\mathbf{L}^h_3]^{4+}$ ion. For comparison, a simulated mass spectrum of a $[Fe_2\mathbf{L}^h_3]^{4+}$ ion assuming natural isotopic abundance (bottom), is also shown over the same m/z range.

Circular dichroism spectra of pairs of flexicate enantiomers were recorded in water at a flexicate concentration of 0.03 mM. In each case it was found that these pairs of spectra were of equal magnitude, but of opposite sign to one another (*i.e.* a reflection in the horizontal axis), confirming that the flexicates are indeed produced in non-racemic pairs of opposite configurations,[17] as might be expected given the aforementioned optical purity of the incorporated diamines (section 2.2.4). The superimposed spectra of $\Lambda_{Fe}$- and $\Delta_{Fe}$-$[Fe_2\mathbf{L}^b_3]Cl_4$ are typical in this respect, and are shown in Figure 2.19 as an illustrative example.

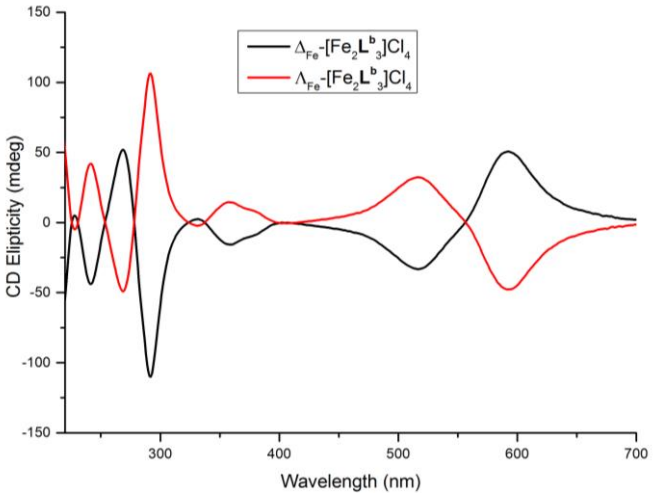


**Figure 2.19: Superimposed CD spectra of [$Fe_2L^b_3$]$Cl_4$ enantiomers**, showing them to be of equal magnitude and opposite sign. Both taken at a concentration of 0.03 mM in water.

## 2.4.2 Water of Crystallisation

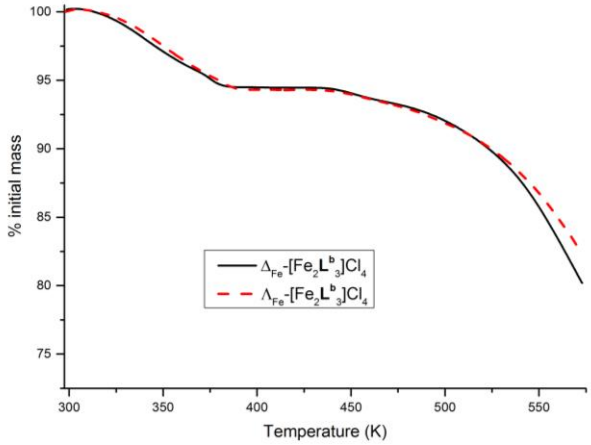


**Figure 2.20: Thermogravimetric analyses of both [$Fe_2L^b_3$]$Cl_4$·6.5$H_2O$ enantiomers,** indicating a characteristic drop in mass as water of crystallisation is lost.

The presence of water molecules in the [$Fe_2$**L**$_3$]$Cl_4$ formulations is evident from the broad O-H stretching modes observed in FTIR spectra and the aforementioned strong $H_2O$ peak in the $^1$H-NMR spectra. Quantification of this water of crystallisation is necessary in order to deduce correct formula weights when calculating molarities, for example in spectroscopic and biomedical assays. In order to determine the water of

crystallisation present with sufficient accuracy, two principal techniques were used in tandem; microanalysis and thermogravimetric analysis (TGA).

TGA data showed a significant mass loss between ambient temperature and 450 K, consistent with the loss of water of crystallisation, before further mass loss at higher temperature. The mass loss demonstrated by TGA, is shown for both $[Fe_2\mathbf{L^b}_3]Cl_4$ enantiomers in Figure 2.20. In that example, approximately 5.8 % of the mass (corresponding to 6.5 water molecules), is lost before the mass remaining reaches a plateau at around 400 K. It was found that these mass losses observed by TGA correlated well with the water of crystallisation predicted by microanalysis data, within the error limits of the two measurements. Microanalysis data for both $[Fe_2\mathbf{L^b}_3]Cl_4$ enantiomers is shown in Table 2.1, where the formulation $[Fe_2\mathbf{L^b}_3]Cl_4{\cdot}6.5H_2O$ (predicted by TGA) fits well with this data.

| Complex | % C | % H | % N |
|---|---|---|---|
| $Fe_2C_{108}H_{102}N_{12}O_6Cl_4{\cdot}6.5H_2O$ | 63.75 | 5.70 | 8.28 |
| $\Delta_{Fe}$-$[Fe_2\mathbf{L^b}_3]Cl_4{\cdot}6.5H_2O$ | 63.66 | 5.83 | 8.09 |
| $\Lambda_{Fe}$-$[Fe_2\mathbf{L^b}_3]Cl_4{\cdot}6.5H_2O$ | 64.08 | 5.68 | 7.98 |

**Table 2.1: Theoretical and recorded microanalysis data for $[Fe_2L^b_3]Cl_4{\cdot}6.5H_2O$ enantiomers.**

### 2.4.3 Aqueous solubility and stability

The solubility and stability of test compounds in aqueous media are important considerations in the planning and interpretation of biomedical experiments. All $[Fe_2\mathbf{L}_3]Cl_4$ flexicates displayed excellent aqueous solubility, however, in more complex aqueous media such as those used in microbiology, precipitation occurred at higher flexicate concentrations, especially for larger complexes, such as the systems $[Fe_2\mathbf{L^{d\text{-}h}}_3]Cl_4$. Therefore, where concentrated stock solutions were required (*e.g.* for

microbiological assays), those solutions were supplemented with methanol (typically 10 % vol.).

In order to assess the stability of flexicates in water, a panel of five flexicates was chosen and each made up to 50 μM in water and incubated for 28 days at 37 °C (average healthy human body temperature, and a commonly used temperature in biomedical experiments). The concentration of flexicate present was monitored at various time points by measuring the absorbance at a wavelength of 573 nm, corresponding to the peak maxima of the flexicate metal-to-ligand charge transfer (MLCT) band; an absorbance that is distinct and unique to the complex. The results are plotted graphically in Figure 2.21. It is obvious from this absorbance-time dependence data that $[Fe_2\mathbf{L}^{a}{}_3]Cl_4$ and $[Fe_2\mathbf{L}^{h}{}_3]Cl_4$ are relatively unstable in water, and this could be verified visually as the two initially purple solutions became pale yellow by the conclusion of the experiment.

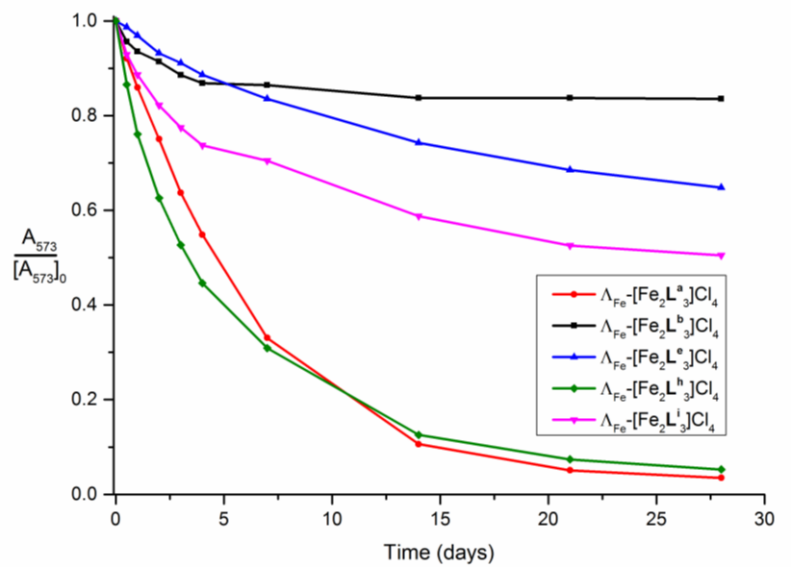


**Figure 2.21: Decomposition of flexicates in water at 37 °C**, from an initial concentration of 0.05 mM. Monitored using the absorbance at λ = 573 nm. Data sets normalised using the initial value ($A_{573}$ at t = 0).

Flexicates $[Fe_2\mathbf{L}^{e}{}_3]Cl_4$, $[Fe_2\mathbf{L}^{i}{}_3]Cl_4$, and particularly $[Fe_2\mathbf{L}^{b}{}_3]Cl_4$, were relatively stable. The cause of this difference is likely a result of the structure and rigidity of the

cation, as observations made of $[Zn_2\mathbf{L}_3][ClO_4]_4$ analogues marked $\mathbf{L^a}$ and $\mathbf{L^h}$ systems as being particularly asymmetric and dynamic, whereas $\mathbf{L^b}$ and $\mathbf{L^i}$ systems were especially rigid. Nonetheless, each of the flexicates analysed were largely intact (>85 %) after 24 hours.

First-order kinetics appear to be the most common rate laws encountered in stability studies,[18] whereby the loss of the starting material may be described using a simple exponential decay model (equation 2.1) containing two parameters; the initial quantity at t = 0 (denoted $[A]_0$ here), and the rate constant, k.

$$[A] = [A]_0 e^{-kt} \qquad \text{Equation 2.1}$$

Whereas $[A]_0$ is effectively an arbitrary choice made as part of the experimental setup, k is dependent on the stability of the compound under the conditions applied (solvent, temperature, *etc.*) and is the parameter that determines the half-life of the compound, as equation 2.1 can be manipulated in order to express the half-life ($t_{1/2}$) as a function where k is the only variable (equation 2.2).

$$t_{1/2} = \frac{\ln(2)}{k} \qquad \text{Equation 2.2}$$

The first-order model described by equation 2.1 could be iteratively fitted to the decay profiles of $[Fe_2\mathbf{L^a}_3]Cl_4$ and $[Fe_2\mathbf{L^h}_3]Cl_4$, with minimal remaining residual error ($R^2$ > 0.97), in spite of the fact that the model does not account for absorptions caused by the breakdown products which accumulate over the course of hydrolysis. Rate constants, half-lives and coefficient of determination ($R^2$) values for these models are tabulated in Table 2.2. OriginPro 9.1 software was used in fitting the model and calculating the parameters obtained. The exponential decay model could not be accurately fitted to the hydrolysis data of $[Fe_2\mathbf{L^{b/e/i}}_3]Cl_4$, however.

| **Complex** | **Apparent rate constant** ($day^{-1}$) | **Half-life** (days) | $\mathbf{R^2}$ |
|---|---|---|---|
| $\Lambda_{Fe}$-$[Fe_2\mathbf{L}^{a}{}_3]Cl_4$ | **0.152** ± 0.005 | **4.549** ± 0.142 | **0.99** |
| $\Lambda_{Fe}$-$[Fe_2\mathbf{L}^{h}{}_3]Cl_4$ | **0.198** ± 0.027 | **3.500** ± 0.473 | **0.98** |

**Table 2.2: Parameters obtained from the fitting of a First-order decay model (equation 2.1) to the hydrolysis data of $[Fe_2L^{a}{}_3]Cl_4$ and $[Fe_2L^{h}{}_3]Cl_4$.** Rate constants and half-lives are shown with 95 % confidence intervals. The R-squared curve-fitting statistic is quoted to two decimal places.

Complexes $[Fe_2\mathbf{L}^{b/e/i}{}_3]Cl_4$ do appear to decay exponentially initially, but this slows or even halts at roughly 5-7 days; preventing the complexes from achieving 50 % loss over the course of the experiment, making a comprehensive analysis difficult. Analysis of the solutions after the conclusion of the experiment showed that there had been negligible fluctuation in the pH of these solutions throughout the duration of the experiment. However, as the solutions were sealed in order to prevent evaporation, there may have been a depletion of molecular oxygen, which may be necessary in breaking down the complexes *via* oxidative routes. It could therefore be postulated that $[Fe_2\mathbf{L}^{b/i}{}_3]Cl_4$ require oxidative processes to occur in order for aqueous decomposition to proceed at an appreciable rate, though further investigation would be necessary in order to better understand the potential role of molecular oxygen in the aqueous decomposition of $[Fe_2\mathbf{L}_3]Cl_4$ class Ia flexicates.

Ultimately, the process of aqueous decomposition for a multi-component, self-assembled system is understandably a rather complex process, requiring several steps and perhaps alternative competing routes (*e.g.* ligand dissociation, oxidation), each of which could conceivably occur at different rates, and be individually influenced by a variety of factors.

## 2.5 Summary

The progress in diamine design/synthesis described in this chapter allowed the development of a diverse range of new class Ia flexicates, and these have in turn been critical in understanding the effect the incorporated linker unit has upon the structure and assembly of the metallohelix. The improved synthetic route proved to be straightforward and easily adapted, making it foreseeably useful in any future investigation.

While we know that helication[19] is not a requirement for formation of the flexicate structures, it is perhaps not surprising to observe that some linker units work slightly against the helicity arising from the metal coordination units. This tends to cause distortion and asymmetry in the structures (*e.g.* $[Zn_2\mathbf{L^a}_3]^{4+}$,[1] $[Zn_2\mathbf{L^d}_3]^{4+}$, and certain class Ib systems[2]). In contrast, for the current compounds *m*-xylenyl-bridged $\mathbf{L^b}$ and dibenzofuran-bridged $\mathbf{L^i}$ appear to be excellent helicands for the formation of class Ia flexicates. This is evidenced in the resistance of flexicates $[Fe_2\mathbf{L^b}_3]Cl_4$ and $[Fe_2\mathbf{L^i}_3]Cl_4$ to aqueous decomposition, and the higher symmetry and large helical twist per unit of inter-metal distance that are observed in their $[Zn_2\mathbf{L}_3][ClO_4]_4$ crystal structures, noting the order obtained: $[Zn_2\mathbf{L^i}_3]^{4+}$ (11.2° Å$^{-1}$) > $[Zn_2\mathbf{L^f}_3]^{4+}$ (10.0° Å$^{-1}$) > $[Zn_2\mathbf{L^b}_3]^{4+}$ (8.1° Å$^{-1}$) >> $[Zn_2\mathbf{L^a}_3]^{4+}$ (2.5° Å$^{-1}$).

Given the similarity in configuration between the linker units of $\mathbf{L^b}$ and $\mathbf{L^i}$, it is unsurprising that they have a similar effect on the geometry of the class Ia flexicates. Both linkers are effectively planar (dihedral angles between dibenzofuran aromatic ring planes are less than 6.5°) and the substituent $C^{Ar}$-$CH_2$ bonds subtend angles of approximately 93.5° for 2,8-dibenzofuran,[20] and 120° for *m*-xylenyl. As a result these linkers are both rigid and introduce a slight fold to the ligand. However, as this fold

becomes very sharp (*o*-xylenyl), the result is a poor helicand, $\mathbf{L^c}$. It is likely that this sharper fold allows the ligand ready access to tetradentate binding modes (*i.e.* chelating a single metal centre), and would also disfavour the formation of $[M_2\mathbf{L}_3]^{4+}$ systems for steric and electrostatic reasons in bringing the two metal centres much closer together than in the *p*- or *m*-xylenyl bridged systems.

Class Ia flexicates with Ar-E-Ar linkers, where E is a single-atom connector, appeared to make reasonably effective helicands, *e.g.* note the aqueous stability of ether-linked $[Fe_2\mathbf{L^e}_3]Cl_4$. However, if this central group is 1,2-ethylene, the resulting ligand ($\mathbf{L^h}$) is much more flexible due to the ability to rotate about the ethylene C-C bond, which allows access to a range of Ar-$CH_2$-$CH_2$-Ar conformations - from linear (*trans*-like) to the sharply bent (*cis*-like). As a result of the increased flexibility in $\mathbf{L^h}$, the complex formed with Zn(II) exists as a number of species in solution, albeit with the threefold symmetric species being dominant at room temperature. Whilst the $[Fe_2\mathbf{L^h}_3]Cl_4$ complex did appear to be threefold symmetric by $^1$H-NMR, broad signals suggest there may be some dynamic processes occurring within the structure. A dynamic class Ia structure is reminiscent of observations made of the class Ia prototype, $[Fe_2\mathbf{L^a}_3]Cl_4$, and it is therefore unsurprising that both of these flexicates displayed relatively poor aqueous stability compared to other class Ia flexicates.

## 2.6 References for Chapter 2


1. S. E. Howson, A. Bolhuis, V. Brabec, G. J. Clarkson, J. Malina, A. Rodger and P. Scott, *Nat. Chem.*, 2012, 4, 31-36.

2. R. A. Kaner, S. J. Allison, A. D. Faulkner, R. M. Phillips, D. I. Roper, S. L. Shepherd, D. H. Simpson, N. R. Waterfield and P. Scott, *Chem. Sci.*, 2016, 7, 951-958.

3. A. D. Faulkner, R. A. Kaner, Q. M. A. Abdallah, G. Clarkson, D. J. Fox, P. Gurnani, S. E. Howson, R. M. Phillips, D. I. Roper, D. H. Simpson and P. Scott, *Nat. Chem.*, 2014, 6, 797-803.

4. H. C. Aspinall, N. Greeves, W. M. Lee, E. G. McIver and P. M. Smith, *Tetrahedron Lett.*, 1997, 38, 4679-4682.

5. S. Yao and K. D. Belfield, *J. Org. Chem.*, 2005, 70, 5126-5132.

6. S. Yao, H. Y. Ahn, X. H. Wang, J. Fu, E. W. Van Stryland, D. J. Hagan and K. D. Belfield, *J. Org. Chem.*, 2010, 75, 3965-3974.

7. F. G. Bordwell, *Acc. Chem. Res.*, 1988, 21, 456-463.

8. S. E. Howson, L. E. N. Allan, N. P. Chmel, G. J. Clarkson, R. van Gorkum and P. Scott, *Chem. Commun.*, 2009, 1727-1729.

9. S. E. Howson, L. E. N. Allan, N. P. Chmel, G. J. Clarkson, R. J. Deeth, A. D. Faulkner, D. H. Simpson and P. Scott, *Dalton Trans.*, 2011, 40, 10416-10433.

10. C. Piguet, G. Bernardinelli and G. Hopfgartner, *Chem. Rev.*, 1997, 97, 2005-2062.

11. D. J. Fox, S. Parris, D. S. Pedersen, C. R. Tyzack and S. Warren, *Org. Biomol. Chem.*, 2006, 4, 3108-3112.

12. J. M. Lehn, A. Rigault, J. Siegel, J. Harrowfield, B. Chevrier and D. Moras, *Proc. Natl. Acad. Sci. USA*, 1987, 84, 2565-2569.

13. S. E. Howson, G. J. Clarkson, A. D. Faulkner, R. A. Kaner, M. J. Whitmore and P. Scott, *Dalton Trans.*, 2013, 42, 14967-14981.

14. B. Rozsondai, J. H. Moore, D. C. Gregory and I. Hargittai, *Acta Chim. Hung.*, 1977, 94, 321-331.

15. P. Mal, B. Breiner, K. Rissanen and J. R. Nitschke, *Science*, 2009, 324, 1697-1699.

16. P. Mal and J. R. Nitschke, *Chem. Commun.*, 2010, 46, 2417-2419.

17. A. Rodger and B. Nordén, *Circular Dichroism and Linear Dichroism*, Oxford University Press, 1997.

18. Y. Qiu, Y. Chen, G. G. Z. Zhang, L. Liu and W. Porter, *Developing Solid Oral Dosage Forms: Pharmaceutical Theory and Practice*, Elsevier Science, 2009.

19. J. L. Atwood and J. M. Lehn, *Comprehensive Supramolecular Chemistry: Supramolecular reactivity and transport : bioinorganic systems*, Pergamon, 1996.

20. O. Dideberg, L. Dupont and J. M. Andre, *Acta Crystallogr. Sect. B: Struct. Sci.*, 1972, 28, 1002-1007.

# Chapter 3

# Evaluation of Antimicrobial Activity

## 3.1 Introduction

Characterising the susceptibility of bacteria to candidate antimicrobial compounds *in vitro* is an essential part of the early discovery process.[1] As outlined in Chapter 1, the assay commonly employed is the macro/microbroth dilution method for determination of minimum inhibitory concentration (MIC).[1-3] This standardised method exposes the test organism to an incremental series of antimicrobial concentrations (typically in the range 1-128 μg/ml or lower).[2, 4, 5] The MIC is defined as the lowest concentration required for complete inhibition of microbial growth over a set incubation period (typically 18-24 h). The MIC is also critical to the setup and/or interpretation of many other evaluations used to investigate antimicrobial activity (as will be described in this chapter).

In this chapter, the new water-soluble class Ia flexicates, *i.e.* $[Fe_2\mathbf{L}^{\mathbf{a\text{-}i}}{}_3]Cl_4$, are screened initially against a small panel of microbes. The most active compounds against Gram-negatives are tested against a larger panel of clinically relevant pathogens. Other evaluations that are relevant to the mode-of-action (MOA) and/or clinical use are undertaken;[1] (i) whether the complexes are bactericidal or bacteriostatic; (ii) the effect on membrane integrity; (iii) the influence on bacterial growth under various conditions; (iv) toxicity toward eukaryote models.

## 3.2 Initial Screening

### 3.2.1 Determination of MICs by broth microdilution: protocol optimisation

The method used in the Bolhuis laboratory (University of Bath) in a previous collaboration with the group was a useful starting point in developing our own protocols for determining MICs[6], especially as they made use of an appropriate growth medium specifically formulated for susceptibility testing: cation-adjusted Mueller-Hinton broth (CAMHB).[7] The constraints imposed upon the protocol to be used are that it must remain as true as possible to the standard procedure[2, 5] and that it ought to closely reproduce the MIC data reported for $[Fe_2\mathbf{L}^{\mathbf{a}}_3]Cl_4$, as well as known antimicrobials. Ideally, the protocol should also be high-throughput.

In order to create the range of solutions required, a 1280 μg/ml stock solution of the flexicate was prepared in water containing 10 % methanol by volume (in order to aid dissolution), which was diluted tenfold in CAMHB-culture as part of the assay to give the highest concentration tested, 128 μg/ml. This stock was repeatedly diluted twofold in CAMHB, allowing the standard 1-128 μg/ml range to be used in the assay, with ≤1 % methanol by volume remaining. Overnight cultures of either *E. coli* strain TOP10 (ATCC PTA-10989) or methicillin-resistant *S. aureus* strain USA300 (ATCC BAA-1717) in CAMHB were diluted in the same medium to an cell concentration of $5 \times 10^5$ cfu/ml. 200 μl of 9:1 microbial culture/flexicate dilution, or appropriate control, were laid out onto a sterile 96-well plate (as in Figure 3.1, for example). After a 20 h incubation at 37 °C with gentle shaking, the plates were visually inspected, in order to determine the MICs.

It was found that for $\Delta_{Fe}$-$[Fe_2\mathbf{L}^{\mathbf{a}}_3]Cl_4$ and $\Lambda_{Fe}$-$[Fe_2\mathbf{L}^{\mathbf{a}}_3]Cl_4$, MICs against *E. coli* TOP10 matched those reported against *E. coli* MC4100, and likewise MICs against

(MRSA) *S. aureus* USA300 corresponded with those reported for *S. aureus* MRSA252[6] (included as part of Table 3.1). These MICs determined from 200 µl cultures on a 96-well plate were consistent with those determined with 1 ml. This is advantageous as a 96-well plate format allows a higher throughput determination of MICs: four compound/strain combinations may be run in triplicate, across a seven-concentration range, with space for appropriate positive and negative controls respectively. An example of such a setup, where a single flexicate is screened against four strains is shown in Figure 3.1, where the demarcation between growth and inhibition, which marks out the MIC, can clearly be made out for each strain. Each plate was repeated to ensure that biological replicates were also performed as part of each determination.

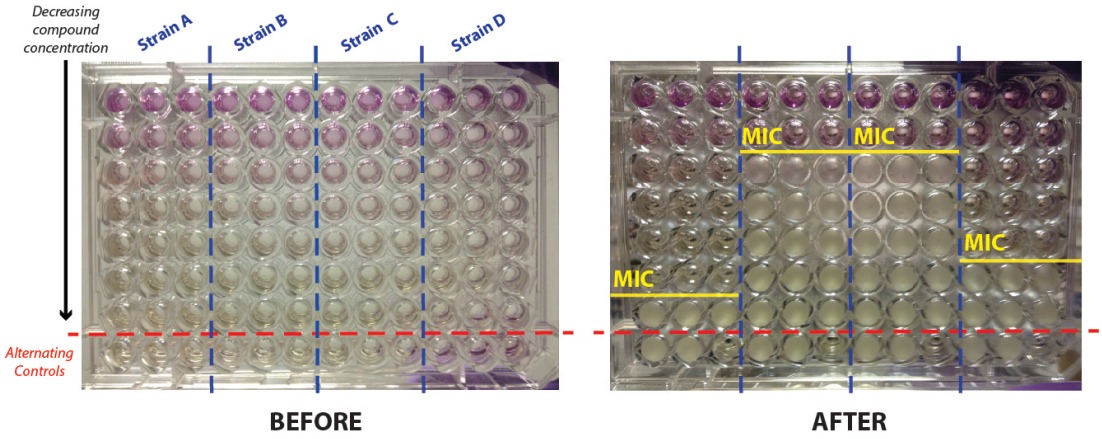


**Figure 3.1: Example of an MIC determination interpreted visually, using a 96-well plate**. Photographs taken before/after incubation have been annotated to show the setup and interpretation respectively. In this example a single flexicate has been tested at concentrations 128-2 µg/ml (descending down the plate) against four strains, each in triplicate. Here, MICs of 4 µg/ml (strain A), 64 µg/ml (strain B), 64 µg/ml (strain C), and 8 µg/ml (strain D) are assigned. Positive (culture only) and negative (medium only) controls have been used to validate results.

MICs were also determined from the 96-well plate setup by monitoring the optical density (turbidity) at a wavelength of 600 nm (commonly abbreviated '$OD_{600}$') at set time intervals, using a plate reader, so that growth curves for each condition could be plotted. This was especially useful in cases where the demarcation between growth

and inhibition was difficult to determine by visual inspection alone. However, the use of a plate reader reduces the turnover of the assay, since only one plate can be incubated/monitored at a time. Growth curves produced from the MIC determination of kanamycin against *E. coli* TOP10 are shown in Figure 3.2, where there is an obvious distinction between the weak growth observed at half the MIC, and complete inhibition at the MIC. For each microbial strain used in this chapter, MICs were determined against the known antimicrobials, kanamycin and tetracycline (see Table 3.1). These determined values closely corresponded to MICs reported for representative *E. coli* and *S. aureus* strains.[2]

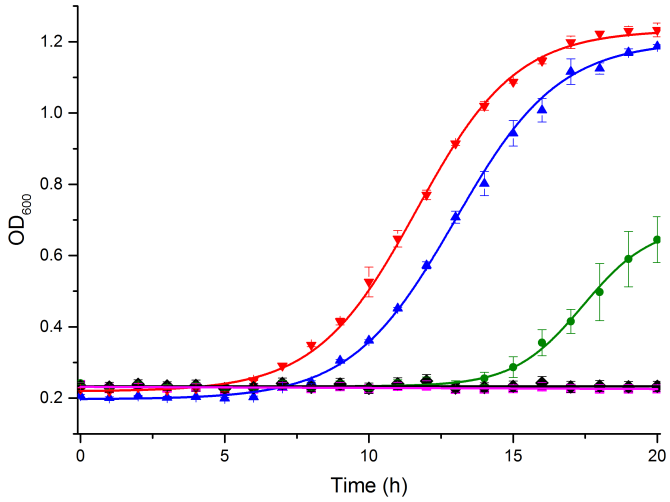


**Figure 3.2: MIC determination of kanamycin against *E. coli* TOP10, using growth curves.** The MIC of 2 µg/ml (pink squares), can be confirmed as this concentration has a 'growth' profile identical to that of the negative control (black diamonds), whereas the next lowest concentration of 1 µg/ml (green circles) shows weak growth. At 0.5 µg/ml (quarter the MIC, blue triangles), the growth approaches that of the positive control (red inverted triangles). Error bars representing 95 % confidence intervals, calculated using replicates, are shown.

### 3.2.2 MIC data and selectivity

Following the above assessment of the protocol and confirmation of the earlier results, a slightly expanded panel comprising two representative Gram-negative and two Gram-positive species, was chosen for the initial screen against the entire new class Ia flexicate library. To accompany the Gram negative model organism,[8] *E. coli*,

represented by the TOP10 strain, physiologically and genetically distinct *P. aeruginosa* (strain PAO1, ATCC 15692) was selected, due to its human pathogenicity and extensive inherent resistance to many established antimicrobials. This makes it a clinically relevant target.[9] To expand on the previous Gram-positive model (*S. aureus* USA300), *B. subtilis* (strain 168, ATCC 6051) was selected since it is also an extensively studied Gram-positive species with significantly different physiology (and no direct clinical relevance) that is genetically unrelated to *S. aureus.*[10]

The MICs determined against this panel of four microbial species are tabulated in Table 3.1. In addition to the water-soluble class Ia flexicates and antibiotic controls, representative subcomponents (*i.e.* starting materials and intermediates) of the flexicate systems were also screened against *E. coli* TOP10 and *S. aureus* USA300. Screening was not possible for the ligands and their corresponding diamines, due to their poor aqueous solubility.

Generally $\Lambda_{Fe}$ class Ia flexicates were more potent than their $\Delta_{Fe}$ counterparts, particularly against *E. coli*, though the differences were subtle *i.e.* 1-2 dilutions. This increased our confidence in the screening results since effectively pairs of independently synthesized compounds are being tested in parallel. This initial screen of class Ia flexicates demonstrates a range of activities, while notably we have recently shown that the related class Ib compounds have little if any antimicrobial activity.[6, 11]

| Group | Compound | MIC/ µg/ml (µM) | | | |
|---|---|---|---|---|---|
| | | *Gram positive* | | *Gram negative* | |
| | | ***S. aureus*** USA300 | ***B. subtilis*** 168 | ***E. coli*** Top10 | ***P. aeruginosa*** PAO1 |
| Class Ia Flexicates | $\Lambda_{Fe}$-[$Fe_2\mathbf{L}^{\mathbf{a}}_3$]$Cl_4$ | **8** (3.9) | **2** (1.0) | **4** (2.0) | **64** (31.3) |
| | $\Delta_{Fe}$-[$Fe_2\mathbf{L}^{\mathbf{a}}_3$]$Cl_4$ | **8** (3.9) | **1** (0.5) | **8** (3.9) | **128** (62.6) |
| | $\Lambda_{Fe}$-[$Fe_2\mathbf{L}^{\mathbf{b}}_3$]$Cl_4$ | **16** (7.9) | **4** (2.0) | **2** (1.0) | **>128** (>60) |
| | $\Delta_{Fe}$-[$Fe_2\mathbf{L}^{\mathbf{b}}_3$]$Cl_4$ | **16** (7.9) | **1** (0.5) | **4** (2.0) | **>128** (>60) |
| | $\Lambda_{Fe}$-[$Fe_2\mathbf{L}^{\mathbf{d}}_3$]$Cl_4$ | **32** (13.5) | **8** (3.4) | **64** (27.1) | **>128** (>60) |
| | $\Delta_{Fe}$-[$Fe_2\mathbf{L}^{\mathbf{d}}_3$]$Cl_4$ | **16** (6.8) | **8** (3.4) | **64** (27.1) | **>128** (>60) |
| | $\Lambda_{Fe}$-[$Fe_2\mathbf{L}^{\mathbf{e}}_3$]$Cl_4$ | **2** (0.8) | **1** (0.4) | **16** (6.7) | **128** (53.9) |
| | $\Delta_{Fe}$-[$Fe_2\mathbf{L}^{\mathbf{e}}_3$]$Cl_4$ | **16** (6.7) | **2** (0.8) | **32** (13.5) | **128** (53.9) |
| | $\Lambda_{Fe}$-[$Fe_2\mathbf{L}^{\mathbf{f}}_3$]$Cl_4$ | **16** (6.6) | **4** (1.6) | **64** (26.2) | **>128** (>60) |
| | $\Delta_{Fe}$-[$Fe_2\mathbf{L}^{\mathbf{f}}_3$]$Cl_4$ | **32** (13.1) | **8** (3.3) | **16** (6.6) | **>128** (>60) |
| | $\Lambda_{Fe}$-[$Fe_2\mathbf{L}^{\mathbf{g}}_3$]$Cl_4$ | **16** (6.6) | **8** (3.3) | **64** (26.6) | **>128** (>60) |
| | $\Delta_{Fe}$-[$Fe_2\mathbf{L}^{\mathbf{g}}_3$]$Cl_4$ | **16** (6.6) | **4** (1.7) | **32** (13.3) | **>128** (>60) |
| | $\Lambda_{Fe}$-[$Fe_2\mathbf{L}^{\mathbf{h}}_3$]$Cl_4$ | **32** (13.1) | **8** (3.3) | **64** (26.2) | **>128** (>60) |
| | $\Delta_{Fe}$-[$Fe_2\mathbf{L}^{\mathbf{h}}_3$]$Cl_4$ | **32** (13.1) | **8** (3.3) | **64** (26.2) | **>128** (>60) |
| | $\Lambda_{Fe}$-[$Fe_2\mathbf{L}^{\mathbf{i}}_3$]$Cl_4$ | **2** (0.8) | **2** (0.8) | **16** (6.6) | **128** (52.8) |
| | $\Delta_{Fe}$-[$Fe_2\mathbf{L}^{\mathbf{i}}_3$]$Cl_4$ | **2** (0.8) | **2** (0.8) | **16** (6.6) | **128** (52.8) |
| Antibiotics | Kanamycin | **1** (2.1) | **0.5** (1.0) | **2** (4.1) | **16** (33.0) |
| | Tetracycline | **0.5** (1.1) | **8** (18.0) | **1** (2.3) | **4** (9.0) |
| Components | Fe(II) gluconate | **>128** (>250) | | **>128** (>250) | |
| | Pyridine-2-carboxaldehyde | **>128** (>1000) | | **>128** (>1000) | |

**Table 3.1: *In vitro* antimicrobial activity (MICs) of class Ia flexicates** and controls against four bacterial strains. MICs quoted in µg/ml, and µM in parentheses.

In terms of Gram-negative activity, while no compounds showed significant activity against *P. aeruginosa*, $\Lambda_{Fe}$-[$Fe_2\mathbf{L}^{\mathbf{b}}_3$]$Cl_4$ slightly exceeded the potency of $\Lambda_{Fe}$-[$Fe_2\mathbf{L}^{\mathbf{a}}_3$]Cl against *E. coli* with MIC of 2 µg/ml - a result comparable to the established control antibiotics, despite the much higher molecular weight of the flexicate. Activity against and selectivity for Gram-negatives are desirable traits in anti-infective candidates since their outer membranes constitute a semi-permeable barrier (see Chapter 1 for more details), indicating lower membrane permeability and

antibiotic susceptibility, making them challenging therapeutic targets. Their restricted outer membrane permeability also often works in synergy with co-determinant resistance mechanisms, such as efflux mechanisms, to bring about antimicrobial resistance (AMR).[12] In contrast to the range of activities in *E. coli* and *S. aureus*, most complexes showed relatively high activity against *B. subtilis*, as discussed later in this chapter.

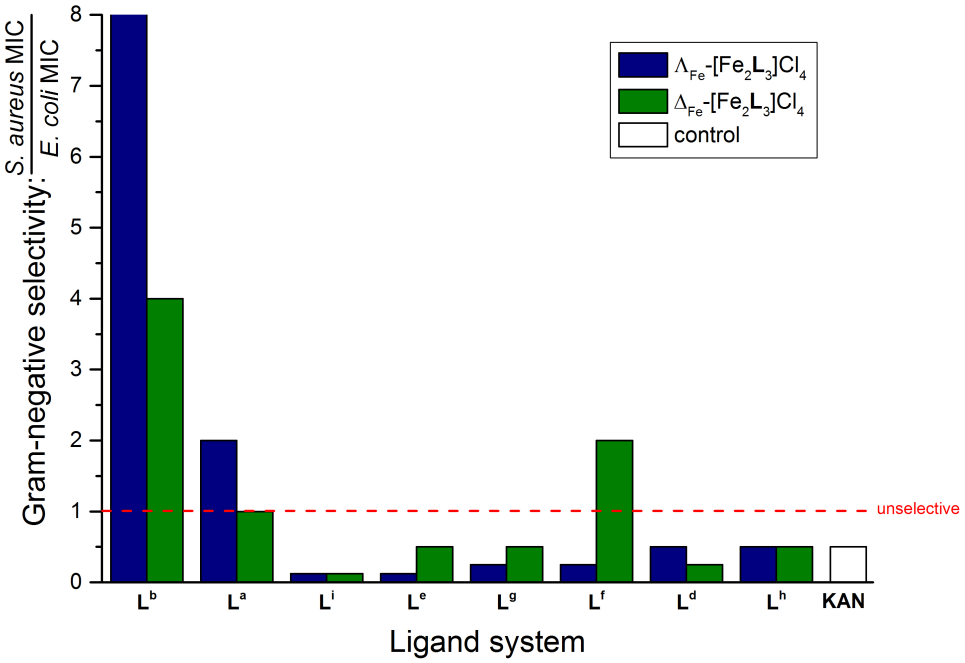


**Figure 3.3: Gram-negative selectivity [*S. aureus* MIC/*E. coli* MIC] of class Ia flexicates** ordered in the *x*-axis by intermetallic distance (increasing left to right). A selectivity ratio of one, *i.e.* where there is no selectivity for either organism, is marked as a dashed red line. Kanamycin (KAN) is included for reference.

In an attempt to assess and compare Gram-negative/Gram-positive selectivity, the ratios of the potency for each compound against *E. coli*/*S. aureus* are plotted in Figure 3.3. The complexes have been ordered in the *x*-axis according to their intermetallic distance using data from the crystal structures of the isostructural Zn(II) analogues (Chapter 2). It is apparent that the selectivity displayed by $\Lambda_{Fe}$-[Fe$_2$**L**$^{\mathbf{b}}$$_3$]Cl$_4$ is rather unique among the active compounds in the series. The compound $\Lambda_{Fe}$-[Fe$_2$**L**$^{\mathbf{a}}$$_3$]Cl$_4$ is the nearest competitor with a marginal selectivity for the Gram-

negative as previously reported.[6] The compound $\Delta_{Fe}$-$[Fe_2\mathbf{L}^{f}_3]Cl_4$ is reasonably selective but has low activity.

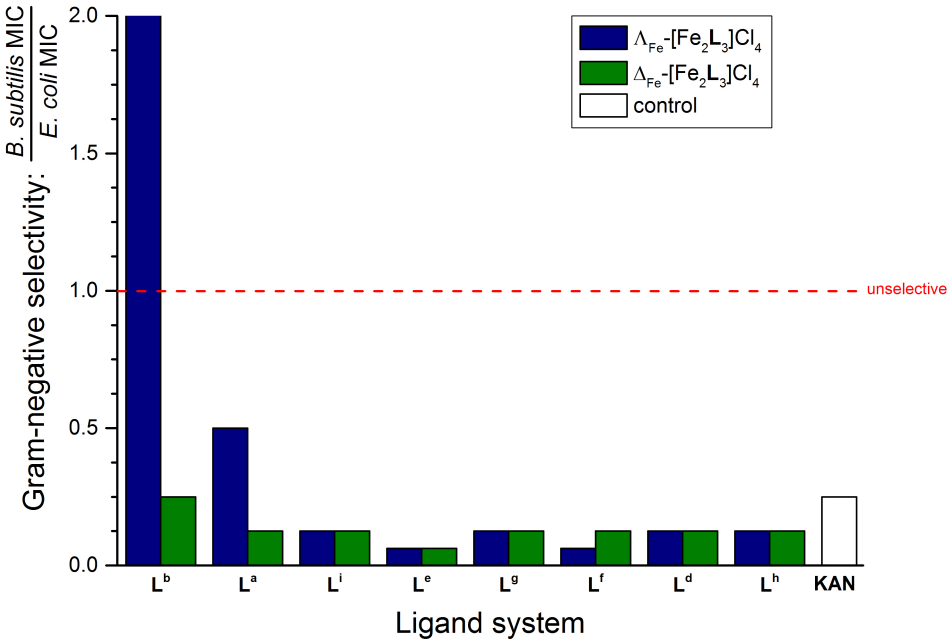


**Figure 3.4: Gram-negative selectivity [*B. subtilis* MIC/*E. coli* MIC] of class Ia flexicates** ordered by intermetallic distance (increasing left to right). A selectivity ratio of one, *i.e.* where there is no selectivity for either organism, is marked as a dashed red line. Kanamycin (KAN) is included in both graphs for reference.

Gram-negative selectivity may also be assessed by plotting the ratios of the MICs for each compound against *E. coli*/*B. subtilis*, as shown in Figure 3.4. In doing so, it would appear that most class Ia flexicates show a selectivity for Gram-positive *B. subtilis* over *E. coli*, however, it is likely that the low values of Gram-negative selectivity suggested by this ratio are predominantly a consequence of the broad antimicrobial sensitivity of *B. subtilis* in liquid.[13] Nevertheless, it serves to further illustrate the unique activity of $\Lambda_{Fe}$-$[Fe_2\mathbf{L}^{b}_3]Cl_4$ as the only compound with a lower MIC against *E. coli* TOP10 than *B. subtilis* 168.

In grouping complexes by size in Figures 3.3 and 3.4, it becomes apparent that there is stronger selectivity for *E. coli* amongst the short flexicates with xylyl bridges - particularly $\Lambda_{Fe}$-$[Fe_2\mathbf{L}^{b}_3]Cl_4$. It is also evident that in complexes $[Fe_2\mathbf{L}^{e}_3]Cl_4$ and

$[Fe_2\mathbf{L}^{i}_3]Cl_4$ where the ligand contains a central ether O atom protruding from the structure, that the selectivity is strongly reversed, making these examples quite Gram-positive selective by this metric. Much longer structures without protruding ether O atoms displayed both lower selectivity and very modest activity, making them poor antimicrobial candidates.

### 3.2.3 Microbial lethality

It is common practice to assess whether the antibacterial activity exhibited by a compound or class of compounds is predominantly bacteriostatic (reversible inhibition of bacterial growth), or bactericidal (bacterial killing). This is useful for judging clinical relevance and for understanding the MOA.[14, 15] For example, efforts made to understand the lethality of proposed Ru(II) antimicrobial metallodrugs were discussed in Chapter 1.[16, 17] The common method employed is to determine minimal bactericidal concentrations (MBCs), and to contrast these against the observed MICs. Such a determination is usually performed in the immediate aftermath of an MIC determination, whereby attempts are made to culture viable organisms that have been exposed to drug concentrations at and above the MIC, on an antimicrobial-free medium. The MBC is usually defined as the concentration where effective eradication (>99.9 %) of viable cells occurs.

MBCs were determined for class Ia flexicates against *E. coli* TOP10 and *S. aureus* USA300 (see Table 3.2), by attempting to recover viable cells by centrifugation from the relevant wells of a completed MIC determination assay, re-suspending the bacterial pellet in sterile phosphate buffered saline (PBS), and plating onto sterile lysogeny broth (LB) agar plates. After incubating these plates overnight at 37 °C, the lowest concentration where viable cells could not be recovered was determined to be

the MBC. Flexicates gave MBC/MIC ratios mostly in the range 1-2 against both species, making these complexes by definition, bactericidal (MBC/MIC ≤ 4).[1]

| Compound | *S. aureus* USA300 | | *E. coli* Top10 | |
|---|---|---|---|---|
| | **MBC** (μg/ml) | MBC / MIC | **MBC** (μg/ml) | MBC / MIC |
| $\Lambda_{Fe}$-[$Fe_2$**L**$^{a}_3$]$Cl_4$ | **16** | 2 | **8** | 2 |
| $\Delta_{Fe}$-[$Fe_2$**L**$^{a}_3$]$Cl_4$ | **16** | 2 | **16** | 2 |
| $\Lambda_{Fe}$-[$Fe_2$**L**$^{b}_3$]$Cl_4$ | **32** | 2 | **8** | 4 |
| $\Delta_{Fe}$-[$Fe_2$**L**$^{b}_3$]$Cl_4$ | **32** | 2 | **16** | 4 |
| $\Lambda_{Fe}$-[$Fe_2$**L**$^{d}_3$]$Cl_4$ | **32** | 1 | **64** | 1 |
| $\Delta_{Fe}$-[$Fe_2$**L**$^{d}_3$]$Cl_4$ | **32** | 2 | **64** | 1 |
| $\Lambda_{Fe}$-[$Fe_2$**L**$^{e}_3$]$Cl_4$ | **2** | 1 | **32** | 2 |
| $\Delta_{Fe}$-[$Fe_2$**L**$^{e}_3$]$Cl_4$ | **16** | 1 | **32** | 1 |
| $\Lambda_{Fe}$-[$Fe_2$**L**$^{f}_3$]$Cl_4$ | **16** | 1 | **128** | 2 |
| $\Delta_{Fe}$-[$Fe_2$**L**$^{f}_3$]$Cl_4$ | **32** | 1 | **32** | 2 |
| $\Lambda_{Fe}$-[$Fe_2$**L**$^{g}_3$]$Cl_4$ | **32** | 2 | **64** | 1 |
| $\Delta_{Fe}$-[$Fe_2$**L**$^{g}_3$]$Cl_4$ | **16** | 1 | **64** | 2 |
| $\Lambda_{Fe}$-[$Fe_2$**L**$^{h}_3$]$Cl_4$ | **32** | 1 | **64** | 1 |
| $\Delta_{Fe}$-[$Fe_2$**L**$^{h}_3$]$Cl_4$ | **32** | 1 | **128** | 2 |
| $\Lambda_{Fe}$-[$Fe_2$**L**$^{i}_3$]$Cl_4$ | **2** | 1 | **32** | 2 |
| $\Delta_{Fe}$-[$Fe_2$**L**$^{i}_3$]$Cl_4$ | **8** | 4 | **32** | 2 |

**Table 3.2: *In vitro* bactericidal activity (MBCs) of class Ia flexicates** against *E. coli* TOP10 and *S. aureus* USA300. MBCs quoted in μg/ml, and as a multiple of the corresponding MIC.

In order to investigate the rate of bacterial killing, time-kill curves were plotted, following a similar method to that described by Bolhuis *et al.*[16] Overnight *E. coli* cultures were diluted in CAMHB (50 ml) to a cell concentration of approximately $10^6$ cfu/ml. Compound was added and samples were taken at regular intervals during 37 °C incubation. For removal of the compound from samples, cells were collected by centrifugation and re-suspended in sterile PBS. The viable count was determined by plating serial dilutions, allowing the cfu/ml to be calculated at each time point. Attention was focussed upon the key relationship between the lead anti-Gram

negative compound, $\Lambda_{Fe}$-[$Fe_2\mathbf{L}^{\mathbf{b}}{}_3$]$Cl_4$ , and the Gram-negative model, *E. coli* TOP10. Figure 3.5 compares several time-kill curves using different concentrations of $\Lambda_{Fe}$-[$Fe_2\mathbf{L}^{\mathbf{b}}{}_3$]$Cl_4$. As expected, the number of viable cells present is shown to decrease in correlation with the concentration of $\Lambda_{Fe}$-[$Fe_2\mathbf{L}^{\mathbf{b}}{}_3$]$Cl_4$ (dose dependent), and the decrease becomes more pronounced the longer the cells are incubated with the compound.

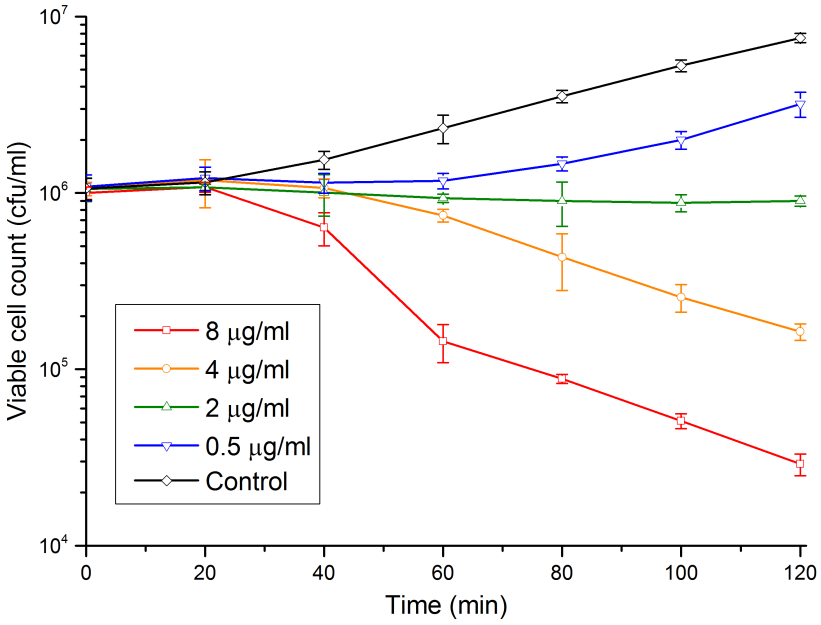


**Figure 3.5: Time kill curves of *E. coli* TOP10 in the presence or absence of $\Lambda_{Fe}$-[$Fe_2L^b{}_3$]$Cl_4$.** The vertical axis has been scaled logarithmically. Error bars representing 95 % confidence intervals, calculated using replicates, are shown.

It is evident from the time-kill assays that the compound is fast acting, taking around 1 h to reduce the number of viable cells tenfold at 8 μg/ml, the observed MBC for this complex against *E. coli* TOP10. However, across the concentration range tested (including the control), it appears the viable cell count is unaffected at t = 20 min, suggesting that there is some initial delay in the action, comparable to the optimal *E. coli* dividing time. A delay, where cells are not initially in logarithmic phase, have been described for the killing kinetics of β-lactam antibiotics, as growth models of time-kill curves typically account for this.[18, 19] Contrastingly, the reports by Ooi *et al.*

of their antimicrobial quaternary amine/porphyrin 'XF' platform showed those agents to rapidly kill *S. aureus* without delay, at concentrations above the MIC and under a range of growth conditions.[20]

At 2 μg/ml of $\Lambda_{Fe}$-$[Fe_2\mathbf{L}^{\mathbf{b}}{}_3]Cl_4$, the viable count stays relatively stable throughout the experiment, confirming the measured MIC, whereby rates of cell growth and death are roughly equivalent. This also shows that the observed MIC is stable to changes in the volume of the culture used.

## 3.3 Cell Membrane Integrity

When bactericidal activity is observed for a proposed antimicrobial agent, it is prudent to make an assessment of the effect it has on the bacterial cell membrane, to establish if cell lysis is the major cause of the observed loss in bacterial viability. Although antimicrobial agents that target cell wall synthesis (*e.g.* β-lactams[21]) or specifically disrupt the prokaryote membrane (*e.g.* pore-forming antimicrobial peptides[22]) may cause cell lysis, there are many compounds, including many biocides, that will nonspecifically compromise the integrity of the bacterial cell membrane, causing, or at least contributing to, cell death. Direct osmotically driven cell lysis (*i.e.* detergency) is not a desirable property for a drug molecule to have, as this will usually correspond to a lack of prokaryotic specificity, leading to an acute toxic effect in mammals.[23]

In order to assess the effect of class Ia flexicates on the cell membrane integrity of bacteria, we employed the commercially available, high-throughput *Bac*Light™ LIVE/DEAD assay (Invitrogen).[24] This fluorescence assay scores cells as 'live'

(intact) or 'dead' (membrane compromised), using two fluorescent DNA binders: SYTO-9 and propidium iodide. Used alone, SYTO-9 labels all bacteria in a population, however, when both dyes are present, propidium iodide penetrates only bacteria with damaged membranes and causes a reduction in the SYTO-9 stain fluorescence.[25] After incubation of these dyes in 1:1 ratio with bacterial cells (to give 200 µl total), the fluorescence emission from excitation at wavelength 470 nm, is predominantly red ($\lambda_{max} \approx 630$ nm) for 'dead'/compromised cells, and green ($\lambda_{max} \approx 530$ nm) for 'live'/intact cells. The green/red emission ratio is therefore proportional to the percentage of 'live'/intact cells in the entire sample; a simple calibration curve is used to translate fluorescence output into the % cell integrity for a given sample. These curves were generated using control samples: untreated cells (100 % intact), cells treated with isopropanol, washed and re-suspended in saline solution (0 % intact), and intentional mixtures of these to give samples at 10, 50, and 90 % intact respectively. A typical calibration curve is shown in Figure 3.6. Ampicillin, (a peptidoglycan synthesis inhibitor) was also used as an antibiotic control, at a clinically-relevant concentration of 4 µg/ml, the *E. coli* MIC.[2]

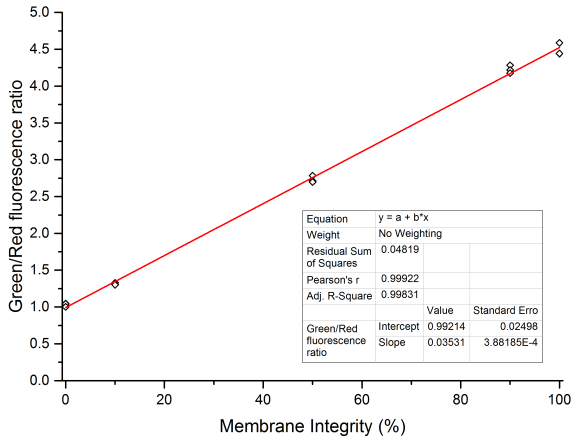


**Figure 3.6: A typical *Bac*Light™ assay calibration curve** plotting the fluorescence output ratio of control samples comprising 0, 10, 50, 90, and 100 % 'live'/intact *E. coli* TOP10 cells, respectively. A linear model has been fitted by linear regression, plotted here as a red line. Output parameters are tabulated under the curve.

Either *S. aureus* USA300 or *E. coli* TOP10 cells grown to stationary phase in LB were collected by centrifugation, washed twice and then re-suspended in sterile 0.9 % saline solution to $OD_{600}$ = 0.2. Enantiomers of $[Fe_2\mathbf{L}^{\mathbf{a}}{}_3]Cl_4$ and $[Fe_2\mathbf{L}^{\mathbf{b}}{}_3]Cl_4$ respectively were incubated with the cells either at the appropriate MIC or at [4 × MIC], as recommended by Chopra,[26, 27] for 45 minutes (37 °C). After a further 15 min room-temperature incubation with the *Bac*Light™ preparation (in darkness), the fluorescence output was measured at 530 nm and 630 nm respectively, from excitation at 485 nm. The calculated % membrane integrity is tabulated in Table 3.3. Saline solutions of flexicates (10-100 μg/ml) were not observed to emit any significant fluorescence output when irradiated with light of wavelength 470 nm, suggesting the compounds themselves do not contribute to false-positive/negative results.

| | **% Membrane Integrity** | | | |
|---|---|---|---|---|
| | ***S. aureus*** USA300 | | ***E. coli*** TOP10 | |
| **Compound** | **1 × MIC** | **4 × MIC** | **1 × MIC** | **4 × MIC** |
| $\Lambda_{Fe}$-$[Fe_2\mathbf{L}^{\mathbf{a}}{}_3]Cl_4$ | **91.0** ± 4.9 (8 μg/ml) | **75.6** ± 1.9 (32 μg/ml) | **100.0** ± 2.0 (4 μg/ml) | **100.0** ± 0.8 (16 μg/ml) |
| $\Delta_{Fe}$-$[Fe_2\mathbf{L}^{\mathbf{a}}{}_3]Cl_4$ | **93.8** ± 3.4 (8 μg/ml) | **82.8** ± 1.2 (32 μg/ml) | **100.5** ±1.0 (8 μg/ml) | **92.0** ± 1.6 (16 μg/ml) |
| $\Lambda_{Fe}$-$[Fe_2\mathbf{L}^{\mathbf{b}}{}_3]Cl_4$ | **85.6** ± 10.0 (16 μg/ml) | **15.1** ± 0.8 (64 μg/ml) | **100.5** ± 8.9 (2 μg/ml) | **96.7** ± 5.7 (8 μg/ml) |
| $\Delta_{Fe}$-$[Fe_2\mathbf{L}^{\mathbf{b}}{}_3]Cl_4$ | **80.8** ± 3.6 (16 μg/ml) | **14.5** ± 2.2 (64 μg/ml) | **99.1** ± 8.3 (4 μg/ml) | **95.7** ± 3.2 (16 μg/ml) |
| Ampicillin | **97.3** ± 3.3 (4 μg/ml) | | **93.2%** ± 6.2 (4 μg/ml) | |

**Table 3.3: Percentage membrane integrity of *S. aureus* and *E. coli* exposed to flexicates** $[Fe_2\mathbf{L}^{\mathbf{a}}{}_3]Cl_4$ and $[Fe_2\mathbf{L}^{\mathbf{b}}{}_3]Cl_4$ for 45 minutes, either at the corresponding MIC, or 4 × MIC. Error representing 95 % confidence intervals, calculated using replicates, are quoted. Absolute concentrations in μg/ml are included for reference, in parentheses.

The data obtained from the application of the *Bac*Light™ assay suggest that, in spite of their bactericidal effect noted in MBC/MIC values and *E. coli* time-kill curves of $\Lambda_{Fe}$-$[Fe_2\mathbf{L}^{\mathbf{b}}{}_3]Cl_4$, the lead class Ia flexicate tested, did not cause significant

membrane damage to *E. coli* TOP10, and only caused significant damage to *S. aureus* USA300 (against which they were less active) at substantial concentrations. This would imply that these flexicates do not act as lytic agents at lower concentrations (<30 μg/ml), at least when tested against stationary phase *E. coli* and *S. aureus*. Ampicillin at 4 μg/ml gave little or no cell lysis, especially against the β-lactam-resistant *S. aureus* USA300. Ooi *et al.* observed similar negative results from a shorter 10 min exposure of *S. aureus* SH1000 to the peptidoglycan synthesis inhibitor, vancomycin.[26] On the other hand, those researchers also observed extensive cell lysis for other membrane-disruptive agents including nisin[28] and cetyltrimethyl-ammonium bromide[29] (CTAB).

## 3.4 Screening Against Pathogenic Gram-Negative Bacteria

### 3.4.1 MIC determination and choice of strains

The initial screening described in section 3.2 identified lead anti-Gram-negative compounds. Model laboratory strains (*e.g. E. coli* TOP10) were included in the initial screen, as they are presumed to be adequate representatives of their parent genus and due to their low hazard category, may be easily handled, making them ideal for rapid screening of a large library. However, in being cultivated for efficient and safe laboratory use over many generations, such model strains have often lost many characteristics of wild-type/pathogenic strains of the same parent species.[30, 31] Therefore we proceeded to screen our leading class Ia flexicates against more recently isolated clinically relevant Gram-negative strains. Two categories of Gram-negative pathogens were chosen: pathogenic *E. coli*, and Gram-negative species belonging to the so-called *ESKAPE* pathogens[9, 32, 33] - *Klebsiella pneumoniae*,

*Acinetobacter baumannii*, and *Enterobacter* species (*Pseudomonas aeruginosa* having already been included in the initial screen). It should be noted that the majority of the strains described herein are classified as biosafety hazard group 2 by relevant authorities,[34] and must be handled appropriately.

Pathogenic *E. coli* strains may be grouped according to the symptoms that they manifest during infections of a human host. For example, enterohemorrhagic *E. coli* (EHEC) strains, most notably strains of the serotype O157:H7, cause acute haemorrhagic diarrhoea, whereas uropathogenic *E. coli* (UPEC) strains are responsible for many urinary tract infections (UTIs). We focussed our attention upon EHEC O157:H7 strains Sakai (ATCC BAA-460) and EDL933 (ATCC 700927), UPEC O6:H1:K2 strain CFT073 (ATCC 700928), and an archetypal K12 *E. coli* strain, MG1655 (ATCC 700926) that, in spite of being a laboratory strain, has undergone minimal genetic manipulation making it a more appropriate control strain than TOP10. A useful physiological and genomic comparison of these four strains may be found in the work of Brzuszkiewicz *et al*.[35]

Amongst Gram-negative *ESKAPE* pathogens, four clinical isolate strains were chosen; *K. pneumoniae* strains K6 (ATCC 700603), widely used in susceptibility testing and exhibiting extended spectrum β-lactam resistance,[36] and KP02 (NCTC 13442), which exhibits carbapenem resistance *via* the OXA-48 β-lactamase;[37] an *A. baumannii* reference strain (NCTC 13420) associated with a multidrug resistant outbreak in the UK;[38, 39] *E. cloacae* strain 684 (NCTC 13405) that exhibits extended spectrum β-lactam resistance *via* the AmpC β-lactamase.[40]

MICs were determined for the class Ia flexicates with leading Gram-negative activity, $[Fe_2\mathbf{L}^{\mathbf{a}}{}_3]Cl_4$ and $[Fe_2\mathbf{L}^{\mathbf{b}}{}_3]Cl_4$ enantiomers respectively, as well as control

antibiotics, against the panel of Gram-negative pathogens using the assay outlined in section 3.2.1. The results obtained are listed in Table 3.4. Species of the family Enterobacteriaceae (*E. coli*, *K. pneumoniae*, and *E. cloacae*) generally exhibited promising susceptibility (MICs of 2-8 μg/ml) to the flexicates tested, especially the lead compound indicated by the initial screen, $\Lambda_{Fe}$-$[Fe_2\mathbf{L}^{b}_{3}]Cl_4$, which frequently demonstrated higher μg/ml activity than the controls. Of particular note was the activity of this compound against EHEC O157:H7 strains (Sakai and EDL933) that matched the activity versus *E. coli* TOP10. Remarkably, of the *E. coli* strains tested, the lab strain MG1655 demonstrated the least susceptibility.

| | | **MIC** (μg/ml) | | | | | | | |
|---|---|---|---|---|---|---|---|---|---|
| **Group** | **Compound** | ***E. coli*** MG1655 | **UPEC** CFT073 | **EHEC** EDL933 | **EHEC** Sakai | ***K. pneumoniae*** K6 | ***K. pneumoniae*** KP02 | ***E. cloacae*** 684 | ***A. baumannii*** NCTC 13420 |
| Class Ia Flexicate | $\Lambda_{Fe}$-$[Fe_2\mathbf{L}^{a}_{3}]Cl_4$ | 8 | 16 | 4 | 16 | 8 | 32 | 64 | 64 |
| | $\Delta_{Fe}$-$[Fe_2\mathbf{L}^{a}_{3}]Cl_4$ | 32 | 16 | 16 | 32 | 128 | 128 | 128 | 64 |
| | $\Lambda_{Fe}$-$[Fe_2\mathbf{L}^{b}_{3}]Cl_4$ | 8 | 4 | 2 | 2 | 4 | 64 | 8 | 64 |
| | $\Delta_{Fe}$-$[Fe_2\mathbf{L}^{b}_{3}]Cl_4$ | 8 | 4 | 4 | 4 | 8 | 128 | 16 | 64 |
| Antibiotic | Kanamycin | 2 | 8 | 4 | 4 | 64 | >64 | 2 | >64 |
| | Tetracycline | 2 | 4 | 4 | 4 | 16 | 32 | 4 | >64 |

**Table 3.4: *In vitro* antimicrobial activity (MICs) of leading class Ia flexicates against pathogenic Gram-negative strains**. Kanamycin and tetracycline controls are also included for reference.

Taking both screens into account, it is evident that class Ia flexicates are not especially active against species of the order Pseudomonadales (*P. aeruginosa*, *A. baumannii*), or against *K. pneumoniae* strain KP02. The latter case is particularly intriguing as it is in stark contrast to the susceptibility exhibited by the other *K. pneumoniae* strain tested, K6. This would seemingly indicate that the mechanism of carbapenem resistance in KP02 also conveys cross-resistance to class Ia flexicates. If

that is the case, it would be an unusual example of resistance to an established antibiotic offering cross-resistance to an entirely anthropogenic compound. Similarity in behaviour to clinically accepted antibiotics supports the notion that the action of an antimicrobial agent is of a specific nature.

Of additional note is that what little susceptibility *P. aeruginosa*, *A. baumannii*, and *K. pneumoniae* KP02 do show, is higher for our initial 'hit' compound, $\Lambda_{Fe}$-$[Fe_2\mathbf{L}^{a}{}_3]Cl_4$, rather than $\Lambda_{Fe}$-$[Fe_2\mathbf{L}^{b}{}_3]Cl_4$. This may indicate that the target site is different for these strains, or that there is a difference in membrane interactions, leading to increased exclusion and/or expulsion from the cell. The latter hypothesis would fit with observations that intrinsic and adaptive AMR mechanisms in species of the order Pseudomonadales are often associated with the cell membrane and the permeability thereof. These mechanisms involve various components such as the membrane and LPS layer themselves, as well as porins and efflux pump proteins that control cellular ingress/egress respectively.[41-44] Compellingly, many OXA-48 positive *K. pneumoniae* clinical isolates, of which KP02 (NCTC 13442) is one, are known to augment β-lactamase activity with loss or down-regulation of certain outer membrane porins (notably OmpK35 and OmpK36) as part of their AMR.[45-48] Given the much lower susceptibility of *K. pneumoniae* KP02 to the leading flexicates compared with the K6 strain, this would again support the hypothesis that interaction of flexicates with the cell membrane is a key factor in their mode of action, if indeed KP02 exhibits lower susceptibility as a result of porin deficiency. It is also worth noting that *Pseudomonas* and similar bacteria can produce a polysaccharide capsule (alginate) that is strongly anionic, and so could absorb and neutralise cationic antimicrobial agents.[49]

Nonetheless, the activity trends observed in Tables 3.1 and 3.4, suggest that there is a specificity to the action of class Ia flexicates, including the lead compound, $\Lambda_{Fe}$-$[Fe_2\mathbf{L}^{\mathbf{b}}{}_3]Cl_4$. Given the particularly strong activity this compound has against EHEC O157:H7 strains, further experiments were therefore conducted to further investigate the activity of $\Lambda_{Fe}$-$[Fe_2\mathbf{L}^{\mathbf{b}}{}_3]Cl_4$ against the EHEC O157:H7 strain, Sakai.

### 3.4.2 Lead compound effect upon *E. coli* Sakai

In order to investigate the kinetics involved in the action of $\Lambda_{Fe}$-$[Fe_2\mathbf{L}^{\mathbf{b}}{}_3]Cl_4$ against *E. coli* Sakai, the MIC was re-measured with a single alteration to the protocol; the plate was incubated at 30 °C rather than the standard 37 °C. The reduced temperature has numerous effects, including; (i) reducing the kinetics of microbial growth; (ii) slowing the interactions that underlie the bactericidal MOA; (iii) reducing membrane fluidity, which may affect rate of compound ingress; (iv) reducing gene expression and enzyme kinetics, ultimately slowing the bacterial response. Under these conditions, the MIC shifted from 2 to 4 μg/ml. This suggests that the potency of the compound is linked to the rates of the various processes involved.

To further examine whether the bactericidal MOA of $\Lambda_{Fe}$-$[Fe_2\mathbf{L}^{\mathbf{b}}{}_3]Cl_4$ necessitates active growth of *E. coli*, an experiment was established to investigate whether $\Lambda_{Fe}$-$[Fe_2\mathbf{L}^{\mathbf{b}}{}_3]Cl_4$ exposure during stationary phase causes a decrease in the viability of *E. coli* Sakai. Cultures of *E. coli* Sakai were grown overnight to stationary phase, collected by centrifugation, and re-suspended to an $OD_{600}$ of 0.1, in 20 ml PBS containing 8 μg/ml (MBC, 4 × MIC) $\Lambda_{Fe}$-$[Fe_2\mathbf{L}^{\mathbf{b}}{}_3]Cl_4$, before incubation for a further three hours at 37 °C. Cells were subsequently harvested by centrifugation and washed twice in clean sterile PBS. The final cell pellet was re-suspended to an $OD_{600}$ of 0.01 in 50 ml CAMHB. These cultures were incubated at 37 °C and monitored for

growth by taking periodic $OD_{600}$ measurements and viability counts over five hours. This data is plotted in Figure 3.7, alongside positive and negative (20 vol% iso-propanol) controls.

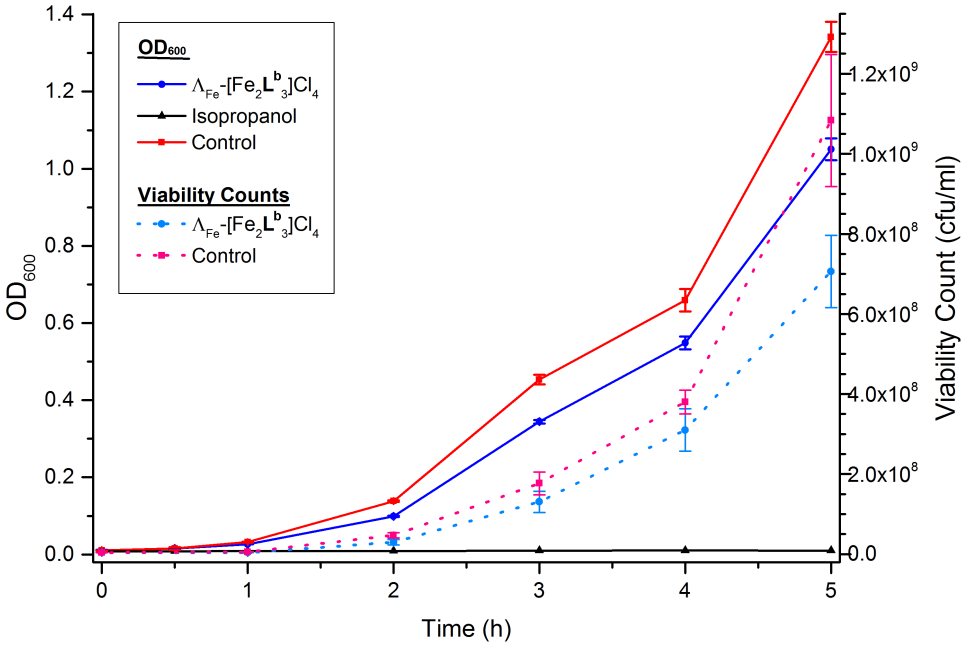


**Figure 3.7: Growth of *E. coli* O157:H7 Sakai after exposure to $\Lambda_{Fe}$-$[Fe_2L^b_3]Cl_4$ at (4 × MIC) during stationary phase**, followed by washing and resuspension in CAMHB. Data compared to a positive control containing no compound, and incubation with the known lytic/cidal agent, isopropanol (20 vol%). $OD_{600}$ measurements (solid lines) and viability counts (dotted lines) are shown. Viability counts are not shown for isopropanol, as no viable cells could be recovered. Error bars representing 95 % confidence intervals are shown, calculated using replicates.

Although at a slower rate than the positive control, Figure 3.7 clearly shows that *E. coli* Sakai grows with near normal kinetics despite the long exposure to (4 × MIC) $\Lambda_{Fe}$-$[Fe_2\mathbf{L}^{\mathbf{b}}_3]Cl_4$ during stationary phase, once the flexicate is removed. A minor deviation from the positive control growth rate suggests limited cell death has occurred. This lack of cell death observed by this treatment is in contrast to the rapid killing seen for the same concentration of $\Lambda_{Fe}$-$[Fe_2\mathbf{L}^{\mathbf{b}}_3]Cl_4$, in Figure 3.5, where the compound was present during log phase. It should be noted that the lack of bacteriocidal action in stationary phase cells is in agreement with the *Bac*Light™

assay data, which suggested negligible membrane damage at lower concentrations, since this assay requires cells to be in stationary phase.

## 3.5 Eukaryote Toxicity

Efforts to advance from *in vitro* antimicrobial screening towards *in vivo* screening in mammalian models can be expedited and de-risked by first attempting to understanding the *in vitro* toxicity of the compounds to mammalian cell lines, and lower metazoan animals such as insects.

### 3.5.1 Insect model

To assess the general toxicity of class Ia flexicates towards a metazoan animal, a straightforward toxicity assay was employed by Dr Nicholas Waterfield and co-workers (Microbiology and Infection Division, University of Warwick) using *Galleria mellonella* larvae: commonly called "wax worms", which have been shown to be a useful model organism for *in vivo* toxicology and pathogenicity testing, making them an alternative to small mammals in early experiments.[50, 51]

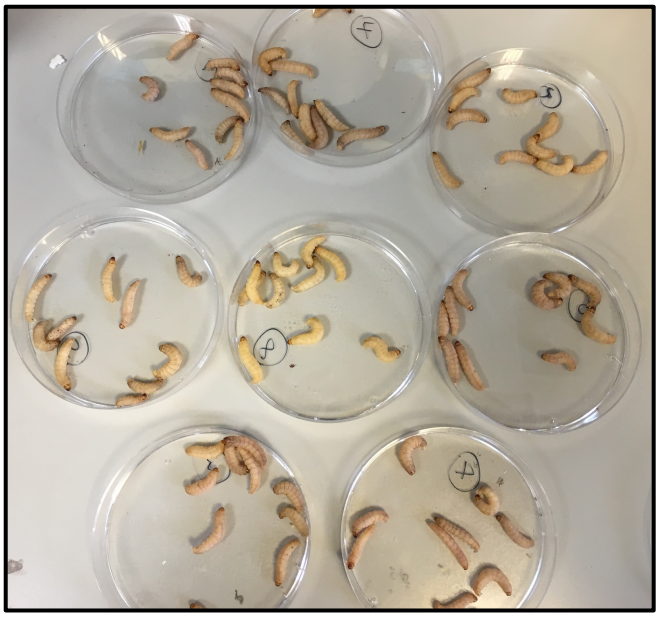

**Figure 3.8: *G. mellonella* larvae injected with solutions of various flexicates,** to a bodily concentration of roughly 32 μg/ml, and incubated for five days. The control (PBS only injection) is shown in the centre.

Solutions of leading class Ia flexicates, $[Fe_2\mathbf{L}^{a\text{-}b}{}_3]Cl_4$ enantiomers, in PBS (10 μl) were carefully injected into the open blood system of cohorts of *G. mellonella* larvae. Larval masses varied slightly but were typically 250 mg, a value that was subsequently used to calculate treatment doses, to give a bodily concentration of 32-64 μg/ml. After the initial injection, larvae (ten per condition), including negative controls injected with PBS only, were incubated over five days while being examined and scored daily, for survival. Figure 3.8 shows several example plates of *G. mellonella* larvae at the endpoint of the experiment. It was found that the injection of the flexicates had no significant effect on larval survival. It would appear from this initial toxicity screen that the class Ia flexicates are not overtly toxic to multicellular eukaryotes, even at this relatively high dosage. This is in agreement with the previously observed low toxicity ($LC_{50}$ > 400 μg/ml) of the class prototype, $[Fe_2\mathbf{L}^{a}{}_3]Cl_4$, to the nematode worm *Caenorhabditis elegans* (*C. elegans*).[6]

### 3.5.2 Human cell line model

In order to investigate the cytotoxicity of the class Ia flexicates to mammalian cells, their ability to kill or otherwise damage immortalised human cells *in vitro*. This was tested by determining the half-maximal lethal concentrations ($IC_{50}$): defined as the concentration of a therapeutic agent at which half of the maximal inhibition (or death) occurs, relative to an untreated control. This was conducted by Samantha Shepherd in the Phillips laboratory (University of Huddersfield) using a colorimetric MTT assay, which measures metabolic activity of a cell line *via* the reduction of the yellow tetrazole, MTT, to purple formazan; a process which can only occur if the cells present are alive and metabolically active. $IC_{50}$ values are quoted for a specific incubation time with the compound, since cells must be harvested in order to recover and measure formazan levels.

$IC_{50}$ values (96 h incubation) were determined for all water-soluble class Ia flexicates against ARPE-19 (ATCC CRL-2302), a non-cancerous retinal cell line. The values obtained are tabulated in Table 3.5. A rough measure of selectivity of the complexes for *E. coli* over non-cancerous cells, calculated as the molar ratio between the APRE-19 $IC_{50}$ and the MIC against *E. coli* TOP10, is also included.

The $IC_{50}$:MIC ratio provides an *ad hoc* index for prokaryote selectivity (therapeutic index), however since $IC_{50}$ and MIC values differ in how they are defined and measured, it makes it somewhat difficult to draw firm conclusions regarding the potential for clinical applicability of a test compound using this index. Nevertheless, this metric is useful in comparing the relative prokaryote selectivity within compound libraries. For class Ia flexicates, it is obvious that xylyl-bridged compounds, $[Fe_2\mathbf{L}^{\mathbf{a\text{-}b}}{}_3]Cl_4$ enantiomers, are much more selective for the prokaryote

organism (*E. coli* TOP10) over human APRE-19 cells, than other compounds of the class, reflective of their relatively low *E. coli* MICs and high ARPE-19 $IC_{50}$ values. This is again in line with the different behaviour observed of these lead compounds in the above *in vitro* assays, compared with other class Ia flexicates.

| | **$IC_{50}$ after 96 h** (μM) | **Prokaryote Selectivity** |
|---|---|---|
| **Compound** | **ARPE-19** | **$\frac{\text{ARPE19 } IC_{50}}{E.coli \text{ TOP10 MIC}}$** |
| $\Lambda_{Fe}$-$[Fe_2\mathbf{L}^{a}_3]Cl_4$ | **13.90** ± 1.14 | **6.95** |
| $\Delta_{Fe}$-$[Fe_2\mathbf{L}^{a}_3]Cl_4$ | **18.69** ± 2.09 | **4.79** |
| $\Lambda_{Fe}$-$[Fe_2\mathbf{L}^{b}_3]Cl_4$ | **6.39** ± 2.36 | **6.39** |
| $\Delta_{Fe}$-$[Fe_2\mathbf{L}^{b}_3]Cl_4$ | **22.44** ± 2.56 | **11.22** |
| $\Lambda_{Fe}$-$[Fe_2\mathbf{L}^{d}_3]Cl_4$ | **0.17** ± 0.07 | **<0.01** |
| $\Delta_{Fe}$-$[Fe_2\mathbf{L}^{d}_3]Cl_4$ | **0.29** ± 0.12 | **0.01** |
| $\Lambda_{Fe}$-$[Fe_2\mathbf{L}^{e}_3]Cl_4$ | **0.89** ± 0.46 | **0.13** |
| $\Delta_{Fe}$-$[Fe_2\mathbf{L}^{e}_3]Cl_4$ | **2.37** ± 0.46 | **0.18** |
| $\Lambda_{Fe}$-$[Fe_2\mathbf{L}^{f}_3]Cl_4$ | **0.29** ± 0.12 | **0.01** |
| $\Delta_{Fe}$-$[Fe_2\mathbf{L}^{f}_3]Cl_4$ | **1.14** ± 0.31 | **0.17** |
| $\Lambda_{Fe}$-$[Fe_2\mathbf{L}^{g}_3]Cl_4$ | **0.67** ± 0.25 | **0.03** |
| $\Delta_{Fe}$-$[Fe_2\mathbf{L}^{g}_3]Cl_4$ | **1.07** ± 0.32 | **0.08** |
| $\Lambda_{Fe}$-$[Fe_2\mathbf{L}^{h}_3]Cl_4$ | **2.26** ± 1.07 | **0.09** |
| $\Delta_{Fe}$-$[Fe_2\mathbf{L}^{h}_3]Cl_4$ | **6.84** ± 1.57 | **0.26** |
| $\Lambda_{Fe}$-$[Fe_2\mathbf{L}^{i}_3]Cl_4$ | **1.98** ± 0.45 | **0.3** |
| $\Delta_{Fe}$-$[Fe_2\mathbf{L}^{i}_3]Cl_4$ | **1.94** ± 0.56 | **0.29** |

**Table 3.5: *In vitro* human cell line inhibition ($IC_{50}$ values) and relative prokaryote selectivity of class Ia flexicates** using non-cancerous ARPE-19 cells. Relative selectivity is given by the ratio of ARPE-19 $IC_{50}$ to the *E. coli* TOP10 MIC in μM.

## 3.6 Summary

The work described in this chapter has demonstrated the range of *in vitro* biological activities displayed by class Ia flexicates, allowing the identification of $\Lambda_{Fe}$-$[Fe_2\mathbf{L}^{\mathbf{b}}{}_3]Cl_4$ as the lead compound (MIC *vs. E. coli* O157:H7 of 2 μg/ml, 1 μM), and made progress towards understanding the underlying MOA. In general, the consistent potent activity of shorter xylyl-bridged flexicates, against Gram-negative Enterobacteriaceae (including against a panel of clinically relevant pathogenic examples), coupled with their relative selectivity for these species over Gram-positive *S. aureus*, Human ARPE-19 cells, and *G. mellonella* larvae, make these compounds strong candidates for further research and development in the field of antimicrobial chemotherapy.

Despite their activity against the Enterobacteriaceae, the lead compounds exhibited far less activity against certain other Gram-negative bacteria tested, namely the Pseudomonadales and a single carbapenem-resistant *K. pneumoniae* strain, KP02. This difference would appear to correlate with differences in the cell membrane composition and permeability (see section 3.4.1) suggesting the outer cell membrane is a key site of interaction for the lead class Ia flexicates, if not the major target site itself.

The MOA of the class Ia library is bacteriocidal in nature, and therefore concerns processes within the microbial cell that are crucial not only for growth, but for survival. However, the difference in cell death between cells that are actively dividing, and those in stationary phase, would appear to demonstrate a much stronger effect upon the actively replicating enterobacterial cell. It would appear that this MOA is specific in nature, since a range of activities is observed across both

complexes and species. Furthermore, despite the hypothesis of the MOA relating to a critical interaction between the lead class Ia flexicates and the enterobacterial cell membrane, it would appear that the MOA is not cytolytic in nature, at least when cells are in stationary phase.

As well as progression towards *in vivo* study (protection assays in mammalian models), future work on the antimicrobial activity of class Ia flexicates will inevitably involve further cycles of synthesis and screening to refine their potency and selectivity. However, the exact molecular interactions that give rise to the observed antimicrobial activity of the lead compound remain unknown; without this information, improvements to the activity of the lead compound will be somewhat serendipitous and therefore inefficient. Research towards deconvoluting the molecular targets, *i.e.* the mechanism of action, is the focus of the next chapter.

## 3.7 References for Chapter 3


1. A. J. O'Neill and I. Chopra, *Expert Opin. Investig. Drugs*, 2004, **13**, 1045-1063.

2. J. M. Andrews, *J. Antimicrob. Chemother.*, 2001, **48**, 5-16.

3. P. G. Engelkirk and J. L. Duben-Engelkirk, *Laboratory Diagnosis of Infectious Diseases: Essentials of Diagnostic Microbiology*, Wolters Kluwer Health/Lippincott Williams & Wilkins, 2008.

4. EUCAST, *Clin. Microbiol. Infect.*, 2003, **9**, ix-xv.

5. CLSI, *Methods for Dilution Antimicrobial Susceptibility Tests for Bacteria That Grow Aerobically; Approved Standard*, CLSI document M07-A9, Wayne (PA), USA, 9th edn., 2012.

6. S. E. Howson, A. Bolhuis, V. Brabec, G. J. Clarkson, J. Malina, A. Rodger and P. Scott, *Nat. Chem.*, 2012, **4**, 31-36.

7. L. M. Koeth, A. King, H. Knight, J. May, L. A. Miller, I. Phillips and J. A. Poupard, *J. Antimicrob. Chemother.*, 2000, **46**, 369-376.

8. B. Alberts, A. Johnson, J. Lewis, M. Raff, K. Roberts and P. Walter, *Molecular Biology of the Cell*, Garland, Oxford, 2002.

9. L. B. Rice, *J. Infect. Dis.*, 2008, **197**, 1079-1081.

10. A. L. Sonenshein, J. A. Hoch and R. Losick, in *Bacillus subtilis and Its Closest Relatives*, American Society of Microbiology, 2002.

11. R. A. Kaner, S. J. Allison, A. D. Faulkner, R. M. Phillips, D. I. Roper, S. L. Shepherd, D. H. Simpson, N. R. Waterfield and P. Scott, *Chem. Sci.*, 2016.

12. R. E. W. Hancock, *Trends Microbiol.*, 1997, **5**, 37-42.

13. N. A. Logan and P. D. Vos, in *Bergey's Manual of Systematics of Archaea and Bacteria*, John Wiley & Sons, Ltd, 2015.

14. M. J. Mulligan and C. G. Cobbs, *Infect. Dis. Clin. North Am.*, 1989, **3**, 389-398.

15. L. R. Peterson and C. J. Shanholtzer, *Clin. Microbiol. Rev.*, 1992, **5**, 420-432.

16. A. Bolhuis, L. Hand, J. E. Marshall, A. D. Richards, A. Rodger and J. Aldrich-Wright, *Eur. J. Pharm. Sci.*, 2011, **42**, 313-317.

17. F. F. Li, J. G. Collins and F. R. Keene, *Chem. Soc. Rev.*, 2015, **44**, 2529-2542.

18. M. Mueller, A. de la Peña and H. Derendorf, *Antimicrob. Agents Chemother.*, 2004, **48**, 369-377.

19. E. I. Nielsen, A. Viberg, E. Löwdin, O. Cars, M. O. Karlsson and M. Sandström, *Antimicrob. Agents Chemother.*, 2007, **51**, 128-136.

20. N. Ooi, K. Miller, C. Randall, W. Rhys-Williams, W. Love and I. Chopra, *J. Antimicrob. Chemother.*, 2010, **65**, 72-78.

21. H. S. Chung, Z. Yao, N. W. Goehring, R. Kishony, J. Beckwith and D. Kahne, *Proc. Natl. Acad. Sci. USA*, 2009, **106**, 21872-21877.

22. K. A. Brogden, *Nature Rev. Microbiol.*, 2005, **3**, 238-250.

23. P. Steinberg, *High-Throughput Screening Methods in Toxicity Testing*, Wiley, 2013.

24. M. Berney, F. Hammes, F. Bosshard, H. U. Weilenmann and T. Egli, *Appl. Environ. Microbiol.*, 2007, **73**, 3283-3290.

25. J. J. Hilliard, R. M. Goldschmidt, L. Licata, E. Z. Baum and K. Bush, *Antimicrob. Agents Chemother.*, 1999, **43**, 1693-1699.

26. N. Ooi, K. Miller, J. Hobbs, W. Rhys-Williams, W. Love and I. Chopra, *J. Antimicrob. Chemother.*, 2009, **64**, 735-740.

27. N. Ooi, I. Chopra, A. Eady, J. Cove, R. Bojar and A. J. Oneill, *J. Antimicrob. Chemother.*, 2013, **68**, 1297-1304.

28. E. Ruhr and H. G. Sahl, *Antimicrob. Agents Chemother.*, 1985, **27**, 841-845.

29. J. Y. Maillard, *J. Appl. Microbiol.*, 2002, **92**, 16S-27S.

30. Z. Palková, *EMBO Rep.*, 2004, **5**, 470-476.

31. J. L. Hobman, C. W. Penn and M. J. Pallen, *Mol. Microbiol.*, 2007, **64**, 881-885.

32. H. W. Boucher, G. H. Talbot, J. S. Bradley, J. E. Edwards, D. Gilbert, L. B. Rice, M. Scheld, B. Spellberg and J. Bartlett, *Clin. Infect. Dis.*, 2009, **48**, 1-12.

33. J. N. Pendleton, S. P. Gorman and B. F. Gilmore, *Expert Rev. Anti Infect. Ther.*, 2013, **11**, 297-308.

34. L. C. Chosewood and D. E. Wilson, *Biosafety in Microbiological and Biomedical Laboratories*, U.S. Government Printing Office, Washington D.C., 5th edn., 2007.

35. E. Brzuszkiewicz, H. Bruggemann, H. Liesegang, M. Emmerth, T. Oschlager, G. Nagy, K. Albermann, C. Wagner, C. Buchrieser, L. Emody, G. Gottschalk, J. Hackert and U. Dobrindt, *Proc. Natl. Acad. Sci. USA*, 2006, **103**, 12879-12884.

36. J. K. Rasheed, G. J. Anderson, H. Yigit, A. M. Queenan, A. Doménech-Sánchez, J. M. Swenson, J. W. Biddle, M. J. Ferraro, G. A. Jacoby and F. C. Tenover, *Antimicrob. Agents Chemother.*, 2000, **44**, 2382-2388.

37. V. Dimou, H. Dhanji, R. Pike, D. M. Livermore and N. Woodford, *J. Antimicrob. Chemother.*, 2012, **67**, 1660-1665.

38. J. F. Turton, M. E. Kaufmann, M. Warner, J. Coelho, L. Dijkshoorn, T. van der Reijden and T. L. Pitt, *J. Hosp. Infect.*, 2004, **58**, 170-179.

39. J. M. Coelho, J. F. Turton, M. E. Kaufmann, J. Glover, N. Woodford, M. Warner, M.-F. Palepou, R. Pike, T. L. Pitt, B. C. Patel and D. M. Livermore, *J. Clin. Microbiol.*, 2006, **44**, 3623-3627.

40. Y. Yang, D. M. Livermore and R. J. Williams, *J. Med. Microbiol.*, 1988, **25**, 227-233.

41. J. Vila, S. Martí and J. Sánchez-Céspedes, *J. Antimicrob. Chemother.*, 2007, **59**, 1210-1215.

42. A. Skiada, A. Markogiannakis, D. Plachouras and G. L. Daikos, *Int. J. Antimicrob. Agents*, 2011, **37**, 187-193.

43. K. Poole, *Front. Microbiol.*, 2011, **2**, 1-13.

44. L. Fernandez and R. E. Hancock, *Clin. Microbiol. Rev.*, 2012, **25**, 661-681.

45. D. Gülmez, N. Woodford, M.-F. I. Palepou, S. Mushtaq, G. Metan, Y. Yakupogullari, S. Kocagoz, O. Uzun, G. Hascelik and D. M. Livermore, *Int. J. Antimicrob. Agents*, 2008, **31**, 523-526.

46. M. Doumith, M. J. Ellington, D. M. Livermore and N. Woodford, *J. Antimicrob. Chemother.*, 2009, **63**, 659-667.

47. C. Pitart, M. Solé, I. Roca, A. Fàbrega, J. Vila and F. Marco, *Antimicrob. Agents Chemother.*, 2011, **55**, 4398-4401.

48. L. Poirel, A. Potron and P. Nordmann, *J. Antimicrob. Chemother.*, 2012, **67**, 1597-1606.

49. A. Boyd and A. M. Chakrabarty, *J. Ind. Microbiol.*, 1995, **15**, 162-168.

50. A. P. Desbois and P. J. Coote, *J. Antimicrob. Chemother.*, 2011, **66**, 1785-1790.

51. C. R. Harding, G. N. Schroeder, J. W. Collins and G. Frankel, *J. Vis. Exp.*, 2013, 50964.

# Chapter 4

## **Towards Target Deconvolution** - Tandem '*omic*' Approaches

### 4.1 Introduction

In the previous chapter, $\Lambda_{Fe}$-$[Fe_2\mathbf{L}^{\mathbf{b}}{}_3]Cl_4$ was established as the lead antimicrobial compound against Gram-negative *Enterobacteriaceae*. The pathogen, *E. coli* O157:H7 Sakai Δ*stx*1-2, proved especially susceptible (MIC = 2 μg/ml), and was therefore used as a model to investigate mode-of-action. This strain is a derivative of a Japanese isolate[1] where both Shiga toxin genes (*stx*1, *stx*2) were knocked-out by Sasakawa and co-workers, who introduced a kanamycin resistance cassette.[2] The strain was later cured of kanamycin resistance by Dr Chrystala Constantinidou and co-workers (unpublished), who kindly donated it for use. It was found that $\Lambda_{Fe}$-$[Fe_2\mathbf{L}^{\mathbf{b}}{}_3]Cl_4$ is bactericidal against *E. coli*, but is most potent against actively replicating cells. However, the key molecular interactions of this compound, *i.e.* the underlying mechanism(s), remain unknown.

Deconvolution of molecular targets has profound implications for the development of antimicrobial candidates identified through phenotypic profiling,[3] as it provides the clarity necessary to allow the establishment of far more precise lines of investigation (*e.g. in silico* docking studies[4]). A good example of this may be found in accounts from the 1980s of the discovery of the penicillin-binding proteins (PBPs), and the effect it had on the research and development of the β-lactams.[5, 6] However, the sheer complexity of the microbial cell has traditionally made target

identification and validation somewhat challenging and therefore an undertaking only attempted for therapeutic agents with a well-established clinical pedigree.[7]

Fields of study grouped together under the neologism *'omics'*,[8] *e.g.* genomics, transcriptomics (RNA) and proteomics, may bring coherence to the complexity of the cellular machine through the categorisation and quantification of a certain group of biological molecules within the cell.[9] Advances in the technology and bioinformatics necessary to produce and process such huge data sets are making tandem *omic* approaches an increasingly viable option in a number of applications, including the development of hypotheses regarding the key molecular targets (mechanism) of a drug candidate.[10]

This chapter explores the -*omic* responses of the clinically relevant *E. coli* Sakai to $\Lambda_{Fe}$-$[Fe_2\mathbf{L}^{\mathbf{b}}_3]Cl_4$, to identify responses that may be indicative of key interactions, allowing the development of credible mechanistic hypotheses.

## 4.2 Characterisation of Tolerant Mutants

Given the number of potential mechanisms by which antimicrobial resistance (AMR) may occur (see Chapter 1), bacterial resistance, or at least tolerance, to an antibacterial agent should be anticipated from large, fast-growing bacterial populations. It should be noted here that resistance could occur through either spontaneous mutation of genes already present in the genome or through the acquisition of specific traits by horizontal gene transfer. In the case of mutation of intrinsic genes, exposure to antibacterial stress alters the relative fitness of different genotypes within a the population, 'selecting' for genotypes encoding lower

susceptibility factors when the antibacterial pressure is sufficient.[11] However, in order for a resistance-conferring mutation to be selected, it must add to the overall fitness of the genome that carries it. Mutations that confer AMR by modification to native pathways, but at too high a cost to the overall fitness of organism tend to be rapidly lost from the population. Therefore the desirable property of an effective antimicrobial with regard to mechanism-of-action, is a scenario where the process of AMR is complex, coming at a high fitness cost to the microbe. Under these circumstances, AMR by horizontal gene transfer (HGT) is more common that native mechanisms.

Considering AMR, what is important to understand of an anti-infective agent is the frequency and extent with which AMR arises when a lethal dose is applied. This information is useful in considering clinical acceptance; hinting as to how AMR may arise with clinical use, and thus which dosage regimes may be the best to use. Additionally, subsequent characterisation of any resistant/tolerant mutants recovered may provide insights into how *in vitro* resistance/tolerance to the candidate antibacterial arises, potentially inferring the mechanism underlying the candidate's antibacterial activity.[12] Analysing the genomes of resistant/tolerant strains in particular can shed light onto these mechanisms. Compellingly, since the first sequencing of a whole bacterial genome by Sanger in the 1970s,[13] the advent of high-throughput sequencing technology (*e.g.* the Illumina whole genome MiSeq platform) has vastly reduced the time and cost of whole-genome sequencing (WGS), making it an accessible tool for many laboratories.[14]

To calculate frequency of spontaneous resistance, the number of resistant mutants arising in a population must be determined. Resistant mutants (RMs) are therefore

frequently isolated from laboratory cultures by challenging these populations to grow on agar plates infused with a sub-lethal dose of antibacterial agent, as this allows RM colonies to be isolated, selected and counted.[15-18] In segregating individual lines of descent (such as colonies), agar methods also benefit genomic analyses, as post-mutation genetic drift (random variation in the relative frequency of different genotypes in a small population, owing to the chance deletion or mutation of particular genes) and mixing of different genotypes are limited, reducing noise. Mutant lines may also be generated in clear lines of descent from individual parent lines, accounting for variation in the original WT. However, it should be noted that environmental factors influence the likelihood of certain resistance mechanisms arising, inferring that the resistance profile or 'resistome' developed on agar may be different to that which would arise *in vivo* during an infection.[11] Nonetheless agar plate methods of RM generation remain a useful initial assessment of resistance to an antibacterial agent, and therefore we chose to apply this method to investigate the physiological and genomic changes that occurred in *E. coli* Sakai cultivated when challenged with lethal doses of $\Lambda_{Fe}$-$[Fe_2\mathbf{L}^{\mathbf{b}}{}_3]Cl_4$.

### 4.2.1 Selection of mutants with increased tolerance to $\Lambda_{Fe}$-$[Fe_2\mathbf{L}^{\mathbf{b}}{}_3]Cl_4$

The ability of *E. coli* Sakai to grow on Mueller-Hinton (MH) agar infused with $\Lambda_{Fe}$-$[Fe_2\mathbf{L}^{\mathbf{b}}{}_3]Cl_4$, was initially assessed by spreading 25 µl of an overnight culture of *E. coli* Sakai onto MH agar infused with 20, 40, and 80 µg/ml of the compound, respectively. After incubation of these plates overnight (37 °C), it was found that agar plates infused with 20 or 40 µg/ml of the compound were covered with a 'lawn' of *E. coli*; it was only at the highest concentration of the compound, 80 µg/ml that individual colonies were resolved. This is surprising given that these concentrations

are much higher (×10-40) than the MIC in liquid broth, which suggests that the effective concentration reaching the growing bacteria is low, possibly reflecting poor diffusion of the compound through agar and/or weak penetration of the biofilms formed by bacterial colonies.

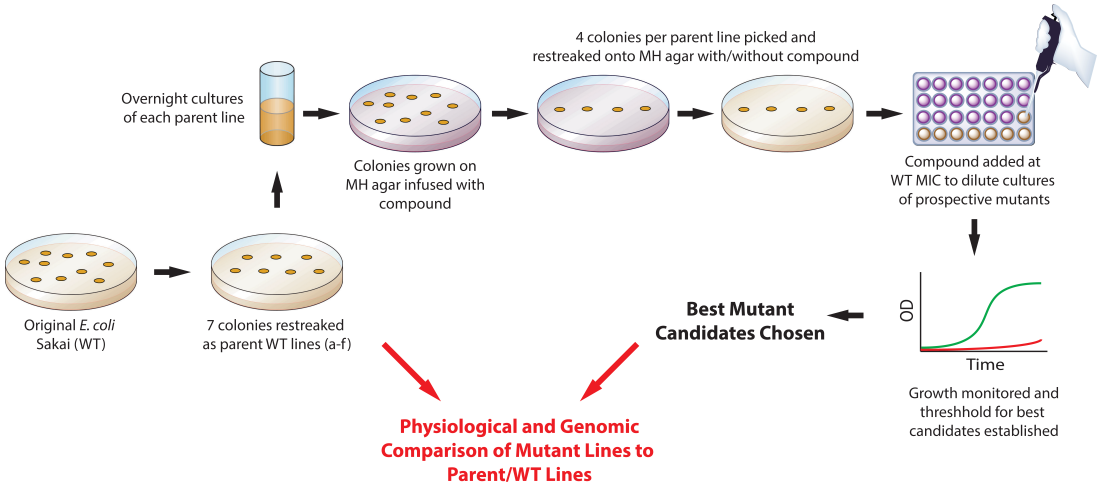


**Figure 4.1: Workflow diagram for the selection, confirmation and study of *E. coli* Sakai mutants exhibiting resistance/tolerance to the lead compound** from wild type lines, as outlined in section 4.2.

Mutant variants of *E. coli* Sakai with reduced susceptibility to $\Lambda_{Fe}$-[$Fe_2\mathbf{L}^{\mathbf{b}}{}_3$]$Cl_4$ were selected for study, using the workflow depicted in Figure 4.1. From an initial population of *E. coli* Sakai, seven colonies (labelled a-f) were re-streaked onto MH agar to serve as parent WT lines. Overnight cultures of these parent lines were grown in CAMHB, and 25 µl of each culture was applied to MH agar containing 80 µg/ml $\Lambda_{Fe}$-[$Fe_2\mathbf{L}^{\mathbf{b}}{}_3$]$Cl_4$, set into a 6-well plate. The remaining overnight cultures were serially diluted and plated onto LB agar in order to establish viable cell counts and thus the total number of *E. coli* present in the cultures, $1.78 \times 10^9$ cfu/ml on average ($\sigma = 0.13 \times 10^9$ cfu/ml). An average of 11.1 ($\sigma = 3.3$) colonies grew from the 25 µl aliquots of overnight culture applied to 6-well plates containing MH agar infused with $\Lambda_{Fe}$-[$Fe_2\mathbf{L}^{\mathbf{b}}{}_3$]$Cl_4$. This suggests a mutation frequency of $2.49 \times 10^{-7}$ ($\sigma = 0.78 \times 10^{-7}$) under those conditions, assuming all colonies did indeed represent *bona fide* RM mutant lines.

### 4.2.2 Characterisation of tolerant phenotypes

Four prospective RM colonies from each of the seven parent lines (twenty-eight colonies in total) were selected for further study. These colonies were re-streaked onto MH agar containing 80 μg/ml of the compound, and then onto MH agar without selection pressure from the compound, removing any false positive "non-mutants" or genetically unstable mutants (having low fitness, resulting in rapid revertance of the mutation) respectively. Only one of the twenty-eight prospective mutants was discounted using this screen. As a test of the ability of the twenty-seven stable mutants to resist the lead compound in agar, six examples were picked and streaked onto lanes of MH agar containing 80 μg/ml of the compound, alongside two parent lines. The resulting plate after overnight incubation (37 °C) is shown in Figure 4.2, where lanes containing prospective RMs streaked towards the centre of the plate resulted in a 'lawn' of *E. coli*, while the WT strain only produced a few colonies at the site of initial inoculation, where the bacterial load would have been highest. This may indicate that on agar, a layer of dead cells is able to protect growing *E. coli* cells from the lethal effect of the lead compound.

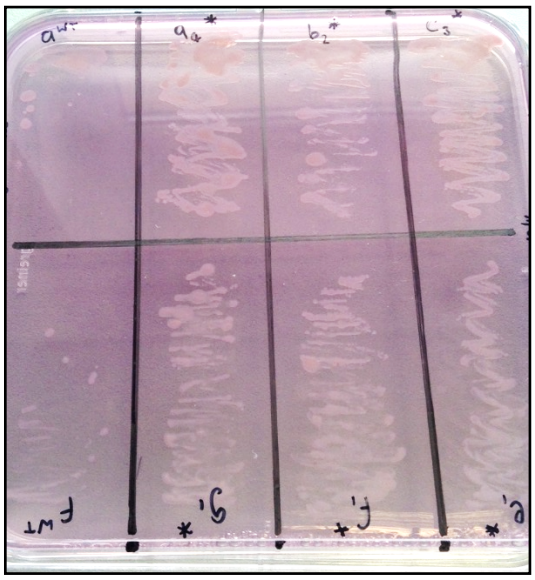

**Figure 4.2: Tolerant mutant and wild type lines of *E. coli* Sakai smeared onto lanes of MH agar infused with the lead compound**, $\Lambda_{Fe}$-$[Fe_2L^b_3]Cl_4$, at 80 μg/ml. Two lanes containing wild type lines are shown on the far left, with the other six lanes hosting selected mutant lines. Picked colonies were smeared along their lanes towards the centre line.

From the twenty-seven prospective stable mutants, overnight cultures in CAMHB were grown. These were diluted to $5 \times 10^5$ cfu/ml in 1 ml CAMHB, containing the lead compound at a concentration of 2 μg/ml (the WT MIC determined by broth microdilution). This was also performed for the seven WT parent lines, and all thirty-four samples plus negative controls were incubated for 20 h (37 °C) in sterile 24-well plates. The $OD_{600}$ was measured for each cell line, and it was found that after subtraction of the baseline (average negative control measurement), the growth varied considerably across cell lines. WT/parent lines showed negligible signs of growth as expected, and while all prospective RM were observed to have grown somewhat (all $OD_{600} > 0.05$), some prospective RMs grew considerably ($OD_{600} > 1$), and others displayed only weak signs of growth. The most promising candidates, *i.e.* those that registered an $OD_{600} > 0.5$, were selected for further study that involved comparing their phenotypes and genotypes to the parent lines. This final selection yielded seventeen RM lines, with at least one RM line sourced from each of the seven original parent lines.

To determine the extent of resistance in the seventeen chosen RM lines, MIC of these best candidates was measured using the protocol described in the previous chapter. The results are tabulated in Table 4.1. This confirmed that the RM candidates were indeed more resistant to the lead compound, $\Lambda_{Fe}$-$[Fe_2\mathbf{L}^{\mathbf{b}}_3]Cl_4$, but with only slight shifts in the MIC (×2-4). This suggests that these lines represent tolerant mutants, rather than fully resistant strains.

### 4.2.3 Whole genome sequencing, bioinformatic analysis, and characterisation of genetic alterations

Cultures of each of the 17 tolerant mutants were grown in CAMHB overnight, alongside WT *E. coli* Sakai. Genomic DNA was collected from these cultures, prepared for whole genome sequencing (WGS) using the Illumina Nextera® XT kit, and sequenced with an Illumina MiSeq™ sequencer (Microbiology & Infection division, University of Warwick), as outlined in Chapter 6.

WGS allowed a search for mutations common to all or some of the 17 tolerant strains. The nature of the Illumina sequencing platform does not provide fully sequenced "closed" genomes, however, the web based Enterobase service[19] could be used to assemble and compare DNA contigs (overlapping DNA sequences that together represent a *contiguous* consensus region of DNA) from the 17 genomes to ascertain any single nucleotide polymorphisms (SNPs), as well as small DNA insertions or deletions. This analysis was carried out by Drs Alexia Hapeshi and Nicholas Waterfield (University of Warwick), and is summarised in Table 4.1.

| ***E. coli* cell line** | **MIC against lead compound** (μg/ml) | **Mutation detected** (Yes or No) | **Mutation type** | **Alteration position** (NCBI reference) | **Change relative to WT** | **Gene(s) affected** | **Plasmid to Chromosome coverage ratio** (relative to WT) |
|---|---|---|---|---|---|---|---|
| **WT** | **2** | **-** | **-** | **-** | **-** | **-** | **1** |
| a1 | 4 | Yes | Deletion | | 550 bases lost | *waaG, waaQ* | 1.53 |
| a4 | 4 | Yes | Deletion | 4971120 | ~1900 bases lost | *btuB* | 0.01 |
| b1 | 8 | Yes | SNP | 1736847 | G to T | *galU* | 1.27 |
| b2 | 4 | Yes | Deletion | 4550911 | 11 bases lost | *waaG* | 0.56 |
| c2 | 8 | Yes | SNP | 1737380 | G to A | *galU* | 1.37 |
| c3 | 4 | Yes | SNP | 4974478 | C to G | *btuB* | 0.03 |
| d4 | 4 | No | | | | | 0.21 |
| e1 | 4 | Yes | SNP | 1737192 | A to C | *galU* | 1.07 |
| e2 | 8 | No | | | | | 0.20 |
| e4 | 8 | No | | | | | 0.07 |
| f1 | 8 | Yes | SNP | 1737192 | A to C | *galU* | 0.67 |
| f3 | 4 | No | | | | | 0.55 |
| f4 | 4 | No | SNP* | | | *galU* | 0.05 |
| g1 | 4 | Yes | Deletion | 4974320 | 1 base (T) lost | *btuB* | 0.56 |
| g2 | 4 | No | Insertion | 4973226 | G inserted | *btuB* | 0.43 |
| g3 | 8 | No | Deletion* | 4973227 | 1 base (G) lost | *btuB* | 0.49 |
| g4 | 4 | Yes | SNP | 4974212 | C to T | *btuB* | 0.55 |

**Table 4.1: Characterisation of *E. coli* Sakai tolerant mutants**, in comparison to the WT strain. Response to the lead compound (MIC) is compared to genomic changes found through EnteroBase. Relative plasmid (pO157) levels found through mapping coverages are also listed. Those identified later *via* Sanger sequencing are marked *.

While most of these 'tolerant mutations' could be grouped into three distinct classes, interestingly no evidence of traditional target site mutations, which would have pointed to a specific target in the cell, was observed. Rather all three groups showed mutations in genes for proteins involved in the maintenance of the outer membrane of the cell.

Two of the mutation groups had acquired mutations that would alter the biophysical properties of the lipopolysaccharide (LPS) outer membrane (see Figure 1.2), presumably lowering the interaction of the lead compound with the cell. Specifically, mutations were observed in the *waaG* glucosyltransferase and *galU*, UTP-glucose-1-phosphate uridylyltransferase genes. The WaaG glycosyltransferase enzyme is involved in the synthesis of LPSs that constitute the outer leaflet of the outer membrane in Gram-negative bacteria, and has previously been identified as a potential antibiotic target.[20] It is located at the cytosolic side of the inner membrane, where it catalyses the transfer of the first outer-core glucose to the inner core during lipopolysaccharide synthesis. Similarly, the GalU enzyme is also involved in LPS synthesis. The LPS O-antigen of EHEC O157:H7 comprises *N*-acetyl-D-perosamine, L-fucose, D-glucose, and *N*-acetyl-D-galactose.[21] This normally has a defensive role against host antimicrobial peptides. As *N*-acetyl-D-galactose is synthesized from galactose by GalE, GalT, GalK, and GalU, [22] these *galU* mutants will have defective O-antigen.

The third class of mutants contain mutations that pre-terminate the vitamin B12 transporter gene, *btuB*. The protein expressed by this gene (BtuB) is responsible for the active translocation of vitamin B12 (cyanocobalamin) across the outer membrane to the periplasmic space. It derives its energy for transport by interacting with the trans-periplasmic membrane protein TonB. It also acts as the receptor for the proteinaceous antibacterial A and E colicins.[23] This transporter may 'promiscuously' contribute to entry of the lead compound into the periplasm, especially given BtuB is thought to mediate colicin action upon *E. coli*. Indeed non-functional mutations to the *E. coli btuB* gene have been shown to confer increased colicin resistance, which

could be reversed by the addition of a plasmid bearing a functioning copy of the *btuB* gene.[24]

It is harder to account for the increase in tolerance in the remaining mutants, in which no chromosomal SNPs or insertion/deletions could be detected, only the loss of the pO157 virulence plasmid (extrachromosomal DNA). The loss of the plasmid could be co-incidental, perhaps just an indication of bacterial stress, with any genuine tolerance SNPs, being missed as a consequence of the incomplete nature of MiSeq based WGS. However, it is noteworthy that pO157 encodes a small operon of genes predicted to be involved in LPS modification.[25] It could therefore be speculated that the loss of these genes may have resulted in increased tolerance observed, again through changes in surface chemistry of the bacteria.

### 4.2.4 Cross resistance

| Compound | **MIC** (μg/ml) **vs. *E. coli* Sakai** | | | |
|---|---|---|---|---|
| | **Mutants** | | | **WT** |
| | **b1** | **b2** | **g4** | |
| $\Lambda_{Fe}$-$[Fe_2\mathbf{L}^{b}_3]Cl_4$ | 8 | 4 | 4 | 2 |
| $\Delta_{Fe}$-$[Fe_2\mathbf{L}^{b}_3]Cl_4$ | 16 | 16 | 16 | 4 |
| $\Lambda_{Fe}$-$[Fe_2\mathbf{L}^{a}_3]Cl_4$ | 8 | 8 | 32 | 16 |
| $\Delta_{Fe}$-$[Fe_2\mathbf{L}^{a}_3]Cl_4$ | 16 | 32 | 64 | 32 |

**Table 4.2: Cross-resistance of *E. coli* Sakai mutants to lead anti-*E. coli* flexicates** determined through MIC measurements. Values for E. coli Sakai WT, and earlier screening against the lead compound, are included for reference.

To determine whether *E. coli* Sakai mutants with tolerance to $\Lambda_{Fe}$-$[Fe_2\mathbf{L}^{b}_3]Cl_4$ (the lead compound) exhibit cross-resistance to closely related compounds, three well-characterised mutants; b1, b2, and g4 (representing alterations to genes *galU*, *waaG*, and *btuB* respectively), were selected for screening against compounds closely

related to the lead compound. These included its antipode, $\Delta_{Fe}$-$[Fe_2\mathbf{L}^{\mathbf{b}}{}_3]Cl_4$, and *p*-xylenyl bridged $[Fe_2\mathbf{L}^{\mathbf{a}}{}_3]Cl_4$ enantiomers. Results are listed in Table 4.2.

Intriguing differences in the responses of mutants to these variant forms of flexicates were observed. The *galU* mutant, b1, was more tolerant to $[Fe_2\mathbf{L}^{\mathbf{b}}{}_3]Cl_4$ enantiomers than the wild-type, and yet this strain is *more susceptible* to $[Fe_2\mathbf{L}^{\mathbf{a}}{}_3]Cl_4$ enantiomers compared to the WT. This finding is reminiscent of the observation made in the previous chapter, that flexicate-resistant *P. aeruginosa* PAO1 and *K. pneumoniae* KP02 were most susceptible to the prototype class Ia flexicate, $\Lambda_{Fe}$-$[Fe_2\mathbf{L}^{\mathbf{a}}{}_3]Cl_4$. The *waaG* mutant, b2, possessed increased resistance to $\Delta_{Fe}$-$[Fe_2\mathbf{L}^{\mathbf{b}}{}_3]Cl_4$, though susceptibility to $[Fe_2\mathbf{L}^{\mathbf{a}}{}_3]Cl_4$ enantiomers remained unchanged. Finally, the *btuB* mutant, g4, exhibited increased resistance to all compounds. This study supports the notion that membrane interactions are indeed key to the interactions of these lead compounds, and is also indicative of some structure-specificity to this interaction.

## 4.3 Transcriptome Response

An alternative approach to investigating the biochemical interactions that define the mechanism of an antimicrobial agent is to study changes in bacterial gene expression (mRNA levels) when the organism is challenged with the antimicrobial compound. In this case it is important to use sub-lethal doses of the agent so that bacteria are affected by the agent and have time to respond through changes in gene expression, but are not actually killed.[26] Bacterial transcriptional responses to stress are typically very rapid, on the timescale of minutes. In order to allow a stress to take effect and elicit a transcriptome response, studies of bacterial transcriptional responses to antimicrobial stress typically measure RNA levels 15-60 min after application of the

agent to a microbial culture.[27-29] Analysing total RNA may also be useful in identifying any small noncoding RNA transcripts (sRNA) that are not translated into protein, but are nevertheless implicit in influencing cellular processes by other regulatory mechanisms.[30]

The current technique for measuring a transcriptomic profile is through RNA sequencing (RNA-seq),[31] which involves conversion of RNA purified from microbial culture to complementary DNA (cDNA). Synthesised cDNA may then be sequenced using second generation high-throughput RNA-seq kits, which use similar technology to whole-genome sequencing that has largely replaced older microarray technology.[32, 33] There are several important considerations that should precede sequencing, however; (i) optimal timing and concentration for the addition of the antimicrobial agent should be determined beforehand, to ensure that the transcriptome is predominantly influenced by the agent, rather than by general stress and/or cell death signalling; (ii) contaminating DNA must be fully depleted from the RNA samples, using *e.g.* DNase; (iii) RNA is readily degraded by environmental RNAases, and therefore must be rapidly protected from degradation by using appropriate handling techniques, and ensuring all workspaces and equipment are sterile and free of RNases; (iv) in order to detect low-level transcripts with enough read depth to infer statistically significant changes, ribosomal RNA (rRNA), which is not a component of the expression profile and comprises the majority (95-99 %) of RNA present in a bacterium,[34] must be depleted. Quality controls may be used during the preparation of RNA sample for sequencing (*e.g.* the Agilent 2100 Bioanalyzer DNA/RNA quality control system), in order to ensure the results obtained are of high quality.

### 4.3.1 Optimisation of experimental conditions

An overnight culture of WT *E. coli* Sakai was diluted to an $OD_{600}$ of 0.025, in 3 × 50 ml CAMHB. The growth of these triplicates was monitored during incubation at 37 °C (with shaking aeration), by taking $OD_{600}$ measurements every 30 min, until stationary phase behaviour was observed (after 8 h). This was repeated with cultures where 0.5 μg/ml of $\Lambda_{Fe}$-$[Fe_2\mathbf{L}^{b}_3]Cl_4$ (¼ of the MIC) was added either initially, or during exponential growth ($OD_{600}$ ≈ 0.5), 200 min into the experiment. Growth curves plotted from $OD_{600}$ data, is shown in Figure 4.3. Since the sub-MIC, 0.5 μg/ml, addition of the lead compound during exponential growth caused minimal deviation in growth from the control, this condition was chosen for the experiment to determine the effect of the compound on the transcriptome.

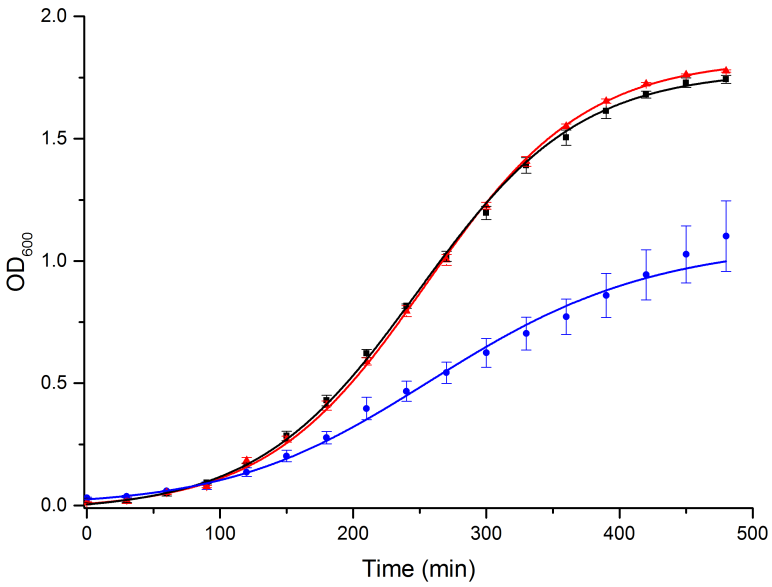


**Figure 4.3: Growth of *E. coli* Sakai WT in response to the lead compound** added at a quarter of the MIC (0.5 μg/ml), either initially (blue circles) or at 200 minutes during exponential phase (red triangles). The control culture is included for reference (black squares). Error bars representing 95 % confidence intervals, calculated using replicates, are shown.

In line with similar experiments,[27-29] it was planned to extract the RNA 40 min after the addition of the compound. The $OD_{600}$ 240 min after inoculation, with addition of the compound at 200 min, is around 0.75 for both this condition and the control culture. This corresponds to approximately $6 \times 10^8$ cfu/ml.

### 4.3.2 Extraction and purification of microbial RNA

In line with the chosen setup described in the previous section, three overnight cultures of WT *E. coli* Sakai were each diluted in 2 × 50 ml CAMHB (one control and one treated culture), to an $OD_{600}$ of 0.025. These cultures were incubated at 37 °C for 200 min, whereupon $\Lambda_{Fe}$-$[Fe_2\mathbf{L}^{\mathbf{b}}_3]Cl_4$ was added to one culture from each pair, to a final concentration of 0.5 μg/ml. After a further 40 min of incubation, 1 ml of each culture was added to separate 2 ml aliquots of RNAprotect® reagent (Qiagen), and vortexed immediately, preserving and stabilising the microbial RNA. After a 5 min incubation at ambient temperature, cells were collected by centrifugation. RNA was then extracted from the samples and prepared for RNA-seq as outlined in Chapter 6.

Samples were finally eluted in 40 μl of RNase-free water per sample. The RNA concentration of each sample was determined from 1 μl of RNA elution, using the Qubit® HS RNA quantification kit (ThermoFisher Scientific). The absence of DNA from the RNA elution was confirmed using a standard polymerase chain reaction (PCR) to attempt the amplification of the gene encoding the *E. coli* 16S ribosomal subunit. The absence of detectable PCR products in subsequent agarose gel electrophoresis, signified the lack of genomic DNA contamination. Additionally, the Agilent 2100 Bioanalyzer instrument was used to check the quality of RNA, using a further 2 μl of RNA elution prepared using the RNA 6000 pico kit (Agilent), according to the manufacturer's instructions. Bioanalyzer electropherograms, which plot fluorescence output (proportional to RNA quantity) versus elution time (proportional to fragment size), are shown in Figure 4.4. The large sharp rRNA peaks (16S and 23S subunits) and reasonably smooth baseline suggests minimal

RNA degradation has occurred, making the remaining RNA elution samples appropriate for further processing towards RNA-seq.

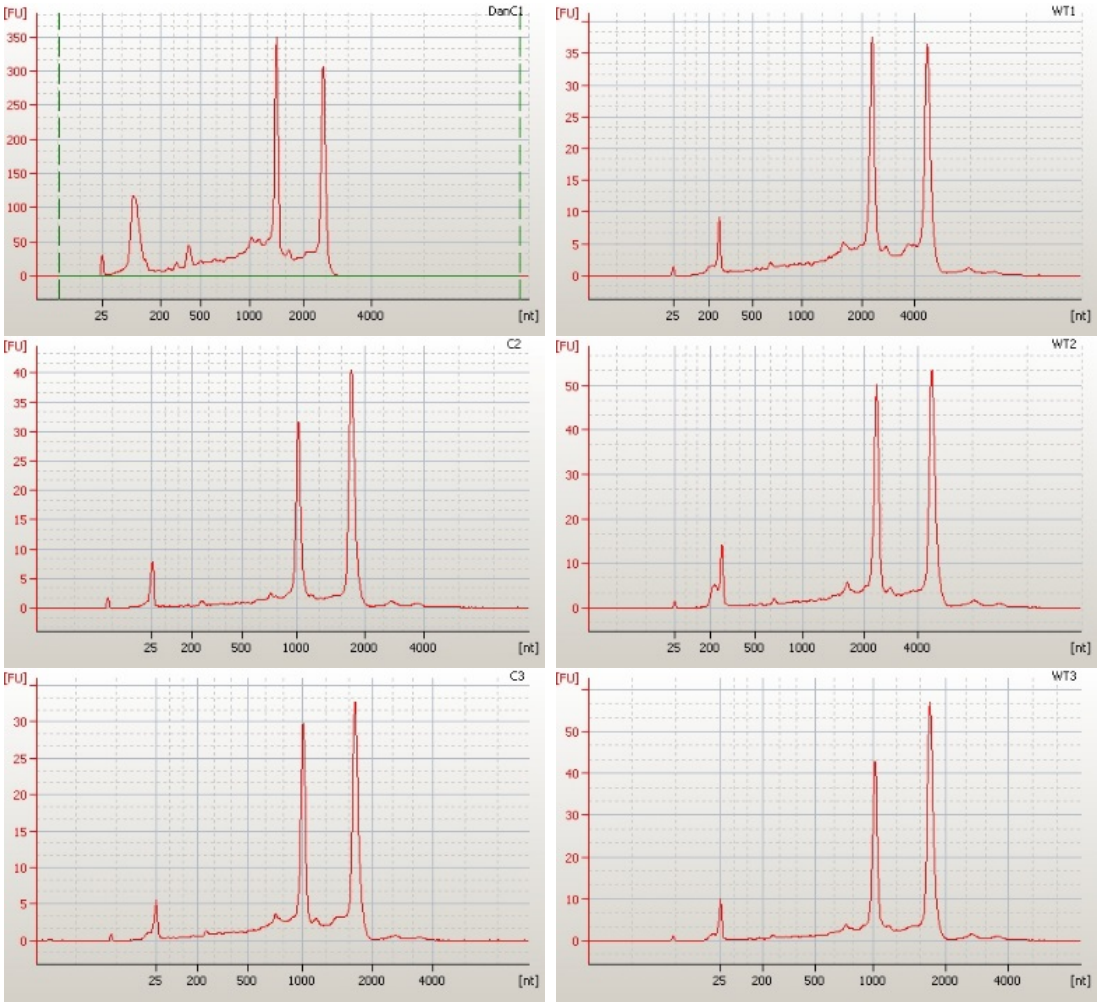


**Figure 4.4: Agilent Bioanalyzer electropherograms of *E. coli* Sakai RNA,** used to determine sample quality. The two largest peaks, towards the right of each electropherogram, are due to the *E. coli* ribosomal 16S and 23S subunits. The three electropherograms on the left are of RNA from *E. coli* treated with the lead compound, and those on the right are of RNA from control groups.

### 4.3.3 Depletion of rRNA

As stated above, rRNA is the dominant form of RNA purified from microbial cells, and this should be significantly depleted to improve read depth of RNA-seq data. The Ribo-Zero™ bacterial rRNA removal kit (Illumina) was used according to the

manufacturer's instructions, to achieve rRNA depletion of 4 µg of input RNA per sample. At the final step, samples were eluted into 5.5 µl RNase-free water.

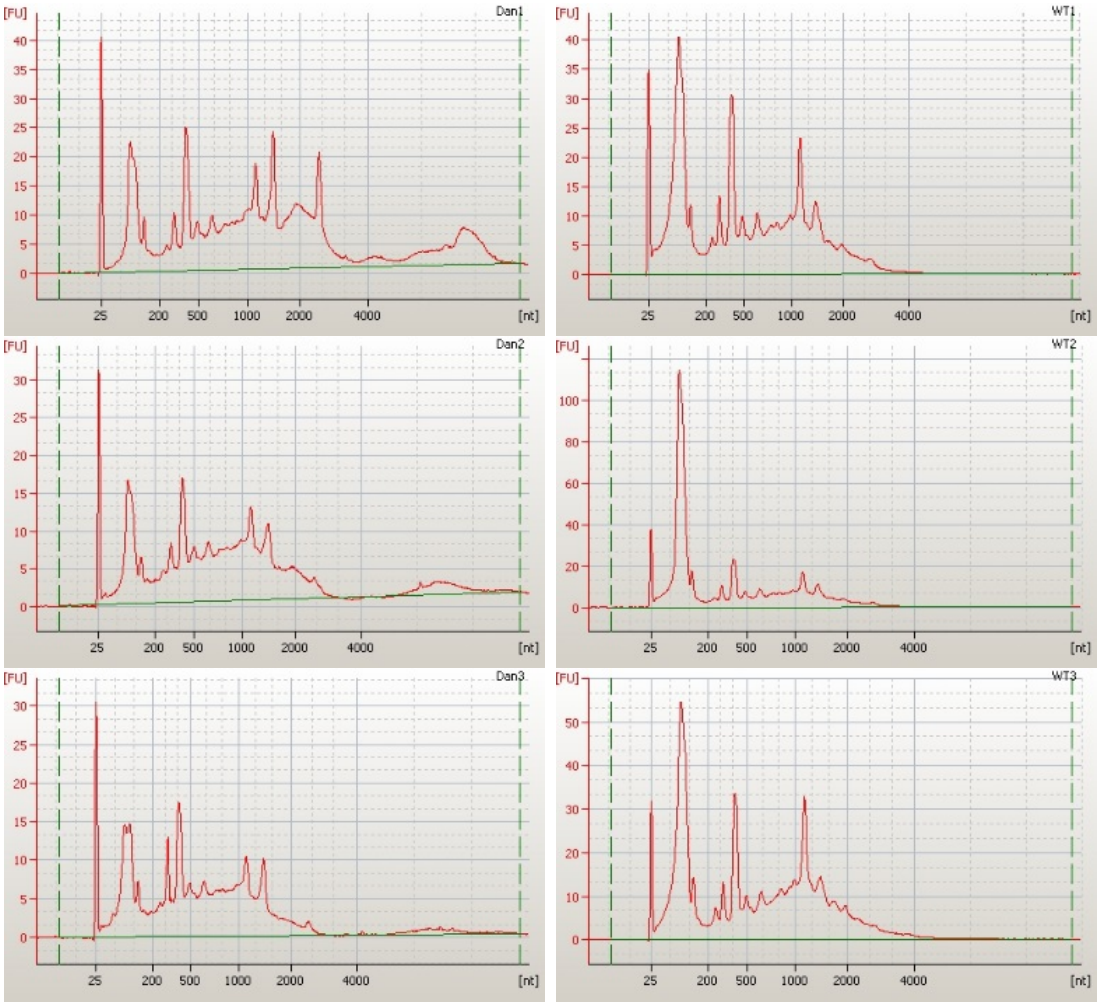


**Figure 4.5: Agilent Bioanalyzer electropherograms of enriched *E. coli* Sakai RNA after rRNA depletion,** used to determine sample quality. The three electropherograms on the left are of enriched RNA from *E. coli* treated with the lead compound, and those on the right are of enriched RNA from control groups.

The Agilent 2100 Bioanalyzer instrument was used to check the quality of RNA, using 0.5 µl of input RNA per sample, prepared using the RNA 6000 pico kit (Agilent) as per kit instructions. Bioanalyzer electropherograms, shown in Figure 4.5, have much smaller 16S and 23S rRNA peaks compared to those of the pre-enriched RNA samples (Figure 4.4), suggesting the rRNA depletion was successful. The remaining 5 µl of each enriched RNA sample was progressed towards conversion to cDNA.

### 4.3.4 Sequencing *via* conversion to cDNA

A modified TruSeq™ (Illumina) magnetic bead format, stranded mRNA sample preparation protocol was used to prepare cDNA libraries for sequencing (see Chapter 6). All steps were carried out in sealable sterile 96-well plates. The prepared cDNA libraries were recovered from this process as 30 µl of supernatant (in TruSeq™ Resuspension buffer). The DNA concentrations of sample libraries were determined using the Qubit® HS dsDNA quantification kit (2 µl of input solution from each library). The Agilent 2100 Bioanalyzer instrument was used to determine the quality and average fragment size of cDNA sample libraries, using 0.5 µl of input DNA each, prepared using the High-Sensitivity DNA kit (Agilent) as per kit instructions. Bioanalyzer electropherograms, shown in Figure 4.6, each show a single shouldered peak of roughly similar fragment size (260-275 bp). This would suggest the conversion to cDNA has been successful and that the samples are of sufficient quality to proceed towards sequencing. The cDNA libraries, prepared using TruSeq™ stranded mRNA kit, were then sequenced on the Illumina MiSeq™ platform, prepared using the paired-end 2 × 75 bp kit as per instructions.

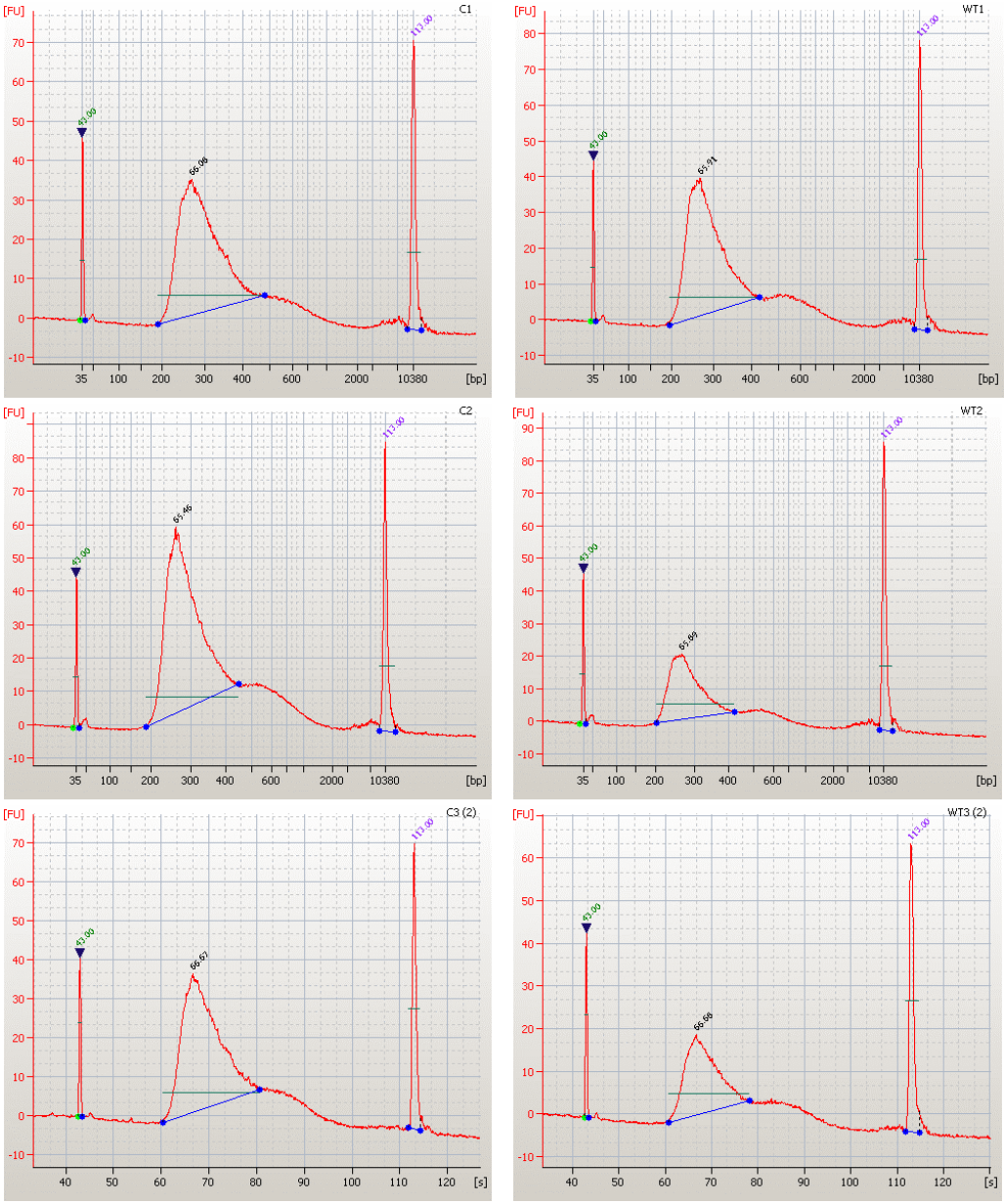


**Figure 4.6: Agilent Bioanalyzer electropherograms of cDNA synthesised from enriched *E.coli* Sakai RNA**, using the TruSeq™ kit, to determine sample quality and average DNA fragment size. The three electropherograms on the left are of cDNA sourced from *E. coli* treated with the lead compound, and those on the right are of sample sourced from control groups. Sharp peaks are due to short and long DNA markers respectively. Annotations (blue lines) demonstrate where fragment sizes were determined.

### 4.3.5 Bioinformatic analyses and results

RNA-seq data was mapped onto the genome sequence of EHEC Sakai and analysed as paired datasets using the DESeq2 program,[35] by Drs Alexia Hapeshi and Nicholas Waterfield (University of Warwick). Using this approach and paired sample analysis, a limited number of statistically significant expression changes, relevant to the activity of the lead compound, were successfully defined. An increase in

transcription of 48 genes (Table 4.3) and a decrease in only 20 (Table 4.4) was observed. A combination of manual analysis; STRING network analysis and KEGG database pathway-mapping tools, was used to further interpret this data (Figure 4.7).

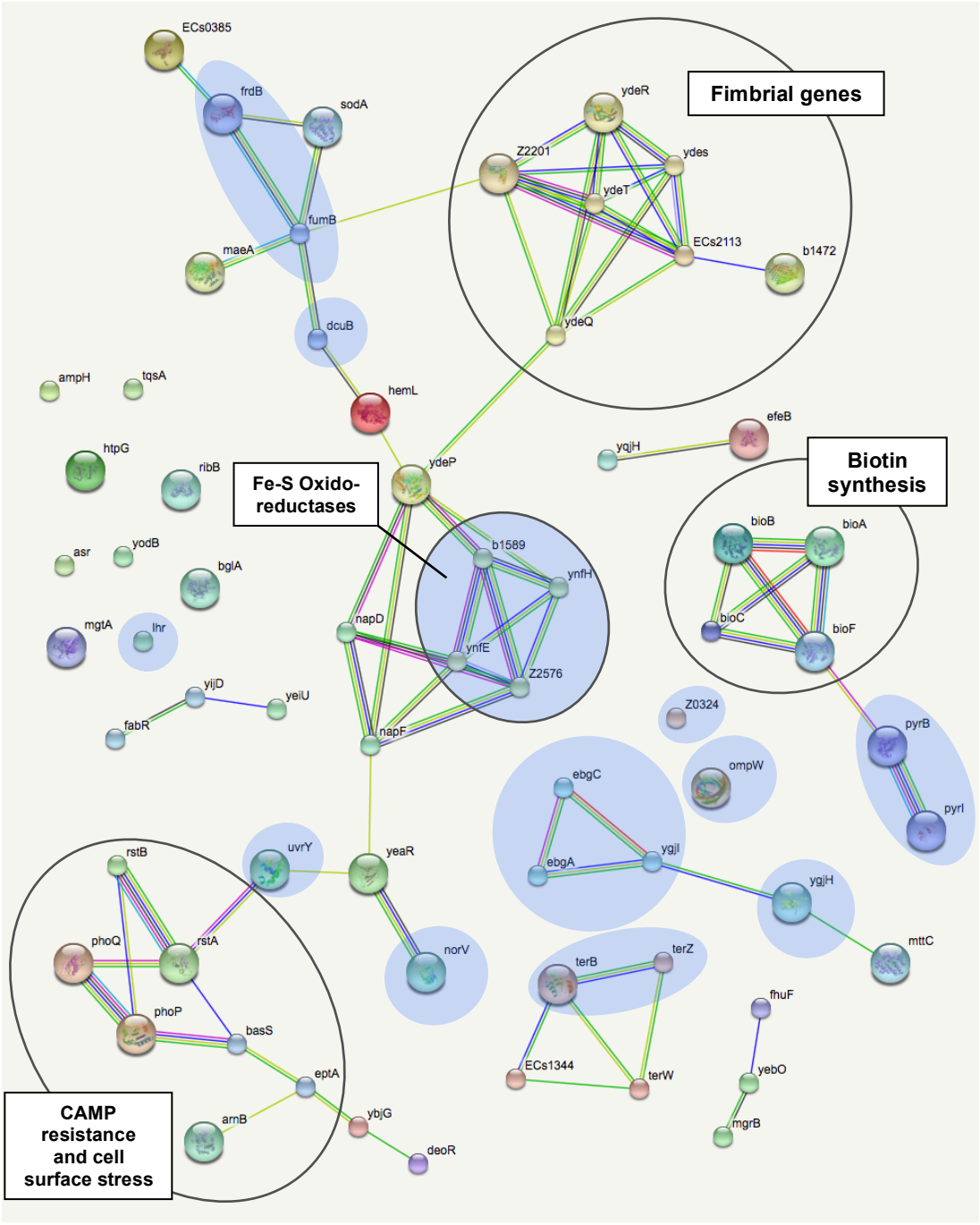


**Figure 4.7: KEGG database pathway-mapping of RNA-seq (*E. coli* Sakai response) data,** illustrating pathway relationships (connective lines) between genes affected by treatment with the lead compound (nodes). Down-regulated genes are shaded blue (others are all upregulated). Important gene clusters are circled and annotated. There is no particular meaning to the node colours, but their size relates to the availability of structural information for the corresponding protein. The nature of the relationships between genes and their corresponding proteins are denoted by line colour: known interactions are turquoise (from curated databases) or magenta (experimentally determined); predicted interactions are green (gene neighbourhood), red (gene fusions), or blue (gene co-occurrence); others are yellow (textmining), black (co-expression), or lilac (protein homology).[36]

| Gene | Product | $Log_2$ fold change | Gene | Product | $Log_2$ fold change |
|---|---|---|---|---|---|
| *fimH* | Fimbiral adhesin FimH | 2.13 | *mdh* | Malate dehydrogenase | 1.26 |
| *ydeR* | Fimbrial-like protein | 2.09 | *bioC* | Biotin synthase BioC | 1.24 |
| *ydeT* | Fimbrial usher protein | 2.08 | *efeB* | Deferrochelatase/ peroxidase | 1.23 |
| ECs2112 | Fimbrial chaperone protein | 2.07 | *bioF* | 8-amino-7-oxononanoate synthase | 1.23 |
| *yodB* | Cytochrome b561 | 1.98 | *ampH* | Endopeptidase AmpH | 1.22 |
| ECs2113 | Major fimbrial subunit | 1.91 | *fabR* | Transcriptional repressor FabR | 1.21 |
| *ribB* | DHBP synthase | 1.87 | *yijD* | Inner-membrane protein | 1.18 |
| *napF* | Ferredoxin protein NapF | 1.84 | ECs0853 | Biotin synthase | 1.17 |
| *yedS* | Fimbrial-like protein | 1.79 | *lpxT* | Lipid A 1-diphosphate synthase LpxT | 1.17 |
| *ybjG* | Undecaprenyl-diphosphatase | 1.75 | *phoE* | Phosphoporin protein PhoE | 1.16 |
| *ydeP* | Oxidoreductase | 1.75 | *yeaR* | $NO_x$ response protein YeaR | 1.15 |
| ECs2713 | Hypothetical protein | 1.70 | *tatD* | Exonuclease | 1.14 |
| *mgtA* | $Mg^{2+}$-transporter | 1.64 | *eptA* | phosphoethanolamine transferase EptA | 1.13 |
| *rstA* | Transcriptional regulator | 1.61 | *bioA* | Adenosylmethionine-8-amino-7-oxononanoate aminotransferase | 1.13 |
| *terW* | Regulator of tellurite resistance *ter* operon | 1.59 | *yqjH* | Ferric-chelate reductase | 1.10 |
| *asr* | Acid shock protein | 1.56 | ECs1344 | Hypothetical protein | 1.10 |
| *rstB* | Sensor protein RstB | 1.53 | *arnB* | UDP-4-amino-4-deoxy-L-arabinose transaminase | 1.07 |
| *yebO* | Membrane protein YebO | 1.49 | *phoP* | PhoP family transcriptional regulator | 1.04 |
| *yebG* | Membrane protein YebG | 1.48 | *deoR* | Transcriptional repressor DeoR | 0.99 |
| *fuhF* | Ferric iron reductase FhuF-like transporter | 1.48 | *prpB* | 2-methylisocitrate lyase | 0.96 |
| *napD* | NapD assembly protein | 1.43 | *pmrB* | Sensor protein PmrB/BasS | 0.95 |
| *sodA* | Superoxide dismutase | 1.38 | *tqsA* | AI-2 transport protein | 0.95 |
| *phoQ* | Sensor protein PhoQ | 1.32 | *bglA* | 6-phospho-β-glucosidase | 0.91 |
| *hemL* | Glutamate-1-semialdehyde aminotransferase | 1.29 | *hsp90* | Heat-shock protein | 0.81 |

**Table 4.3: Genes found to be significantly upregulated in treated samples (0.5 µg/ml lead compound),** relative to the untreated control, using EnteroBase. All *p*-values <0.001.

| Gene | Product | $Log_2$ fold change | Gene | Product | $Log_2$ fold change |
|---|---|---|---|---|---|
| *ygjH* | Putative tRNA synthetase | -1.74 | *egbC* | β-D-galactosidase | -1.14 |
| *norV* | Anaerobic NO-reductase flavorubredoxin | -1.63 | *ynfE* | Oxidoreductase | -1.13 |
| *dcuB* | Anaerobic C4-dicarboxylate transporter | -1.55 | *csrB* | sRNA Inhibitor of CsrA | -1.08 |
| *egbA* | β-D-galactosidase | -1.53 | *lhr* | ATP-dependent helicase | -1.00 |
| *ompW* | Outer membrane porin | -1.46 | *pyrI* | Aspartate carbamoyltransferase | -0.98 |
| *fumB* | Fumarase B | -1.35 | *pyrB* | Aspartate carbamoyltransferase | -0.94 |
| *dmsA* | DMSO-reductase | -1.25 | *terB* | Tellurite, colicin & phage resistance protein | -0.94 |
| *dmsB* | DMSO-reductase | -1.23 | *frdB* | Fumarate reductase | -0.87 |
| *dmsC* | DMSO-reductase | -1.21 | *int* | Integrase for prophage CP-933I | -0.87 |
| *ygjL* | Oxidoreductase | -1.14 | *terZ* | Tellurite, colicin & phage resistance protein | -0.87 |

**Table 4.4: Genes found to be significantly down-regulated in treated samples (0.5 µg/ml lead compound),** relative to the untreated control, using EnteroBase**.** All *p*-values <0.001.

Full details of the mapping and analyses (STRING/KEGG) can be found in Chapter 6. Some of the key findings are discussed in the following sections.

### 4.3.6 Cationic antimicrobial peptide resistance and membrane maintenance

A crucial finding was that *E. coli* induced expression of genes for sensors, regulators and LPS modification that are known to be up regulated in response to attack by cationic antimicrobial peptides (CAMPs).[37] These include the genes for PhoPQ, a two component (2C) sensor/regulator pair, and MgrB, which modulates the PhoQ sensor response range.[38] While the analysis does not directly indicate whether the sensor is being activated or not, the increase in transcription of auto-regulated *phoPQ* genes themselves[39] along with known regulon genes strongly suggests that this is the case. This 2C system is known to up regulate genes for LPS modification in response to CAMP insult,[39] and indeed observed an up regulation in

transcription of the *arnB* gene, encoding a UDP-4-amino-4-deoxy-l-arabinose-oxoglutarate aminotransferase, was observed. This transamindase is an enzyme that acts in a pathway that modifies lipid A phosphates with 4-amino-4-deoxy-l-arabinose, causing an increase the surface positive charge of the cell, reducing interaction with CAMPs and an giving increased resistance to polymyxins.[40] Several other PhoPQ regulated genes are also up regulated upon exposure to the lead compound. These include genes for the proteins, PhoE (an outer membrane phosphoporin allowing for passive diffusion of small molecules), MgtA (a magnesium-transporting ATPase), HemL (glutamate-1-semialdehyde aminotransferase involved in the process of heme synthesis and also regulated by $Mg^{2+}$ levels) and RstAB (a 2C sensor/regulator system which supresses RpoS expression and is itself also regulated by $Mg^{2+}$ levels). It should be noted that the *phoPQ* genes are also under the control of a $Mg^{2+}$ responsive promoter, suggesting 'cross-talk' between several stimuli. While the PhoE porin showed transcriptional up regulation, it is noted that a second porin, OmpW showed a significant down regulation. OmpW functions in transport of small, hydrophobic molecules across the outer membrane, related to cell survival under microaerobic conditions. It also serves as a receptor for the antimicrobial protein, Colicin S4.

Increased transcription of the gene for the YbjG undecaprenyl pyrophosphate phosphatase is also relevant as BcrC/YbjG family proteins confer bacitracin resistance.[41] Disruption of *ybjG* causes increased bacitracin sensitivity, while overexpression causes increased resistance to bacitracin. Interestingly an increase in transcription of the gene for the regulator FabR was also observed. FabR is known to repress the transcription of *fabB*, involved in unsaturated fatty acid (UFA) biosynthesis.[42] By controlling UFA production, FabR directly influences the

physical properties of the membrane bilayer. Despite this, no significant difference in *fabB* transcription was detected at this time point, so the involvement of FabR in the regulation of other genes cannot be ruled out. Two further tightly-linked genes, also relevant to CAMP resistance[43] and showing increased transcription, are those for the EptA phosphoethanolamine transferase and its regulator sensor protein, PmrB. The sensor domain of PmrB is known to respond to several stimuli including acidic pH and an excess of Fe(III).[44] Again, indirect evidence for the activation of PmrAB system comes from the increase in *pmrB* transcription itself, consistent with its known auto-regulation, and the up regulation of *eptA* transcription. EptA catalyses the addition of a phosphoethanolamine moiety to the KDO component of lipid A.[43] This phosphoethanolamine modification of LPS is required for resistance to polymyxin and also to prevent excessive and damaging Fe(III) binding to the LPS. Interestingly, this modification is also induced in cells grown under mild acidic conditions, which provides a link to a group of up regulated genes involved in coping with acid stress (*vide infra*). While not strictly involved in cell membrane maintenance it is also noted an upregulation in a fimbrial biogenesis operon (suggesting an attempt by the cell to initiate a biofilm), in addition to the β-lactam binding protein, AmpH, which is a DD-alanine-peptidase associated with recycling and remodelling of the peptidoglycan cell wall.[45]

### 4.3.7 Acid stress response

In addition to the PmrB response the transcriptional upregulation of several other genes involved in acid stress response (ASR) were observed. Interestingly, transcriptional ASR and resistance to various membrane-active environmental

stresses, *e.g.* polymyxin B, have been observed in other bacteria, suggesting a mechanistic link.[46, 47] Another up regulated gene involved in both ASR and LPS synthesis is *lpxT*. LpxT is the lipid A 1-diphosphate synthase enzyme, which is induced under acidic aerobic conditions. It catalyses the phosphorylation of lipid A, transferring a phosphate group from undecaprenyl-pyrophosphate to the position 1 phosphate of approximately one-third of lipid A molecules, to create lipid A 1-diphosphate. This is surprising as this would have the effect of increasing the negative charge of the bacterial surface, acting antagonistically to the roles of EptA and ArnB (*vide supra*). It should be noted however that the overall transcription level of this gene is significantly lower than the levels of *eptA* and *arnB* suggesting its effects may be outcompeted. This observation nevertheless highlights the complexities associated with the structural remodelling of Gram-negative lipopolysaccharides. Another gene known to be dependent upon PhoB and RstA (*vide supra*) that can be seen to increase is *asr*, which facilitates an acid-induced protective response in cells exposed to very low pH. A further three up regulated genes known to be involved with ASR are those encoding for EfeB (which extracts iron from exogenous heme and believed to function under acid-stress conditions), YdeP (an oxidoreductase) and RibB (which catalyses the first committed step in the biosynthesis of riboflavin when induced by low pH). In addition to acid stress we also observed the up regulation of response genes for other forms of stress including the heat shock protein Hsp90 and TerW, which is involved in tellurite resistance. On the other hand we also observe down regulation of the *terZ* and *terB* genes, which are also involved in tellurite resistance. The significance of this is unclear.

Interestingly, an increase in transcription of genes relating to oxidative stress was seen, including; *sodA* superoxide dismutase, *yeaR* which is induced by nitric oxide,

*napF* a ferredoxin-type protein predicted to play a role in the oxidative stress response and *tatD* (mttC) a DNase potentially involved with the repair of peroxide-induced DNA damage. It is possible that the up regulation of *yeaR*, we observed is a result of the down regulation of the *norV* gene, which encodes a cytoplasmic nitric oxide reductase, used for the detoxification of nitric oxide.

### 4.3.8 Metabolism and redox state

While the majority of up regulated genes are accounted for in the stress responses described above, significant increases in the transcription of several genes involved in various aspects of metabolism and redox state maintenance were also observed. These include 2-methylisocitrate lyase, which catalyzes the formation of pyruvate and succinate from 2-methylisocitrate and NAD-dependent malate dehydrogenase both of which are involved with energy generation and the citric acid (TCA - tricarboxylic acid) cycle. Conversely a down-regulation of genes for two other TCA related proteins was seen; FrdB fumarate reductase (one of a class of membrane-bound, FAD-containing enzymes that are responsible for the catalysis of fumarate and succinate interconversion) and FumB fumarase (typically more abundant during anaerobic growth and down-regulated by heme limitation). There was also an up regulation in the gene encoding YodB, a cytoplasmic membrane protein (cytochrome b561) that is part of the electron transport respiratory chain. Genes for proteins involved in anabolic and catabolic processes that showed increased transcription include 6-phospho-β-glucosidase, with a likely role in carbohydrate metabolism, and four biotin cofactor synthesis genes, which are necessary for many processes, *e.g.* the production of fatty acids, and the metabolism of fats and amino acids. Two

additional genes encoding enzymes with roles in iron homeostasis are up regulated; YqjH, an NADPH-dependent ferric reductase and FhuF which is involved in the reduction of ferric iron in cytoplasmic ferrioxamine B.

The significance of the down regulation of several other genes involved in metabolic processes remains unclear. These include an operon of four genes that encode membrane localised an anaerobic dimethyl sulfoxide reductase complex and *dcuB,* encoding an anaerobic C4-dicarboxylate transporter responsible for the transport of C4-dicarboxylates from the periplasm across the inner membrane. Finally, a down-regulation was observed in genes *ebgA* and *ebgC*, which encode subunits of a cryptic β-D-galactosidase, believed to be an evolved alternative to LacZ.

## 4.4 Proteome Response

Changes to the transcriptome are only one aspect of the response of a bacterium to stress. To mount a physiologically useful response, newly synthesised or pre-existing mRNA needs to be translated into protein product. Since the processes of translation, localisation, modification and degradation that maintain the proteome have individual kinetics independent of transcription, the proteomic responses do not necessarily correlate strongly with responses at the RNA level.[48] It is therefore prudent in obtaining a full perspective of the physiological response, and how the cellular machinery executes this response, to examine both proteomic and transcriptomic responses in tandem.[49] Until recently, questions of global protein abundances had been difficult to address. However, with advances in mass spectrometry (MS), notably the development of the Orbitrap mass detector,[50] large scale analysis of full cellular proteomes has become feasible. MS proteomic methods

rely on the notion the partially digested proteins will fragment into a predictable distribution of masses, since all natural polypeptides (proteins) use the same set of ~20 amino acids and a limited suite of post-translational modifications.[51] Comparing MS data to an in silico derived protein fragmentation database can therefore be used to deduce a global protein profile.

### 4.4.1 Setup and protein extraction

Several research teams have reported integrated transcriptomic and proteomic analyses of stress-perturbed bacterial culture, typically using mass spectrometry to profile and quantify proteins, at the same time point(s) as the trascriptome was analysed.[52-54] It was therefore chosen to conduct a similar proteomic analysis of *E. coli* Sakai to the lead compound ($\Lambda_{Fe}$-$[Fe_2\mathbf{L}^{\mathbf{b}}{}_3]Cl_4$), with culture and perturbation conditions identical to those used to measure the transcriptomic response (see section 4.2); with samples taken 40 min after addition of 0.5 μg/ml compound, during exponential phase, including three replicates of the experiment and control cultures respectively. The cells can then be washed and lysed, allowing protein to be extracted using SDS polyacrylamide gel electrophoresis (SDS-PAGE), and prepared for liquid chromatography mass spectrometry (LCMS) analysis.

Protein was extracted at the relevant time point by first collecting cells by centrifugation, before washing with, and resuspending in, PBS. Cell lysis followed by SDS-PAGE were then performed as detailed in Chapter 6. Those gel images are shown in Figure 4.8; the consistency of the sample lanes attest to the homogeneity of samples produced by this protocol, in terms of the major protein bands present and total protein loading.

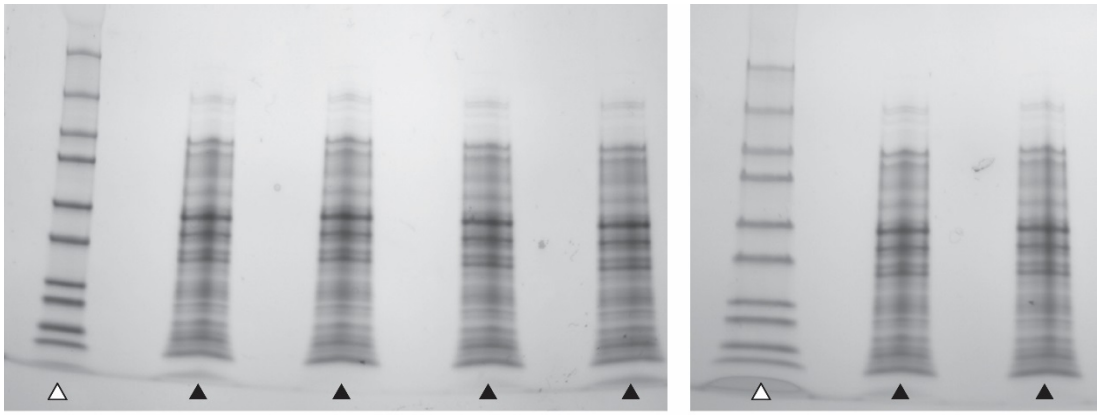

**Figure 4.8: SDS-PAGE gels of *E. coli* Sakai protein (~40 µg)** extracted from cultures with/without exposure to the lead compound during exponential growth. Hollow triangles mark lanes where a NE BioLabs broad range protein reference ladder was applied, and filled triangles mark sample lanes.

### 4.4.2 LCMS: preparation and analysis

Each sample lane from the SDS-PAGE gels were carefully extricated and cut into small pieces, which were prepared separately. Peptide samples within gel pieces were prepared for LCMS using the heterophase digestion method outlined by Shevchenko, Mann and co-workers.[55] Briefly, each sample was; reduced using dithiothreitol (DTT) to break up disulfide bridges; alkylated at reactive sites using iodoacetamide; digested using trypsin (2.5 ng/µl, 18 h incubation at 37 °C); extracted from the gel pieces by sonication in 3:1 water/acetonitrile containing 5 % formic acid. Extracts from the same SDS-PAGE lane were then recombined, and the six samples were dried under gentle vacuum (SpeedVac). These samples were stored at -20 °C, and later thawed gradually when required for LCMS analysis.

Dry peptide samples were resuspended by sonication in 55 µl of water containing 2.5 % acetonitrile and 0.05 % trifluoroacetic acid, purified using C18 desalting tips, and again dried *via* SpeedVac. Samples were finally resuspended into 1:1 methanol/water (50 µl) and a 10 µl aliquot was analysed by *nano*LC-ESI-MS/MS.

### 4.4.3 Data analysis and results

Proteins were identified from raw LCMS data (referenced against the Uniprot Escherichia_coli_O157H7 database) and label-free quantification (LFQ) values for each protein were calculated using MaxQuant software.[56] Data were inputted to Perseus[57] for normalisation and further analysis, establishing the fold difference between *E. coli* Sakai proteins (treated *vs.* control samples) and the statistical significance of those differences using the significance analysis of microarrays (SAM) technique.[58] SAM identifies statistically significant genes by carrying out protein-specific t-tests and computes a statistic $d_i$ for each protein $i$, which effectively scores the strength of the relationship between protein counts and treatment group A and B, using the difference between mean counts for each treatment and the standard error, $s_i$ (Equation 4.1). This was undertaken by Dr Alexia Hapeshi (University of Warwick) and further details are included in Chapter 6.

$$d_i = \frac{\overline{x_A}(i) - \overline{x_B}(i)}{s_i + s_0} \qquad \text{Equation 4.1}$$

The false discovery rate[59] (FDR) was set to 0.01, to match the RNA-seq analysis. The value $s_0$, a parameter used to alter the weighting given to fold difference over statistical significance in scoring, was set to typical values of either 0.2 or 0.5.[60] These settings suggested only one or four proteins had significantly different counts across treatments, respectively. Volcano plots (scatter plots of fold difference against statistical significance) illustrating this analysis are shown in Figure 4.9, and the proteins found to have significant differential counts are listed in Table 4.5.

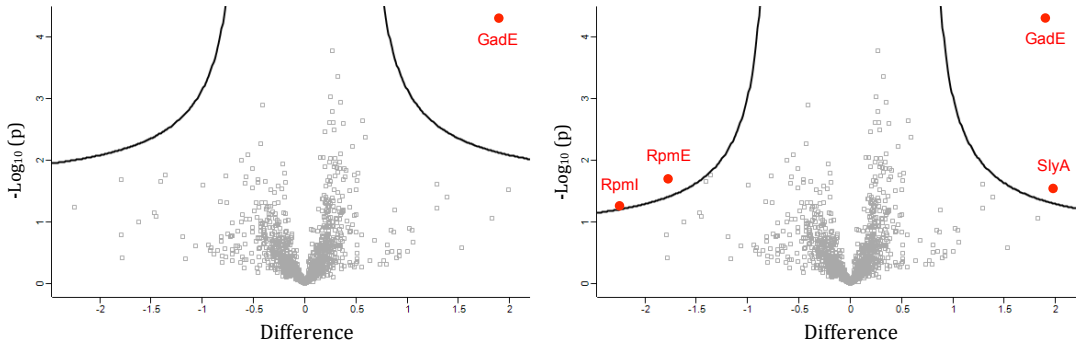


**Figure 4.9: Volcano plots of proteomic data, identifying significant protein changes between treated and control *E. coli* Sakai cells.** The difference in $\log_2$ LFQ (treated *vs.* control) is plotted against -$\log_{10}$ p-value for each protein, with selection thresholds set at $s_0$ = 0.2 (left) or 0.5 (right) shown as black curves. Proteins exceeding these thresholds are marked with red circles and annotations.

| Protein | Function | *Log₂* LFQ fold change | *-Log₁₀* p-value |
|---|---|---|---|
| GadE* | Regulates the expression of several genes involved in acid resistance | 1.89 | 4.29 |
| SlyA | Regulates the expression of several genes involved in acid resistance | 1.99 | 1.51 |
| RpmI | 50S ribosomal protein L35 | -2.25 | 1.23 |
| RpmE | 50S ribosomal protein L31 | -1.79 | 1.68 |

**Table 4.5: Proteins counts found to be significantly different in treated samples (0.5 µg/ml lead compound),** relative to the untreated control, using SAM analysis ($s_0$ = 0.5, FDR = 0.01) on Perseus software**.** Proteins that remain significant with $s_0$ = 0.2, are marked * (GadE).

The difficulty in finding significant changes in protein counts under the treatment conditions applied (40 min after an addition of the lead compound at 0.5 µg/ml), especially in contrast to the RNA-seq findings, suggest that this treatment was too subtle to detect many overt changes to the proteome. This is consistent with the low fold changes and relatively mild response observed in the RNA-seq data for the same treatment/incubation time. A higher dosage and/or a longer incubation with the complex would thus foreseeably be worthy of consideration in any future proteomic study of the antimicrobial action of the lead compound.

GadE was identified as the protein having the most significant LFQ difference across treatments, having a higher count in *E. coli* Sakai cells treated with the lead compound, in spite of a lack of significant up-regulation in the RNA-seq data. GadE

is a transcriptional regulator involved in glutamate-dependent mechanisms of acid stress response (ASR). It is required for the expression of gadA and gadBC, amongst others. This makes GadE the essential regulator for the GAD (Glutamate decarboxylase) system, which consumes protons by converting glutamate to γ-aminobutyric acid (GABA), removing them from solution.[61] This is of interest in relation to the RNA-seq data, as a number of genes linked to ASR were found to be differentially expressed (see section 4.3.7). Taken together, this would suggest the lead compound is affecting the intracellular pH. This effect could be directly or indirectly critical to the mechanism (though there may be several), or it could be the result of another mechanism, *e.g.* disruption of the proton-motive force could cause a build-up of protons in the cell.

Compellingly, another protein with a higher count in treated cells, albeit with much lower statistical significance (p-value ≈ 0.03), was the transcriptional regulator, SlyA. As well as being another protein associated with ASR, SlyA is also associated with resistance to CAMPs,[62] another process where associated genes were seen to be upregulated in the RNA-study (see section 4.3.6). The only proteins showing any remotely significant lowering of their counts after treatment with the lead compound were both ribosomal proteins. This may suggest that the cell is diverting resources away from ribosome assembly in response to the activation of specific stress pathway. However, for both proteins the p-values associated with these lower counts (0.02-0.06) are rather high, making these differences more ambiguous.

## 4.5 Summary

This chapter described tandem "omics" approaches that investigated the mechanism of the lead class Ia flexicate, $\Lambda_{Fe}$-[$Fe_2\mathbf{L}^{\mathbf{b}}_3$]$Cl_4$, against *E. coli* Sakai, with the aim of developing credible hypotheses. Firstly a genomic study of mutants selected against the lead compound, followed by studies of the transcriptomic and proteomic responses respectively to the lead compound. To our knowledge, this is the most comprehensive mechanistic study of an antimicrobial metallodrug to date.

In spite of the high concentration of the lead compound (80 μg/ml) required to select single colonies at ×40 the MIC in broth, under these conditions a mutation frequency of $2.49 \times 10^{-7}$ ($\sigma = 0.78 \times 10^{-7}$) was obtained. This is higher than many antibiotics typically used in the clinic,[63] though some yield similar values, *e.g.* rifampicin against *S. aureus*.[64] However, it is noteworthy that none of these mutants were truly resistant; as only two- to four- fold increases in MIC were observed. WGS (MiSeq) followed by genome assembly *via* EntroBase was a critical indicator of potential mechanistic targets in identifying gene modifications that lead to tolerance: genes encoding LPS modification enzymes, *waaG* and *galU*, and a vitamin B12 transporter gene, *btuB*. Each of these would point to the Gram-negative outer membrane being either a primary target or at least a critical interaction for reasons such as ingress. Mutations to *waaG* and *galU* gave no cross-resistance or even increased susceptibility to other lead flexicates ([$Fe_2\mathbf{L}^{\mathbf{a}}_3$]$Cl_4$), compared to the WT. This suggests that the LPS layer (which WaaG and GalU modify), is not only critical to the action of $\Lambda_{Fe}$-[$Fe_2\mathbf{L}^{\mathbf{b}}_3$]$Cl_4$, but is specific in its interaction with this compound and its structure.

An unexpected outcome of the mutant selection and WGS, was a potential link between the level of the pO157 plasmid and tolerance. Early data from ongoing Sanger sequencing experiments on these mutants by Drs Kathryn Styles and Nick Waterfield would suggest that the observed loss is genuine (not the result of irregularities in DNA extraction or genome mapping). The cause of this loss remains unknown as the experiment was not designed to investigate this effect, and further work will be necessary to better understand the plasmid loss. As well as speculatively containing genes encoding LPS modifiers, the plasmid contains many virulence factors, thus its loss under this selection pressure could be of clinical interest.

The RNA-seq response (analysed by DEseq2) could be grouped into three main classes; (i) CAMP resistance and membrane maintenance; (ii) acid stress response; (iii) Metabolism and redox state. The ability to group most of the genes identified into those categories and often related cellular pathways (Figure 4.7) adds confidence to these findings. The response appeared to be moderate, with only 68 genes found to have significantly different expression after treatment with the lead compound at quarter the MIC, for 40 min. In addition, overt differences were not seen as fold changes were all within the range: $2.13 > \boldsymbol{log_2}(\text{fold change}) > -1.74$. However, this moderate response appears to have beneficially aided the analysis (as intended), since there is an absence of chaotic or erratic changes that may result from the early stages of cell death, which could otherwise confound interpretation of the results.

Proteomic analysis could only reliably identify a single protein, GadE, as being differentially expressed in treated cells with a high degree of confidence. This is

likely due to the re-use of the treatment conditions used in the RNA study, which elicited a moderate transcriptome response, while it is likely the proteome would take longer to show a response. Any future proteomic investigation should take this finding into account by using a longer incubation time with the flexicate and/or a concentration closer to the MIC. Indeed, with additional resources it is typical to perform proteomic analyses as time-series.[49] Nonetheless a higher count of GadE is supportive of the lead compound inducing an ASR, in line with RNA-seq findings.

With the outer membrane, acid stress and redox/metabolism all being implicated in the action of the lead compound, it may be hypothesised that the compound is acting upon the outer membrane in such a way to either disrupt ion (*e.g.* proton) transport or permeablise this layer somewhat. This general mechanism would be compatible with all of these effects, and would certainly be consistent with observations from Chapter 3 such as the stark difference in the susceptibility of *K. pneumoniae* strains to the lead compound. Another hypothesis, potentially congruent with the first, is that the lead compound may be mimicking the activity of CAMPs. This was alluded to in some specific RNA responses and would certainly be consistent with membrane interactions being critical to their action. Notably, a somewhat similar RNA response to that described in this chapter has been reported for *Streptococcus pneumoniae* treated with a designed CAMP.[65] In addition, the first report of class Ia flexicates did allude to their structural similarity to certain CAMPs[66] where the seats of cationic charge are held at opposite ends of an otherwise hydrophobic protein, *e.g.* protegrin. It would certainly be prudent to investigate these hypotheses further in any future investigations of these molecules and their antimicrobial activity.

## 4.6 References for Chapter 4


1. H. Watanabe, A. Wada, Y. Inagaki, K. Itoh and K. Tamura, *Lancet*, 1996, **348**, 831-832.

2. S. Dahan, S. Knutton, R. K. Shaw, V. F. Crepin, G. Dougan and G. Frankel, *Infect. Immun.*, 2004, **72**, 5452-5459.

3. G. C. Terstappen, C. Schlupen, R. Raggiaschi and G. Gaviraghi, *Nat. Rev. Drug Discov.*, 2007, **6**, 891-903.

4. S. Ghosh, A. Nie, J. An and Z. Huang, *Curr. Opin. Chem. Biol.*, 2006, **10**, 194-202.

5. B. G. Spratt, *J. Gen. Microbiol.*, 1983, **129**, 1247-1260.

6. D. J. Tipper, *Pharmacol. Ther.*, 1985, **27**, 1-35.

7. L. L. Silver, *Clin. Microbiol. Rev.*, 2011, **24**, 71-109.

8. J. Lederberg and A. T. McCray, *Scientist*, 2001, **15**, 8-8.

9. W. Zhang, F. Li and L. Nie, *Microbiology*, 2010, **156**, 287-301.

10. J. Lee and M. Bogyo, *Curr. Opin. Chem. Biol.*, 2013, **17**, 118-126.

11. R. C. MacLean, A. R. Hall, G. G. Perron and A. Buckling, *Nat. Rev. Genet.*, 2010, **11**, 405-414.

12. N. Woodford and M. J. Ellington, *Clin. Microbiol. Infect.*, 2007, **13**, 5-18.

13. F. Sanger, S. Nicklen and A. R. Coulson, *Proc. Natl. Acad. Sci. USA*, 1977, **74**, 5463-5467.

14. N. J. Loman, C. Constantinidou, J. Z. M. Chan, M. Halachev, M. Sergeant, C. W. Penn, E. R. Robinson and M. J. Pallen, *Nat. Rev. Microbiol.*, 2012, **10**, 599-606.

15. G. Wang, T. J. M. Wilson, Q. Jiang and D. E. Taylor, *Antimicrob. Agents Chemother.*, 2001, **45**, 727-733.

16. N. Mani, C. H. Gross, J. D. Parsons, B. Hanzelka, U. Muh, S. Mullin, Y. Liao, A. L. Grillot, D. Stamos, P. S. Charifson and T. H. Grossman, *Antimicrob. Agents Chemother.*, 2006, **50**, 1228-1237.

17. S. Min, K. Ingraham, J. Huang, L. McCloskey, S. Rilling, A. Windau, J. Pizzollo, D. Butler, K. Aubart, L. A. Miller, M. Zalacain, D. J. Holmes and K. O'Dwyer, *Antimicrob. Agents Chemother.*, 2015, **59**, 4644-4652.

18. T. Warrier, K. Kapilashrami, A. Argyrou, T. R. Ioerger, D. Little, K. C. Murphy, M. Nandakumar, S. Park, B. Gold, J. Mi, T. Zhang, E. Meiler, M. Rees, S. Somersan-Karakaya, E. Porras-De Francisco, M. Martinez-Hoyos, K. Burns-Huang, J. Roberts, Y. Ling, K. Y. Rhee, A. Mendoza-Losana, M. Luo and C. F. Nathan, *Proc. Natl. Acad. Sci. USA*, 2016, **113**, E4523-E4530.

19. EnteroBase, http://enterobase.warwick.ac.uk, (accessed May 2017).

20. J. Liebau, P. Pettersson, S. Szpryngiel and L. Mäler, *Biophys. J.*, 2015, **109**, 552-563.

21. M. B. Perry, L. MacLean and D. W. Griffith, *Biochem. Cell Biol.*, 1986, **64**, 21-28.

22. P. Genevaux, P. Bauda, M. S. DuBow and B. Oudega, *Arch. Microbiol.*, 1999, **172**, 1-8.

23. N. Cadieux, P. G. Phan, D. S. Cafiso and R. J. Kadner, *Proc. Natl. Acad. Sci. USA*, 2003, **100**, 10688-10693.

24. F. Calcuttawala, C. Hariharan, G. P. Pazhani, S. Ghosh and T. Ramamurthy, *Antimicrob. Agents Chemother.*, 2015, **59**, 152-158.

25. J. Y. Lim, J. W. Yoon and C. J. Hovde, *J. Microbiol. Biotechnol.*, 2010, **20**, 5-14.

26. T. Wecke and T. Mascher, *J. Antimicrob. Chemother.*, 2011, **66**, 2689-2704.

27. N. Kaldalu, R. Mei and K. Lewis, *Antimicrob. Agents Chemother.*, 2004, **48**, 890-896.

28. M. E. Laubacher and S. E. Ades, *J. Bacteriol.*, 2008, **190**, 2065-2074.

29. C. Lorenz, T. J. Dougherty and S. Lory, *J. Bacteriol.*, 2016, **198**, 3162-3175.

30. K. Papenfort and J. Vogel, *Cell Host & Microbe*, **8**, 116-127.

31. N. J. Croucher and N. R. Thomson, *Curr. Opin. Microbiol.*, 2010, **13**, 619-624.

32. R. Hitzemann, D. Bottomly, P. Darakjian, N. Walter, O. Iancu, R. Searles, B. Wilmot and S. McWeeney, *Genes, Brain and Behav.*, 2013, **12**, 1-12.

33. A. H. M. van Vliet, *FEMS Microbiol. Lett.*, 2010, **302**, 1-7.

34. C. Rosenow, R. M. Saxena, M. Durst and T. R. Gingeras, *Nucleic Acids Res.*, 2001, **29**, e112-e112.

35. M. I. Love, W. Huber and S. Anders, *Genome Biol.*, 2014, **15**, 550.

36. D. Szklarczyk, J. H. Morris, H. Cook, M. Kuhn, S. Wyder, M. Simonovic, A. Santos, N. T. Doncheva, A. Roth, P. Bork, L. J. Jensen and C. von Mering, *Nucleic Acids Res.*, 2017, **45**, D362-D368.

37. J. S. Gunn, *J. Endotoxin Res.*, 2001, **7**, 57-62.

38. A. M. Lippa and M. Goulian, *PLOS Genetics*, 2009, **5**, e1000788.

39. S. Richards, K. Strandberg, M. Conroy and J. Gunn, *Front. Cell. Infect. Microbiol.*, 2012, **2**.

40. S. D. Breazeale, A. A. Ribeiro, A. L. McClerren and C. R. H. Raetz, *J. Biol. Chem.*, 2005, **280**, 14154-14167.

41. M. E. Ghachi, A. Derbise, A. Bouhss and D. Mengin-Lecreulx, *J. Biol. Chem.*, 2005, **280**, 18689-18695.

42. Y. Feng and J. E. Cronan, *Mol. Microbiol.*, 2011, **80**, 195-218.

43. C. M. Herrera, J. V. Hankins and M. S. Trent, *Mol. Microbiol.*, 2010, **76**, 1444-1460.

44. M. M. S. M. Wösten, L. F. F. Kox, S. Chamnongpol, F. C. Soncini and E. A. Groisman, *Cell*, 2000, **103**, 113-125.

45. S. M. González-Leiza, M. A. de Pedro and J. A. Ayala, *J. Bacteriol.*, 2011, **193**, 6887-6894.

46. P. I. Ramos, M. G. Custodio, G. D. Quispe Saji, T. Cardoso, G. L. da Silva, G. Braun, W. M. Martins, R. Girardello, A. T. de Vasconcelos, E. Fernandez, A. C. Gales and M. F. Nicolas, *BMC Genomics*, 2016, **17**, 737.

47. G. J. Leyer and E. A. Johnson, *Appl. Environ. Microbiol.*, 1993, **59**, 1842-1847.

48. T. Maier, M. Guell and L. Serrano, *FEBS Lett.*, 2009, **583**, 3966-3973.

49. C. Vogel and E. M. Marcotte, *Nat. Rev. Genet.*, 2012, **13**, 227-232.

50. Q. Hu, R. J. Noll, H. Li, A. Makarov, M. Hardman and R. Graham Cooks, *J. Mass Spectrom.*, 2005, **40**, 430-443.

51. B. Alberts, A. Johnson, J. Lewis, M. Raff, K. Roberts and P. Walter, *Molecular Biology of the Cell*, Garland, Oxford, 2002.

52. K. P. Jayapal, R. J. Philp, Y.-J. Kok, M. G. S. Yap, D. H. Sherman, T. J. Griffin and W.-S. Hu, *PLOS ONE*, 2008, **3**, e2097.

53. T. Maier, A. Schmidt, M. Guell, S. Kuhner, A. C. Gavin, R. Aebersold and L. Serrano, *Mol. Syst. Biol.*, 2011, **7**, 12.

54. T. King, C. Kocharunchitt, K. Gobius, J. P. Bowman and T. Ross, *PLOS ONE*, 2014, **9**.

55. A. Shevchenko, H. Tomas, J. Havlis, J. V. Olsen and M. Mann, *Nat. Protoc.*, 2007, **1**, 2856-2860.

56. S. Tyanova, T. Temu and J. Cox, *Nat. Protoc.*, 2016, **11**, 2301-2319.

57. S. Tyanova, T. Temu, P. Sinitcyn, A. Carlson, M. Y. Hein, T. Geiger, M. Mann and J. Cox, *Nat. Methods*, 2016, **13**, 731-740.

58. V. G. Tusher, R. Tibshirani and G. Chu, *Proc. Natl. Acad. Sci. USA*, 2001, **98**, 5116-5121.

59. Y. Benjamini and Y. Hochberg, *J. Roy. Stat. Soc. Ser. B. (Stat. Method.)*, 1995, **57**, 289-300.

60. N. Grassl, N. A. Kulak, G. Pichler, P. E. Geyer, J. Jung, S. Schubert, P. Sinitcyn, J. Cox and M. Mann, *Genome Med.*, 2016, **8**, 44.

61. J. W. Foster, *Nat. Rev. Microbiol.*, 2004, **2**, 898-907.

62. H. Song, W. Kong, N. Weatherspoon, G. Qin, W. Tyler, J. Turk, R. Curtiss and Y. Shi, *J. Biol. Chem.*, 2008, **283**, 28158-28168.

63. A. J. O'Neill and I. Chopra, *Expert Opin. Investig. Drugs*, 2004, **13**, 1045-1063.

64. A. J. O'Neill, J. H. Cove and I. Chopra, *J. Antimicrob. Chemother.*, 2001, **47**, 647-650.

65. C.-F. Le, R. Gudimella, R. Razali, R. Manikam and S. D. Sekaran, *Sci. Rep.*, 2016, **6**, 26828.

66. S. E. Howson, A. Bolhuis, V. Brabec, G. J. Clarkson, J. Malina, A. Rodger and P. Scott, *Nat. Chem.*, 2012, **4**, 31-36.

# Chapter 5

# General Conclusions and Future Work

## 5.1 The Antimicrobial Discovery Process

Chapters 2 and 3 outline the synthesis and screening that allowed the discovery of new antimicrobial class Ia flexicates, with a particular focus on compounds showing activity against Gram-negative species. The assembly $\Lambda_{Fe}$-$[Fe_2\mathbf{L}^{\mathbf{b}}_3]Cl_4$ was discovered as an exceptionally potent antimicrobial against the *Enterobacteriaceae*, particularly *E. coli*, with MICs as low as 2 μg/ml.

Optimisation of this compound may now be considered. Chapter 2 outlined how a range of linkers may be incorporated into the class Ia flexicate system, however the subcomponent assembly of these metallohelices foreseeable allows for a wider range of synthetic modifications (see Scheme 2.4). For example, modification of the pyridine units or replacement with other *N*-heterocyclic systems is highly feasible.[1-3]

Likewise, the screening presented in Chapter 3 could be expanded through the use of a panel incorporating a greater diversity of bacterial strains and species. Notably, promising Gram-positive activity was observed for certain compounds such as $[Fe_2\mathbf{L}^{\mathbf{i}}_3]Cl_4$ enantiomers, but not explored further since Gram-negative systems are a priority.[4, 5] Just as the Gram-negative panel was expanded through the use of ESKAPE pathogens to give novel insights, the Gram-positive panel might be similarly increased by the addition of *Enterococcus faecium* strains, several of which are well-known pathogens,[6] and various strains of *Staphylococcus aureus* that would better represent the diversity of that species.[7] Additionally there are many other

documented examples of Gram-positive genera containing many pathogenic strains *e.g. Streptococci,*[8] *Listeria,*[9] *Clostridium*.[10] Furthermore, simpler antimicrobial screens such as that outlined in this work necessitate the use of strains that may be accommodated by an unmodified macro/micro-broth dilution method of assessing susceptibility. The screening of strains requiring specific growth conditions not accounted for by this method (*e.g.* anaerobes require a low $O_2$ environment) require sophisticated modification, but could thus allow the testing compounds against a broader range of pathogens.[11]

In understanding the activity observed from the screening described in this work, and its origin, it must noted that broth dilution methods of MIC determination measure bacterial susceptibility as a function of the concentration applied to solution. However, this is not necessarily correlated to the 'effective concentration', *i.e.* the bioavailability, of the compound as experienced by the bacterium, or the cellular uptake of the compound. To determine bioavailability, the extent to which compounds are removed from solution by the factors their environment must be considered.[12] While the aqueous solubility and stability of the compounds described in this work is addressed, further work is required to determine whether the bioavailability of the compounds in biological media such as CAMHB is an important factor of the activity observed. A simple experiment to determine whether binding to broth components inactivates a compound, may be a simple incubation in broth at a set concentration followed by filtration through a size-exclusion filter that removes large molecules such as proteins, but would allow an unbound metallohelix to pass through.[13] The concentration of the complex passing through such a filter post-incubation would allow a rough estimate of non-specific binding, measured for example using the flexicate MLCT absorption band, as used in Chapter 2 in

determining aqueous stability. Bioavailability *in vivo* is much more complex, but nonetheless means of addressing this issue have been described.[14]

In practice the measurement of cellular uptake is often challenging. For metallodrugs containing non-native elements [*e.g.* Ru(II) complexes], the problem is simplified as the presence of these elements, acting as proxies for the complex, is relatively easy to determine and quantify, for example by inductively coupled plasma mass spectrometry (ICP-MS). For compounds entirely composed of elements native to bacteria, as is the case for the class Ia flexicates screened in this work, spectroscopic handles may be into the molecule without affecting the chemistry by the introduction of radioisotopes such as $^{3}H$ (tritium), $^{14}C$, or $^{55}Fe$ that have sufficient half-lives to allow for synthesis, preparation, *etc.*, is a plausible route that allow for quantitative detection in-cell.[15, 16]

The work of Chapter 3 put forward simple structure-activity relationship (SARs) for Class Ia flexicates with regard to *E. coli* and *S. aureus* respectively, and these may be developed further by gathering additional quantitative information about the physical properties of this class,[17] such as lipophilicity [*e.g.* log (P)] or redox potential for example. Correlation between factors such as these and observed antimicrobial activity could be crucial in understanding which properties are necessary in driving the activity, stimulating better mechanistic understanding and guiding future synthetic work.

## 5.2 Mechanistic Hypotheses

Chapter 4 outlined hypotheses regarding the mechanism causing the potent bactericidal activity of the lead compound in *E. coli* ($\Lambda_{Fe}$-[$Fe_2\mathbf{L}^{\mathbf{b}}_3$]$Cl_4$). This compound was seen to influence the cell membrane, acid-stress, and cell metabolism/redox, with the enticing notion that this may hint at a similarity in behaviour between this compound and cationic antimicrobial peptides (CAMPs). Immediate further work in this area could focus on testing these hypotheses using orthogonal approaches to mechanistic investigation.

Recently, fluorescence-based 'reporter strains' have been reported, whereby the target bacterium is modified such that it fluoresces in response to stress caused by the inhibition of a particular critical cellular process.[18] In 2007, a Bayer HealthCare research team reported that they had successfully produced and tested five *Bacillus subtilis* reporter strains, with different promoters associated with certain stress responses, fused to a luciferase (fluorescent reporter) gene.[19] These five stains were collectively capable of 'reporting' inhibition of: DNA synthesis, RNA synthesis, protein synthesis, cell membrane synthesis (or cell wall damage) and fatty acid synthesis. The team tested against several antibiotic compounds with well-understood mechanisms and the reporter strains proved effective in highlighting the processes being targeted; *e.g.* bleomycin induces the *yorB* promoter associated with DNA damage, vancomycin induces the promoter *ypuA* associated with cell wall stress. The system has some drawbacks such as a limited drug concentration range and difficulty identifying mechanisms for compounds with diverse MOAs (*e.g.* ethidium bromide). Understandably, the potential of such high-throughput

biotechnology for facile, rapid understanding of the mechanism of action for novel, antimicrobials, is considerable.

Another means of validating the importance of a certain cellular pathway to the antimicrobial activity of a compound, is to test the susceptibility of 'knockout mutant' strains, *e.g.* the Keio collection, a library of *E. coli* K-12 mutants.[20, 21] These stains differ from typical wild-type stains of the same species in that they lack a certain nonessential gene (or lack the means to express said gene), which causes a pathway to be shut down. Libraries of such knockout mutant strains have been devised in order to assist in the triangulation of antimicrobial agents' mechanism or key cellular targets.

With confirmation of a key target of targets, specific information regarding these interactions such as binding kinetics may be explored and leveraged to improve the antimicrobial activity through molecular modification.

## 5.3 References for Chapter 5


1. C. P. Sebli, S. E. Howson, G. J. Clarkson and P. Scott, *Dalton Trans.*, 2010, **39**, 4447-4454.

2. S. E. Howson, L. E. N. Allan, N. P. Chmel, G. J. Clarkson, R. J. Deeth, A. D. Faulkner, D. H. Simpson and P. Scott, *Dalton Trans.*, 2011, **40**, 10416-10433.

3. A. D. Faulkner, R. A. Kaner, Q. M. A. Abdallah, G. Clarkson, D. J. Fox, P. Gurnani, S. E. Howson, R. M. Phillips, D. I. Roper, D. H. Simpson and P. Scott, *Nat. Chem.*, 2014, **6**, 797-803.

4. R. E. W. Hancock, *Trends Microbiol.*, 1997, **5**, 37-42.

5. R. Tommasi, D. G. Brown, G. K. Walkup, J. I. Manchester and A. A. Miller, *Nat. Rev. Drug Discov.*, 2015, **14**, 529-542.

6. C. J. Kristich, L. B. Rice and C. A. Arias, in *Enterococci: From Commensals to Leading Causes of Drug Resistant Infection*, eds. M. S. Gilmore, D. B. Clewell, Y. Ike and N. Shankar, Boston, 2014.

7. S. Y. C. Tong, J. S. Davis, E. Eichenberger, T. L. Holland and V. G. Fowler, *Clin. Microbiol. Rev.*, 2015, **28**, 603-661.

8. R. Facklam, *Clin. Microbiol. Rev.*, 2002, **15**, 613-630.

9. M. Hamon, H. Bierne and P. Cossart, *Nat. Rev. Microbiol.*, 2006, **4**, 423-434.

10. C. L. Hatheway, *Clin. Microbiol. Rev.*, 1990, **3**, 66-98.

11. A. N. Schuetz, *Clin. Infect. Dis.*, 2014, **59**, 698-705.

12. M. A. Zeitlinger, H. Derendorf, J. W. Mouton, O. Cars, W. A. Craig, D. Andes and U. Theuretzbacher, *Antimicrob. Agents Chemother.*, 2011, **55**, 3067-3074.

13. J. Beer, C. C. Wagner and M. Zeitlinger, *AAPS J.*, 2009, **11**, 1.

14. D. Williams, *Br. J. Clin. Pharmacol.*, 2014, **77**, 913-914.

15. M. Winterhalter and M. Ceccarelli, *Eur. J. Pharm. Biopharm.*, 2015, **95**, 63-67.

16. G. Lappin and S. Temple, *Radiotracers in Drug Development*, CRC Press, New York, 2006.

17. J.-P. Renaud, C.-w. Chung, U. H. Danielson, U. Egner, M. Hennig, R. E. Hubbard and H. Nar, *Nat. Rev. Drug Discov.*, 2016, **15**, 679-698.

18. J. R. van der Meer and S. Belkin, *Nature Rev. Microbiol.*, 2010, **8**, 511-522.

19. A. Urban, S. Eckermann, B. Fast, S. Metzger, M. Gehling, K. Ziegelbauer, H. Rubsamen-Waigmann and C. Freiberg, *Appl. Environ. Microbiol.*, 2007, **73**, 6436-6443.

20. T. Baba, T. Ara, M. Hasegawa, Y. Takai, Y. Okumura, M. Baba, K. A. Datsenko, M. Tomita, B. L. Wanner and H. Mori, *Mol. Syst. Biol.*, 2006, **2**, 2006.0008-2006.0008.

21. N. Yamamoto, K. Nakahigashi, T. Nakamichi, M. Yoshino, Y. Takai, Y. Touda, A. Furubayashi, S. Kinjyo, H. Dose, M. Hasegawa, K. A. Datsenko, T. Nakayashiki, M. Tomita, B. L. Wanner and H. Mori, *Mol. Syst. Biol.*, 2009, **5**, 335.

# Chapter 6

# Materials and Methods

## 6.1 Experimental Details for Chapter 2

### 6.1.1 Solvents and chemicals

All solvents and chemicals purchased from commercial sources (Sigma-Aldrich, Acros, Fisher Scientific, Alfa Aesar or Invitrogen) were used without further purification unless otherwise stated. Sodium hydride dispersions in mineral oil were placed in a Schlenk vessel under an inert atmosphere and washed three times with diethyl ether to remove the oil, then dried and stored under argon in an MBraun dry box. Where necessary solvents were dried by heating to reflux for 3 d under dinitrogen over the appropriate drying agents (potassium for tetrahydrofuran, and calcium hydride for methanol and DCM) and degassed before use. Tetrahydrofuran was additionally pre-dried over sodium wire. Dried solvents were stored in glass ampoules under argon. Deuterated solvents were purchased from Sigma-Aldrich or Cambridge Isotope Laboratories and pre-dried over molecular sieves (3 Å for methanol, dimethyl sulfoxide and acetonitrile; 4 Å for chloroform), for 24 h prior to use. Perchlorate salts pose an explosion risk, particularly when heated, and were therefore only used on a small scale and never exposed to excess heat.

### 6.1.2 Equipment and instrumentation

Where appropriate, reactions were carried out under argon using a dual manifold argon/vacuum line and standard Schlenk techniques, or an MBraun dry box. All

glassware and cannulae for these techniques were stored in an oven at >375 K for 48 h prior to use.

NMR spectra were recorded on Bruker Advance III HD300/400/500 spectrometers. Routine NMR assignments were confirmed by $^{1}H$-$^{1}H$ (COSY) and $^{13}C$-$^{1}H$ (HSQC) correlation experiments where necessary. The spectra were internally referenced using the residual protio solvent ($CDCl_3$, $CD_3CN$ *etc.*) resonance relative to tetramethylsilane ($\delta = 0$ ppm). ESI mass spectra were recorded in a methanol/water mixture (4:1) on either an Agilent Technologies 1260 Infinity spectrometer or a Bruker Daltonics MicroTOF spectrometer. Fourier-transformed infra-red (FTIR) spectra were measured using a Bruker Alpha-P FTIR spectrometer (undergraduate laboratory, University of Warwick). Elemental analyses were performed by Medac Ltd. Chobham, Surrey, UK GU24 8JB. Optical rotation measurements were performed on a Perkin Elmer Polarimeter 341 by Warwick Analytical Services, Coventry, UK. In all cases the following parameters were used: solvent methanol, temperature 21 °C, pathlength 100 mm, wavelength 589 nm.

Suitable single crystals for diffractometry were mounted on glass fibre with Fomblin oil on a Bruker-Nonius FR591 rotating anode diffractometer with a Bruker-Nonius APEX II CCD camera on k-goniostat. The crystals were kept at 120 ± 2 K during data collection. Using Olex2,1 the structure was solved with the ShelXS2 structure solution program using Direct Methods and refined with the ShelXL2 refinement package using Least Squares minimisation. This was performed by Dr Guy Clarkson, and data is tabulated in the appendix.

UV-Visible absorbance spectra were recorded using a Jasco V-660 spectrometer. Measurements were collected from a 1 cm path-length quartz cuvette and, unless

otherwise mentioned, the standard parameters used were: bandwidth 1 nm, response time 1 sec, wavelength scan range 200-700 nm, data pitch 0.2 nm, scanning speed 200 nm/min, with four accumulation taken per sample to give an average spectrum with reduced noise. CD spectra were measured on a Jasco J-815 spectrometer. Measurements were collected using a 1 cm path-length quartz cuvette and unless otherwise mentioned the standard parameters used were: bandwidth 2 nm, response time 1 sec, wavelength scan range 200-700 nm, data pitch 1 nm, scanning speed 200 nm/min, with four accumulation taken per sample to give an average spectrum with reduced noise.

Thermogravimetric analysis (TGA) was performed using a Mettler Toledo TGA/DSC 1 STAR® system instrument. Samples were weighed accurately into a pre-weighed 40 μl TGA/DSC aluminium crucible (DSC consumables Inc.) and heated 298 to 573 K (25 to 300 °C), at 5 K/min under a nitrogen atmosphere. The mass of the sample was recorded at various temperature points along this range.

### 6.1.3 Synthesis and characterisation of small organic molecules

**(*R*)-2-phenylglycinol[1] [(*R*)-1]**

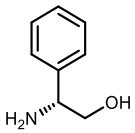


D-Phenylglycine (20.0 g, 0.13 mol, 1 eq.) was suspended in anhydrous tetrahydrofuran (100 ml) under argon, and added dropwise to a stirred solution of lithium aluminium hydride (10.0 g, 0.26 mol, 2 eq.) in anhydrous tetrahydrofuran (100 ml) at 0 °C. The suspension was allowed to warm to ambient temperature and then heated at reflux (70

°C) for 16 h. After cooling to 0 °C the reaction mixture was quenched by adding saturated potassium carbonate solution (250 ml) dropwise. The solid was filtered off to give a yellow solution. The solvent was removed under reduced pressure to give a yellow solid, which upon recrystallisation from minimum hot toluene gave a white crystalline solid.

Yield: 10.37 g, 75.6 mmol, 58 %.

$^{1}$H NMR (300 MHz, 298 K, $CDCl_3$): $\delta_H$ 7.31-7.17 (5H, m, Ph), 3.97 (1H, dd, $^{3}J_{HH}$ = 4.4 Hz, 8.3 Hz, CH), 3.67 (1H, dd, $^{2}J_{HH}$ = 10.7 Hz, $^{3}J_{HH}$ = 4.4 Hz, $CH_2$), 3.48 (1H, dd, $^{2}J_{HH}$ = 10.7 Hz, $^{3}J_{HH}$ = 8.3 Hz, $CH_2$), 1.78 (2H, br s, $NH_2$).

$^{13}$C{$^{1}$H NMR (75 MHz, 298 K, $CDCl_3$): $\delta_C$ 142.9 (Ph), 128.8 (Ph), 127.7 (Ph), 126.6 (Ph), 68.2 ($CH_2$), 57.5 (CH).

MS (ESI): m/z 297.1 $[2M+Na]^+$, 160.0 $[M+Na]^+$, 138.1 $[M+H]^+$, 121.1 $[M-NH_2]^+$.

FTIR: ν $cm^{-1}$ 2834 w, 1605 w, 1496 w, 1452 w, 1360 w, 1197 w, 1078 m, 1045 m, 979 w, 883 m, 816 m, 755 s, 700 s.

Elemental analysis found (calculated for $C_8H_{11}NO$): % C 69.76 (70.04), H 8.19 (8.08), N 10.19 (10.21).

Melting point: 76-78 °C (lit. 76-78 °C).[1]

Optical rotation: -26.04° (6.61 g/100 ml, 21 °C) [lit. value -25.99° (6.62 g/100 ml, 20 °C)].[1]

**(*S*)-2-phenylglycinol [(*S*)-1]**

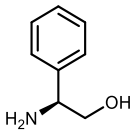


Synthesised using the procedure described for (*R*)-2-phenylglycinol, substituting D-phenylglycine for L-phenylglycine.

Yield: 11.48 g, 83.7 mmol, 65 %.

$^{1}$H NMR (300 MHz, 298 K, $CDCl_3$): $\delta_H$ 7.31-7.17 (5H, m, Ph), 3.97 (1H, dd, $^{3}J_{HH}$ = 4.4 Hz, 8.3 Hz, CH), 3.67 (1H, dd, $^{2}J_{HH}$ = 10.7 Hz, $^{3}J_{HH}$ = 4.4 Hz, $CH_2$), 3.48 (1H, dd, $^{2}J_{HH}$ = 10.7 Hz, $^{3}J_{HH}$ = 8.3 Hz, $CH_2$), 1.78 (2H, br s, $NH_2$).

$^{13}C\{^{1}H\}$ NMR (75 MHz, 298 K, $CDCl_3$): $\delta_C$ 142.9 (Ph), 128.8 (Ph), 127.7 (Ph), 126.6 (Ph), 68.2 ($CH_2$), 57.5 (CH).

MS (ESI): m/z 297.1 $[2M+Na]^+$, 160.0 $[M+Na]^+$, 138.1 $[M+H]^+$, 121.1 $[M-NH_2]^+$.

FTIR: ν $cm^{-1}$ 2834 w, 1605 w, 1496 w, 1452 w, 1360 w, 1197 w, 1078 m, 1045 m, 979 w, 883 m, 816 m, 755 s, 700 s.

Elemental analysis found (calculated for $C_8H_{11}NO$): % C 69.87 (70.04), H 8.27 (8.08), N 10.12 (10.21).

Melting point: 76-79 °C.

Optical rotation: 26.17° (6.67 g/100 ml, 21 °C).

**_bis_-4-(Bromomethyl)phenyl ether[2] (2e)**

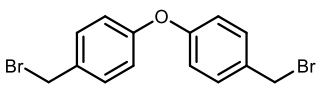


Diphenyl ether (5.67 g, 33.3 mmol) and paraformaldehyde (4.0 g, 0.13 mol, 4 eq.), were suspended in a solution of 33 wt% HBr in glacial acetic acid (36 ml). The mixture was stirred at ambient temperature for 48 h. The white solid formed was collected by filtration, washed with water (100 ml) and 2:1 *n*-hexane/ethyl acetate (80 ml), and dried in air. The product was recrystallised from hot toluene/*n*-hexane, to give a white crystalline solid, which was collected by filtration and dried overnight at 50°C *in vacuo*.

Yield: 6.74 g, 18.9 mmol, 57 %.

$^{1}$H NMR (300 MHz, 298 K, $CDCl_3$): $\delta_H$ 7.37 (4H, d, $^{3}J_{HH}$ = 8.5 Hz, Ph), 6.97 (4H, d, $^{3}J_{HH}$ = 8.5 Hz, Ph), 4.51 (4H, s, $CH_2$).

$^{13}C\{^{1}H\}$ NMR (75 MHz, 298 K, $CDCl_3$): $\delta_C$ 157.1 (Ph), 133.1 (Ph), 130.8 (Ph), 119.3 (Ph), 33.3 ($CH_2$).

MS (CGMS): m/z 277.7 $[M\text{-}Br]^+$, 275.7 $[M\text{-}Br]^+$, 197.4 $[M\text{-}2Br+H]^+$.

FTIR: $\nu$ $cm^{-1}$ 1592 w, 1495 m, 1439 w, 1231 s, 1198 s, 1160 m, 1088 m, 1015 w, 869 m, 860 m, 839 s, 813 m.

Elemental analysis found (calculated for $C_{14}H_{12}Br_2O$): % C 46.76 (47.23) H 3.35 (3.40) N <0.1 (0).

**_bis_-4-(bromomethyl)phenyl sulfide[2] (2f)**

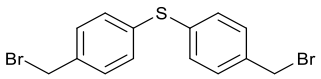


Diphenyl sulfide (2.8 ml, 3.1 g, 16.6 mmol, 1.0 eq.) and paraformaldehyde (1.8 g, 59.9 mmol, 3.6 eq.) were added to a solution of 33 wt% HBr in glacial acetic acid (18 ml). The mixture was stirred under reflux at 50 °C overnight. Upon cooling, the addition of water (100 ml) caused a white precipitate to form, which was collected by filtration, washed with water (100 ml) and 2:1 *n*-hexane/ethyl acetate (80 ml), and dried in air. The product was recrystallised from hot toluene/*n*-hexane, to give a white crystalline solid, which was collected by filtration and dried overnight at 50°C *in vacuo*.

Yield: 4.01 g, 10.8 mmol, 65 %.

$^{1}$H NMR (500 MHz, 298 K, $CDCl_3$): $\delta_H$ 7.34-7.29 (8H, m, Ar), 4.47 (4H, s, $CH_2$).

$^{13}C\{^{1}H\}$ NMR (125 MHz, 298 K, $CDCl_3$): $\delta_C$ 137.0 (Ph), 136.0 (Ph), 131.4 (Ph), 130.1 (Ph), 33.0 ($CH_2$).

MS (CGMS): m/z 372.9 $[M+H]^+$, 293.7 $[M-Br]^+$, 292.3 $[M-Br]^+$, 213.2 $[M-2Br+H]^+$.

FTIR: ν $cm^{-1}$ 1487 w, 1222 m, 1196 m, 1086 w, 1016 w, 839 s, 804 w.

Elemental analysis found (calculated for $C_{14}H_{12}Br_2S$): % C 44.91 (45.19), H 3.30 (3.25), N <0.1 (0).

***bis*-4-(bromomethyl)phenylmethane[3] (2g)**

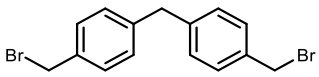


Diphenylmethane (5.0 g, 29.7 mmol, 1.0 eq) and paraformaldehyde (5.35 g 0.178 mol, 6.0 eq.) were suspended in a mixture of aqueous 48 wt% HBr solution (80 ml) and glacial acetic acid (25 ml). Tetradecyltrimethylammonium bromide (0.16 g) was added and the suspension was stirred under reflux at 125 °C overnight. Upon cooling, the yellow solid formed was collected by filtration, washed with water (100 ml) and dried in air. The product was recrystallised from hot toluene/*n*-hexane, to give a white powder, which was collected by filtration and dried overnight at 70 °C *in vacuo*.

Yield: 3.85 g, 10.9 mmol, 37 %.

$^{1}$H NMR (300 MHz, 298 K, $CDCl_3$): $\delta_H$ 7.32 (4H, d, $^{3}J_{HH}$ = 7.4 Hz, Ph), 7.15 (4H, d, $^{3}J_{HH}$ = 7.4 Hz, Ph), 4.48 (4H, s, $CH_2Br$), 3.96 (2H, s, $CH_2$).

$^{13}C\{^{1}H\}$ NMR (75 MHz, 298 K, $CDCl_3$): $\delta_C$ 141.2 (Ph), 135.9 (Ph), 129.5 (Ph), 129.4 (Ph), 41.5 ($CH_2$), 33.6 ($CH_2Br$).

MS (CGMS): m/z 275.7 $[M\text{-}Br]^+$, 273.7 $[M\text{-}Br]^+$.

FTIR: ν $cm^{-1}$ 1511 w, 1432 w, 1416 w, 1226 m, 1198 s, 1022 w, 864 m, 823 s, 765 m, 721 m, 715 s.

Elemental analysis found (calculated for $C_{15}H_{14}Br_2$): % C 51.53 (50.88), H 3.96 (3.99), N <0.1 (0).

**1,2-*bis*-4-(bromomethyl)phenylethane (2h)**

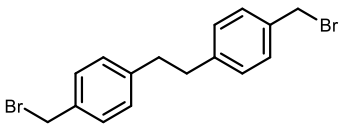


Bibenzyl (5.42 g, 29.7 mmol, 1.0 eq) and paraformaldehyde (5.35 g 0.178 mol, 6.0 eq.) were suspended in a mixture of aqueous 48 wt% HBr solution (80 ml) and glacial acetic acid (25 ml). Tetradecyltrimethylammonium bromide (0.16 g) was added and the suspension was stirred under reflux at 125 °C overnight. Upon cooling, the yellow solid formed was collected by filtration, washed with water (100 ml) and dried in air. The product was recrystallised from hot DCM/*n*-hexane, to give a yellow powder, which was collected by filtration and dried overnight at 50 °C *in vacuo*.

Yield: 1.95 g, 5.3 mmol, 18 %.

$^{1}$H NMR (300 MHz, 298 K, $CDCl_3$): 7.31 (4H, d, $^{3}J_{HH}$ = 7.3 Hz, Ph), 7.17 (4H, d, $^{3}J_{HH}$ = 7.3 Hz, Ph), 4.49 (4H, s, $CH_2Br$), 2.91 (4H, s, $CH_2$).

$^{13}C\{^{1}H\}$ NMR (75 MHz, 298 K, $CDCl_3$): $\delta_C$ 142.1 (Ph), 135.7 (Ph), 129.3 (Ph), 129.0 (Ph), 37.5 ($CH_2$), 33.8 ($CH_2Br$).

MS (CGMS): m/z 289.8 $[M\text{-}Br]^+$, 287.8 $[M\text{-}Br]^+$, 243.8 $[M\text{-}2Br+Cl]^+$, 184.9 $[C_8H_8Br]^+$, 182.9 $[C_8H_8Br]^+$, 139.5 $[C_8H_8Cl]^+$, 104.5 $[C_8H_8]^+$.

FTIR: ν $cm^{-1}$ 1611 w, 1511 m, 1437 w, 1418 m, 1226 s, 1211 s, 1200 s, 1081 w, 1017 w, 830 s, 749 m.

Elemental analysis found (calculated for $C_{16}H_{16}Br_2$): % C 52.88 (52.21), H 4.46 (4.38), N <0.1 (0).

**2,8-*bis*(bromomethyl)dibenzofuran (2i)**

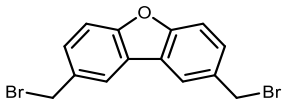


Dibenzofuran (1.0 g, 5.9 mmol, 1.0 eq) and paraformaldehyde (0.78 g, 26.0 mol, 4.38 eq) were suspended in a solution of 33 wt% HBr in glacial acetic acid (10 ml). 90 wt% phosphoric acid (5 ml) was added and the mixture stirred under reflux at 65 °C for 1 h, then at ambient temperature overnight, before cooling. The reaction contents were added to ice-cold water (150 ml), and the white solid collected by filtration and dried in air. The crude product was dissolved into a minimal volume of hot toluene, before adding an excess (~100 ml) of *n*-hexane. The product was recrystallised from hot toluene/*n*-hexane, to give a white powder, which was collected by filtration and dried overnight at 50°C *in vacuo*.

Yield: 1.00 g, 2.8 mmol, 48 %.

$^{1}$H NMR (300 MHz, 298 K, $CDCl_3$): $\delta_H$ 7.98 (2H, s, Ph), 7.56-7.48 (4H, m, Ph), 4.69 (4H, s, $CH_2$).

$^{13}C\{^{1}H\}$ NMR (100 MHz, 298 K, $CDCl_3$): $\delta_C$ 156.6 (Ph), 132.9 (Ph), 128.9 (Ph), 124.4 (Ph), 121.6 (Ph), 112.3 (Ph), 34.0 ($CH_2Br$).

MS (CGMS): m/z 275.7 $[M\text{-}Br]^+$, 274.3 $[M\text{-}Br]^+$, 229.8 $[M\text{-}2Br+Cl]^+$, 194.9 $[M\text{-}2Br]^+$.

FTIR: ν $cm^{-1}$ 1601 w, 1486 w, 1458 w, 1219 s, 1205 s, 1187 s, 1126 m, 1024 m, 882 m, 822 s, 736 m.

Elemental analysis found (calculated for $C_{14}H_{10}Br_2O$): % C 47.16 (47.50), H 2.88 (2.85), N <0.1 (0).

**2,7-*bis*(bromomethyl)fluorene (2j)**

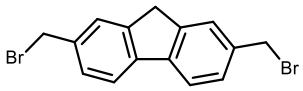


Adapted from a synthesis of 2,7-*bis*(bromomethyl)-9,9-diethylfluorene.[4]

Fluorene (5.0 g, 30.1 mmol, 1.0 eq) and paraformaldehyde (3.9 g, 0.13 mol, 4.3 eq.) were suspended in a solution of 33 wt% HBr in glacial acetic acid (75 ml). 90 w% phosphoric acid (25 ml) was added and the mixture stirred under reflux at 65 °C for 1 h, then at ambient temperature overnight. The flocculent reaction mixture was added to ice-cold water (300 ml), and the white solid collected by filtration and dried in air. Recrystalisation from 5:1 acetone/*n*-hexane gave the desired product as a white powder, which was dried overnight at 50 °C *in vacuo.*

Yield: 2.91 g, 8.3 mmol, 27 %.

$^1$H NMR (300 MHz, 298 K, $CDCl_3$): $\delta_H$ 7.73 (2H, d, $^3J_{HH}$ = 7.8 Hz, Ph), 7.58 (2H, s, Ph), 7.41 (2H, d, $^3J_{HH}$ = 7.8 Hz, Ph), 4.60 (4H, s, $CH_2Br$), 3.90 (2H, s, $CH_2$).

$^{13}C\{^1H\}$ NMR (100 MHz, 298 K, $CDCl_3$): $\delta_C$ 144.3 (Ph), 141.6 (Ph), 136.8 (Ph), 128.2 (Ph), 126.0 (Ph), 120.5 (Ph), 36.8 ($CH_2$), 34.4 ($CH_2Br$).

MS (CGMS): m/z 262.8 $[M-2Br+2Cl]^+$, 227.9 $[M-2Br+Cl]^+$, 193.0 $[M-2Br]^+$.

FTIR: $\nu$ $cm^{-1}$ 1420 m, 1396 s, 1227 m, 1210 s, 1201 s, 825 s, 732 m, 725 m,706 s.

Elemental analysis found (calculated for $C_{15}H_{12}Br_2$): % C 51.72 (51.17) H 3.43 (3.44) N <0.1 (0).

### 6.1.4 Synthesis and characterisation of chiral diamines (3a-i)[5]

**(*R*,*R*)-α,α'-*bis*(2-amino-2-phenylethoxy)-*p*-xylene [(*R*,*R*)-3a]**

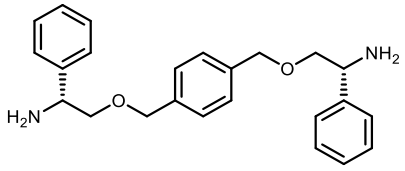


Under inert atmosphere, (*R*)-2-phenylglycinol (2.0 g, 14.6 mmol, 2.2 eq.) was dissolved in anhydrous THF (50 ml), to which 1 ml (1.11 g, 5.0 mmol, 0.8 eq.) [15]-crown-[5] was added by injection. The solution was then added dropwise to neat sodium hydride (0.72 g, 31.3 mmol, 4.8 eq.). The effervescent mixture was carefully placed under static vacuum and stirred at ambient temperature for 1 h. A solution of α,α'-dibromo-*p*-xylene (1.73 g, 6.6 mmol, 1 eq.) in anhydrous THF (40 ml) was then added dropwise. The reaction mixture was then stirred under static vacuum; for 1 h at ambient temperature, then 5 h at 65 °C. The bright yellow reaction mixture was allowed to cool before quenching with 2:1 saturated KCl aq./water (60 ml). The crude product was extracted using diethyl ether (3 × 100 ml), dried over sodium sulfate, filtered through celite, and the solvent removed under reduced pressure to leave a yellow oil. This crude product was purified by Kügelrohr distillation (150 °C, 45 min) to remove [15]-crown-[5] and unreacted excess phenylglycinol.

Yield: 1.63 g, 4.3 mmol, 66 %.

$^{1}$H NMR (400 MHz, 298 K, $CDCl_3$): $\delta_H$ 7.36-7.20 (14H, m, Ph), 4.51 (4H, s, OC*H*$_2$Ph), 4.20 (2H, dd, $^{3}J_{HH}$ = 9.0 Hz, 3.8 Hz, CH), 3.57 (2H, dd, $^{2}J_{HH}$ = 9.0 Hz, $^{3}J_{HH}$ = 3.8 Hz, OC*H*$_2$CH), 3.41 (2H, t, $^{2}J_{HH}$/$^{3}J_{HH}$ = 9.0, OC*H*$_2$CH), 1.70 (4H, br s, $NH_2$).

$^{13}$C{$^{1}$H} NMR (100 MHz, 298 K, $CDCl_3$): $\delta_C$ 142.6 (Ph), 137.8 (Ph), 128.5 (Ph), 127.9 (Ph), 127.5 (Ph), 127.0 (Ph), 76.8 (O*C*H$_2$CH), 73.1 (O*C*H$_2$Ph), 55.7 (CH).

MS (ESI): m/z 377.2 $[M+H]^+$, 189.1 $[M+2H]^{2+}$.

FTIR: ν cm$^{-1}$ 2873 m, 1602 w, 1515 w, 1471 m, 1452 w, 1420 w, 1354 m, 1308 w, 1212 w, 1088 s, 1020 m, 848 m, 759 s, 701 s.

Elemental analysis found (calculated for $C_{24}H_{28}N_2O_2$): % C 75.95 (76.56) H 7.34 (7.50) N 7.07 (7.44).

**(*S*,*S*)-*α*,*α*'-*bis*(2-amino-2-phenylethoxy)-*p*-xylene [(*S*,*S*)-3a]**

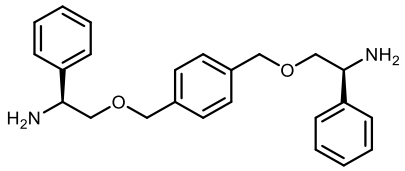


Synthesised according to the procedure described for (*R*,*R*)-**3a**; substituting (*R*)-2-phenylglycinol for (*S*)-2-phenylglycinol.

Yield: 1.71 g, 4.5 mmol, 69 %.

$^{1}$H NMR (400 MHz, 298 K, $CDCl_3$): $\delta_H$ 7.36-7.20 (14H, m, Ph), 4.51 (4H, s, OC*H*$_2$Ph), 4.20 (2H, dd, $^{3}J_{HH}$ = 9.0 Hz, 3.8 Hz, CH), 3.57 (2H, dd, $^{2}J_{HH}$ = 9.0 Hz, $^{3}J_{HH}$ = 3.8 Hz, OC*H*$_2$CH), 3.41 (2H, t, $^{2}J_{HH}$/$^{3}J_{HH}$ = 9.0, OC*H*$_2$CH), 1.70 (4H, br s, $NH_2$).

$^{13}C\{^{1}H\}$ NMR (100 MHz, 298 K, $CDCl_3$): $\delta_C$ 142.6 (Ph), 137.8 (Ph), 128.5 (Ph), 127.9 (Ph), 127.5 (Ph), 127.0 (Ph), 76.8 (O*C*$H_2$CH), 73.1 (O*C*$H_2$Ph), 55.7 (*C*H).

MS (ESI): m/z 399.2 $[M+Na]^+$, 377.2 $[M+H]^+$, 189.1 $[M+2H]^{2+}$.

FTIR: ν $cm^{-1}$ 2873 m, 1602 w, 1515 w, 1471 m, 1452 w, 1420 w, 1354 m, 1308 w, 1212 w, 1088 s, 1020 m, 848 m, 759 s, 701 s.

Elemental analysis found (calculated for $C_{24}H_{28}N_2O_2$): % C 75.95 (76.56) H 7.99 (7.50) N 6.94 (7.44).

**(*R*,*R*)-*α*,*α*'-*bis*(2-amino-2-phenylethoxy)-*m*-xylene [(*R*,*R*)-3b]**

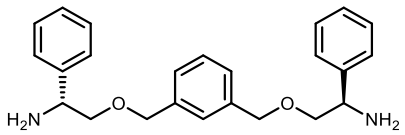


Under inert atmosphere, (*R*)-2-phenylglycinol (1.14 g, 8.3 mmol, 2.2 eq.) was dissolved in anhydrous THF (50 ml), to which 1.2 ml (1.33 g, 6.0 mmol, 1.6 eq.) [15]-crown-[5] was added by injection. The solution was then added dropwise to neat sodium hydride (0.42 g, 17.5 mmol, 4.6 eq.). The effervescent mixture was carefully placed under static vacuum and stirred at ambient temperature for 1 h. A solution of α,α'-dibromo-*m*-xylene (1.0 g, 3.8 mmol, 1 eq.) in anhydrous THF (40 ml) was then added dropwise. The reaction mixture was then stirred under static vacuum; for 1 h at ambient temperature, then 5 h at 65 °C. The pink reaction mixture was allowed to cool before quenching with 2:1 saturated KCl aq./water (60 ml). The crude product was extracted using diethyl ether (3 × 100 ml), dried over sodium sulfate, filtered through celite, and the solvent removed under reduced pressure to leave a yellow oil. This

crude product was purified by Kügelrohr distillation (150 °C, 45 min) to remove [15]-crown-[5] and unreacted excess phenylglycinol.

Yield: 1.22 g, 3.2 mmol, 81 %.

$^{1}$H NMR (300 MHz, 298 K, $CDCl_3$): $\delta_H$ 7.40-7.23 (14H, m, Ph), 4.55 (4H, s, OC*H*$_2$Ph), 4.24 (2H, dd, $^{3}J_{HH}$ = 9.0 Hz, 3.8 Hz, CH), 3.61 (2H, dd, $^{2}J_{HH}$ = 9.0 Hz, $^{3}J_{HH}$ = 3.8 Hz, OC*H*$_2$CH), 3.46 (2H, t, $^{2}J_{HH}$/$^{3}J_{HH}$ = 9.0, OC*H*$_2$CH), 1.75 (4H, br s, $NH_2$).

$^{13}$C{$^{1}$H} NMR (75 MHz, 298 K, $CDCl_3$): $\delta_C$ 142.6 (Ph), 138.5 (Ph), 128.7 (Ph), 128.6 (Ph), 127.5 (Ph), 127.2 (Ph), 127.1 (Ph), 127.0 (Ph), 76.9 (O*C*H$_2$CH), 73.3 (O*C*H$_2$Ph), 55.7 (CH).

MS (ESI): m/z 399.2 $[M+Na]^+$, 377.2 $[M+H]^+$, 189.1 $[M+2H]^{2+}$.

FTIR: $\nu$ cm$^{-1}$ 2853 m, 1602 w, 1492 m, 1452 m, 1254 m, 1155 m, 1084 s, 1027 m, 860 m, 791 w, 759 s, 701 s.

Elemental analysis found (calculated for $C_{24}H_{28}N_2O_2$): % C 75.74 (76.56) H 7.94 (7.50) N 7.30 (7.44).

**(*S*,*S*)-α,α'-*bis*(2-amino-2-phenylethoxy)-*m*-xylene [(*S*,*S*)-3b]**

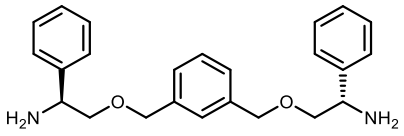


Synthesised according to the procedure described for (*R*,*R*)-**3b**; substituting (*R*)-2-phenylglycinol for (*S*)-2-phenylglycinol.

Yield: 1.16 g, 3.1 mmol, 85 %.

$^{1}$H NMR (300 MHz, 298 K, $CDCl_3$): $\delta_H$ 7.40-7.23 (14H, m, Ph), 4.55 (4H, s, OC*H*$_2$Ph), 4.24 (2H, dd, $^{3}J_{HH}$ = 9.0 Hz, 3.8 Hz, CH), 3.61 (2H, dd, $^{2}J_{HH}$ = 9.0 Hz, $^{3}J_{HH}$ = 3.8 Hz, OC*H*$_2$CH), 3.46 (2H, t, $^{2}J_{HH}/^{3}J_{HH}$ = 9.0, OC*H*$_2$CH), 1.75 (4H, br s, $NH_2$).

$^{13}$C{$^{1}$H} NMR (75 MHz, 298 K, $CDCl_3$): $\delta_C$ 142.6 (Ph), 138.5 (Ph), 128.7 (Ph), 128.6 (Ph), 127.5 (Ph), 127.2 (Ph), 127.1 (Ph), 127.0 (Ph), 76.9 (O*C*H$_2$CH), 73.3 (O*C*H$_2$Ph), 55.7 (CH).

MS (ESI): m/z 399.2 $[M+Na]^+$, 377.2 $[M+H]^+$, 189.1 $[M+2H]^{2+}$.

FTIR: $\nu$ cm$^{-1}$ 2853 m, 1602 w, 1492 m, 1452 m, 1254 m, 1155 m, 1084 s, 1027 m, 860 m, 791 w, 759 s, 701 s.

Elemental analysis found (calculated for $C_{24}H_{28}N_2O_2$): % C 75.72 (76.56) H 7.61 (7.50) N 7.17 (7.44).

**(*S*,*S*)-*α*,*α*'-*bis*(2-amino-2-phenylethoxy)-*o*-xylene [(*S*,*S*)-3c]**

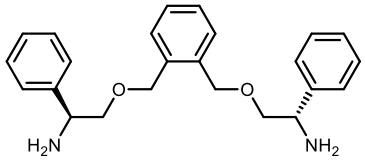


Under inert atmosphere, (*S*)-2-phenylglycinol (0.69 g, 5.0 mmol, 2.2 eq.) was dissolved in anhydrous THF (40 ml), to which 0.6 ml (0.67 g, 3.0 mmol, 1.3 eq.) [15]-crown-[5] was added by injection. The solution was then added dropwise to neat sodium hydride (0.25 g, 10.4 mmol, 4.6 eq.). The effervescent mixture was carefully placed under static vacuum and stirred at ambient temperature for 1 h. A solution of

α,α'-dibromo-*o*-xylene (0.6 g, 2.3 mmol, 1 eq.) in anhydrous THF (30 ml) was then added dropwise. The reaction mixture was then stirred under static vacuum; for 1 h at ambient temperature, then 5 h at 65 °C. The dark brown reaction mixture was allowed to cool before quenching with 2:1 saturated KCl aq./water (50 ml). The crude product was extracted using diethyl ether (3 × 100 ml), dried over sodium sulfate, filtered through celite, and the solvent removed under reduced pressure to leave a yellow oil. This crude product was purified by Kügelrohr distillation (150 °C, 45 min) to remove [15]-crown-[5] and unreacted excess phenylglycinol.

Yield: 0.59 g, 1.6 mmol, 68 %.

$^{1}$H NMR (400 MHz, 298 K, $CDCl_3$): $\delta_H$ 7.29-7.12 (14H, m, Ph), 4.44 (4H, s, OC*H*$_2$Ph), 4.13 (2H, dd, $^{3}J_{HH}$ = 8.9 Hz, 3.8 Hz, CH), 3.50 (2H, dd, $^{2}J_{HH}$ = 8.9 Hz, $^{3}J_{HH}$ = 3.8 Hz, OC*H*$_2$CH), 3.35 (2H, t, $^{2}J_{HH}$/$^{3}J_{HH}$ = 8.90, OC*H*$_2$CH), 1.73 (4H, br s, $NH_2$).

$^{13}$C{$^{1}$H} NMR (75 MHz, 298 K, $CDCl_3$): $\delta_C$ 142.7 (Ph), 136.4 (Ph), 130.0 (Ph), 128.5 (Ph), 128.0 (Ph), 127.5 (Ph), 127.0 (Ph), 76.9 (O*C*H$_2$CH), 71.0 (O*C*H$_2$Ph), 55.7 (CH).

MS (ESI): m/z 377.2 $[M+H]^+$.

FTIR: ν $cm^{-1}$ 2853 m, 1724 w, 1603 w, 1584 w, 1492 w, 1452 m, 1354 w, 1216 w, 1186 w, 1120 m, 1080 s, 1027 m, 943 w, 861 w, 753 s, 700 s.

Elemental analysis found (calculated for $C_{24}H_{28}N_2O_2$): % C 76.14 (76.56) H 7.83 (7.50) N 6.91 (7.44).

**(*R*,*R*)-4,4'-*bis*[(2-amino-2-phenylethoxy)methyl]-1,1'-biphenyl [(*R*,*R*)-3d]**

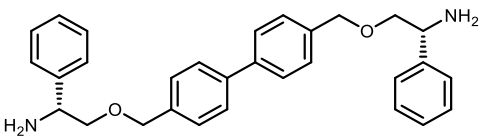


Under inert atmosphere, (*R*)-2-phenylglycinol (0.86 g, 6.3 mmol, 2.1 eq.) was dissolved in anhydrous THF (50 ml), to which 0.6 ml (0.67 g, 3.0 mmol, 1.0 eq.) [15]-crown-[5] was added by injection. The solution was then added dropwise to neat sodium hydride (0.31 g, 12.9 mmol, 4.3 eq.). The effervescent mixture was carefully placed under static vacuum and stirred at ambient temperature for 1 h. A solution of 4,4'-*bis*(chloromethyl)-1,1'-biphenyl (0.75 g, 3.0 mmol, 1 eq.) in anhydrous THF (40 ml) was then added dropwise. The reaction mixture was then stirred under static vacuum; for 1 h at ambient temperature, then 5 h at 65 °C. The yellow reaction mixture was allowed to cool before quenching with 2:1 saturated KCl aq./water (60 ml). The crude product was extracted using diethyl ether (3 × 100 ml), dried over sodium sulfate, filtered through celite, and the solvent removed under reduced pressure to leave a yellow oil. This crude product was purified by Kügelrohr distillation (150 °C, 45 min) to remove [15]-crown-[5] and unreacted excess phenylglycinol. Upon standing, the product solidified to give a pale yellow wax.

Yield: 0.82 g, 1.8 mmol, 61 %.

$^{1}$H NMR (300 MHz, 298 K, $CDCl_3$): $\delta_H$ 7.49 (4H, d, $^{3}J_{HH}$ = 8.1 Hz, Ph), 7.34-7.16 (14H, m, Ph), 4.52 (4H, s, OC*H*$_2$Ph), 4.19 (2H, dd, $^{2}J_{HH}$ = 8.9 Hz, $^{3}J_{HH}$ = 3.8 Hz, CH), 3.57 (2H, dd, $^{2}J_{HH}$ = 8.9 Hz, $^{3}J_{HH}$ = 3.8 Hz, OC*H*$_2$CH), 3.41 (2H, t, $^{2}J_{HH}/^{3}J_{HH}$ = 9.0, OC*H*$_2$CH), 1.73 (4H, br s, $NH_2$).

$^{13}C\{^{1}H\}$ NMR (75 MHz, 298 K, $CDCl_3$): $\delta_C$ 142.6 (Ph), 140.4 (Ph), 137.4 (Ph), 128.5 (Ph), 128.3 (Ph), 127.5 (Ph), 127.2 (Ph), 127.0 (Ph), 76.8 (O*C*$H_2$CH), 73.0 (O*C*$H_2$Ph), 55.7 (CH).

MS (ESI): m/z 475. 2 $[M+Na]^+$, 453.2 $[M+H]^+$, 227.1 $[M+2H]^{2+}$.

FTIR: ν $cm^{-1}$ 3383 w, 2853 m, 1561 w, 1502 w, 1492 m, 1454 m, 1396 w, 1373 w, 1348 m, 1305 m, 1210 w, 1183 w, 1108 s, 1015 m, 1003 m, 936 w, 860 m, 801 s, 758 s, 700 s.

Elemental analysis found (calculated for $C_{30}H_{32}N_2O_2$): % C 79.27 (79.61) H 7.25 (7.13) N 5.93 (6.19).

**(*S*,*S*)-4,4'-*bis*[(2-amino-2-phenylethoxy)methyl]-1,1'-biphenyl [(*S*,*S*)-3d]**

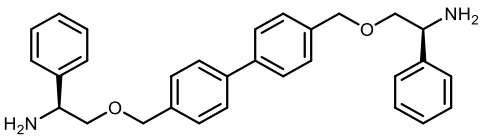


Synthesised according to the procedure described for (*R*,*R*)-**3d**; substituting (*R*)-2-phenylglycinol for (*S*)-2-phenylglycinol.

Yield: 1.05 g, 2.3 mmol, 78 %.

$^{1}H$ NMR (300 MHz, 298 K, $CDCl_3$): $\delta_H$ 7.49 (4H, d, $^{3}J_{HH}$ = 8.1 Hz, Ph), 7.34-7.16 (14H, m, Ph), 4.52 (4H, s, OC*H*$_2$Ph), 4.19 (2H, dd, $^{2}J_{HH}$ = 8.9 Hz, $^{3}J_{HH}$ = 3.8 Hz, CH), 3.57 (2H, dd, $^{2}J_{HH}$ = 8.9 Hz, $^{3}J_{HH}$ = 3.8 Hz, OC*H*$_2$CH), 3.41 (2H, t, $^{2}J_{HH}/^{3}J_{HH}$ = 8.9, OC*H*$_2$CH), 1.73 (4H, br s, $NH_2$).

$^{13}C\{^{1}H\}$ NMR (75 MHz, 298 K, $CDCl_3$): $\delta_C$ 142.6 (Ph), 140.4 (Ph), 137.4 (Ph), 128.5 (Ph), 128.3 (Ph), 127.5 (Ph), 127.2 (Ph), 127.0 (Ph), 76.8 (O*C*$H_2$CH), 73.0 (O*C*$H_2$Ph), 55.7 (CH).

MS (ESI): m/z 475. 2 $[M+Na]^+$, 453.2 $[M+H]^+$, 227.1 $[M+2H]^{2+}$.

FTIR: ν $cm^{-1}$ 3383 w, 2853 m, 1561 w, 1502 w, 1492 m, 1454 m, 1396 w, 1373 w, 1348 m, 1305 m, 1210 w, 1183 w, 1108 s, 1015 m, 1003 m, 936 w, 860 m, 801 s, 758 s, 700 s.

Elemental analysis found (calculated for $C_{30}H_{32}N_2O_2$): % C 79.27 (79.61) H 7.31 (7.13) N 5.92 (6.19).

**(*R*,*R*)-4,4'-*bis*[(2-amino-2-phenylethoxy)methyl]-diphenyl ether [(*R*,*R*)-3e]**

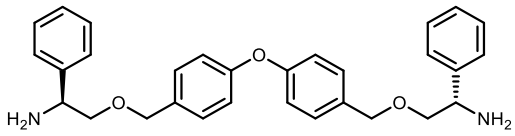


Under inert atmosphere, (*R*)-2-phenylglycinol (0.66 g, 4.8 mmol, 2.1 eq.) was dissolved in anhydrous THF (50 ml), to which 0.6 ml (0.67 g, 3.0 mmol, 1.3 eq.) [15]-crown-[5] was added by injection. The solution was then added dropwise to neat sodium hydride (0.25 g, 10.4 mmol, 4.6 eq.). The effervescent mixture was carefully placed under static vacuum and stirred at ambient temperature for 1 h. A solution of **2e** (0.8 g, 2.3 mmol, 1 eq.) in anhydrous THF (40 ml) was then added dropwise. The reaction mixture was then stirred under static vacuum; for 1 h at ambient temperature, then 5 h at 65 °C. The brick red reaction mixture was allowed to cool before quenching with 2:1 saturated KCl aq./water (60 ml). The crude product was extracted using

diethyl ether (3 × 100 ml), dried over sodium sulfate, filtered through celite, and the solvent removed under reduced pressure to leave a yellow oil. This crude product was purified by Kügelrohr distillation (150 °C, 45 min) to remove [15]-crown-[5] and unreacted excess phenylglycinol.

Yield: 0.78 g, 1.6 mmol, 72 %.

$^{1}$H NMR (300 MHz, 298 K, $CDCl_3$): $\delta_H$ 7.40-7.22 (14H, m, Ph), 6.96 (4H, d, $^{3}J_{HH}$ = 8.3 Hz, Ph), 4.51 (4H, s, OC*H*$_2$Ph), 4.23 (2H, dd, $^{2}J_{HH}$ = 8.9 Hz, $^{3}J_{HH}$ = 3.7 Hz, CH), 3.61 (2H, dd, $^{2}J_{HH}$ = 8.9 Hz, $^{3}J_{HH}$ = 3.7 Hz, OC*H*$_2$CH), 3.45 (2H, t, $^{2}J_{HH}/^{3}J_{HH}$ = 8.9, OC*H*$_2$CH), 1.74 (4H, br s, $NH_2$).

$^{13}$C{$^{1}$H} NMR (75 MHz, 298 K, $CDCl_3$): $\delta_C$ 156.8 (Ph), 142.6 (Ph), 133.2 (Ph), 129.4 (Ph), 128.5 (Ph), 127.5 (Ph), 126.9 (Ph), 118.9 (Ph), 76.7 (O*C*H$_2$CH), 72.9 (O*C*H$_2$Ph), 55.7 (CH).

MS (ESI): m/z 491.2 $[M+Na]^+$, 469.2 $[M+H]^+$, 235.1 $[M+2H]^{2+}$.

FTIR: ν cm$^{-1}$ 3027 w, 2855 w, 1601 m, 1500 s, 1452 w, 1354 w, 1236 s, 1166 w, 1087 s, 1014 w, 874 m, 853 m, 760 s, 701 s.

Elemental analysis found (calculated for $C_{30}H_{32}N_2O_3$): % C 76.47 (76.90) H 7.14 (6.88) N 5.65 (5.98).

**(*S*,*S*)-4,4'-*bis*[(2-amino-2-phenylethoxy)methyl]-diphenyl ether [(*S*,*S*)-3e]**

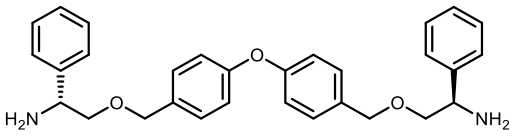

Synthesised according to the procedure described for (*R*,*R*)-**3e**; substituting (*R*)-2-phenylglycinol for (*S*)-2-phenylglycinol.

Yield: 0.77 g, 1.6 mmol, 73 %.

$^{1}$H NMR (300 MHz, 298 K, $CDCl_3$): $\delta_H$ 7.40-7.22 (14H, m, Ph), 6.96 (4H, d, $^{3}J_{HH}$ = 8.3 Hz, Ph), 4.51 (4H, s, OC*H*$_2$Ph), 4.23 (2H, dd, $^{2}J_{HH}$ = 8.9 Hz, $^{3}J_{HH}$ = 3.7 Hz, CH), 3.61 (2H, dd, $^{2}J_{HH}$ = 8.9 Hz, $^{3}J_{HH}$ = 3.7 Hz, OC*H*$_2$CH), 3.45 (2H, t, $^{2}J_{HH}/^{3}J_{HH}$ = 8.9, OC*H*$_2$CH), 1.74 (4H, br s, $NH_2$).

$^{13}$C{$^{1}$H} NMR (75 MHz, 298 K, $CDCl_3$): $\delta_C$ 156.8 (Ph), 142.6 (Ph), 133.2 (Ph), 129.4 (Ph), 128.5 (Ph), 127.5 (Ph), 126.9 (Ph), 118.9 (Ph), 76.7 (O*C*H$_2$CH), 72.9 (O*C*H$_2$Ph), 55.7 (CH).

MS (ESI): m/z 491.2 $[M+Na]^+$, 469.2 $[M+H]^+$, 235.1 $[M+2H]^{2+}$.

FTIR: ν cm$^{-1}$ 3027 w, 2855 w, 1601 m, 1500 s, 1452 w, 1354 w, 1236 s, 1166 w, 1087 s, 1014 w, 874 m, 853 m, 760 s, 701 s.

Elemental analysis found (calculated for $C_{30}H_{32}N_2O_3$): % C 76.48 (76.90) H 7.22 (6.88) N 5.65 (5.98).

**(*R*,*R*)-4,4'-*bis*[(2-amino-2-phenylethoxy)methyl]-diphenyl sulfide [(*R*,*R*)-3f]**

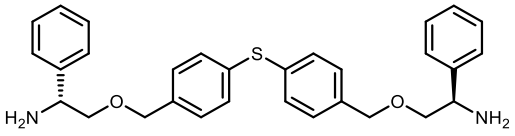


Under inert atmosphere, (*R*)-2-phenylglycinol (0.64 g, 4.7 mmol, 2.1 eq.) was dissolved in anhydrous THF (50 ml), to which 0.6 ml (0.67 g, 3.0 mmol, 1.4 eq.) [15]-

crown-[5] was added by injection. The solution was then added dropwise to neat sodium hydride (0.24 g, 10.0 mmol, 4.7 eq.). The effervescent mixture was carefully placed under static vacuum and stirred at ambient temperature for 1 h. A solution of **2f** (0.8 g, 2.2 mmol, 1 eq.) in anhydrous THF (40 ml) was then added dropwise. The reaction mixture was then stirred under static vacuum; for 1 h at ambient temperature, then 5 h at 65 °C. The dark purple reaction mixture was allowed to cool before quenching with 2:1 saturated KCl aq./water (60 ml). The crude product was extracted using diethyl ether (3 × 100 ml), dried over sodium sulfate, filtered through celite, and the solvent removed under reduced pressure to leave a yellow oil. This crude product was purified by Kügelrohr distillation (150 °C, 45 min) to remove [15]-crown-[5] and unreacted excess phenylglycinol.

Yield: 0.88 g, 1.8 mmol, 84 %.

$^{1}$H NMR (300 MHz, 298 K, $CDCl_3$): $\delta_H$ 7.41-7.23 (18H, m, Ph), 4.53 (4H, s, OC*H*$_2$Ph), 4.25 (2H, dd, $^{2}J_{HH}$ = 8.8 Hz, $^{3}J_{HH}$ = 3.7 Hz, CH), 3.62 (2H, dd, $^{2}J_{HH}$ = 8.8 Hz, $^{3}J_{HH}$ = 3.7 Hz, OC*H*$_2$CH), 3.46 (2H, t, $^{2}J_{HH}$/$^{3}J_{HH}$ = 8.8, OC*H*$_2$CH), 1.76 (4H, br s, $NH_2$).

$^{13}$C{$^{1}$H} NMR (75 MHz, 298 K, $CDCl_3$): $\delta_C$ 142.6 (Ph), 137.4 (Ph), 135.1 (Ph), 131.2 (Ph), 128.6 (Ph), 128.5 (Ph), 127.5 (Ph), 126.9 (Ph), 76.9 (O*C*H$_2$CH), 72.9 (O*C*H$_2$Ph), 55.7 (CH).

MS (ESI): m/z 507.2 $[M+Na]^+$, 485.2 $[M+H]^+$, 243.1 $[M+2H]^{2+}$.

FTIR: ν $cm^{-1}$ 2855 m, 1602 w, 1492 w, 1452 m, 1421 w, 1354 m, 1212 w, 1084 s, 1084 m, 848 m, 757 m, 700 s.

Elemental analysis found (calculated for $C_{30}H_{32}N_2O_2S$): % C 73.53 (74.35) H 6.83 (6.66) N 5.42 (5.78).

**(*S*,*S*)-4,4'-*bis*[(2-amino-2-phenylethoxy)methyl]-diphenyl sulfide [(*S*,*S*)-3f]**

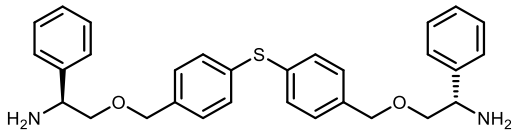


Synthesised according to the procedure described for (*R*,*R*)-**3f**; with the substitution of (*R*)-2-phenylglycinol for (*S*)-2-phenylglycinol.

Yield: 0.58 g, 1.2 mmol, 56 %.

$^{1}$H NMR (300 MHz, 298 K, $CDCl_3$): $\delta_H$ 7.41-7.23 (18H, m, Ph), 4.53 (4H, s, OC*H*$_2$Ph), 4.25 (2H, dd, $^{2}J_{HH}$ = 8.8 Hz, $^{3}J_{HH}$ = 3.7 Hz, CH), 3.62 (2H, dd, $^{2}J_{HH}$ = 8.8 Hz, $^{3}J_{HH}$ = 3.7 Hz, OC*H*$_2$CH), 3.46 (2H, t, $^{2}J_{HH}$/$^{3}J_{HH}$ = 8.8, OC*H*$_2$CH), 1.76 (4H, br s, $NH_2$).

$^{13}$C{$^{1}$H} NMR (75 MHz, 298 K, $CDCl_3$): $\delta_C$ 142.6 (Ph), 137.4 (Ph), 135.1 (Ph), 131.2 (Ph), 128.6 (Ph), 128.5 (Ph), 127.5 (Ph), 126.9 (Ph), 76.9 (O*C*H$_2$CH), 72.9 (O*C*H$_2$Ph), 55.7 (CH).

MS (ESI): m/z 507.2 $[M+Na]^+$, 485.2 $[M+H]^+$, 243.1 $[M+2H]^{2+}$.

FTIR: ν $cm^{-1}$ 2855 m, 1602 w, 1492 w, 1452 m, 1421 w, 1354 m, 1212 w, 1084 s, 1084 m, 848 m, 757 m, 700 s.

Elemental analysis found (calculated for $C_{30}H_{32}N_2O_2S$): % C 73.96 (74.35) H 6.89 (6.66) N 5.42 (5.78).

**(*R*,*R*)-4,4'-*bis*[(2-amino-2-phenylethoxy)methyl]-diphenylmethane [(*R*,*R*)-3g]**

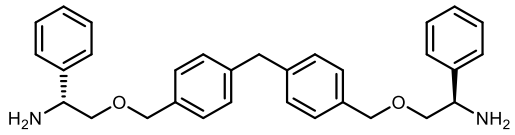


Under inert atmosphere, (*R*)-2-phenylglycinol (0.67 g, 4.9 mmol, 2.2 eq.) was dissolved in anhydrous THF (50 ml), to which 0.6 ml (0.67 g, 3.0 mmol, 1.3 eq.) [15]-crown-[5] was added by injection. The solution was then added dropwise to neat sodium hydride (0.24 g, 10.0 mmol, 4.4 eq.). The effervescent mixture was carefully placed under static vacuum and stirred at ambient temperature for 1 h. A solution of **2g** (0.8 g, 2.3 mmol, 1 eq.) in anhydrous THF (40 ml) was then added dropwise. The reaction mixture was then stirred under static vacuum; for 1 h at ambient temperature, then 5 h at 65 °C. The orange-brown reaction mixture was allowed to cool before quenching with 2:1 saturated KCl aq./water (60 ml). The crude product was extracted using diethyl ether (3 × 100 ml), dried over sodium sulfate, filtered through celite, and the solvent removed under reduced pressure to leave a yellow oil. This crude product was purified by Kügelrohr distillation (150 °C, 45 min) to remove [15]-crown-[5] and unreacted excess phenylglycinol.

Yield: 0.74 g, 1.6 mmol, 70 %.

$^{1}$H NMR (300 MHz, 298 K, $CDCl_3$): $\delta_H$ 7.41-7.14 (18H, m, Ph), 4.52 (4H, s, OC*H*$_2$Ph), 4.24 (2H, dd, $^{2}J_{HH}$ = 8.9 Hz, $^{3}J_{HH}$ = 3.7 Hz, CH), 3.97 (2H, s, PhC*H*$_2$Ph), 3.61 (2H, dd, $^{2}J_{HH}$ = 8.9 Hz, $^{3}J_{HH}$ = 3.7 Hz, OC*H*$_2$CH), 3.45 (2H, t, $^{2}J_{HH}$/$^{3}J_{HH}$ = 8.9, OC*H*$_2$CH), 1.72 (4H, br s, $NH_2$).

$^{13}C\{^{1}H\}$ NMR (75 MHz, 298 K, $CDCl_3$): $\delta_C$ 142.7 (Ph), 140.7 (Ph), 136.1 (Ph), 129.1 (Ph), 128.5 (Ph), 128.1 (Ph), 127.5 (Ph), 127.0 (Ph), 76.9 (O*C*$H_2$CH), 73.3 (O*C*$H_2$Ph), 55.7 (CH), 41.5 (Ph*C*$H_2$Ph).

MS (ESI): m/z 489.1 $[M+Na]^+$, 467.1 $[M+H]^+$.

FTIR: ν $cm^{-1}$ 3057 w, 2896 w, 2853 m, 1603 w, 1511 w, 1492 w, 1452 m, 1418 w, 1354 w, 1182 w, 1088 s, 1020 m, 849 m, 804 w, 758 s, 701 s.

Elemental analysis found (calculated for $C_{31}H_{34}N_2O_2$): % C 80.20 (79.80) H 7.22 (7.34) N 5.23 (6.00).

**(*S*,*S*)-4,4'-*bis*[(2-amino-2-phenylethoxy)methyl]-diphenylmethane [(*S*,*S*)-3g]**

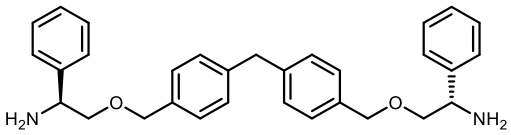


Synthesised according to the procedure described for (*R*,*R*)-**3g**; with the substitution of (*R*)-2-phenylglycinol for (*S*)-2-phenylglycinol.

Yield: 0.75 g, 1.6 mmol, 71 %.

$^{1}H$ NMR (300 MHz, 298 K, $CDCl_3$): $\delta_H$ 7.41-7.14 (18H, m, Ph), 4.52 (4H, s, OC*H*$_2$Ph), 4.24 (2H, dd, $^{2}J_{HH}$ = 8.9 Hz, $^{3}J_{HH}$ = 3.7 Hz, CH), 3.97 (2H, s, PhC*H*$_2$Ph), 3.61 (2H, dd, $^{2}J_{HH}$ = 8.9 Hz, $^{3}J_{HH}$ = 3.7 Hz, OC*H*$_2$CH), 3.45 (2H, t, $^{2}J_{HH}/^{3}J_{HH}$ = 8.9, OC*H*$_2$CH), 1.72 (4H, br s, $NH_2$).

$^{13}C\{^{1}H\}$ NMR (75 MHz, 298 K, $CDCl_3$): $\delta_C$ 142.7 (Ph), 140.7 (Ph), 136.1 (Ph), 129.1 (Ph), 128.5 (Ph), 128.1 (Ph), 127.5 (Ph), 127.0 (Ph), 76.9 (O*C*$H_2$CH), 73.3 (O*C*$H_2$Ph), 55.7 (CH), 41.5 (Ph*C*$H_2$Ph).

MS (ESI): m/z 489.1 $[M+Na]^+$, 467.1 $[M+H]^+$.

FTIR: ν $cm^{-1}$ 3057 w, 2896 w, 2853 m, 1603 w, 1511 w, 1492 w, 1452 m, 1418 w, 1354 w, 1182 w, 1088 s, 1020 m, 849 m, 804 w, 758 s, 701 s.

Elemental analysis found (calculated for $C_{31}H_{34}N_2O_2$): % C 80.34 (79.80) H 7.55 (7.34) N 5.27 (6.00).

**(*R*,*R*)-4,4'-bis[(2-amino-2-phenylethoxy)methyl]-1,2-diphenylethane [(*R*,*R*)-3h]**

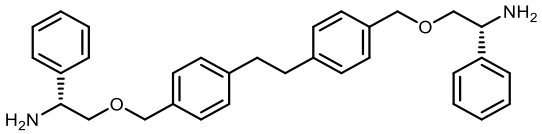


Under inert atmosphere, (*R*)-2-phenylglycinol (0.66 g, 4.8 mmol, 2.2 eq.) was dissolved in anhydrous THF (50 ml), to which 0.6 ml (0.67 g, 3.0 mmol, 1.4 eq.) [15]-crown-[5] was added by injection. The solution was then added dropwise to neat sodium hydride (0.24 g, 10.0 mmol, 4.6 eq.). The effervescent mixture was carefully placed under static vacuum and stirred at ambient temperature for 1 h. A solution of **2h** (0.8 g, 2.2 mmol, 1 eq.) in anhydrous THF (40 ml) was then added dropwise. The reaction mixture was then stirred under static vacuum; for 1 h at ambient temperature, then 5 h at 65 °C. The grey-brown reaction mixture was allowed to cool before

quenching with 2:1 saturated KCl aq./water (60 ml). The crude product was extracted using diethyl ether (3 × 100 ml), dried over sodium sulfate, filtered through celite, and the solvent removed under reduced pressure to leave a yellow oil. This crude product was purified by Kügelrohr distillation (150 °C, 45 min) to remove [15]-crown-[5] and unreacted excess phenylglycinol. Upon standing, the product solidified to give a yellow wax.

Yield: 0.8 g, 1.7 mmol, 77 %.

$^{1}$H NMR (300 MHz, 298 K, $CDCl_3$): $\delta_H$ 7.41-7.14 (18H, m, Ph), 4.53 (4H, s, OC*H*$_2$Ph), 4.24 (2H, dd, $^{2}J_{HH}$ = 8.9 Hz, $^{3}J_{HH}$ = 3.7 Hz, CH), 3.61 (2H, dd, $^{2}J_{HH}$ = 8.9 Hz, $^{3}J_{HH}$ = 3.7 Hz, OC*H*$_2$CH), 3.45 (2H, t, $^{2}J_{HH}$/$^{3}J_{HH}$ = 8.9, OC*H*$_2$CH), 2.91 (4H, s, $CH_2CH_2$), 1.73 (4H, br s, $NH_2$).

$^{13}$C{$^{1}$H} NMR (75 MHz, 298 K, $CDCl_3$): $\delta_C$ 142.7 (Ph), 141.4 (Ph), 135.9 (Ph), 128.6 (Ph), 128.5 (Ph), 128.0 (Ph), 127.5 (Ph), 127.0 (Ph), 76.8 (O*C*H$_2$CH), 73.3 (O*C*H$_2$Ph), 55.7 (CH), 37.7 ($CH_2CH_2$).

MS (ESI): m/z 481.2 $[M+H]^+$.

FTIR: ν $cm^{-1}$ 3384 w, 3058 w, 3027 w, 2854 m, 1601 m, 1514 w, 1491 w, 1451 m, 1421 w, 1352 w, 1308 w, 1291 w, 1114 s, 1091 s, 1020 m, 820 s, 753 s, 700 s.

Elemental analysis found (calculated for $C_{32}H_{36}N_2O_2$): % C 79.71 (79.97) H 7.69 (7.55) N 5.69 (5.83).

**(*S*,*S*)-4,4'-bis[(2-amino-2-phenylethoxy)methyl]-1,2-diphenylethane [(*S*,*S*)-3h]**

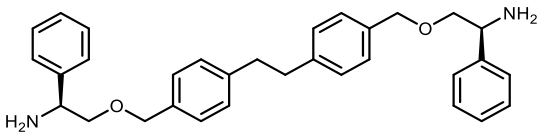


Synthesised according to the procedure described for (*R*,*R*)-**3h**; with the substitution of (*R*)-2-phenylglycinol for (*S*)-2-phenylglycinol.

Yield: 0.84 g, 1.7 mmol, 80 %.

$^{1}$H NMR (300 MHz, 298 K, $CDCl_3$): $\delta_H$ 7.41-7.14 (18H, m, Ph), 4.53 (4H, s, OC*H*$_2$Ph), 4.24 (2H, dd, $^{2}J_{HH}$ = 8.9 Hz, $^{3}J_{HH}$ = 3.7 Hz, CH), 3.61 (2H, dd, $^{2}J_{HH}$ = 8.9 Hz, $^{3}J_{HH}$ = 3.7 Hz, OC*H*$_2$CH), 3.45 (2H, t, $^{2}J_{HH}$/$^{3}J_{HH}$ = 8.9, OC*H*$_2$CH), 2.91 (4H, s, $CH_2CH_2$), 1.73 (4H, br s, $NH_2$).

$^{13}$C{$^{1}$H} NMR (75 MHz, 298 K, $CDCl_3$): $\delta_C$ 142.7 (Ph), 141.4 (Ph), 135.9 (Ph), 128.6 (Ph), 128.5 (Ph), 128.0 (Ph), 127.5 (Ph), 127.0 (Ph), 76.8 (O*C*H$_2$CH), 73.3 (O*C*H$_2$Ph), 55.7 (CH), 37.7 ($CH_2CH_2$).

MS (ESI): m/z 481.2 $[M+H]^+$.

FTIR: ν $cm^{-1}$ 3384 w, 3058 w, 3027 w, 2854 m, 1601 m, 1514 w, 1491 w, 1451 m, 1421 w, 1352 w, 1308 w, 1291 w, 1114 s, 1091 s, 1020 m, 820 s, 753 s, 700 s.

Elemental analysis found (calculated for $C_{32}H_{36}N_2O_2$): % C 80.05 (79.97) H 7.66 (7.55) N 5.69 (5.83).

**(*R*,*R*)-2,8-*bis*[(2-amino-2-phenylethoxy)methyl]-dibenzofuran [(*R*,*R*)-3i]**

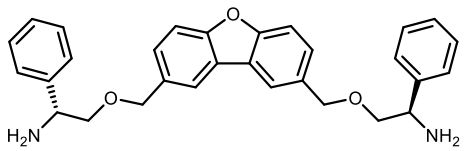


Under inert atmosphere, (*R*)-2-phenylglycinol (0.67 g, 6.0 mmol, 2.2 eq.) was dissolved in anhydrous THF (50 ml), to which 0.6 ml (0.67 g, 3.0 mmol, 1.3 eq.) [15]-crown-[5] was added by injection. The solution was then added dropwise to neat sodium hydride (0.4 g, 10.0 mmol, 4.4 eq.). The effervescent mixture was carefully placed under static vacuum and stirred at ambient temperature for 1 h. A solution of **2i** (0.8 g, 2.3 mmol, 1 eq.) in anhydrous THF (40 ml) was then added dropwise. The reaction mixture was then stirred under static vacuum; for 1 h at ambient temperature, then 5 h at 65 °C. The dark green-grey reaction mixture was allowed to cool before quenching with 2:1 saturated KCl aq./water (60 ml). The crude product was extracted using diethyl ether (3 × 100 ml), dried over sodium sulfate, filtered through celite, and the solvent removed under reduced pressure to leave a yellow oil. This crude product was purified by Kügelrohr distillation (150 °C, 45 min) to remove [15]-crown-[5] and unreacted excess phenylglycinol.

Yield: 0.78 g, 1.7 mmol, 74 %.

$^{1}$H NMR (300 MHz, 298 K, $CDCl_3$): $\delta_H$ 7.81 (2H, s, Ph), 7.45 (2H, d, $^{3}J_{HH}$ = 8.5 Hz, Ph), 7.36-7.17 (12H, m, Ph), 4.62 (4H, s, OC*H*$_2$Ph), 4.20 (2H, dd, $^{2}J_{HH}$ = 8.9 Hz, $^{3}J_{HH}$ = 3.7 Hz, CH), 3.59 (2H, dd, $^{2}J_{HH}$ = 8.9 Hz, $^{3}J_{HH}$ = 3.7 Hz, OC*H*$_2$CH), 3.44 (2H, t, $^{2}J_{HH}/^{3}J_{HH}$ = 8.9, OC*H*$_2$CH), 1.74 (4H, br s, $NH_2$).

$^{13}C\{^{1}H\}$ NMR (75 MHz, 298 K, $CDCl_3$): $\delta_C$ 156.2 (Ph), 142.6 (Ph), 132.9 (Ph), 128.5 (Ph), 127.5 (Ph), 127.3 (Ph), 126.9 (Ph), 124.3 (Ph), 120.3 (Ph), 111.6 (Ph), 76.7 (O*C*$H_2$CH), 73.5 (O*C*$H_2$Ph), 55.7 (CH).

MS (ESI): m/z 489.2 $[M+Na]^+$, 467.2 $[M+H]^+$, 234.1 $[M+2H]^{2+}$.

FTIR: ν $cm^{-1}$ 3057 w, 3027 w, 2854 m, 1603 w, 1488 m, 1452 m, 1420 w, 1355 w, 1248 w, 1208 m, 1189 m, 1083 s, 1027 m, 876 m, 850 m, 808 m, 759 m, 700 s.

Elemental analysis found (calculated for $C_{30}H_{30}N_2O_3$): % C 76.36 (77.23) H 6.83 (6.48) N 5.83 (6.00).

**(*S*,*S*)-2,8-*bis*[(2-amino-2-phenylethoxy)methyl]-dibenzofuran [(*S*,*S*)-3i]**

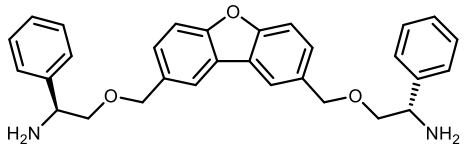


Synthesised according to the procedure described for (*R*,*R*)-**3i**; with the substitution of (*R*)-2-phenylglycinol for (*S*)-2-phenylglycinol.

Yield: 0.82 g, 1.8 mmol, 78 %.

$^{1}H$ NMR (300 MHz, 298 K, $CDCl_3$): $\delta_H$ 7.81 (2H, s, Ph), 7.45 (2H, d, $^{3}J_{HH}$ = 8.5 Hz, Ph), 7.36-7.17 (12H, m, Ph), 4.62 (4H, s, OC*H*$_2$Ph), 4.20 (2H, dd, $^{2}J_{HH}$ = 8.9 Hz, $^{3}J_{HH}$ = 3.7 Hz, CH), 3.59 (2H, dd, $^{2}J_{HH}$ = 8.9 Hz, $^{3}J_{HH}$ = 3.7 Hz, OC*H*$_2$CH), 3.44 (2H, t, $^{2}J_{HH}/^{3}J_{HH}$ = 8.9, OC*H*$_2$CH), 1.74 (4H, br s, $NH_2$).

$^{13}C\{^{1}H\}$ NMR (75 MHz, 298 K, $CDCl_3$): $\delta_C$ 156.2 (Ph), 142.6 (Ph), 132.9 (Ph), 128.5 (Ph), 127.5 (Ph), 127.3 (Ph), 126.9 (Ph), 124.3 (Ph), 120.3 (Ph), 111.6 (Ph), 76.7 (O*C*$H_2$CH), 73.5 (O*C*$H_2$Ph), 55.7 (CH).

MS (ESI): m/z 489.2 $[M+Na]^+$, 467.2 $[M+H]^+$, 234.1 $[M+2H]^{2+}$.

FTIR: ν $cm^{-1}$ 3057 w, 3027 w, 2854 m, 1603 w, 1488 m, 1452 m, 1420 w, 1355 w, 1248 w, 1208 m, 1189 m, 1083 s, 1027 m, 876 m, 850 m, 808 m, 759 m, 700 s.

Elemental analysis found (calculated for $C_{30}H_{30}N_2O_3$): % C 76.36 (77.23) H 6.83 (6.48) N 5.83 (6.00).

### 6.1.5 Synthesis and analysis of Mosher diamides[6]

Mosher amide derivatives were prepared using (*R*)-(+)-Mosher's acid (α-methoxy-α-trifluoromethyl-phenylacetic acid), and analysed using $^{1}H$ and $^{19}F$ NMR. The chemical shifts of Mosher diamide methyl and trifluoromethyl groups are listed in Table 6.1 (see Figure 2.3 for overlaid spectra of **3b** derivatives).

Mosher's acid (90 mg, 0.38 mmol) was dissolved in anhydrous DCM (8 ml) and cooled to 0 °C. Oxalyl chloride (0.4 ml, 0.59 g, 4.7 mmol) was added, followed by 1 drop of DMF. After stirring for 1 hour the reaction mixture was concentrated *in vacuo* and the residue was suspended in hexane (10 ml) and concentrated *in vacuo* [$^{19}F$ NMR (400 MHz, $CDCl_3$) $\delta_F$ -70.2]. The product was dissolved in anhydrous DCM (10 ml) to give a 38 mM solution of Mosher's acid chloride. The diamine (0.01 g, 20-30 µmol) was dissolved in DCM (5 ml) and 2.5 ml of the Mosher's acid chloride solution in DCM (95 µmol >3 eq.) was added, followed by saturated aqueous sodium carbonate (2 ml). After stirring overnight the phases are separated and the organic phase dried

(magnesium sulfate), filtered and concentrated *in vacuo* to give crude Mosher's diamide. Kügelrohr distillation (120 °C, 20 min) was used to remove excess Mosher's acid and Mosher's acid chloride from the product, which was analysed without further purification.

| | **Mosher diamide NMR chemical shift** (400 MHz, $CDCl_3$) | |
|---|---|---|
| **Parent diamine** | $\delta_H$ ($OCH_3$) | $\delta_F$ ($CF_3$) |
| (*R*,*R*)-**3a** | 3.38 | -68.9 |
| (*S*,*S*)-**3a** | 3.30 | -68.9 |
| *rac*-**3a** | 3.38, 3.31 | -68.9 |
| (*R*,*R*)-**3b** | 3.37 | -68.9 |
| (*S*,*S*)-**3b** | 3.29 | -68.9 |
| *rac*-**3b** | 3.37, 3.30 | -68.9 |
| (*R*,*R*)-**3d** | 3.40 | -68.8 |
| (*S*,*S*)-**3d** | 3.32 | -68.8 |
| (*R*,*R*)/(*S*,*S*)-**3d** | 3.40, 3.32 | -68.8 |

**Table 6.1: Chemical shifts of Mosher diamide derivatives (of 3a, 3b, and 3d), used to determine optical purity**. The $^1$H-NMR shift corresponding to -$OCH_3$ protons that are sensitive to the chirality of the parent diamine, and $^{19}$F-NMR shift corresponding to -$CF_3$ F atoms are listed.

### 6.1.6 Synthesis and characterisation of $[Zn_2L_3][ClO_4]_4$ complexes

#### General Procedure[5]

The appropriate optically pure diamine (3.0 eq.) and 2-pyridinecarboxaldehyde (6.0 eq.) were dissolved in acetonitrile (30 ml) and stirred for 30 min at ambient temperature to form a yellow solution containing the ligand. Zinc (II) perchlorate hexahydrate (2.0 eq.) was added was added and no colour change was observed as the solution was stirred at ambient temperature for 4 h. The volume of the solution was reduced to ~10 ml under reduced pressure, and ethyl acetate was added dropwise to cause precipitation of a white solid, which was collected by filtration, washed with ethyl acetate (20 ml), and dried in air.

**$\Delta_{Zn}$-[$Zn_2L^b_3$][$ClO_4$]$_4$·3$H_2O$**

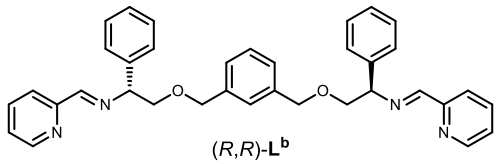

(*R*,*R*)-**L$^b$**

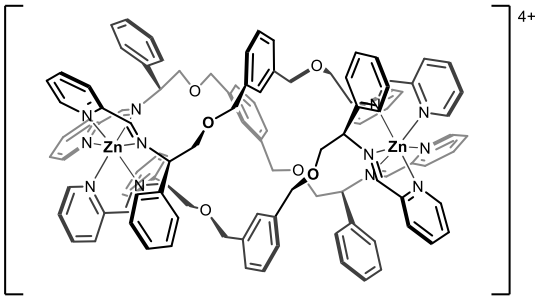

$\Delta_{Zn}$-[$Zn_2$**L$^b$**$_3$]$^{4+}$

Yield: 64 %.

$^1$H NMR (500 MHz, 298 K, $CD_3CN$): $\delta_H$ 8 .65 (6H, s, HC=N), 8.30 (3H, s, Ph), 7.82 (6H, t, $^3J_{HH}$ = 7.8 Hz, Py), 7.65-7.60 (12H, m, Ph/Py), 7.53 (3H, t, $^3J_{HH}$ = 7.5, Ph), 7.34 (6H, dd , $^3J_{HH}$ = 7.5 Hz, 5.3 Hz, Py), 7.25 (6H, d, $^3J_{HH}$ = 7.8 Hz, Py), 6.95 (6H, t, $^3J_{HH}$ = 7.6 Hz, Ph), 6.75 (12H, t, $^3J_{HH}$ = 7.6 Hz, Ph), 6.36 (12H, d, $^3J_{HH}$ = 7.6 Hz, Ph), 5.63 (6H, dd, $^3J_{HH}$ = 11.1 Hz, 2.6 Hz, CH), 5.01 (6H, d, $^2J_{HH}$ = 10.7 Hz, OC*H*$_2$Ph), 4.86 (6H, d, $^2J_{HH}$ = 10.7 Hz, OC*H*$_2$Ph), 4.11 (6H, t, $^2J_{HH}$ /$^3J_{HH}$ = 11.4 Hz, OC*H*$_2$CH), 3.17 (6H, dd, $^2J_{HH}$ = 11.4 Hz, $^3J_{HH}$ = 3.0 Hz, OC*H*$_2$CH).

$^{13}$C{$^1$H} NMR (125 MHz, 298 K, $CD_3CN$): $\delta_C$ 163.3 (C=N), 148.9 (Ar), 147.1 (Ar), 142.7 (Ar), 139.3 (Ar), 135.6 (Ar), 130.5 (Ar), 130.1 (Ar), 130.0 (Ar), 129.6 (Ar), 129.5 (Ar), 129.0 (Ar), 128.1 (Ar), 127.2 (Ar), 75.2 (O*C*H$_2$Ph), 73.0 (O*C*H$_2$CH), 67.8 (CH).

MS (ESI): m/z 448.67 [$Zn_2$**L$^b$**$_3$]$^{4+}$, 309.10 [$Zn_2$**L$^b$**]$^{2+}$.

Elemental analysis found (calculated for $C_{108}H_{102}Cl_4N_{12}O_{22}Zn_2$.3$H_2O$): % C 57.49 (57.74) H 4.46 (4.85) N 7.62 (7.48).

**$\Delta_{Zn}$-[$Zn_2L^d_3$][$ClO_4$]$_4$·10$H_2O$**

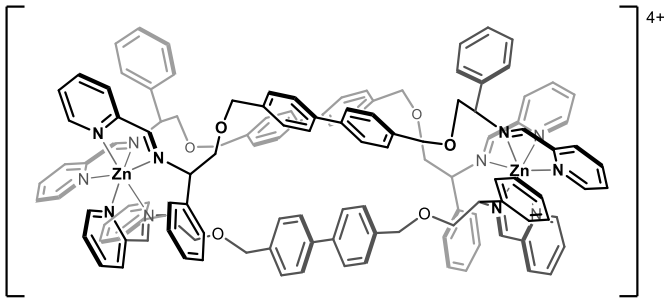


$\Delta_{Zn}$-[$Zn_2\mathbf{L}^{\mathbf{d}}_3$]$^{4+}$

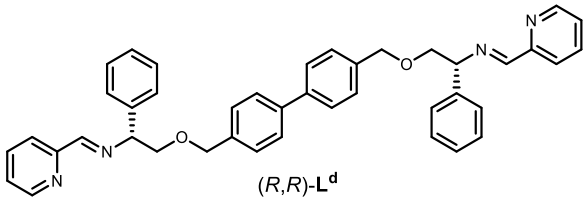

(*R*,*R*)-$\mathbf{L}^{\mathbf{d}}$

Yield: 53 %.

$^1$H NMR (500 MHz, 298 K, $CD_3CN$): $\delta_H$ 8.76 (6H, s, HC=N), 7.93 (6H, t, $^3J_{HH}$ = 7.8 Hz, Py), 7.72 (6H, d, $^3J_{HH}$ = 4.9 Hz, Py), 7.45 (6H, dd , $^3J_{HH}$ = 7.6 Hz, 5.5 Hz, Py), 7.40-7.35 (18H, m, Ph/Py), 7.25 (12H, d, $^3J_{HH}$ = 8.1 Hz, Ph), 7.08 (6H, t, $^3J_{HH}$ = 7.4 Hz, Ph), 6.96 (12H, t, $^3J_{HH}$ = 7.6 Hz, Ph), 6.74 (12H, d, $^3J_{HH}$ = 7.6 Hz, Ph), 5.75 (6H, dd, $^3J_{HH}$ = 10.3 Hz, 2.9 Hz, CH), 5.11 (6H, d, $^2J_{HH}$ = 13.5 Hz, OC*H*$_2$Ph), 4.61 (6H, d, $^2J_{HH}$ = 13.5 Hz, OC*H*$_2$Ph), 4.09 (6H, t, $^2J_{HH}$ /$^3J_{HH}$ = 10.9 Hz, OC*H*$_2$CH), 3.81 (6H, dd, $^2J_{HH}$ = 10.9 Hz, $^3J_{HH}$ = 3.2 Hz, OC*H*$_2$CH).

$^{13}$C{$^1$H} NMR (125 MHz, 298 K, $CD_3CN$): $\delta_C$ 164.1 (C=N), 149.1 (Ar), 147.3 (Ar), 142.8 (Ar), 140.7 (Ar), 137.9 (Ar), 136.2 (Ar), 130.6 (Ar), 129.8 (Ar), 129.15 (Ar(, 129.1 (Ar), 128.1 (Ar), 127.4 (Ar), 72.9 (O*C*H$_2$Ph), 71.8 (O*C*H$_2$CH), 68.2 (CH).

MS (ESI): m/z 631.3 [$\mathbf{L}^{\mathbf{d}}$+H]$^+$.

Elemental analysis found (calculated for $C_{126}H_{114}Cl_4N_{12}O_{22}Zn_2 \cdot 10H_2O$): % C 57.79 (58.18) H 4.44 (5.19) N 6.15 (6.46).

**$\Lambda_{Zn}$-$[Zn_2L^e_3][ClO_4]_4 \cdot 8H_2O$**

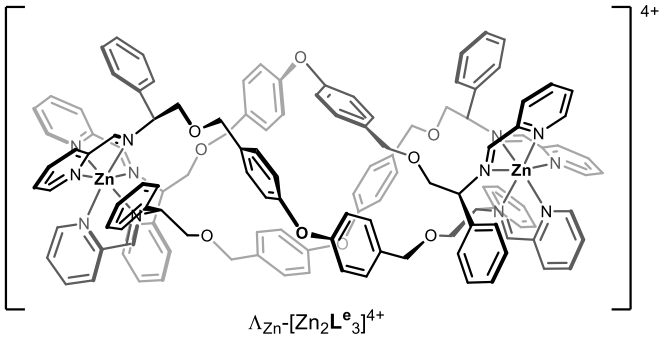


$\Lambda_{Zn}$-$[Zn_2\mathbf{L^e}_3]^{4+}$

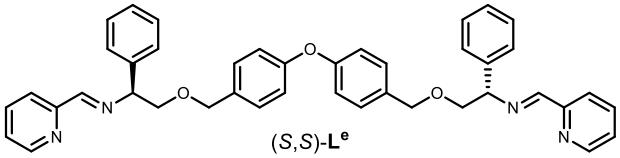

(*S*,*S*)-$\mathbf{L^e}$

Yield: 78 %.

$^1$H NMR (500 MHz, 298 K, $CD_3CN$): $\delta_H$ 8.74 (6H, s, HC=N), 7.85 (6H, t, $^3J_{HH}$ = 7.8 Hz, Py), 7.65 (6H, d, $^3J_{HH}$ = 4.9 Hz, Py), 7.45 (12H, d, $^3J_{HH}$ = 8.5 Hz, Ph), 7.36 (6H, dd , $^3J_{HH}$ = 7.0 Hz, 5.2 Hz, Py), 7.31 (6H, d, $^3J_{HH}$ = 7.7 Hz, Py), 7.02 (6H, t, $^3J_{HH}$ = 7.4 Hz, Ph), 6.88 (12H, t, $^3J_{HH}$ = 7.6 Hz, Ph), 6.73 (12H, d, $^3J_{HH}$ = 8.5 Hz, Ph), 6.60 (12H, d, $^3J_{HH}$ = 7.6 Hz, Ph), 5.75 (6H, dd, $^3J_{HH}$ = 5.7 Hz, $^3J_{HH}$ = 2.0 Hz, CH), 4.95 (6H, d, $^2J_{HH}$ = 12.2 Hz, OC*H*$_2$Ph), 4.42 (6H, d, $^2J_{HH}$ = 12.2 Hz, OC*H*$_2$Ph), 4.19 (6H, t, $^2J_{HH}$ /$^3J_{HH}$ = 11.0 Hz, OC*H*$_2$CH), 3.36 (6H, dd, $^2J_{HH}$ = 11.0 Hz, $^3J_{HH}$ = 2.6 Hz, OC*H*$_2$CH).

$^{13}$C{$^1$H} NMR (125 MHz, 298 K, $CD_3CN$): $\delta_C$ 163.4 (C=N), 157.6 (Ar), 148.9 (Ar), 147.2 (Ar), 142.7 (Ar), 136.0 (Ar), 134.3 (Ar), 130.6 (Ar), 129.8 (Ar), 129.7 (Ar),

129.6 (Ar), 129.1 (Ar), 127.2 (Ar), 119.5 (Ar), 73.1 (O*C*H$_2$Ph), 72.3 (O*C*H$_2$CH), 68.3 (CH).

MS (ESI): m/z 669.3 [**L$^e$**+Na]$^+$, 647.3 [**L$^e$**+H]$^+$.

Elemental analysis found (calculated for $C_{126}H_{114}Cl_4N_{12}O_{25}Zn_2.8H_2O$): % C 57.87 (57.98) H 4.25 (4.90) N 6.33 (6.44).

**$\Lambda_{Zn}$-[Zn$_2$L$^f_3$][ClO$_4$]$_4$.5H$_2$O**

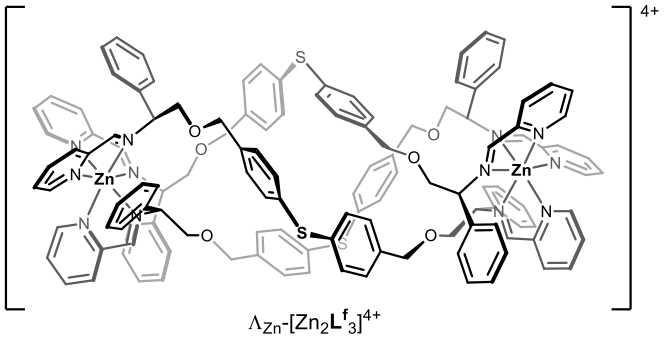


$\Lambda_{Zn}$-[Zn$_2$**L$^f_3$**]$^{4+}$

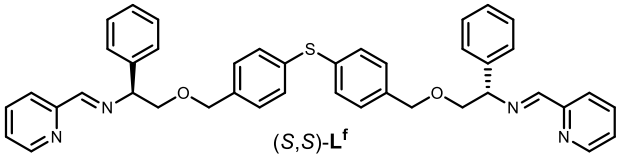


(*S*,*S*)-**L$^f$**

Yield: 76 %.

$^1$H NMR (500 MHz, 298 K, $CD_3CN$): $\delta_H$ 8.72 (6H, s, HC=N), 7.83 (6H, t, $^3J_{HH}$ = 7.8 Hz, Py), 7.60 (6H, d, $^3J_{HH}$ = 4.8 Hz, Py), 7.45 (12H, d, $^3J_{HH}$ = 8.2 Hz, Ph), 7.33 (6H, dd , $^3J_{HH}$ = 7.5 Hz, 5.6 Hz, Py), 7.28 (6H, d, $^3J_{HH}$ = 8.0 Hz, Py), 7.07 (12H, d, $^3J_{HH}$ = 8.2 Hz, Ph), 7.01 (6H, t, $^3J_{HH}$ = 7.4 Hz, Ph), 6.88 (12H, t, $^3J_{HH}$ = 7.6 Hz, Ph), 6.56 (12H, d, $^3J_{HH}$ = 7.6 Hz, Ph), 5.66 (6H, d, $^3J_{HH}$ = 10.4 Hz, CH), 4.92 (6H, d, $^2J_{HH}$ = 12.1

Hz, OC*H*$_2$Ph), 4.39 (6H, d, $^2J_{HH}$ = 12.1 Hz, OC*H*$_2$Ph), 4.20 (6H, t, $^2J_{HH}$ /$^3J_{HH}$ = 11.0 Hz, OC*H*$_2$CH), 3.13 (6H, dd, $^2J_{HH}$ = 11.0 Hz, $^3J_{HH}$ = 2.5 Hz, OC*H*$_2$CH).

$^{13}C\{^1H\}$ NMR (125 MHz, 298 K, $CD_3CN$): $\delta_C$ 163.1 (C=N), 148.8 (Ar), 145.2 (Ar), 142.7 (Ar), 138.1 (Ar), 135.9 (Ar), 135.6 (Ar), 131.0 (Ar), 130.6 (Ar), 129.8 (Ar), 129.5 (Ar), 129.2 (Ar), 127.1 (Ar), 73.2 (O*C*H$_2$Ph), 72.7 (O*C*H$_2$CH), 68.2 (CH).

MS (ESI): m/z 739.0 $[Zn_2\mathbf{L^f}_3][ClO_4]^{3+}$, 684.9 $[\mathbf{L^f}+Na]_+$, 529.4 $[Zn_2\mathbf{L^f}_3]^{4+}$.

Elemental analysis found (calculated for $C_{126}H_{114}Cl_4N_{12}O_{22}S_3Zn_2.5H_2O$): C 57.71 (57.98) H 4.36 (4.90) N 6.23 (6.44).

**$\Lambda_{Zn}$-$[Zn_2\mathbf{L^g}_3][ClO_4]_4\cdot 2H_2O\cdot 2EtOAc$**

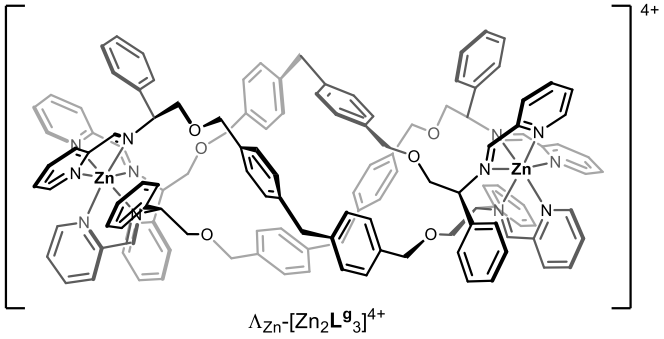


$\Lambda_{Zn}$-$[Zn_2\mathbf{L^g}_3]^{4+}$

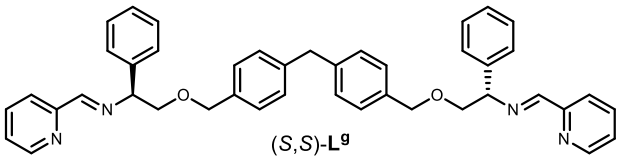

(*S*,*S*)-$\mathbf{L^g}$

Yield: 68 %.

$^1H$ NMR (500 MHz, 298 K, $CD_3CN$): $\delta_H$ 8.71 (6H, s, HC=N), 7.85 (6H, t, $^3J_{HH}$ = 7.8 Hz, Py), 7.64 (6H, d, $^3J_{HH}$ = 4.8 Hz, Py), 7.37-7.31 (24H, m, Ph/Py), 7.02 (6H, t, $^3J_{HH}$ = 7.4 Hz, Ph), 6.91 (12H, d, $^3J_{HH}$ = 8.0 Hz, Ph), 6.88 (12H, t, $^3J_{HH}$ = 7.7 Hz, Ph), 6.58

(12H, d, $^{3}J_{HH}$ = 7.6 Hz, Ph), 5.69 (6H, dd, $^{3}J_{HH}$ = 10.3 Hz, $^{3}J_{HH}$ = 2.2 Hz, CH), 4.83 (6H, d, $^{2}J_{HH}$ = 12.0 Hz, OC*H*$_2$Ph), 4.37 (6H, d, $^{2}J_{HH}$ = 12.0 Hz, OC*H*$_2$Ph), 4.13 (6H, t, $^{2}J_{HH}$ /$^{3}J_{HH}$ = 10.9 Hz, OC*H*$_2$CH), 3.83 (6H, s, PhC*H*$_2$Ph), 3.32 (6H, dd, $^{2}J_{HH}$ = 10.9 Hz, $^{3}J_{HH}$ = 2.9 Hz, OC*H*$_2$CH).

$^{13}C\{^{1}H\}$ NMR (125 MHz, 298 K, $CD_3CN$): $\delta_C$ 163.5 (C=N), 148.9 (Ar), 147.2 (Ar), 142.7 (Ar), 141.4 (Ar), 136.6 (Ar), 136.1 (Ar), 130.5 (Ar), 129.8 (Ar), 129.7 (Ar), 129.6 (Ar), 129.1 (Ar), 128.4 (Ar), 127.3 (Ar), 73.6 (O*C*H$_2$Ph), 72.5 (O*C*H$_2$CH), 68.1 (CH), 41.0 (Ph*C*H$_2$Ph).

MS (ESI): m/z 667.3 [**L**$^{g}$+Na]$^{+}$, 645.3 [**L**$^{g}$+H]$^{+}$.

Elemental analysis found (calculated for $C_{129}H_{120}Cl_4N_{12}O_{22}Zn_2 \cdot 2H_2O \cdot 2EtOAc$): % C 61.47 (61.51) H 4.75 (5.28) N 6.03 (6.28).

**Λ$_{Zn}$-[Zn$_2$L$^{h}_3$][ClO$_4$]$_4$** (partial characterisation of main conformer)

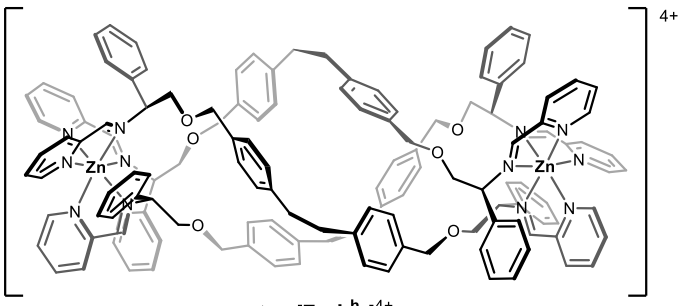


Λ$_{Zn}$-[Zn$_2$**L**$^{h}_3$]$^{4+}$

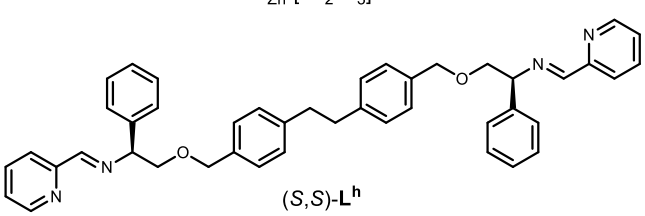

(*S*,*S*)-**L**$^{h}$

$^{1}$H NMR (500 MHz, 298 K, $CD_3CN$): $\delta_H$ 8.67 (6H, s, HC=N), 7.89 (6H, t, $^{3}J_{HH}$ = 7.7 Hz, Py), 7.65 (6H, d, $^{3}J_{HH}$ = 4.9 Hz, Py), 7.42-7.33 (24H, m, Ph/Py), 7.12 (12H, d, $^{3}J_{HH}$ = 7.9 Hz, Ph), 7.04 (6H, t, $^{3}J_{HH}$ = 7.4 Hz, Ph), 6.89 (12H, t, $^{3}J_{HH}$ = 7.7 Hz, Ph), 6.63 (12H, d, $^{3}J_{HH}$ = 7.6 Hz, Ph), 5.63 (6H, dd, $^{3}J_{HH}$ = 10.3 Hz, $^{3}J_{HH}$ = 2.7 Hz, CH), 4.86 (6H, d, $^{2}J_{HH}$ = 12.2 Hz, OC*H*$_2$Ph), 4.50 (6H, d, $^{2}J_{HH}$ = 12.2 Hz, OC*H*$_2$Ph), 4.02 (6H, t, $^{2}J_{HH}$ /$^{3}J_{HH}$ = 10.7 Hz, OC*H*$_2$CH), 3.59 (6H, dd, $^{2}J_{HH}$ = 11.2 Hz, $^{3}J_{HH}$ = 3.2 Hz, OC*H*$_2$CH), 2.79 (12H, s, $CH_2CH_2$).

$^{13}$C{$^{1}$H} NMR (125 MHz, 298 K, $CD_3CN$): $\delta_C$ 163.8 (C=N), 149.0 (Ar), 147.2 (Ar), 142.7 (Ar), 143.6 (Ar), 136.4 (Ar), 136.2 (Ar), 130.6 (Ar), 129.7 (Ar), 129.6 (Ar), 129.2 (Ar), 129.1 (Ar), 127.4 (Ar), 73.8 (O*C*H$_2$Ph), 72.1 (O*C*H$_2$CH), 68.1 (CH), 37.9 ($CH_2CH_2$).

MS (ESI): m/z 681.3 [$\mathbf{L^h}$+Na]$^+$, 659.3 [$\mathbf{L^h}$+H]$^+$.

**$\Delta_{Zn}$-[$Zn_2\mathbf{L^i}_3$][$ClO_4$]$_4$·8$H_2O$**

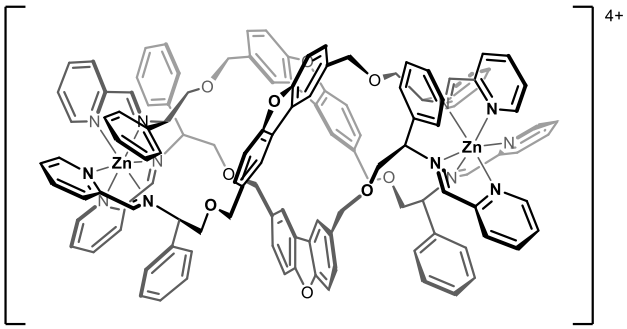


$\Delta_{Zn}$-[$Zn_2\mathbf{L^i}_3$]$^{4+}$

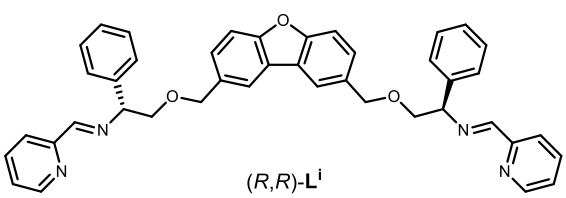

(*R*,*R*)-$\mathbf{L^i}$

Yield: 53 %.

$^{1}$H NMR (500 MHz, 298 K, $CD_3CN$): $\delta_H$ 8.95 (6H, s, Ph), 8.47 (6H, s, HC=N), 7.77 (6H, t, $^{3}J_{HH}$ = 7.8 Hz, Py), 7.72 (6H, d, $^{3}J_{HH}$ = 8.4 Hz, Ph), 7.64 (6H, d, $^{3}J_{HH}$ = 8.4 Hz, Ph), 7.48 (6H, d, $^{3}J_{HH}$ = 4.7 Hz, Py), 7.27 (6H, dd , $^{3}J_{HH}$ = 7.2 Hz, 5.2 Hz, Py), 7.20 (6H, d, $^{3}J_{HH}$ = 7.8 Hz, Py), 6.93 (6H, t, $^{3}J_{HH}$ = 7.4 Hz, Ph), 6.75 (12H, t, $^{3}J_{HH}$ = 7.6 Hz, Ph), 6.18 (12H, d, $^{3}J_{HH}$ = 7.6 Hz, Ph), 5.26 (6H, dd, $^{3}J_{HH}$ = 10.5 Hz, $^{3}J_{HH}$ = 2.6 Hz, CH), 4.44 (6H, d, $^{2}J_{HH}$ = 9.6 Hz, OC*H*$_2$Ph), 3.81 (6H, d, $^{2}J_{HH}$ = 9.6 Hz, OC*H*$_2$Ph), 3.70 (6H, t, $^{2}J_{HH}$ /$^{3}J_{HH}$ = 10.9 Hz, OC*H*$_2$CH), 2.59 (6H, d, $^{2}J_{HH}$ = 9.9 Hz, OC*H*$_2$CH).

$^{13}$C{$^{1}$H} NMR (125 MHz, 298 K, $CD_3CN$): $\delta_C$ 163.3 (C=N), 157.5 (Ar), 148.7 (Ar), 147.1 (Ar), 142.6 (Ar), 135.6 (Ar), 134.1 (Ar), 130.7 (Ar), 130.5 (Ar), 129.6 (Ar), 129.4 (Ar), 129.0 (Ar), 127.3 (Ar), 125.0 (Ar), 122.0 (Ar), 112.8 (Ar), 74.2 (O*C*H$_2$Ph), 72.8 (O*C*H$_2$CH), 67.9 (CH).

MS (ESI): m/z 667.3 [**L**$^{i}$+Na]$^{+}$, 645.3 [**L**$^{i}$+H]$^{+}$.

Elemental analysis found (calculated for $C_{126}H_{108}Cl_4N_{12}O_{25}Zn_2 \cdot 8H_2O$): % C 58.02 (58.05) H 4.17 (4.79) N 6.32 (6.45).

### 6.1.7 Synthesis and characterisation of $[Fe_2L_3]Cl_4$ complexes

**General procedure[5]**

The appropriate optically pure diamine (3.0 eq.) and 2-pyridinecarboxaldehyde (6.0 eq.) were dissolved in methanol (50 ml) and stirred for 2 h at ambient temperature to form a yellow solution containing the ligand. Anhydrous iron (II) chloride (2.0 eq.) was added, and an immediate colour change to deep purple was observed. The solution was then heated at reflux (80 °C) for 48 hours. After filtering through fluted filter

paper, the solvent was removed under reduced pressure to give the desired product as a dark purple solid, which was dried overnight at 50 °C *in vacuo.*

**$\Delta_{Fe}$-[$Fe_2L^a_3$]$Cl_4$·6$H_2O$**

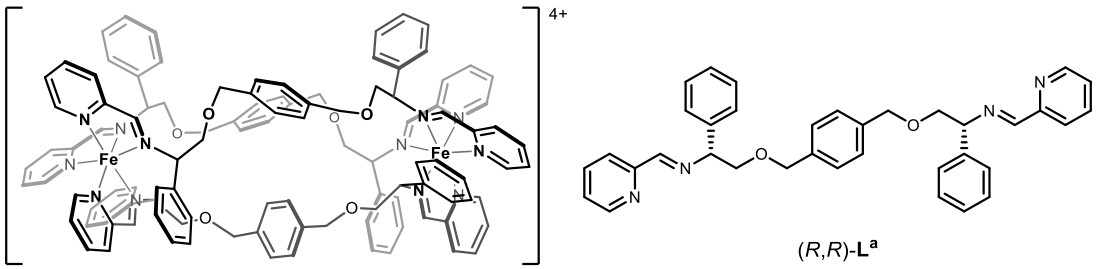


$\Delta_{Fe}$-[$Fe_2$**L**$^a_3$]$^{4+}$ (*R*,*R*)-**L**$^a$

0.7 g (1.86 mmol) of diamine used.

Yield: 1.18 g, 0.58 mmol, 92 %.

$^1$H NMR (400 MHz, 298 K, $CD_3OD$): $\delta_H$ 9.30 (6H, s, HC=N), 7.80 (6H, t, $^3J_{HH}$ = 7.0 Hz, Py), 7.58 (6H, d, $^3J_{HH}$ = 7.0 Hz, Py), 7.55 (12H, s, Ph), 7.29 (6H, t, $^3J_{HH}$ = 7.0 Hz, Py), 7.11 (6H, t, $^3J_{HH}$ = 7.5 Hz, Ph), 7.02 (12H, t, $^3J_{HH}$ = 7.5 Hz, Ph), 6.85-6.80 (18H, m, Py/Ph), 5.97 (6H, dd, $^3J_{HH}$ = 11.0 Hz, $^3J_{HH}$ = 3.5 Hz, CH), 5.12 (6H, d, $^2J_{HH}$ = 13.0 Hz, OC*H*$_2$Ph), 4.61 (6H, d, $^2J_{HH}$ = 13.0 Hz, OC*H*$_2$Ph), 4.34 (6H, t, $^2J_{HH}$/$^3J_{HH}$ = 11.0 Hz, OC*H*$_2$CH), 3.58 (6H, dd, $^2J_{HH}$ = 11.0 Hz, $^3J_{HH}$ = 3.5 Hz, OC*H*$_2$CH).

$^{13}$C{$^1$H} NMR (125 MHz, 298 K, $CD_3OD$): $\delta_C$ 173.3 (C=N), 160.4 (Ar), 154.6 (Ar), 139.9 (Ar), 138.7 (Ar), 136.5 (Ar), 130.5 (Ar), 129.5 (Ar), 129.4 (Ar), 128.9 (Ar), 127.1 (Ar), 73.7 (O*C*H$_2$Ph), 73.1 (O*C*H$_2$CH), 73.0 (CH).

MS (ESI): m/z 443.8 [$Fe_2$**L**$^a_3$]$^{4+}$, 577.3 [**L**$^a$+Na]$^+$.

FTIR: ν $cm^{-1}$ 3346 br, 3024 w, 2860 m, 1635 w, 1612 m, 1591 w, 1494 w, 1472 m, 1452 m, 1358 w, 1298 w, 1241 w, 1104 m, 1074 s, 1019 m, 1000 m, 936 w, 837 w, 757 s, 700 s.

Elemental analysis found (calculated for $C_{108}H_{106}Cl_4Fe_2N_{12}O_6 \cdot 6H_2O$): % C 64.08 (63.91) H 5.40 (5.86) N 7.99 (8.28).

**$\Lambda_{Fe}$-$[Fe_2L^a_3]Cl_4 \cdot 6H_2O$**

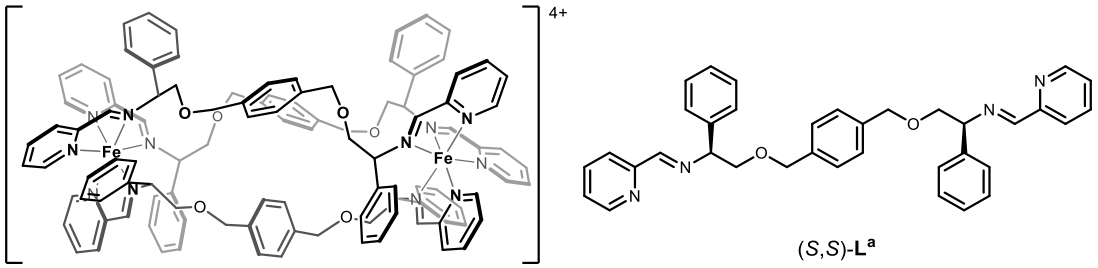


$\Lambda_{Fe}$-$[Fe_2L^a_3]^{4+}$ (*S*,*S*)-$L^a$

0.7 g (1.86 mmol) of diamine used.

Yield: 1.18 g, 0.58 mmol, 93 %.

$^1$H NMR (400 MHz, 298 K, $CD_3OD$): $\delta_H$ 9.30 (6H, s, HC=N), 7.80 (6H, t, $^3J_{HH}$ = 7.0 Hz, Py), 7.58 (6H, d, $^3J_{HH}$ = 7.0 Hz, Py), 7.55 (12H, s, Ph), 7.29 (6H, t, $^3J_{HH}$ = 7.0 Hz, Py), 7.11 (6H, t, $^3J_{HH}$ = 7.5 Hz, Ph), 7.02 (12H, t, $^3J_{HH}$ = 7.5 Hz, Ph), 6.85-6.80 (18H, m, Py/Ph), 5.97 (6H, dd, $^3J_{HH}$ = 11.0 Hz, $^3J_{HH}$ = 3.5 Hz, CH), 5.12 (6H, d, $^2J_{HH}$ = 13.0 Hz, OC*H*$_2$Ph), 4.61 (6H, d, $^2J_{HH}$ = 13.0 Hz, OC*H*$_2$Ph), 4.34 (6H, t, $^2J_{HH}$/$^3J_{HH}$ = 11.0 Hz, OC*H*$_2$CH), 3.58 (6H, dd, $^2J_{HH}$ = 11.0 Hz, $^3J_{HH}$ = 3.5 Hz, OC*H*$_2$CH).

$^{13}$C{$^1$H} NMR (125 MHz, 298 K, $CD_3OD$): $\delta_C$ 173.3 (C=N), 160.4 (Ar), 154.6 (Ar), 139.9 (Ar), 138.7 (Ar), 136.5 (Ar), 130.5 (Ar), 129.5 (Ar), 129.4 (Ar), 128.9 (Ar), 127.1 (Ar), 73.7 (O*C*H$_2$Ph), 73.1 (O*C*H$_2$CH), 73.0 (CH).

MS (ESI): m/z 443.8 $[Fe_2\mathbf{L^a}_3]^{4+}$, 577.3 $[\mathbf{L^a}+Na]^+$.

FTIR: ν $cm^{-1}$ 3346 br, 3024 w, 2860 m, 1635 w, 1612 m, 1591 w, 1494 w, 1472 m, 1452 m, 1358 w, 1298 w, 1241 w, 1104 m, 1074 s, 1019 m, 1000 m, 936 w, 837 w, 757 s, 700 s.

Elemental analysis found (calculated for $C_{108}H_{106}Cl_4Fe_2N_{12}O_6{\cdot}6H_2O$): % C 63.41 (63.91) H 5.61 (5.86) N 7.96 (8.28).

**$\Delta_{Fe}$-$[Fe_2\mathbf{L^b}_3]Cl_4{\cdot}6.5H_2O$**

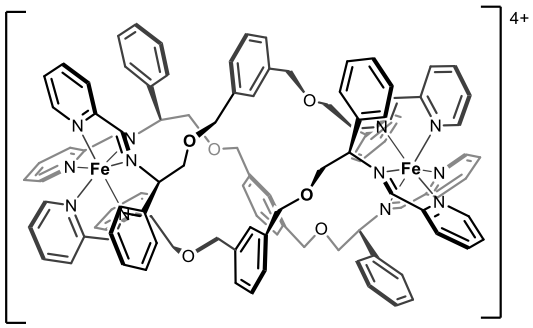


$\Delta_{Fe}$-$[Fe_2\mathbf{L^b}_3]^{4+}$

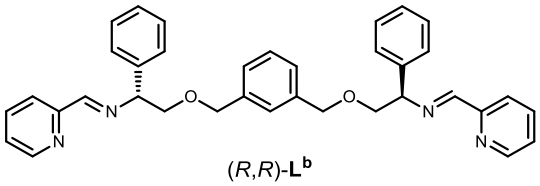


(*R*,*R*)-$\mathbf{L^b}$

0.7 g (1.86 mmol) of diamine used.

Yield: 1.21 g, 0.59 mmol, 96 %.

$^1$H NMR (400 MHz, 298 K, $CD_3OD$): $\delta_H$ 9.22 (6H, s, HC=N), 8.37 (3H, s, Ph), 7.73 (6H, t, $^3J_{HH}$ = 7.6 Hz, Py), 7.66 (6H, d, $^3J_{HH}$ = 7.6 Hz, Py), 7.52-7.47 (9H, m, Ph), 7.22 (6H, t, $^3J_{HH}$ = 6.5 Hz, Py), 7.02 (6H, t, $^3J_{HH}$ = 7.3 Hz, Ph), 6.86 (12H, t, $^3J_{HH}$ = 6.5 Hz, Ph), 6.78 (6H, d, $^3J_{HH}$ = 5.3 Hz, Py), 6.55 (12H, br s, Ph), 5.86 (6H, dd, $^3J_{HH}$ = 11.0 Hz, $^3J_{HH}$ = 2.1 Hz, CH), 5.03 (6H, d, $^2J_{HH}$ = 10.8 Hz, OC*H*$_2$Ph), 4.40 (6H, t, $^2J_{HH}/^3J_{HH}$ = 11.4 Hz, OC*H*$_2$CH), 3.05 (6H, dd, $^2J_{HH}$ = 11.4 Hz, $^3J_{HH}$ = 2.5 Hz, OC*H*$_2$CH). The

presence of water ($\delta_H$ 4.91-4.85) obscures the second OC*H*$_2$Ph peak, which could nonetheless be detected by 2D-NMR (HSQC).

$^{13}$C NMR (125 MHz, 298 K, $CD_3OD$): $\delta_C$ 172.9 (C=N), 160.3 (Ar), 154.5 (Ar), 139.9 (Ar), 139.4 (Ar), 135.8 (Ar), 130.5 (Ar), 130.4 (Ar), 130.2 (Ar), 129.3 (Ar), 128.8 (Ar), 75.9 (O*C*H$_2$Ph), 74.4 (O*C*H$_2$CH), 72.4 (CH).

MS (ESI): m/z 443.8 $[Fe_2\mathbf{L^b}_3]^{4+}$, 577.3 $[\mathbf{L^b}+Na]^+$.

FTIR: ν cm$^{-1}$ 3356 br, 3028 w, 2864 w, 1612 w, 1590 w, 1494 w, 1472 m, 1451 m, 1385 w, 1357 w, 1298 m, 1240 w, 1156 w, 1105 m, 1072 s, 1003 m, 1030 w, 887 w, 834 w, 756 s.

Elemental analysis found (calculated for $C_{108}H_{106}Cl_4Fe_2N_{12}O_6{\cdot}6.5H_2O$): % C 63.65 (63.63) H 5.84 (5.88) N 8.09 (8.24).

**$\Lambda_{Fe}$-$[Fe_2\mathbf{L^b}_3]Cl_4{\cdot}6.5H_2O$**

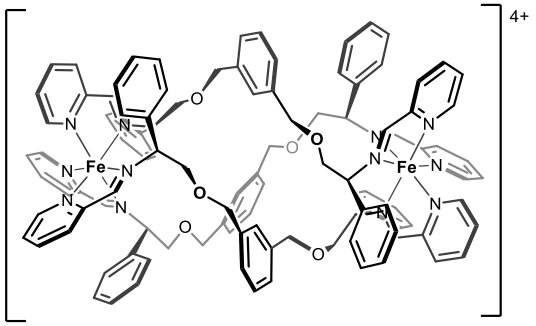


$\Lambda_{Fe}$-$[Fe_2\mathbf{L^b}_3]^{4+}$

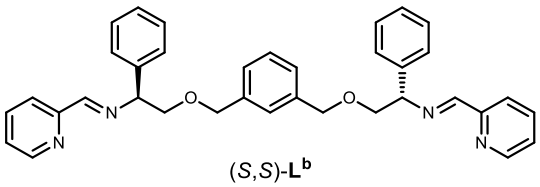

(*S*,*S*)-$\mathbf{L^b}$

0.7 g (1.86 mmol) of diamine used.

Yield: 1.19 g, 0.58 mmol, 94 %.

$^{1}$H NMR (400 MHz, 298 K, $CD_3OD$): $\delta_H$ 9.22 (6H, s, HC=N), 8.37 (3H, s, Ph), 7.73 (6H, t, $^{3}J_{HH}$ = 7.6 Hz, Py), 7.66 (6H, d, $^{3}J_{HH}$ = 7.6 Hz, Py), 7.52-7.47 (9H, m, Ph), 7.22 (6H, t, $^{3}J_{HH}$ = 6.5 Hz, Py), 7.02 (6H, t, $^{3}J_{HH}$ = 7.3 Hz, Ph), 6.86 (12H, t, $^{3}J_{HH}$ = 6.5 Hz, Ph), 6.78 (6H, d, $^{3}J_{HH}$ = 5.3 Hz, Py), 6.55 (12H, br s, Ph), 5.86 (6H, dd, $^{3}J_{HH}$ = 11.0 Hz, $^{3}J_{HH}$ = 2.1 Hz, CH), 5.03 (6H, d, $^{2}J_{HH}$ = 10.8 Hz, OC*H*$_2$Ph), 4.40 (6H, t, $^{2}J_{HH}$/$^{3}J_{HH}$ = 11.4 Hz, OC*H*$_2$CH), 3.05 (6H, dd, $^{2}J_{HH}$ = 11.4 Hz, $^{3}J_{HH}$ = 2.5 Hz, OC*H*$_2$CH). The presence of water ($\delta_H$ 4.91-4.85) obscures the second OC*H*$_2$Ph peak, which could nonetheless be detected by 2D-NMR (HSQC).

$^{13}$C{$^{1}$H} NMR (125 MHz, 298 K, $CD_3OD$): $\delta_C$ 172.9 (C=N), 160.3 (Ar), 154.5 (Ar), 139.9 (Ar), 139.4 (Ar), 135.8 (Ar), 130.5 (Ar), 130.4 (Ar), 130.2 (Ar), 129.3 (Ar), 128.8 (Ar), 75.9 (O*C*H$_2$Ph), 74.4 (O*C*H$_2$CH), 72.4 (CH).

MS (ESI): m/z 443.8 $[Fe_2\mathbf{L^b}_3]^{4+}$, 577.3 $[\mathbf{L^b}+Na]^{+}$.

FTIR: ν cm$^{-1}$ 3356 br, 3028 w, 2864 w, 1612 w, 1590 w, 1494 w, 1472 m, 1451 m, 1385 w, 1357 w, 1298 m, 1240 w, 1156 w, 1105 m, 1072 s, 1003 m, 930 w, 887 w, 834 w, 756 s.

Elemental analysis found (calculated for $C_{108}H_{106}Cl_4Fe_2N_{12}O_6{\cdot}6.5H_2O$): % C 64.08 (63.63) H 5.68 (5.88) N 7.98 (8.24).

**$\Delta_{Fe}$-[$Fe_2L^d_3$]$Cl_4$·12$H_2O$**

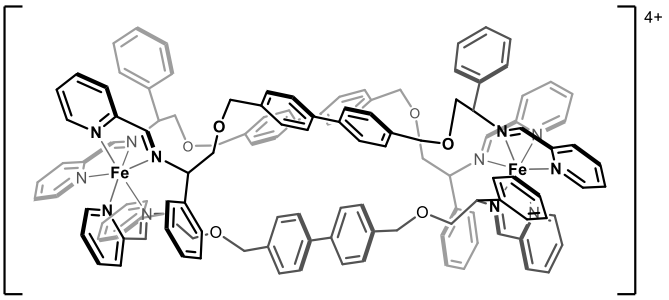


$\Delta_{Fe}$-[$Fe_2\mathbf{L}^{\mathbf{d}}_3$]$^{4+}$

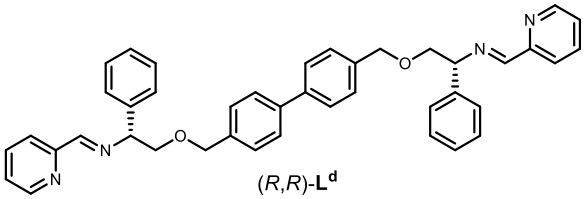

(*R*,*R*)-$\mathbf{L}^{\mathbf{d}}$

0.25 g (0.55 mmol) of diamine used.

Yield: 0.364 g, 0.15 mmol, 84 %.

$^1$H NMR (500 MHz, 298 K, $CD_3OD$): $\delta_H$ 9.39 (6H, s, HC=N), 7.82 (6H, t, $^3J_{HH}$ = 6.8 Hz, Py), 7.62 (6H, d, $^3J_{HH}$ = 6.3 Hz, Py), 7.33-7.26 (18H, m, Ph/Py), 7.16-7.06 (30H, m, Ph), 6.92-6.87 (18H, m, Ph/Py), 6.09 (6H, d, $^3J_{HH}$ = 9.8 Hz, CH), 5.21 (6H, d, $^2J_{HH}$ = 9.6 Hz, OC*H*$_2$Ph), 4.70 (6H, d, $^2J_{HH}$ = 13.7 Hz, OC*H*$_2$Ph/$H_2O$), 4.39 (6H, t, $^2J_{HH}$/$^3J_{HH}$ = 10.6 Hz, OC*H*$_2$CH), 3.82 (6H, d, $^2J_{HH}$ = 9.8 Hz, OC*H*$_2$CH).

$^{13}$C{$^1$H} NMR (100 MHz, 298 K, $CD_3OD$): $\delta_C$ 173.5 (C=N), 160.6 (Ar), 154.7 (Ar), 141.4 (Ar), 139.9 (Ar), 137.7 (Ar), 136.5 (Ar), 130.6 (Ar), 130.5 (Ar), 129.5 (Ar), 128.9 (Ar) 128.6 (Ar), 127.1 (Ar), 73.1 (O*C*H$_2$Ph), 72.9 (CH), 72.8 (O*C*H$_2$CH).

MS (ESI): m/z 500.9 [$Fe_2\mathbf{L}^{\mathbf{d}}_3$]$^{4+}$.

FTIR: ν cm$^{-1}$ 3350 br, 2862 w, 1612 w, 1556 w, 1494 m, 1471 m, 1451 m, 1382 w, 1360 w, 1298 w, 1207 w, 1102 m, 1073 s, 1023 m, 1004 m, 934 w, 804 m, 758 s, 700s.

Elemental analysis found (calculated for $C_{126}H_{118}Cl_4Fe_2N_{12}O_6 \cdot 12H_2O$): % C 63.86 (63.96) H 5.46 (6.05) N 6.88 (7.10).

**$\Lambda_{Fe}$-[$Fe_2L^d_3$]$Cl_4 \cdot 12H_2O$**

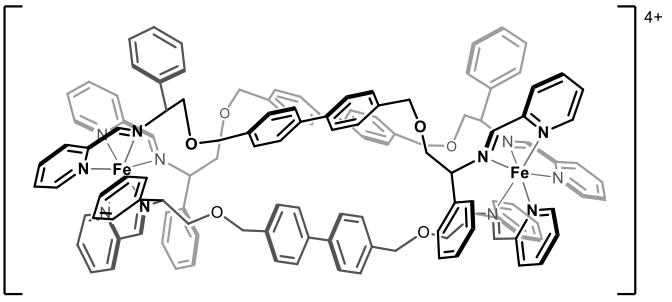


$\Lambda_{Fe}$-[$Fe_2L^d_3$]$^{4+}$

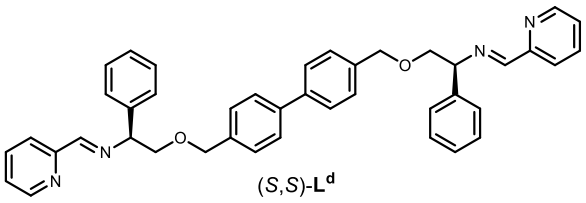

(*S*,*S*)-$L^d$

0.25 g (0.55 mmol) of diamine used.

Yield: 0.347 g, 0.15 mmol, 80 %.

$^1$H NMR (500 MHz, 298 K, $CD_3OD$): $\delta_H$ 9.39 (6H, s, HC=N), 7.82 (6H, t, $^3J_{HH}$ = 6.8 Hz, Py), 7.62 (6H, d, $^3J_{HH}$ = 6.3 Hz, Py), 7.33-7.26 (18H, m, Ph/Py), 7.16-7.06 (30H, m, Ph), 6.92-6.87 (18H, m, Ph/Py), 6.09 (6H, d, $^3J_{HH}$ = 9.8 Hz, CH), 5.21 (6H, d, $^2J_{HH}$ = 9.6 Hz, OC*H*$_2$Ph), 4.70 (6H, d, $^2J_{HH}$ = 13.7 Hz, OC*H*$_2$Ph/$H_2O$), 4.39 (6H, t, $^2J_{HH}$/$^3J_{HH}$ = 10.6 Hz, OC*H*$_2$CH), 3.82 (6H, d, $^2J_{HH}$ = 9.8 Hz, OC*H*$_2$CH).

$^{13}$C{$^1$H} NMR (100 MHz, 298 K, $CD_3OD$): $\delta_C$ 173.5 (C=N), 160.6 (Ar), 154.7 (Ar), 141.4 (Ar), 139.9 (Ar), 137.7 (Ar), 136.5 (Ar), 130.6 (Ar), 130.5 (Ar), 129.5 (Ar), 128.9 (Ar) 128.6 (Ar), 127.1 (Ar), 73.1 (O*C*H$_2$Ph), 72.9 (CH), 72.8 (O*C*H$_2$CH).

MS (ESI): m/z 500.9 $[Fe_2\mathbf{L}^{\mathbf{d}}{}_3]^{4+}$.

FTIR: ν $cm^{-1}$ 3350 br, 2862 w, 1612 w, 1556 w, 1494 m, 1471 m, 1451 m, 1382 w, 1360 w, 1298 w, 1207 w, 1102 m, 1073 s, 1023 m, 1004 m, 934 w, 804 m, 758 s, 700s.

Elemental analysis found (calculated for $C_{126}H_{118}Cl_4Fe_2N_{12}O_6 \cdot 12H_2O$): % C 63.97 (63.96) H 5.28 (6.05) N 6.86 (7.10).

**$\Delta_{Fe}$-$[Fe_2\mathbf{L}^{\mathbf{e}}{}_3]Cl_4 \cdot 10.5H_2O$**

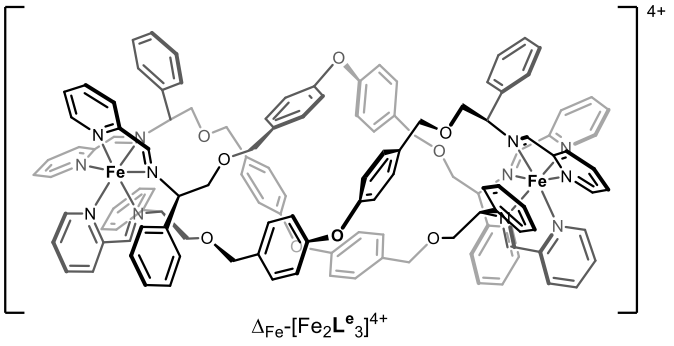


$\Delta_{Fe}$-$[Fe_2\mathbf{L}^{\mathbf{e}}{}_3]^{4+}$

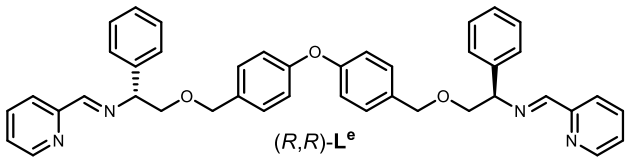

(*R*,*R*)-$\mathbf{L}^{\mathbf{e}}$

0.25 g (0.53 mmol) of diamine used.

Yield: 0.347 g, 0.15 mmol, 82 %.

$^1$H NMR (500 MHz, 298 K, $CD_3OD$): $\delta_H$ 9.33 (6H, s, HC=N), 7.76 (6H, t, $^3J_{HH}$ = 7.6 Hz, Py), 7.55 (6H, d, $^3J_{HH}$ = 7.6 Hz, Py), 7.45 (12H, d, $^3J_{HH}$ = 8.3 Hz, Ph), 7.25 (6H, t, $^3J_{HH}$ = 6.5 Hz, Py), 7.08 (6H, t, $^3J_{HH}$ = 7.3 Hz, Ph), 6.97 (12H, t, $^3J_{HH}$ = 7.5 Hz, Ph), 6.80-6.68 (30H, m, Py/Ph), 6.00 (6H, dd, $^3J_{HH}$ = 10.9 Hz, $^3J_{HH}$ = 1.8 Hz, CH), 5.03 (6H, d, $^2J_{HH}$ = 11.9 Hz, OC*H*$_2$Ph), 4.52 (6H, t, $^2J_{HH}$/$^3J_{HH}$ = 10.9 Hz, OC*H*$_2$CH), 4.40

(6H, d, $^{2}J_{HH}$ = 11.9 Hz, OC*H*$_2$Ph), 3.25 (6H, dd, $^{2}J_{HH}$ = 10.9 Hz, $^{3}J_{HH}$ = 2.0 Hz, OC*H*$_2$CH).

$^{13}C\{^{1}H\}$ NMR (125 MHz, 298 K, $CD_3OD$): $\delta_C$ 172.8 (C=N), 160.4 (Ar), 158.4 (Ar), 154.5 (Ar), 139.8 (Ar), 136.4 (Ar), 134.2 (Ar), 130.5 (Ar), 130.4 (Ar), 130.1 (Ar), 129.4 (Ar), 128.8 (Ar), 127.0 (Ar), 74.1 (O*C*H$_2$Ph), 73.7 (O*C*H$_2$CH), 73.0 (CH).

MS (ESI): m/z 512.7 $[Fe_2\mathbf{L^e}_3]^{4+}$.

FTIR: ν $cm^{-1}$ 3339 br, 2860 w, 1601 m, 1500 s, 1472 m, 1451 m, 1385 w, 1358 w, 1299 w, 1231 s, 1166 w, 1103 m, 1077 s, 1013 m, 1001 m, 873 m, 836 m, 817 w, 758 s, 700 s.

Elemental analysis found (calculated for $C_{126}H_{118}Cl_4Fe_2N_{12}O_9 \cdot 10.5H_2O$): % C 63.21 (63.40) H 5.48 (5.87) N 6.73 (7.04).

**$\Lambda_{Fe}$-$[Fe_2\mathbf{L^e}_3]Cl_4 \cdot 10.5H_2O$**

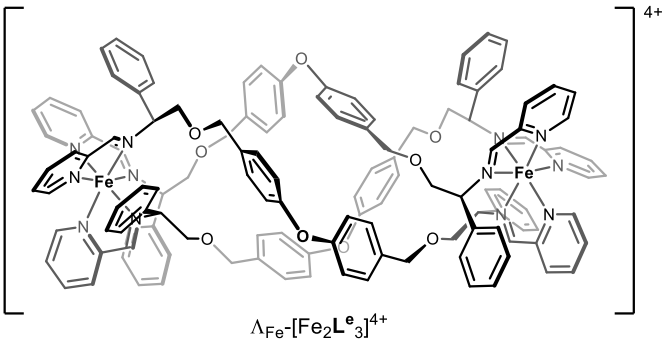


$\Lambda_{Fe}$-$[Fe_2\mathbf{L^e}_3]^{4+}$

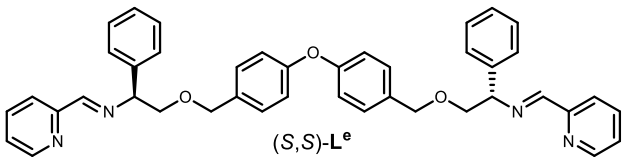

(*S*,*S*)-$\mathbf{L^e}$

0.25 g (0.53 mmol) of diamine used.

Yield: 0.332 g, 0.14 mmol, 78 %.

$^{1}$H NMR (500 MHz, 298 K, $CD_3OD$): $\delta_H$ 9.33 (6H, s, HC=N), 7.76 (6H, t, $^{3}J_{HH}$ = 7.6 Hz, Py), 7.55 (6H, d, $^{3}J_{HH}$ = 7.6 Hz, Py), 7.45 (12H, d, $^{3}J_{HH}$ = 8.3 Hz, Ph), 7.25 (6H, t, $^{3}J_{HH}$ = 6.5 Hz, Py), 7.08 (6H, t, $^{3}J_{HH}$ = 7.3 Hz, Ph), 6.97 (12H, t, $^{3}J_{HH}$ = 7.5 Hz, Ph), 6.80-6.68 (30H, m, Py/Ph), 6.00 (6H, dd, $^{3}J_{HH}$ = 10.9 Hz, $^{3}J_{HH}$ = 1.8 Hz, CH), 5.03 (6H, d, $^{2}J_{HH}$ = 11.9 Hz, OC*H*$_2$Ph), 4.52 (6H, t, $^{2}J_{HH}$/$^{3}J_{HH}$ = 10.9 Hz, OC*H*$_2$CH), 4.40 (6H, d, $^{2}J_{HH}$ = 11.9 Hz, OC*H*$_2$Ph), 3.25 (6H, dd, $^{2}J_{HH}$ = 10.9 Hz, $^{3}J_{HH}$ = 2.0 Hz, OC*H*$_2$CH).

$^{13}$C{$^{1}$H} NMR (125 MHz, 298 K, $CD_3OD$): $\delta_C$ 172.8 (C=N), 160.4 (Ar), 158.4 (Ar), 154.5 (Ar), 139.8 (Ar), 136.4 (Ar), 134.2 (Ar), 130.5 (Ar), 130.4 (Ar), 130.1 (Ar), 129.4 (Ar), 128.8 (Ar), 127.0 (Ar), 74.1 (O*C*H$_2$Ph), 73.7 (O*C*H$_2$CH), 73.0 (CH).

MS (ESI): m/z 512.7 $[Fe_2\mathbf{L}^{e}_3]^{4+}$.

FTIR: ν cm$^{-1}$ 3339 br, 2860 w, 1601 m, 1500 s, 1472 m, 1451 m, 1385 w, 1358 w, 1299 w, 1231 s, 1166 w, 1103 m, 1077 s, 1013 m, 1001 m, 873 m, 836 m, 817 w, 758 s, 700 s.

Elemental analysis found (calculated for $C_{126}H_{118}Cl_4Fe_2N_{12}O_9 \cdot 10.5H_2O$): % C 63.05 (63.40) H 5.17 (5.87) N 6.71 (7.04).

**$\Delta_{Fe}$-[$Fe_2L^f_3$]$Cl_4$·11$H_2O$**

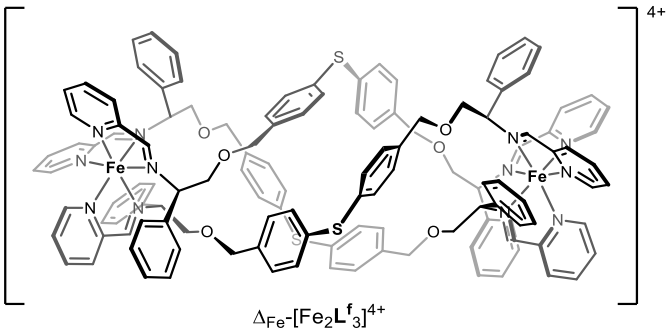


$\Delta_{Fe}$-[$Fe_2\mathbf{L}^f_3$]$^{4+}$

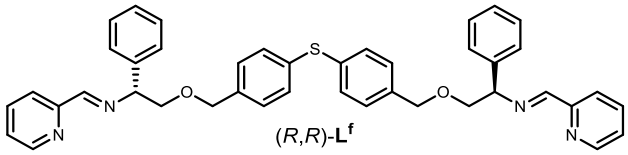


(*R*,*R*)-$\mathbf{L}^f$

0.25 g (0.52 mmol) of diamine used.

Yield: 0.359 g, 0.15 mmol, 85 %.

$^1$H NMR (500 MHz, 298 K, $CD_3OD$): $\delta_H$ 9.34 (6H, s, HC=N), 7.74 (6H, t, $^3J_{HH}$ = 7.4 Hz, Py), 7.53 (6H, d, $^3J_{HH}$ = 7.4 Hz, Py), 7.45 (12H, d, $^3J_{HH}$ = 7.8 Hz, Ph), 7.25 (6H, t, $^3J_{HH}$ = 6.4 Hz, Py), 7.08-7.04 (18H, m, Ph), 6.96 (12H, t, $^3J_{HH}$ = 7.0 Hz, Ph), 6.76-6.66 (18H, m, Ph/Py), 5.93 (6H, d, $^3J_{HH}$ = 10.7 Hz, CH), 4.99 (6H, d, $^2J_{HH}$ = 11.6 Hz, OC*H*$_2$Ph), 4.52 (6H, t, $^2J_{HH}$/$^3J_{HH}$ = 10.7 Hz, OC*H*$_2$CH), 4.38 (6H, d, $^2J_{HH}$ = 11.7 Hz, OC*H*$_2$Ph), 3.04 (6H, d, $^2J_{HH}$ = 10.7 Hz, OC*H*$_2$CH).

$^{13}$C{$^1$H} NMR (125 MHz, 298 K, $CD_3OD$): $\delta_C$ 172.6 (C=N), 160.3 (Ar), 154.4 (Ar), 139.8 (Ar), 138.1 (Ar), 136.5 (Ar), 136.2 (Ar), 131.4 (Ar), 130.5 (Ar), 130.4 (Ar), 129.7 (Ar), 129.5 (Ar), 128.8 (Ar), 127.1 (Ar), 73.9 (O*C*H$_2$Ph), 73.7 (O*C*H$_2$CH), 73.0 (CH).

MS (ESI): m/z 524.7 [$Fe_2\mathbf{L}^f_3$]$^{4+}$.

FTIR: ν $cm^{-1}$ 3360 br, 3027 w, 2862 w, 1613 w, 1592 w, 1492 m, 1472 m, 1452 m, 1384 w, 1353 w, 1299 w, 1242 w, 1102 m, 1079 s, 1015 s, 1001 m, 841 w, 804 m, 758 s, 700 s.

Elemental analysis found (calculated for $C_{126}H_{118}Cl_4Fe_2N_{12}O_6S_3 \cdot 11H_2O$): % C 61.66 (61.92) H 5.20 (5.77) N 6.61 (6.88).

**$\Lambda_{Fe}$-[$Fe_2L^f_3$]$Cl_4 \cdot 11H_2O$**

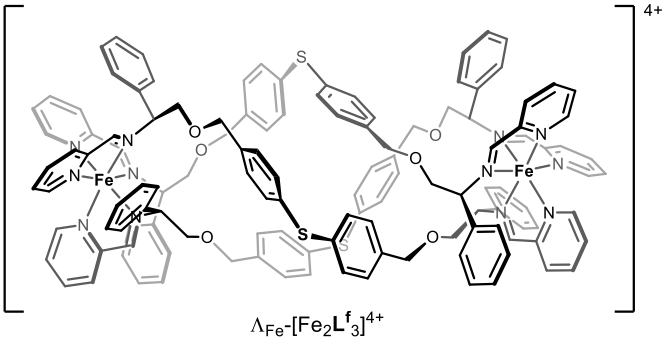


$\Lambda_{Fe}$-[$Fe_2L^f_3$]$^{4+}$

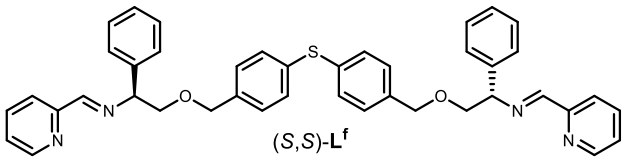


(*S*,*S*)-$L^f$

0.25 g (0.52 mmol) of diamine used.

Yield: 0.29 g, 0.12 mmol, 69 %.

$^1$H NMR (500 MHz, 298 K, $CD_3OD$): $\delta_H$ 9.34 (6H, s, HC=N), 7.74 (6H, t, $^3J_{HH}$ = 7.4 Hz, Py), 7.53 (6H, d, $^3J_{HH}$ = 7.4 Hz, Py), 7.45 (12H, d, $^3J_{HH}$ = 7.8 Hz, Ph), 7.25 (6H, t, $^3J_{HH}$ = 6.4 Hz, Py), 7.08-7.04 (18H, m, Ph), 6.96 (12H, t, $^3J_{HH}$ = 7.0 Hz, Ph), 6.76-6.66 (18H, m, Ph/Py), 5.93 (6H, d, $^3J_{HH}$ = 10.7 Hz, CH), 4.99 (6H, d, $^2J_{HH}$ = 11.6 Hz, OC*H*$_2$Ph), 4.52 (6H, t, $^2J_{HH}/^3J_{HH}$ = 10.7 Hz, OC*H*$_2$CH), 4.38 (6H, d, $^2J_{HH}$ = 11.7 Hz, OC*H*$_2$Ph), 3.04 (6H, d, $^2J_{HH}$ = 10.7 Hz, OC*H*$_2$CH).

$^{13}C\{^{1}H\}$ NMR (125 MHz, 298 K, $CD_3OD$): $\delta_C$ 172.6 (C=N), 160.3 (Ar), 154.4 (Ar), 139.8 (Ar), 138.1 (Ar), 136.5 (Ar), 136.2 (Ar), 131.4 (Ar), 130.5 (Ar), 130.4 (Ar), 129.7 (Ar), 129.5 (Ar), 128.8 (Ar), 127.1 (Ar), 73.9 (O*C*$H_2$Ph), 73.7 (O*C*$H_2$CH), 73.0 (CH).

MS (ESI): m/z 524.7 $[Fe_2\mathbf{L}^{\mathbf{f}}_3]^{4+}$.

FTIR: ν $cm^{-1}$ 3360 br, 3027 w, 2862 w, 1613 w, 1592 w, 1492 m, 1472 m, 1452 m, 1384 w, 1353 w, 1299 w, 1242 w, 1102 m, 1079 s, 1015 s, 1001 m, 841 w, 804 m, 758 s, 700 s.

Elemental analysis found (calculated for $C_{126}H_{118}Cl_4Fe_2N_{12}O_6S_3\cdot 11H_2O$): % C 61.81 (61.92) H 5.22 (5.77) N 6.57 (6.88).

**$\Delta_{Fe}$-$[Fe_2\mathbf{L}^{\mathbf{g}}_3]Cl_4\cdot 11H_2O$**

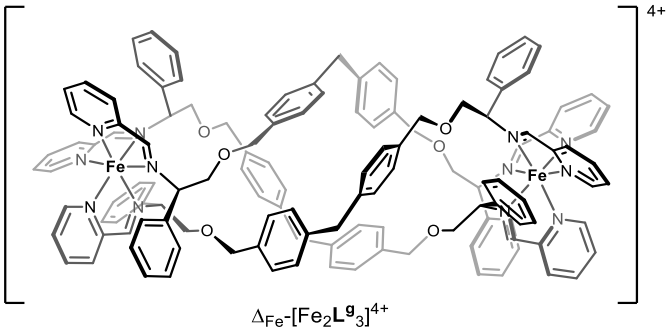


$\Delta_{Fe}$-$[Fe_2\mathbf{L}^{\mathbf{g}}_3]^{4+}$

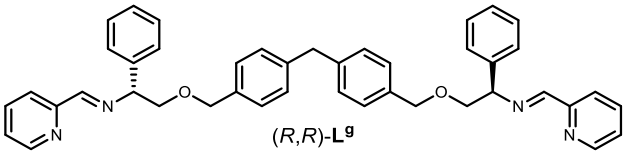

(*R*,*R*)-$\mathbf{L}^{\mathbf{g}}$

0.25 g (0.52 mmol) of diamine used.

Yield: 0.25 g, 0.10 mmol, 60 %.

$^{1}$H NMR (500 MHz, 298 K, $CD_3OD$): $\delta_H$ 9.28 (6H, s, HC=N), 7.75 (6H, t, $^{3}J_{HH}$ = 7.1 Hz, Py), 7.53 (6H, d, $^{3}J_{HH}$ = 7.1 Hz, Py), 7.36 (12H, d, $^{3}J_{HH}$ = 7.6 Hz, Ph), 7.23 (6H, t, $^{3}J_{HH}$ = 6.2 Hz, Py), 7.06 (6H, t, $^{3}J_{HH}$ = 7.0 Hz, Ph), 6.94 (12H, t, $^{3}J_{HH}$ = 7.1 Hz, Ph), 6.89 (12H, d, $^{3}J_{HH}$ = 7.6 Hz, Ph), 6.77 (6H, d, $^{3}J_{HH}$ = 5.0 Hz, Py), 6.69 (12H, d, $^{3}J_{HH}$ = 7.0 Hz, Ph), 5.96 (6H, d, $^{3}J_{HH}$ = 9.8 Hz, CH), 4.45 (6H, t, $^{2}J_{HH}/^{3}J_{HH}$ = 10.9 Hz, OC$H_2$CH), 4.37 (6H, d, $^{2}J_{HH}$ = 11.5 Hz, OC$H_2$Ph), 3.86 (6H, s, PhC$H_2$Ph), 3.23 (6H, d, $^{2}J_{HH}$ = 9.8 Hz, OC$H_2$CH).

$^{13}$C{$^{1}$H} NMR (125 MHz, 298 K, $CD_3OD$): $\delta_C$ 172.8 (C=N), 160.4 (Ar), 154.5 (Ar), 141.9 (Ar), 139.8 (Ar), 136.6 (Ar), 136.4 (Ar), 130.4 (Ar), 130.2 (Ar), 129.3 (Ar), 128.8 (Ar), 127.1 (Ar), 74.2 (O$C$H$_2$Ph), 73.9 (O$C$H$_2$CH), 72.9 (CH), 41.5 (Ph$C$H$_2$Ph).

MS (ESI): m/z 511.4 $[Fe_2\mathbf{L}_3]^{4+}$.

FTIR: ν cm$^{-1}$ 3360 br, 3043 w, 2915 w, 2858 m, 1612 w, 1512 w, 1494 w, 1471 m, 1451 m, 1360 w, 1299 w, 1240 w, 1105 m, 1076 s, 1019 m, 1001 m, 757 s, 700 s.

Elemental analysis found (calculated for $C_{129}H_{124}Cl_4Fe_2N_{12}O_6 \cdot 11H_2O$): % C 65.34 (64.83) H 5.91 (6.16) N 6.52 (7.03).

**$\Lambda_{Fe}$-[$Fe_2L^g_3$]$Cl_4$·11$H_2O$**

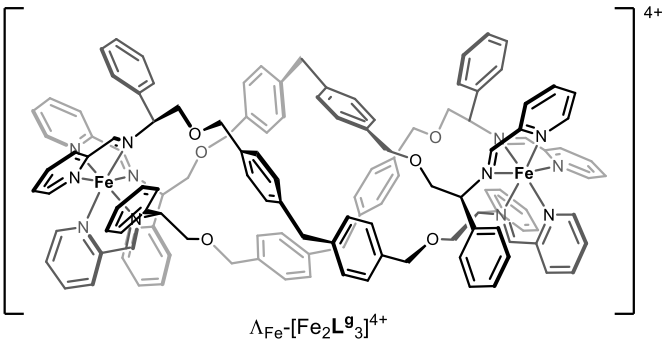


$\Lambda_{Fe}$-[$Fe_2\mathbf{L}^{\mathbf{g}}_3$]$^{4+}$

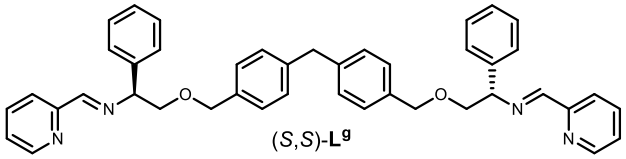

(*S*,*S*)-$\mathbf{L}^{\mathbf{g}}$

0.25 g (0.52 mmol) of diamine used.

Yield: 0.25 g, 0.10 mmol, 60 %.

$^1$H NMR (500 MHz, 298 K, $CD_3OD$): $\delta_H$ 9.28 (6H, s, HC=N), 7.75 (6H, t, $^3J_{HH}$ = 7.1 Hz, Py), 7.53 (6H, d, $^3J_{HH}$ = 7.1 Hz, Py), 7.36 (12H, d, $^3J_{HH}$ = 7.6 Hz, Ph), 7.23 (6H, t, $^3J_{HH}$ = 6.2 Hz, Py), 7.06 (6H, t, $^3J_{HH}$ = 7.0 Hz, Ph), 6.94 (12H, t, $^3J_{HH}$ = 7.1 Hz, Ph), 6.89 (12H, d, $^3J_{HH}$ = 7.6 Hz, Ph), 6.77 (6H, d, $^3J_{HH}$ = 5.0 Hz, Py), 6.69 (12H, d, $^3J_{HH}$ = 7.0 Hz, Ph), 5.96 (6H, d, $^3J_{HH}$ = 9.8 Hz, CH), 4.45 (6H, t, $^2J_{HH}/^3J_{HH}$ = 10.9 Hz, OC*H*$_2$CH), 4.37 (6H, d, $^2J_{HH}$ = 11.5 Hz, OC*H*$_2$Ph), 3.86 (6H, s, PhC*H*$_2$Ph), 3.23 (6H, d, $^2J_{HH}$ = 9.8 Hz, OC*H*$_2$CH).

$^{13}$C{$^1$H} NMR (125 MHz, 298 K, $CD_3OD$): $\delta_C$ 172.8 (C=N), 160.4 (Ar), 154.5 (Ar), 141.9 (Ar), 139.8 (Ar), 136.6 (Ar), 136.4 (Ar), 130.4 (Ar), 130.2 (Ar), 129.3 (Ar), 128.8 (Ar), 127.1 (Ar), 74.2 (O*C*H$_2$Ph), 73.9 (O*C*H$_2$CH), 72.9 (CH), 41.5 (Ph*C*H$_2$Ph).

MS (ESI): m/z 511.4 [$Fe_2\mathbf{L}^{\mathbf{g}}_3$]$^{4+}$.

FTIR: ν $cm^{-1}$ 3360 br, 3043 w, 2915 w, 2858 m, 1612 w, 1512 w, 1494 w, 1471 m, 1451 m, 1360 w, 1299 w, 1240 w, 1105 m, 1076 s, 1019 m, 1001 m, 757 s, 700 s.

Elemental analysis found (calculated for $C_{129}H_{124}Cl_4Fe_2N_{12}O_6 \cdot 11H_2O$): % C 64.76 (64.83) H 5.50 (6.16) N 6.39 (7.03).

**$\Delta_{Fe}$-[$Fe_2L^h_3$]$Cl_4 \cdot 11.5H_2O$**

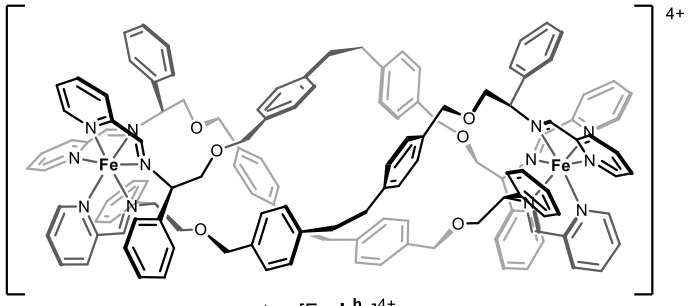


$\Delta_{Fe}$-[$Fe_2\mathbf{L}^h_3$]$^{4+}$

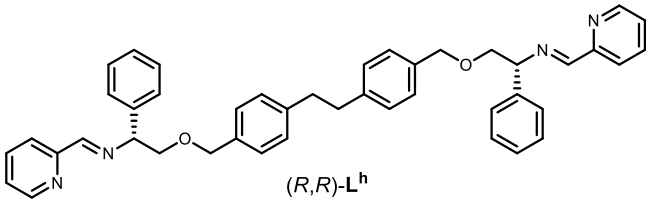

(*R*,*R*)-$\mathbf{L}^h$

0.25 g (0.52 mmol) of diamine used.

Yield: 0.32 g, 0.13 mmol, 77 %.

$^{13}C\{^1H\}$ NMR (125 MHz, 298 K, $CD_3OD$): $\delta_C$ 173.3 (C=N), 160.4 (Ar), 154.6 (Ar), 143.2 (Ar), 139.8 (Ar), 136.5 (Ar), 130.3 (Ar), 130.0 (Ar), 129.8 (Ar), 129.7 (Ar), 129.3 (Ar), 128.8 (Ar), 127.2 (Ar), 74.5 (O*C*$H_2$Ph), 73.3 (O*C*$H_2$CH), 72.7 (CH), 38.1 ($CH_2CH_2$).

MS (ESI): m/z 521.9 [$Fe_2\mathbf{L}^h_3$]$^{4+}$.

FTIR: ν $cm^{-1}$ 3372 br, 3023 w, 2921 w, 2855 m, 1612 w, 1589 w, 1513 w, 1494 w, 1471 m, 1451 m, 1385 1241 w, 1103 m, 1074 s, 1018 m, 1002 m, 815 w, 158 s, 700 s.

Elemental analysis found (calculated for $C_{132}H_{126}Cl_4Fe_2N_{12}O_6 \cdot 11.5H_2O$): % C 65.44 (65.05) H 5.87 (6.16) N 6.69 (6.90).

**$\Lambda_{Fe}$-[$Fe_2L^h_3$]$Cl_4 \cdot 11.5H_2O$**

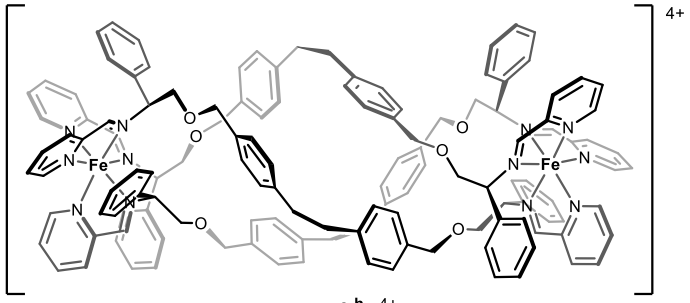


$\Lambda_{Fe}$-[$Fe_2\mathbf{L}^h_3$]$^{4+}$

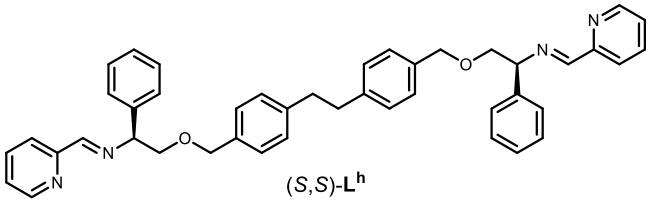

(*S*,*S*)-$\mathbf{L}^h$

0.25 g (0.52 mmol) of diamine used.

Yield: 0.32 g, 0.13 mmol, 78 %.

$^{13}C\{^1H\}$ NMR (125 MHz, 298 K, $CD_3OD$): $\delta_C$ 173.3 (C=N), 160.4 (Ar), 154.6 (Ar), 143.2 (Ar), 139.8 (Ar), 136.5 (Ar), 130.3 (Ar), 130.0 (Ar), 129.8 (Ar), 129.7 (Ar), 129.3 (Ar), 128.8 (Ar), 127.2 (Ar), 74.5 (O*C*$H_2$Ph), 73.3 (O*C*$H_2$CH), 72.7 (CH), 38.1 ($CH_2CH_2$).

MS (ESI): m/z 521.9 [$Fe_2\mathbf{L}^h_3$]$^{4+}$.

FTIR: ν $cm^{-1}$ 3372 br, 3023 w, 2921 w, 2855 m, 1612 w, 1589 w, 1513 w, 1494 w, 1471 m, 1451 m, 1385 1241 w, 1103 m, 1074 s, 1018 m, 1002 m, 815 w, 158 s, 700 s.

Elemental analysis found (calculated for $C_{132}H_{126}Cl_4Fe_2N_{12}O_6 \cdot 11.5H_2O$): % C 64.48 (65.05) H 5.66 (6.16) N 6.69 (6.90).

**$\Delta_{Fe}$-[$Fe_2L^i_3$]$Cl_4 \cdot 13H_2O$**

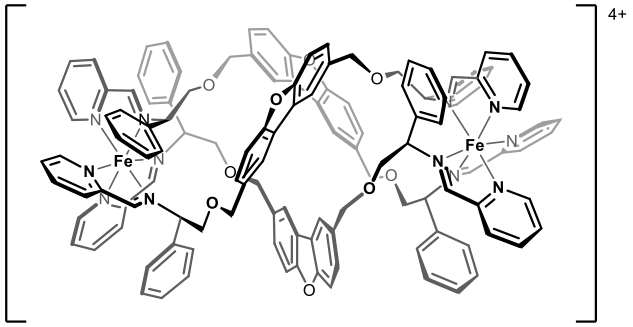


$\Delta_{Fe}$-[$Fe_2L^i_3$]$^{4+}$

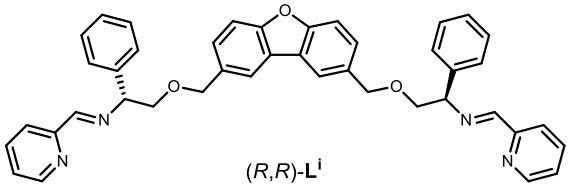

(*R*,*R*)-$L^i$

0.25 g (0.54 mmol) of diamine used.

Yield: 0.38 g, 0.16 mmol, 88 %.

$^1$H NMR (500 MHz, 298 K, $CD_3OD$): $\delta_H$ 9.10 (6H, s, HC=N), 9.00 (6H, s, DBF), 7.76 (6H, d, $^3J_{HH}$ = 8.3 Hz, DBF), 7.69 (6H, t, $^3J_{HH}$ = 7.7 Hz, Py), 7.59 (6H, d, $^3J_{HH}$ = 8.3 Hz, DBF), 7.46 (6H, d, $^3J_{HH}$ = 7.7 Hz, Py), 7.14 (6H, t, $^3J_{HH}$ = 6.6 Hz, Py), 7.05 (6H, t, $^3J_{HH}$ = 7.4 Hz, Ph), 6.95 (12H, t, $^3J_{HH}$ = 7.4 Hz, Ph), 6.65 (6H, d, $^3J_{HH}$ = 5.6 Hz, Py), 6.50 (6H, d, $^3J_{HH}$ = 5.3 Hz, Ph), 5.55 (6H, dd, $^3J_{HH}$ = 10.8 Hz, $^3J_{HH}$ = 2.7 Hz, CH), 4.51

(6H, d, $^{2}J_{HH}$ = 9.2 Hz, OC*H*$_2$Ph), 4.02 (6H, t, $^{2}J_{HH}$/$^{3}J_{HH}$ = 11.0 Hz, OC*H*$_2$CH), 3.75 (6H, d, $^{2}J_{HH}$ = 9.2 Hz, OC*H*$_2$Ph), 2.34 (6H, dd, $^{2}J_{HH}$ = 10.8 Hz, $^{3}J_{HH}$ = 2.7 Hz, OC*H*$_2$CH).

$^{13}C\{^{1}H\}$ NMR (125 MHz, 298 K, $CD_3OD$): $\delta_C$ 172.7 (C=N), 160.4 (Ar), 158.2 (Ar), 154.3 (Ar), 139.7 (Ar), 135.8 (Ar), 133.6 (Ar), 131.7 (Ar), 130.3 (Ar), 130.1 (Ar), 129.4 (Ar), 128.6 (Ar), 125.0 (Ar), 123.2 (Ar), 113.1 (Ar), 74.8 (O*C*H$_2$Ph), 73.9 (O*C*H$_2$CH), 72.3 (CH).

MS (ESI): m/z 645.2 [$\mathbf{L^i}$+H]$^{+}$, 511.3 [$Fe_2\mathbf{L^i}_3$]$^{4+}$.

FTIR: ν cm$^{-1}$ 3378 br, 3030 w, 2856 m, 1612 w, 1591 w, 1488 w, 1472 m, 1452 m, 1385 m, 1360 w, 1242 w, 1212 m, 1185 m, 1104 m, 1073 s, 1027 m, 1002 m, 830 w, 806 w, 758 s, 700s.

Elemental analysis found (calculated for $C_{126}H_{112}Cl_4Fe_2N_{12}O_9 \cdot 13H_2O$): % C 62.60 (62.38) H 5.13 (5.73) N 6.69 (6.93).

**$\Lambda_{Fe}$-[$Fe_2L^i_3$]$Cl_4$·13$H_2O$**

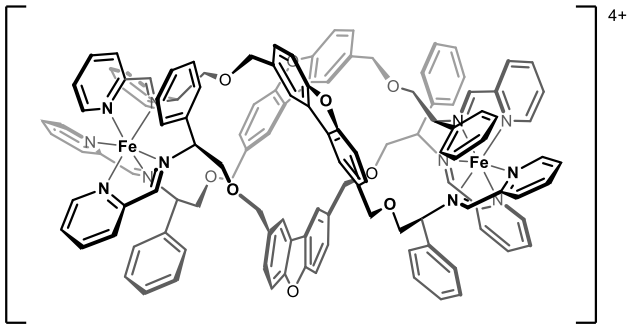


$\Lambda_{Fe}$-[$Fe_2L^i_3$]$^{4+}$

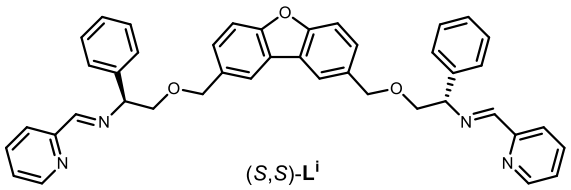

(*S*,*S*)-$L^i$

0.25 g (0.54 mmol) of diamine used.

Yield: 0.36 g, 0.15 mmol, 83 %.

$^1$H NMR (500 MHz, 298 K, $CD_3OD$): $\delta_H$ 9.10 (6H, s, HC=N), 9.00 (6H, s, DBF), 7.76 (6H, d, $^3J_{HH}$ = 8.3 Hz, DBF), 7.69 (6H, t, $^3J_{HH}$ = 7.7 Hz, Py), 7.59 (6H, d, $^3J_{HH}$ = 8.3 Hz, DBF), 7.46 (6H, d, $^3J_{HH}$ = 7.7 Hz, Py), 7.14 (6H, t, $^3J_{HH}$ = 6.6 Hz, Py), 7.05 (6H, t, $^3J_{HH}$ = 7.4 Hz, Ph), 6.95 (12H, t, $^3J_{HH}$ = 7.4 Hz, Ph), 6.65 (6H, d, $^3J_{HH}$ = 5.6 Hz, Py), 6.50 (6H, d, $^3J_{HH}$ = 5.3 Hz, Ph), 5.55 (6H, dd, $^3J_{HH}$ = 10.8 Hz, $^3J_{HH}$ = 2.7 Hz, CH), 4.51 (6H, d, $^2J_{HH}$ = 9.2 Hz, OC*H*$_2$Ph), 4.02 (6H, t, $^2J_{HH}$/$^3J_{HH}$ = 11.0 Hz, OC*H*$_2$CH), 3.75 (6H, d, $^2J_{HH}$ = 9.2 Hz, OC*H*$_2$Ph), 2.34 (6H, dd, $^2J_{HH}$ = 10.8 Hz, $^3J_{HH}$ = 2.7 Hz, OC*H*$_2$CH).

$^{13}$C{$^1$H} NMR (125 MHz, 298 K, $CD_3OD$): $\delta_C$ 172.7 (C=N), 160.4 (Ar), 158.2 (Ar), 154.3 (Ar), 139.7 (Ar), 135.8 (Ar), 133.6 (Ar), 131.7 (Ar), 130.3 (Ar), 130.1 (Ar), 129.4 (Ar), 128.6 (Ar), 125.0 (Ar), 123.2 (Ar), 113.1 (Ar), 74.8 (O*C*H$_2$Ph), 73.9 (O*C*H$_2$CH), 72.3 (CH).

MS (ESI): m/z 645.2 $[\mathbf{L^i}+H]^+$, 511.3 $[Fe_2\mathbf{L^i}_3]^{4+}$.

FTIR: ν $cm^{-1}$ 3378 br, 3030 w, 2856 m, 1612 w, 1591 w, 1488 w, 1472 m, 1452 m, 1385 m, 1360 w, 1242 w, 1212 m, 1185 m, 1104 m, 1073 s, 1027 m, 1002 m, 830 w, 806 w, 758 s, 700s.

Elemental analysis found (calculated for $C_{126}H_{112}Cl_4Fe_2N_{12}O_9 \cdot 13H_2O$): % C 62.18 (62.38) H 4.95 (5.73) N 6.71 (6.93).

### 6.1.8 Absorption spectra for $[Fe_2L_3]Cl_4$ flexicates

### UV-visible spectra

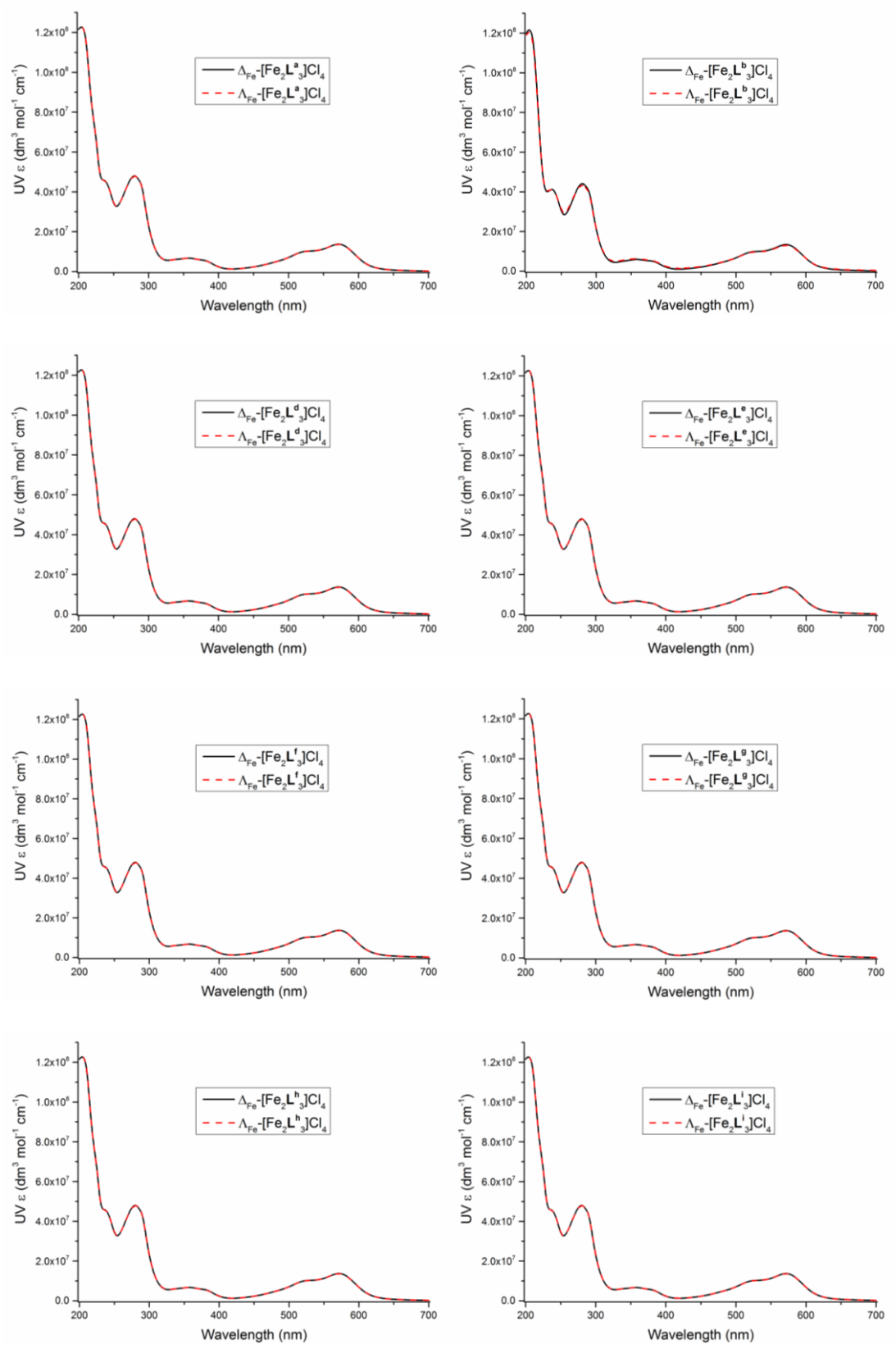

## CD spectra

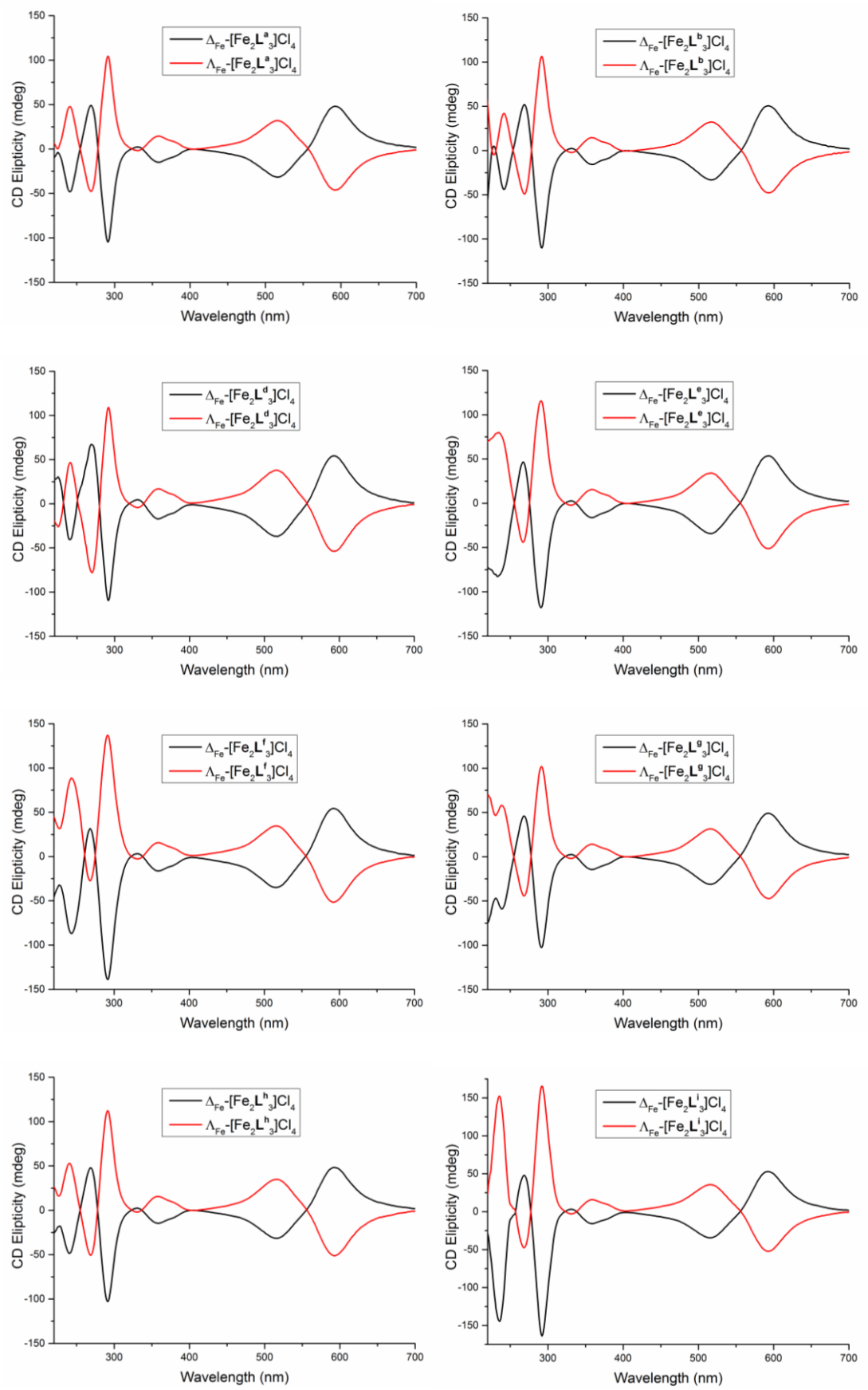
ΔFe-[Fe2La3]Cl4
ΛFe-[Fe2La3]Cl4
ΔFe-[Fe2Lb3]Cl4
ΛFe-[Fe2Lb3]Cl4
ΔFe-[Fe2Ld3]Cl4
ΛFe-[Fe2Ld3]Cl4
ΔFe-[Fe2Le3]Cl4
ΛFe-[Fe2Le3]Cl4
ΔFe-[Fe2Lf3]Cl4
ΛFe-[Fe2Lf3]Cl4
ΔFe-[Fe2Lg3]Cl4
ΛFe-[Fe2Lg3]Cl4
ΔFe-[Fe2Lh3]Cl4
ΛFe-[Fe2Lh3]Cl4
ΔFe-[Fe2Li3]Cl4
ΛFe-[Fe2Li3]Cl4
CD Elipticity (mdeg)
Wavelength (nm)

### 6.1.9 TGA data for $[Fe_2L_3]Cl_4$ flexicates

Illustrating mass decrease due to loss of water of crystallisation and decomposition.

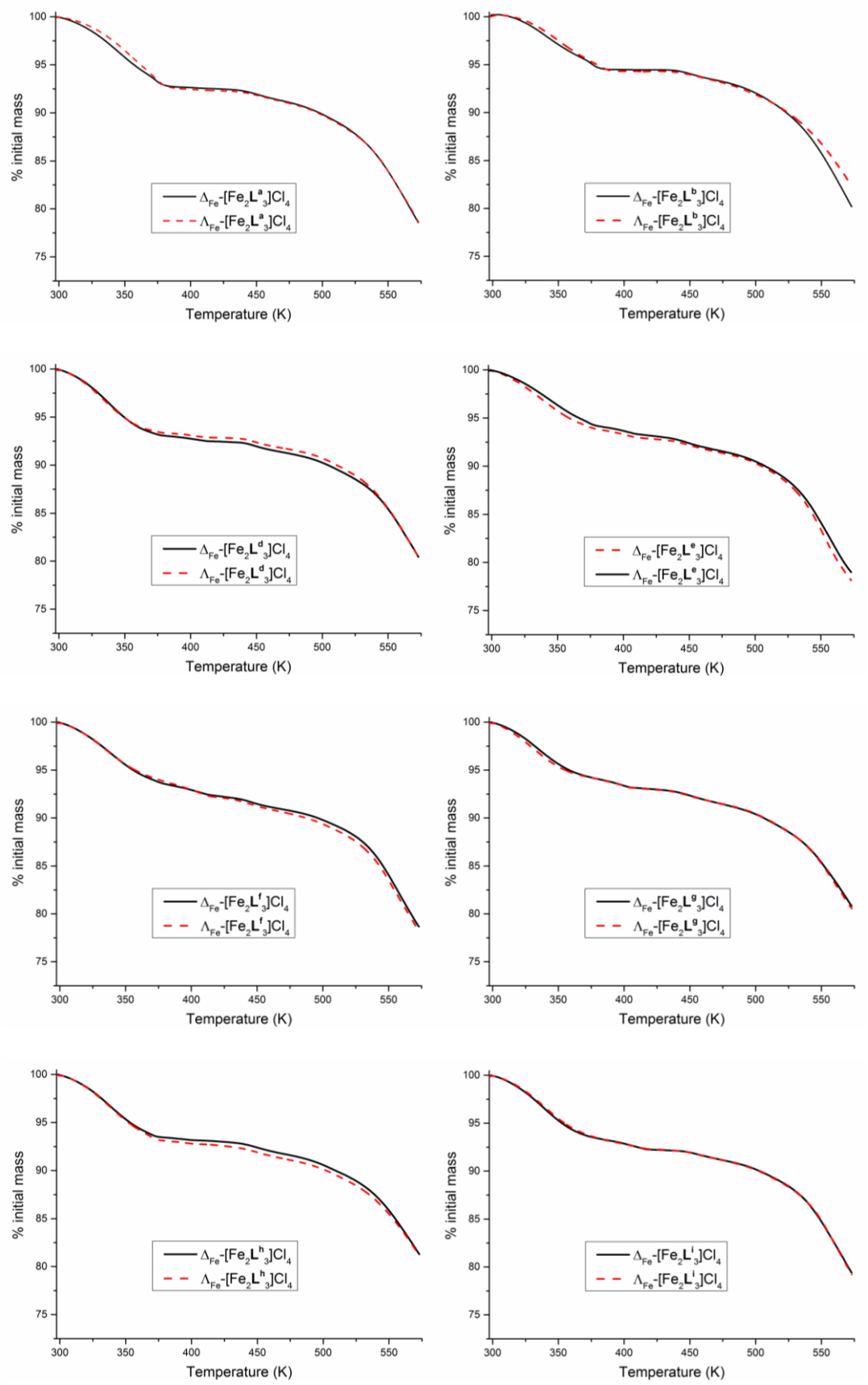

### 6.1.10 Aqueous stability study of $[Fe_2L_3]Cl_4$ flexicates

For all solutions tested, flexicate concentrations of 50 μM were made up in distilled water supplemented with 1 % methanol. Aliquots of 3 ml were sealed into plastic macrocuvettes (Fisher) using [10 mm × 10 mm] LDPE cuvette lids (Sigma) and parafilm to prevent evaporation. After taking initial UV-vis spectra across the wavelength range 450-600 nm - otherwise using the parameters detailed in section 5.1.1, these cuvettes were incubated at 37 °C using a cuvette incubator rack (Grant instruments) for 28 days. Intermittent UV-vis spectra using the same parameters were taken during this time, with the cuvettes being carefully cleaned with lens tissues beforehand. UV-vis spectra of a 3 ml solution of 1 % methanol in water were also taken alongside the flexicate solutions, to be used as a baseline measurement that was subtracted from experimental data.

# 6.2 Experimental Details for Chapters 3 and 4

### 6.2.1 General considerations

All procedures were carried out using appropriate aseptic techniques; for routine work, surfaces were thoroughly washed with 4:1 ethanol/water beforehand, and work was carried out close to a lit flame (Bunsen burner); extensive and/or sensitive work was carried out using a sterile class II microbiological laminar flow cabinet (*e.g.* ThermoFisher 1300 series). Where necessary, equipment and reagents were either bought sterile or sterilised in-house, using an autoclave. Cation-adjusted Müller-Hinton broth (CAMHB) was purchased from Sigma, where it is listed as Mueller Hinton Broth 2. Sterile growth media, agar plates, and antibiotic stock solutions were prepared by the media preparation unit of the University of Warwick's School of Life science (stored at 4 °C until required), unless stated otherwise. Where accurate weighing of small masses was essential, *e.g.* in making flexicate stock solutions, this was done using a 7-figure balance (Sartorius). The optical density at 600 nm ($OD_{600}$) of bacterial broth cultures was measured on a benchtop spectrophotometer (*e.g.* Jenway 6300 or ISS Cell Density Meter). Routine centrifugations were performed using a benchtop centrifuge, *e.g.* Eppendorf 4418 model, for small volumes (≤2 ml liquid), or an Eppendorf 5810R centrifuge for larger volumes (up to 50 ml).

For the incubation of multi-well (typically 96-well) plates, the Falcon™ plates (Fisher) containing bacterial culture were either incubated using a plate thermos-shaker (BioSan PST-100HL), or where turbidity (*i.e.* optical density) was monitored during incubation, using a microplate reader (BMG labtech SPECTROstar nano, or Labsystems iEMS reader) set to periodically measure $OD_{600}$ output of each well used. In either case the plates were incubated with the clear polystyrene lid applied, at 37 °C with shaking (200-400 rpm depending on the assay). Appropriate positive/negative

controls were incorporated. At least two biological replicates were performed for each plate.

### 6.2.2 Bacterial strains

Strains and their origins are listed in table 6.2. Bacterial stocks were stored long-term in either Müller-Hinton broth or Lysogeny broth (LB) supplemented with 20-40 % glycerol, and frozen to -80 °C. When required, frozen bacterial stocks were slowly thawed on ice and then streaked onto MH agar or LB agar plates, which were subsequently incubated overnight to give single colonies. Inoculated agar plates were incubated overnight in a precision incubator (LEEC) set to 37 °C.

| Strain | Wild-type ascension code | Notes and references | Source |
|---|---|---|---|
| *A. baumannii* | NCTC 13420 | Reference MDR strain[7] | Biota Ltd. (now defunct) Pathogen library |
| *B. subtilis* 168 | ATCC 6051 | Legacy strain[8] | Dowson laboratory (University of Warwick) |
| *E. cloacae* 684 | NCTC 13405 | AmpC positive isolate[9] | Biota Pathogen library |
| *E. coli* TOP10 | ATCC PTA-10989 | DH10β strain[10] | Invitrogen |
| *E. coli* MG1655 | ATCC 700926 | K12 strain[11] | Constantinidou laboratory (University of Warwick) |
| *E. coli* CFT073 | ATCC 700928 | UPEC O6:H1:K2[12] | Constantinidou laboratory |
| *E. coli* Sakai | ATCC BAA-460 | Japanese EHEC O157:H7 Δ*stx*1-2[13, 14] | Constantinidou laboratory |
| *E. coli* EDL933 | ATCC 700927 | American EHEC O157:H7 Δ*stx*1-2[15] | Constantinidou laboratory |
| *K. pneumoniae* K6 | ATCC 700603 | Reference strain, SHV-18 positive[16] | Biota Pathogen library |
| *K. pneumoniae* KP02 | NCTC 13442 | OXA-48 positive isolate[17] | Biota Pathogen library |
| *P. aeruginosa* PAO1 | ATCC 15692 | Legacy strain[18] | Biota Pathogen library |
| *S. aureus* USA300 | ATCC BAA-1717 | MRSA, FPR3757 isolate[19] | Nebraska Transposon Mutant Library |

**Table 6.2: Information regarding the strains used in this work, and their origins.**

Overnight bacterial cultures in liquid were grown by seeding 5-10 ml of sterile broth (CAMHB unless specifically stated) with bacteria picked from a single colony grown on an agar plate. A sterile 25 ml tube

All incubations of liquid culture (except for 96-well plates) were carried out using a MaxQ® 8000 (ThermoFisher) or Innovia® 44 (New Brunswick scientific) thermoshaker, set to 37 °C with shaking at 150-400 rpm, or for some larger cultures using a shaking water bath (Grant instruments) with the same parameters.

### 6.2.3 Minimum inhibitory concentration (MIC) determination[20-22]

A 1280 μg/ml stock solution of each flexicate was prepared in water containing 10 % methanol, corresponding to a tenfold concentration of the highest concentration tested, 128 μg/ml. This stock was repeatedly diluted twofold in CAMHB, allowing the standard 1-128 μg/ml range to be used in the assay upon further tenfold dilution.

Overnight cultures of each bacterial strain in CAMHB (antibiotic-free) were diluted in the same medium to an cell concentration of $5 \times 10^5$ cfu/ml. Aliquots of 9:1 microbial culture/flexicate dilution or appropriate control (200 μl), were distributed out onto a sterile 96-well plate, set up as described in section 5.2.1. They were then either incubated and later visually inspected, or $OD_{600}$ data was recorded and used to determine bacterial growth, allowing the MIC (the lowest concentration that inhibits growth) to be determined. In either case, plates were incubated at 37 °C (unless specified otherwise) for 20 h, with gentle shaking.

Appropriate positive (culture only, no antimicrobial) and negative controls (media only) were used in each plate. Every plate was repeated at least in duplicate. Known antimicrobials (*e.g.* kanamycin) were used to validate this methodology.

### 6.2.4 Minimum bactericidal concentration (MBC) determination[23]

Determination of MBCs was carried out for strain/compound pairings where an MIC ≤128 μg/ml was determined, immediately following that assay. For each 'culture' with compound concentration in the range 128 μg/ml to the MIC (inclusive), 100 μl of the bacteria/compound mix was recovered from the microtitre plate for analysis. Cell and/or debris was collected from samples by centrifugation and resuspended in 100 μl sterile PBS, which was streaked onto a sterile antimicrobial-free LB/agar plate. Upon overnight incubation (37 °C), plates were inspected and the MBC was determined to be the lowest concentration of compound at which this dilution/culturing assay showed no visible signs of bacterial growth. This was performed at least in duplicate for each pairing of compound concentration and bacterial strain.

### 6.2.5 *Bac*Light™ LIVE/DEAD assay and fluorometric measurements

Overnight cultures of the appropriate bacterial strain in CAMHB (antibiotic-free) were divided into two equal portions and cells collected by centrifugation (4000 *g* for 10 min) and resuspeded in aqueous saline solution (0.85 % NaCl by weight). One pellet, going on to comprise live/intact cells, was resuspended in fresh saline solution (10 ml). The second pellet, (which would go on to comprise dead/compromised bacterial cells) was resuspended using the same volume of 70 % aqueous isopropanol, in order to obtain dead/compromised cells. Both suspensions were incubated, with

gentle shaking, for 1 h at room temperature, before harvesting by centrifugation (4000*g* for 10 min). Both pellets were resuspended in fresh saline solution to yield a cell suspension of $OD_{600}$ = 0.2.

Flexicate solutions of 10× the desired final concentration were prepared in saline containing 10 % methanol, and they were added to the live (intact) cell suspension at a ratio of 9:1 (cells:flexicate). These were distributed into separate wells of a sterile Falcon™ 96-well plate (100 µl each). Additionally, different proportions of live and dead cells were mixed to obtain cell suspensions containing different proportions of live/intact cells (100 %, 90 %, 50 %, 10 % and 0 %). Aliquots of these mixtures (100 µl) were applied to each plate as controls. Plates were incubated for 40 min at 37 °C, then 100 µL of *Bac*Light™ LIVE/DEAD dye solution (prepared according to the manufacturer's instructions) was added. After 15 min incubation in a darkroom at ambient temperature, fluorescence output of the samples was measured using a VarioSkan Flash (ThermoFisher) plate reader, set to measure the output at wavelength 530 nm and 630 nm respectively (12 nm bandwidth, 100 ms measurement time), from an excitation at wavelength 485 nm. A delay of 200 ms was included between measurements.

Cell membrane integrity was quantitatively determined using the controls to plot a standard curve (for an example, see Figure 3.6). Experimental samples were repeated five times, and controls were repeated in triplicate.

### 6.2.6 Whole genome sequencing (WGS)

The appropriate *E. coli* cells were collected from 0.5 ml of overnight culture (~$5 \times 10^8$ cells), by centrifugation. Genomic DNA was collected from each of these samples

using a DNeasy® blood and tissue genomic DNA extraction kit (Qiagen), according to the manufacturer's instructions. The purified genomic DNA from each sample was eluted into 100 µl of the elution buffer and the DNA concentration (ng/µl) of each sample was determined using the Qubit® high-sensitivity dsDNA quantification kit (ThermoFisher Scientific).

The Illumina Nextera® XT kit was used to prepare genomic DNA libraries (250 bp fragments) that are suitable for sequencing, and ensure each sample is uniquely identifiable during sequencing. This was done according to the manufacturer's instructions, using the DNA concentrations determined using the Qubit® assay to normalise the quantity of input genomic DNA used (1 ng in 5 µl). After the preparation of genomic DNA libraries, the DNA concentration of each library was determined using the Qubit® HS dsDNA quantification kit. This allowed DNA libraries to be normalised (4 mM), pooled together (5 µl of each library), and finally prepared for sequencing according to Illumina Nexteria® XT guidelines. The prepared pool of DNA libraries was loaded onto an Illumina MiSeq™ sequencer (machine time courtesy of the Microbiology and Infection Division, University of Warwick), by either Dr Gemma Kay, or Dr Alexia Hapeshi. The paired-end 2 × 250 bp kit was used for the whole-genome sequencing.

### 6.2.7 Extraction and purification of microbial RNA

To extract RNA from *E. coli* culture, $6 \times 10^8$ cells (*e.g.* 1 ml of culture at $OD_{600} \approx 0.75$) were added to an aliquots of RNAprotect® reagent (Qiagen) of twice the volume, and vortexed immediately, preserving and stabilising the microbial RNA. After a 5 min incubation at ambient temperature, cells were collected by centrifugation.

To facilitate the breakdown of the *E. coli* cell wall, cells were resuspended into 100 µl Tris-EDTA (TE) buffer containing 20 µl proteinase K (Qiagen) and 1 mg/ml lysozyme, and incubation for 5 min at ambient temperature with gentle shaking. RNA was then extracted from the samples using the miRNeasy spin-column format kit (Qiagen) as per the manufacturer's instructions, with the inclusion of a double on-column DNA digestion (using RNase-free DNase). The final elution was performed using 40 µl of RNase-free water per sample. The RNA concentration of each sample was determined from 1 µl of RNA elution, using the Qubit® HS RNA quantification kit (ThermoFisher Scientific).

### 6.2.8 Determining quality of microbial RNA

The absence of DNA from the RNA elution was confirmed using a standard polymerase chain reaction (PCR) to attempt the amplification of the gene encoding the *E. coli* 16S ribosomal subunit.[24]

The PCR primers for 16S rRNA were:

`5'-AGAGTTTGATCMTGGCTCAG-3'` (forward)

`5'-GGTTACCTTGTTACGACTT-3'` (reverse)

The PCR conditions were:

1) Initial denaturation at 94 °C for 3 min.
2) Denaturation at 94 °C for 30 sec.
3) Annealing at 55 °C for 30 sec.
4) Extension at 68 °C for 1 min.
5) Steps 2-4 repeated ×29 times.

6) Final extension at 68 °C for 5 min.

The absence of detectable PCR products in subsequent agarose gel electrophoresis, signified the lack of genomic DNA contamination.

Additionally, the Agilent 2100 Bioanalyzer instrument was used to check the quality of RNA, using a further 2 µl of RNA elution prepared using the RNA 6000 pico kit (Agilent), according to the manufacturer's instructions. Bioanalyzer electropherograms are shown in Figure 4.4.

### 6.2.9 Generation of cDNA libraries

A modified TruSeq™ Stranded mRNA (Illumina) library preparation protocol was used to prepare cDNA libraries for sequencing. All steps were carried out in sterile, sealable 96-well plates.

Firstly, RNA was fragmented and converted to cDNA *via* DNA/RNA hybrid. RNA depleted of rRNA (5 µl) was mixed with TruSeq™ 'Fragment, Prime, Finish mix' (13 µl) and incubated at 94 °C for 8 min. The 96-well plate was briefly centrifuged (280 g), incubated for 5 min at ambient temperature and 17 µl of the sample transferred to a new well on the same plate. Superscript II (Fisher) was mixed with TruSeq™ First Strand Synthesis Act D in a 1:9 ratio, and 8 µl of this mix was added to each sample. The plate was then incubated at 25 °C for 10 min, 42 °C for 15 min and 70 °C for 15 min. Next, to each sample was added; TruSeq™ End Repair Control diluted 1:50 in Resuspension buffer (5 µl), and TruSeq™ Second Strand Marking Master Mix (20 µl). Plates were then incubated at 16 °C for 1 h.

An initial purification was performed by adding 90 μl of Agencourt® AMPure® XP magnetic beads, and incubating the plate at ambient temperature for 15 min, then placing it on a suitable magnetic rack for 5 min at ambient temperature. The supernatant was discarded and the beads were washed twice by cycles of adding 200 μl of 80% aq. ethanol, incubating for 30 sec on the magnetic rack and discarding the supernatant. Beads were dried in air for 15 min and resuspended in 17.5 μl of resuspension buffer. The plate was incubated at ambient temperature for 2 min, placed on the magnetic rack for 5 min and 15 μl of the supernatant, containing cDNA, was transferred to a new well.

In preparation for sequencing, cDNA 3' ends were adenylated. To achieve this, for each sample TruSeq™ A-Tailing Control diluted 1:100 in Resuspension buffer (2.5 μl) and TruSeq™ A-Tailing mix (12.5 μl) were added, and the plate was incubated at 37 °C for 30 min, then 70 °C for 5 min. Then, TruSeq™ Ligation Control diluted 1:100 in Resuspension buffer (2.5 μl), TruSeq™ Ligation mix (2.5 μl), and of Index adapter (2.5 μl) were added to each sample. The plate was centrifuged (280 g, 1 min) and then incubated at 30 °C for 1 h. TruSeq™ Stop Ligation buffer (5 μl) was added to stop the reaction. A second purification (using 42 μl of Agencourt® AMPure® XP beads) was carried out as described for the initial purification: beads were washed with 80 % aq. ethanol, resuspended in 52.5 μl of Resuspension buffer and 50 μl of supernatant was transferred to a new well. A third purification (using 50 μl of Agencourt® AMPure® XP beads) was performed immediately after: beads were washed with 80 % aq. ethanol, resuspended in 22.5 μl of Resuspension buffer and 20 μl of supernatant was transferred to a new well.

Enrichment of the samples using PCR was performed. To each sample, PCR Primer Cocktail (5 µl) and PCR Master mix (25 µl) were added, and the following PCR setup enacted:

1) Initial denaturation at 98 °C for 30 sec.
2) Denaturation at 98 °C for 10 sec.
3) Annealing at 60 °C for 30 sec.
4) Extension at 72 °C for 30 sec.
5) Repeat steps 2-4 14 more times.
6) Final extension at 72 °C for 5 min.

A final purification was performed as previously described using 50 µl of Agencourt® AMPure® XP beads: beads were washed with 80 % aq. ethanol and resuspended in 32.5 µl of Resuspension buffer. The supernatant (30 µl), containing completed cDNA library, was then transferred to a new well. Prior to sequencing DNA concentration and fragment size were determined, as these parameters are critical to the setup. The former was measured using the Qubit® High Sensitivity DNA assay kit, and the latter using was determined using the (Agilent 2100) Bioanalyzer High Sensitivity DNA kit as per the manufacturer's instructions.

### 6.2.10 Protein extraction and sodium dodecyl sulfate polyacrylamide gel electrophoreisis (SDS-PAGE)

Protein was extracted at the relevant time point by first collecting ~$6.4 \times 10^8$ cells (equivalent to 1 ml of culture at an $OD_{600} = 0.8$) by centrifugation and resuspension twice into 1 ml PBS, before resuspending the final cell pellets into 100 µl PBS. To initiate lysis of *E. coli* cells, 100 µl of a combined ×2 loading buffer/SDS-PAGE

loading dye (see composition below) was thoroughly mixed into the samples, then after a 5 min incubation at 95 °C, samples were left to stand for 18 h at ambient temperature. SDS-PAGE (4–15% Mini-PROTEAN® TGX™, BioRad) was then performed using 12 µl from each lysate sample per lane (preliminary protein quantification assays suggested that this volume contains ~40 µg of *E. coli* protein). After staining for 1 h with InstantBlue (Expedeon) and removing excess dye by immersing the gels in water for 18 h, gels were imaged using a G:BOX Chemi XRQ (SYNGENE).

Combined loading buffer/SDS-PAGE loading dye composition (×2 concentration): 1 ml Tris/HCl buffer (1 M, pH 7.5), 4 ml 10 % SDS, 4 ml 50 % glycerol, 200 µl β-mercaptoethanol, 200 µl bromophenol blue [40 mg/ml], 600 µl deionised water.

### 6.2.11 Protein preparation for proteomics: in-gel digest

Protocol adapted from the methodology outlined by Shevchenko, Mann and co-workers,[25] by the proteomics division of the School of Life Sciences, University of Warwick. Work performed jointly by the author and Dr Alexia Hapeshi.

Each sample lane from the SDS-PAGE gels was carefully extricated and cut into small pieces (6 per lane), which were prepared separately. Gel pieces were washed (and destained) by adding 50% ethanol in 50 mM ammonium bicarbonate and incubating for 20 min, with shaking and heating at 50 °C. This was repeated twice, before dehydrating the gel pieces by adding 100% ethanol, incubating for 5 min at 55°C with shaking, then removing the liquid.

Protein disulfide bonds were reduced by adding 10 mM dithiothreitol (DTT) in 50 mM ammonium bicarbonate (180 µl) and incubating for 45 min at 56 ºC, with shaking, then removing excess liquid. Cysteine residues could then be alkylated by adding 55 mM iodoacetimide (IAA) in 50 mM ammonium bicarbonate for 30 min (at ambient temperature, in the dark), then removing excess liquid. Gel pieces were again washed (using 50 % ethanol in 50 mM ammonium bicarbonate) and dehydrated (using 100% ethanol) as previously described.

For the tryptic digest, 2.5 ng/µl trypsin (40 µl) was added and the gel pieces allowed to rehydrate for 10 mins. Sufficient additional 50 mM ammonium bicarbonate to cover the gel pieces was then added and samples incubated overnight with shaking (37 ºC).

To stop the digestion and extract the peptides from the gel pieces, 5 % formic acid in 25 % acetonitrile was added (40 µl). Samples were sonicate for 10 min and the supernatant extracted. This was repeated three times, pooling the collected supernatants for each sample. The samples originating from the same SDS-PAGE lane were then recombined and the peptide samples dried using a Speed-Vac, overnight (40 °C).

Dry peptide samples were resuspended by sonication (30 min) in 55 µl of water containing 2.5 % acetonitrile and 0.05 % trifluoroacetic acid. Samples were purified using C18 desalting tips, and dried using by SpeedVac evaporation. Samples were finally resuspended into 1:1 methanol/water (50 µl) and a 10 µl aliquot was analysed by *nano*LC-ESI-MS/MS using an Ultimate 3000 Orbitrap Fusion™ instrument (Thermo Fisher) with a 120 min LC separation on a 25 cm column, for each sample.

### 6.2.12 Bioinformatics: whole genome analysis

[As performed by Drs Alexia Hapeshi and Nicholas Waterfield]

Fastq reads from the whole genome sequencing of WT and tolerant clones were uploaded to EnteroBase[26] and assembled into *contigs*. The genomes of the tolerant clones were then aligned against the WT assembly whilst all genomes including the WT were also aligned against the reference *E. coli* O157:H7 Sakai genome (Assembly: GCF_000008865.1) for SNP and indel detection.

In addition, for confirmation of the EnteroBase analysis, alignment of raw reads to the reference *E. coli* O157:H7 Sakai genome (Assembly: GCF_000008865.1) including plasmids pO157 and pOSAK1 (Accession numbers: NC_002695 for the chromosome, NC_002127 for pOSAK1 and NC_002128 for pO157) was performed using Bowtie2.[27] For the purposes of mapping, the chromosome and two plasmids were used as reference in a single multifasta file. Bam files were sorted and indexed using Samtools[28] and visualised in Artemis genome browser[29] for manual validation. Qualimap[30] was used to calculate mapping statistics. Finally, SNP and small indel detection was also performed using VarScan2.[31]

### 6.2.13 Bioinformatics: transcriptomic analysis

[As performed by Drs Alexia Hapeshi and Nicholas Waterfield]

Fastq reads were mapped using Bowtie2 against the *E. coli* O157:H7 Sakai genome. As for the genome analysis, the chromosomal and pO157 and pOSAK1 plasmid sequences were introduced in a single fasta file, which was used as the reference for

Bowtie2. Alignment statistics are shown below. Only mapped reads were then used to create bam files and read counts per gene were calculated using BEDtools coverageBed.[32] Differential expression analysis was performed using DESeq2.[33] A multi-factor design was used to account for sample pairing and hence differences between the samples, whilst measuring the effect of the treatment. The design formula used was thus dds <- DESeqDataSet(se, design = ~replicate + condition), whereby condition refers to treatment. Results show differentially expressed genes with a Benjamini-Hochberg false discovery rate[34] (FDR) cutoff of 0.05 and a p-adjusted value less than 0.05. To identify overrepresented biological pathways in the dataset, the KEGG mapper Search&Color Pathway tool[35] was used and STRING[36] was used to visualise connections between differentially expressed genes. Table 6.3 lists the number of paired reads and % alignment rate for each sample.

| **Sample** | **Number of reads** (paired) | **Alignment rate** (%) |
|---|---|---|
| Control replicate 1 | 7746362 | 84.98 |
| Control replicate 2 | 5809414 | 99.77 |
| Control replicate 3 | 7168291 | 98.25 |
| Treated replicate 1 | 5529284 | 99.57 |
| Treated replicate 2 | 7553893 | 99.44 |
| Treated replicate 3 | 9714225 | 99.80 |

**Table 6.3: RNAseq (paired) read numbers and alignment rate for each sample.**

### 6.2.14 Bioinformatics: proteomic analysis

[As performed by Dr Alexia Hapeshi]

Raw LCMS data was introduced into MaxQuant software[37] to calculate label-free quantification (LFQ) values for each protein identified (referenced against peptide sequences from the Uniprot Escherichia_coli_O157H7 database). These were used in

Perseus[38] for further analysis. Total protein distributions were normalised for each sample, base-2 logarithms of LFQ fold differences (treated *vs.* control samples) were taken, and paired t-tests were used to calculate p-values. These parameters were used to calculate significance thresholds: the false discovery rate (FRD), set to 0.01, and $s_0$ (see Equation 4.1) set to 0.2 or 0.5.

## 6.3 References for Chapter 6


1. S. E. Howson, L. E. N. Allan, N. P. Chmel, G. J. Clarkson, R. J. Deeth, A. D. Faulkner, D. H. Simpson and P. Scott, *Dalton Trans.*, 2011, **40**, 10416-10433.

2. S. Yao, H. Y. Ahn, X. H. Wang, J. Fu, E. W. Van Stryland, D. J. Hagan and K. D. Belfield, *J. Org. Chem.*, 2010, **75**, 3965-3974.

3. R. H. Mitchell and V. S. Iyer, *Synlett*, 1989, **1989**, 55-57.

4. S. Yao and K. D. Belfield, *J. Org. Chem.*, 2005, **70**, 5126-5132.

5. S. E. Howson, A. Bolhuis, V. Brabec, G. J. Clarkson, J. Malina, A. Rodger and P. Scott, *Nat. Chem.*, 2012, **4**, 31-36.

6. D. J. Fox, S. Parris, D. S. Pedersen, C. R. Tyzack and S. Warren, *Org. Biomol. Chem.*, 2006, **4**, 3108-3112.

7. J. F. Turton, M. E. Kaufmann, M. Warner, J. Coelho, L. Dijkshoorn, T. van der Reijden and T. L. Pitt, *J. Hosp. Infect.*, 2004, **58**, 170-179.

8. P. R. Burkholder and N. H. Giles, *Am. J. Bot.*, 1947, **34**, 345-348.

9. Y. Yang, D. M. Livermore and R. J. Williams, *J. Med. Microbiol.*, 1988, **25**, 227-233.

10. S. G. Grant, J. Jessee, F. R. Bloom and D. Hanahan, *Proc. Natl. Acad. Sci. USA*, 1990, **87**, 4645-4649.

11. F. R. Blattner, G. Plunkett, C. A. Bloch, N. T. Perna, V. Burland, M. Riley, J. Collado-Vides, J. D. Glasner, C. K. Rode, G. F. Mayhew, J. Gregor, N. W. Davis, H. A. Kirkpatrick, M. A. Goeden, D. J. Rose, B. Mau and Y. Shao, *Science*, 1997, **277**, 1453-1462.

12. H. L. Mobley, D. M. Green, A. L. Trifillis, D. E. Johnson, G. R. Chippendale, C. V. Lockatell, B. D. Jones and J. W. Warren, *Infect. Immun.*, 1990, **58**, 1281-1289.

13. H. Watanabe, A. Wada, Y. Inagaki, K. Itoh and K. Tamura, *Lancet*, 1996, **348**, 831-832.

14. S. Dahan, S. Knutton, R. K. Shaw, V. F. Crepin, G. Dougan and G. Frankel, *Infect. Immun.*, 2004, **72**, 5452-5459.

15. J. K. Bender, J. Praszkier, M. J. Wakefield, K. Holt, M. Tauschek, R. M. Robins-Browne and J. Yang, *Appl. Environ. Microbiol.*, 2012, **78**, 5083-5092.

16. J. K. Rasheed, G. J. Anderson, H. Yigit, A. M. Queenan, A. Doménech-Sánchez, J. M. Swenson, J. W. Biddle, M. J. Ferraro, G. A. Jacoby and F. C. Tenover, *Antimicrob. Agents Chemother.*, 2000, **44**, 2382-2388.

17. V. Dimou, H. Dhanji, R. Pike, D. M. Livermore and N. Woodford, *J. Antimicrob. Chemother.*, 2012, **67**, 1660-1665.

18. B. W. Holloway, *Microbiology*, 1955, **13**, 572-581.

19. B. A. Diep, S. R. Gill, R. F. Chang, T. H. Phan, J. H. Chen, M. G. Davidson, F. Lin, J. Lin, H. A. Carleton, E. F. Mongodin, G. F. Sensabaugh and F. Perdreau-Remington, *The Lancet*, 2006, **367**, 731-739.

20. J. M. Andrews, *J. Antimicrob. Chemother.*, 2001, **48**, 5-16.

21. EUCAST, *Clin. Microbiol. Infect.*, 2003, **9**, ix-xv.

22. CLSI, *Methods for Dilution Antimicrobial Susceptibility Tests for Bacteria That Grow Aerobically; Approved Standard*, CLSI document M07-A9, Wayne (PA), USA, 9th edn., 2012.

23. V. Lorian and B. A. Atkinson, *J. Clin. Microbiol.*, 1982, **16**, 70-76.

24. D. J. Lane, in *Nucleic Acid Techniques in Bacterial Systematics*, eds. E. Stackebrandt and M. Goodfellow, John Wiley and Sons, Chichester, 1991, pp. 115–175.

25. A. Shevchenko, H. Tomas, J. Havlis, J. V. Olsen and M. Mann, *Nat. Protocols*, 2007, **1**, 2856-2860.

26. EnteroBase, http://enterobase.warwick.ac.uk.

27. B. Langmead and S. L. Salzberg, *Nat. Methods*, 2012, **9**, 357-359.

28. H. Li, B. Handsaker, A. Wysoker, T. Fennell, J. Ruan, N. Homer, G. Marth, G. Abecasis and R. Durbin, *Bioinformatics*, 2009, **25**, 2078-2079.

29. K. Rutherford, J. Parkhill, J. Crook, T. Horsnell, P. Rice, M. A. Rajandream and B. Barrell, *Bioinformatics*, 2000, **16**, 944-945.

30. F. Garcia-Alcalde, K. Okonechnikov, J. Carbonell, L. M. Cruz, S. Gotz, S. Tarazona, J. Dopazo, T. F. Meyer and A. Conesa, *Bioinformatics*, 2012, **28**, 2678-2679.

31. D. C. Koboldt, Q. Zhang, D. E. Larson, D. Shen, M. D. McLellan, L. Lin, C. A. Miller, E. R. Mardis, L. Ding and R. K. Wilson, *Genome Res.*, 2012, **22**, 568-576.

32. A. R. Quinlan and I. M. Hall, *Bioinformatics*, 2010, **26**, 841-842.

33. M. I. Love, W. Huber and S. Anders, *Genome Biol.*, 2014, **15**, 550.

34. Y. Benjamini and Y. Hochberg, *J. Roy. Stat. Soc. Ser. B. (Stat. Method.)*, 1995, **57**, 289-300.

35. M. Kanehisa, S. Goto, Y. Sato, M. Furumichi and M. Tanabe, *Nucleic Acids Res.*, 2012, **40**, D109-114.

36. C. von Mering, L. J. Jensen, B. Snel, S. D. Hooper, M. Krupp, M. Foglierini, N. Jouffre, M. A. Huynen and P. Bork, *Nucleic Acids Res.*, 2005, **33**, D433-437.

37. S. Tyanova, T. Temu and J. Cox, *Nat. Protoc.*, 2016, **11**, 2301-2319.

38. S. Tyanova, T. Temu, P. Sinitcyn, A. Carlson, M. Y. Hein, T. Geiger, M. Mann and J. Cox, *Nat. Methods*, 2016, **13**, 731-740.

# Appendix

## Crystallographic Data

### $[Zn_2L^b_3][ClO_4]_4 \cdot 2CH_3CN$

| | |
|---|---|
| Empirical formula | $C_{112}H_{108}Cl_4N_{14}O_{22}Zn_2$ |
| Formula weight | 2274.66 |
| Temperature/K | 150(2) |
| Crystal system | monoclinic |
| Space group | $P2_1$ |
| a/Å | 12.3149(4) |
| b/Å | 40.4691(4) |
| c/Å | 12.3281(2) |
| α/° | 90 |
| β/° | 117.839(3) |
| γ/° | 90 |
| Volume/Å$^3$ | 5432.9(2) |
| Z | 2 |
| $\varrho_{calc}$g/cm$^3$ | 1.390 |
| μ/mm$^{-1}$ | 2.091 |
| F(000) | 2364.0 |
| Crystal size/mm$^3$ | 0.124 × 0.116 × 0.074 colourless block |
| Radiation | CuKα (λ = 1.54178) |
| 2Θ range for data collection/° | 8.118 to 152.936 |
| Index ranges | -13 ≤ h ≤ 11, -50 ≤ k ≤ 47, -13 ≤ l ≤ 15 |
| Reflections collected | 19477 |
| Independent reflections | 13837 [$R_{int}$ = 0.0262, $R_{sigma}$ = 0.0327] |
| Data/restraints/parameters | 13837/377/1615 |
| Goodness-of-fit on $F^2$ | 1.041 |
| Final R indexes [I>=2σ (I)] | $R_1$ = 0.0482, $wR_2$ = 0.1332 |
| Final R indexes [all data] | $R_1$ = 0.0492, $wR_2$ = 0.1346 |
| Largest diff. peak/hole / e Å$^{-3}$ | 0.42/-0.54 |
| Flack parameter | -0.014(15) |

### $[Zn_2L^f_3][ClO_4]_4 \cdot 6CH_3CN \cdot 5H_2O$

| | |
|---|---|
| Empirical formula | $C_{138}H_{142}Cl_4N_{18}O_{27}S_3Zn_2$ |
| Formula weight | 2853.41 |
| Temperature/K | 100(2) |
| Crystal system | monoclinic |
| Space group | C2/c |
| a/Å | 38.9929(5) |
| b/Å | 22.5983(2) |

| | |
|---|---|
| c/Å | 36.9118(6) |
| α/° | 90 |
| β/° | 104.4640(10) |
| γ/° | 90 |
| Volume/Å$^3$ | 31494.8(7) |
| Z | 8 |
| $\varrho_{calc}$g/cm$^3$ | 1.204 |
| μ/mm$^{-1}$ | 1.937 |
| F(000) | 11904.0 |
| Crystal size/mm$^3$ | 0.29 × 0.11 × 0.1 |
| Radiation | CuKα (λ = 1.54178) |
| 2Θ range for data collection/° | 4.556 to 134.798 |
| Index ranges | -46 ≤ h ≤ 46, -27 ≤ k ≤ 27, -44 ≤ l ≤ 43 |
| Reflections collected | 210348 |
| Independent reflections | 28266 [$R_{int}$ = 0.0614, $R_{sigma}$ = 0.0286] |
| Data/restraints/parameters | 28266/377/1849 |
| Goodness-of-fit on F$^2$ | 1.360 |
| Final R indexes [I>=2σ (I)] | $R_1$ = 0.1046, $wR_2$ = 0.3130 |
| Final R indexes [all data] | $R_1$ = 0.1218, $wR_2$ = 0.3332 |
| Largest diff. peak/hole / e Å$^{-3}$ | 1.21/-0.84 |

## $[Zn_2L^i_3][ClO_4]_4 \cdot CH_3CN \cdot 1.5H_2O$

| | |
|---|---|
| Empirical formula | $C_{128.5}H_{114.75}Cl_3N_{13.25}O_{22.5}Zn_2$ |
| Formula weight | 2441.67 |
| Temperature/K | 100(2) |
| Crystal system | triclinic |
| Space group | P-1 |
| a/Å | 19.4621(5) |
| b/Å | 24.0209(9) |
| c/Å | 30.5735(16) |
| α/° | 90.960(4) |
| β/° | 99.274(3) |
| γ/° | 89.987(3) |
| Volume/Å$^3$ | 14104.2(10) |
| Z | 4 |
| $\varrho_{calc}$g/cm$^3$ | 1.150 |
| μ/mm$^{-1}$ | 0.462 |
| F(000) | 5078.0 |
| Crystal size/mm$^3$ | 0.20 × 0.12 × 0.03 |
| Radiation | MoKα (λ = 0.71073) |
| 2Θ range for data collection/° | 4.308 to 55.424 |
| Index ranges | -23 ≤ h ≤ 25, -31 ≤ k ≤ 31, -39 ≤ l ≤ 39 |
| Reflections collected | 159842 |
| Independent reflections | 63160 [$R_{int}$ = 0.1545, $R_{sigma}$ = 0.1643] |
| Data/restraints/parameters | 63160/351/3038 |

| | |
|---|---|
| Goodness-of-fit on $F^2$ | 1.272 |
| Final R indexes [I>=2σ (I)] | $R_1 = 0.1738$, $wR_2 = 0.4171$ |
| Final R indexes [all data] | $R_1 = 0.2757$, $wR_2 = 0.4778$ |
| Largest diff. peak/hole / e $Å^{-3}$ | 4.64/-0.92 |